VALORIZATION OF LIGNOCELLULOSIC WASTE ABUNDANT IN TÜRKİYE FOR POTENTIAL APPLICATION IN SUSTAINABLE LITHIUM RECOVERY

A Thesis Submitted to
the Graduate School of
İzmir Institute of Technology
in Partial Fulfillment of the Requirements for the Degree of

DOCTOR OF PHILOSOPHY

in Chemical Engineering

by
Yaşar Kemal RECEPOĞLU

December 2023
İZMİR

We approve the thesis of **Yaşar Kemal RECEPOĞLU**

Examining Committee Members:

Assoc. Prof. Dr. Aslı YÜKSEL ÖZŞEN
Supervisor, Department of Chemical Engineering, Izmir Institute of Technology

Prof. Dr. Nalan KABAY
Department of Chemical Engineering, Ege University

Prof. Dr. Levent BALLİCE
Department of Chemical Engineering, Ege University

Prof. Dr. S. Fehime ÖZKAN ÇAKICIOĞLU
Department of Chemical Engineering, Izmir Institute of Technology

Prof. Dr. Mustafa M. DEMİR
Department of Materials Science and Engineering, Izmir Institute of Technology

5 December 2023

Prof. Dr. Aysun SOFUĞLU
Head of the Department of
Chemical Engineering

Prof. Dr. Mehtap EANES
Dean of the Graduate School of
Engineering and Science

ACKNOWLEDGMENTS

This thesis was financially supported by The Scientific and Technological Research Council of Türkiye-TUBITAK 1001 (Project no. 219M219) from the beginning to the end. Izmir Institute of Technology Scientific Research Projects Coordination Unit (Project No. 2019IYTE0178) is also acknowledged for providing financial support to initiate this thesis study.

I wish to convey my appreciation to Assoc. Prof. Dr. Aslı YÜKSEL ÖZŞEN, my supervisor, whose guidance has been invaluable throughout the course of this thesis. I also extend my heartfelt thanks to the members of my PhD Thesis Committee and Jury, namely Prof. Dr. S. Fehime ÖZKAN ÇAKICIOĞLU and Prof. Dr. Mustafa M. DEMİR, for generously sharing their expertise, which significantly enhanced the quality of my thesis.

Assoc. Prof. Dr. Özgür ARAR at Ege University, Department of Chemistry, is greatly acknowledged for his endless support, both for his knowledge in the development of this thesis and technically - such as Li analysis in a flame photometer. I would like to express my gratitude to the experts at the Center for Materials Research, as well as the Environmental Development Application and Research Center at İzmir Institute of Technology Integrated Research Center, for their generous assistance and technical support.

Finally, I want to express my gratitude to my mother Nursel DEMİREL, who assisted me in overcoming challenges and provided invaluable moral support throughout my PhD journey. I feel incredibly fortunate to have you by my side.

ABSTRACT

VALORIZATION OF LIGNOCELLULOSIC WASTE ABUNDANT IN TÜRKİYE FOR POTENTIAL APPLICATION IN SUSTAINABLE LITHIUM RECOVERY

The demand for lithium (Li) is increasing by its pivotal role in energy storage and transportation electrification nowadays. The surge in demand has prompted a global quest for sustainable and cost-effective methods to extract Li from water sources. This thesis centers on valorizing abundant lignocellulosic waste, specifically hazelnut shell waste, abundant in Türkiye starting with the phosphorylation of pristine cellulose, contributing to the development of innovative biosorbents tailored for extracting Li from aqueous solutions. Comprehensive material characterization was conducted using SEM–EDS, FTIR, XPS, BET, XRD, and TGA analyses. Various factors influencing the process, such as biosorbent dosage, initial concentration, temperature, contact time, pH, and coexisting ions were explored. The maximum sorption capacity was determined to be 9.60 mg/g for phosphorylated functional cellulose (FC) and 7.71 mg/g for phosphorylated functional hazelnut shell waste (FHS) at 25°C, by the Langmuir model. Impressively, Li sorption reached equilibrium within a 3-minute, indicating the rapid kinetic properties of biosorbents. Furthermore, FC and FHS were employed in a packed bed column, leading to a threefold increase in sorption capacity under dynamic flow, especially at lower flow rates, regardless of bed height. Remarkably, a mere 15.75 mL of 5% H_2SO_4 solution was adequate to desorb approximately 100% of Li from the saturated biosorbents. The column data interpreted with theoretical models, affirmed the potential for large-scale implementation of these biosorbents. Preliminary tests on Li recovery from geothermal water using FC and FHS were also conducted to assess their applicability in real brine conditions, with a comparison made to the commercial ion exchange resin, Lewatit® TP 260.

ÖZET

SÜRDÜRÜLEBİLİR LİTYUM GERİ KAZANIMINDA POTANSİYEL UYGULAMA İÇİN TÜRKİYE'DE YAYGIN BULUNAN LİGNOSELÜLOZİK ATIKLARIN DEĞERLENDİRİLMESİ

Lityumun (Li) enerji depolama teknolojilerinde ve taşımacılığın elektrifikasyonunda oynadığı kilit rol nedeniyle talebi günümüzde artmaktadır. Bu artan talep, sürdürülebilir ve düşük maliyetli yöntemler arayışını küresel ölçekte tetiklemiştir. Bu tez, Türkiye'de bol miktarda bulunan özellikle fındık kabuk atığı gibi lignoselülozik atıkların değerlendirilmesine odaklanmaktadır. Süreç, ham selülozun fosforilasyonu ile başlayarak, sulu çözeltilerden Li kazanmak için özel olarak tasarlanmış yenilikçi biyosorbentlerin geliştirilmesine katkı sağlamıştır. SEM–EDS, FTIR, XPS, BET, XRD ve TGA analizleri kullanılarak kapsamlı malzeme karakterizasyonu gerçekleştirilmiştir. Süreç üzerinde etkili olan biosorbent dozajı, başlangıç derişimi, sıcaklık, temas süresi, pH ve ortak iyonlar gibi çeşitli faktörler araştırılmıştır. Maksimum sorpsiyon kapasitesi, 25°C'de Langmuir modeline göre fosforile edilmiş fonksiyonel selüloz (FC) için 9.60 mg/g ve fosforile edilmiş fonksiyonel fındık kabuk atığı (FHS) için 7.71 mg/g olarak belirlenmiştir. Etkileyici bir şekilde, Li sorpsiyonu 3 dakika içinde dengeye ulaşarak biyosorbentlerin hızlı kinetik özelliklerini kanıtlamıştır. Ayrıca, FC ve FHS dolgulu bir kolon kullanılarak, akış hızı ve yatak yüksekliği gibi değişken işletme koşullarında özellikle yükseklikten bağımsız olarak düşük akış hızlarında Li'nin sudan geri kazanımında üç kat artış sağlanmıştır. Dikkat çekici bir şekilde, doymuş biyosorbentlerden Li'nin yaklaşık %100'ünü sıyırmak için yalnızca 15.75 mL %5'lik H_2SO_4 çözeltisi yeterli olmuştur. Teorik modellerle yorumlanan kolon verileri, bu biyosorbentlerin büyük ölçekte uygulanma potansiyelini doğrulamıştır. FC ve FHS kullanılarak jeotermal sudan Li geri kazanımına yönelik bazı ön denemeler ayrıca gerçek tuzlu su koşullarında uygulanabilirliklerini değerlendirmek amacıyla yapılarak Lewatit® TP 260 ticari iyon değiştirici reçinesi ile karşılaştırılmıştır.

This thesis is dedicated to my acquaintances who lost their lives in the earthquake of February 6, 2023…

TABLE OF CONTENTS

LIST OF FIGURES

Figure **Page**

Figure **Page**

Figure **Page**

Figure **Page**

Figure **Page**

LIST OF TABLES

Table **Page**

Table **Page**

CHAPTER 1

INTRODUCTION

The increasing demand for lithium (Li), a crucial component in batteries for electric vehicles, portable electronics, and renewable energy storage systems, has led to the exploration of sustainable methods for its recovery (Meng et al., 2021; Swain, 2017). According to recent market analysis, 35% of the Li market share is composed of batteries, 32% is ceramic, and 9% is lubricants (Li et al., 2018). However, Li demand is expected to increase significantly due to the development of automobile technology. Electric vehicles are expected to replace fossil-fuel-powered vehicles, and demand for developing storage and battery-to-battery systems will double every 5-10 years. By the year 2030, over 55 million electric cars will be on the road (IEA, 2021). The cost of lithium hydroxide and lithium carbonate is expected to increase by two folds in the future, from 8000 US$ per ton to 12000 US$ in 2025 (Baba et al., 2019; Li et al., 2018).

Li is difficult to separate and recover from water because of its low concentrations compared to Na, Mg, and other similar cations, even though saline water resources are much more widespread and less expensive to process than rocks containing minerals like amblygonite, lepidolite, petalite, and spodumene (Recepoğlu et al., 2017a). Various methods such as ion exchange (Aljarrah et al., 2023; Arroyo et al., 2019; Zandvakili and Ranjbar, 2018), adsorption (Jiang et al., 2020; Marthi et al., 2021), solvent extraction (Mao et al., 2022; Sun et al., 2022; Zhang et al., 2018), solar evaporation (Yu et al., 2022), co-precipitation (Battaglia et al., 2022; Shin et al., 2022) and membrane processes (Sun et al., 2022; Xiao et al., 2022; Xu et al., 2022) have been investigated to recover Li from water. Among all others, the adsorption process is the most efficient, promising and most widely used method in hydrometallurgy and wastewater treatment, since it is basically simple, economically, and technically feasible and socially acceptable (Nouri et al., 2007). Because of their exceptional physicochemical features that improve affinity for metal ions, synthetic adsorbents have a high adsorption capacity. Some inorganic adsorbents such as $H_4Mn_5O_{12}$ nanotubes lithium ion sieve (Xu et al., 2019), iron-doped

lithium titanium oxides (Wang et al., 2018), titanium type ion sieve (H_xTiO_3) (Wang et al., 2017), and λ-MnO_2 (Kitajou et al., 2006; Park et al., 2012; Recepoğlu et al., 2017a, 2018a; Yoshizuka et al., 2002) have been used in the majority of research on Li recovery from a combination of various cations with higher concentrations. Namely, Lawagon et al. (2016) studied lithium-ion sieve (Metatitanic acid (H_2TiO_3)-LIS) to adsorb Li ions from seawater at pH 11.5, initial concentration of 70 mg/L and at 30℃, the adsorption capacity of 94.5 mg/g was achieved (Lawagon et al., 2016). However, they are very cost-constrained, have sophisticated synthesis procedures, are non-biodegradable, and are generally unfavorable to the environment. Therefore, there is a growing interest in the development of new functional adsorbents with high selectivity, large capacity, and high sorption rates for the removal of hazardous pollutants as well as the recovery of precious metals from water. Particularly, because they are environmentally friendly, adsorbents developed from natural polymers are the most preferred ones (Recepoğlu et al., 2018b). Currently, agro-biomass wastes have proved potential and sustainable sources of biosorbents for Li and other metal ions (Nampeera et al., 2022). To generate more accessible, long-lasting, and environmentally acceptable adsorbents for the remediation of metal ions and contaminants from aqueous sources, the agro-wastes are targeted and modified (Bulgariu and Bulgariu, 2018; Yousef and Qiblawey, 2020). Coffee husks (Berhe et al., 2015; Cheruiyot et al., 2019; Torres Castillo et al., 2021), rice husks (Johar et al., 2012), Rhizophora mucronate stem-barks (Oloo et al., 2020), orange peels (Akinhanmi et al., 2020), cabbage wastes (Wekoye et al., 2020), have served as biomass supplies for the synthesis of biosorbents that remove dyes, pollutants, heavy metals, and other contaminants. Cellulose is a suitable substitute matrix to develop functional materials for eliminating pollutants. It has hydroxyl groups that can be modified with various techniques to produce novel sorbents with different functional groups (Yetgin et al., 2022).

The key objective of this thesis is to develop low-cost biosorbent that promote sustainability and circular economy, by modifying the cellulose-based materials (pristine cellulose and hazelnut shell waste) to obtain value-added Li capable functional materials through phosphorylation. Elaborative characterization studies were performed for the novel phosphorylated functional cellulose (FC) and hazelnut shell waste (FHS). Batch and dynamic packed column sorption experiments for the recovery of Li from water with several process parameters were considered in detail. Some preliminary tests were done

for the Li recovery from geothermal water samples obtained from different thermal regions of Türkiye using FC and FHS. The synthesized biosorbents, FC and FHS, also compared with commercially available ion exchange resin, Lewatit® TP 260.

1.1. Motivation

In my thesis, I had motivations of varied dimensions. My objective on a larger scale was to connect two regional key challenges to provide an effective solution. Those issues were: (i) the valorization of lignocellulosic wastes mainly hazelnut shell wastes that are abundant and used only for heating purposes in Türkiye by converting them into a value-added product such as biosorbent and, (ii) the utilization of those biosorbents in sustainable lithium recovery from aqueous sources such as geothermal water as lithium is a critical raw material and strategic metal of 21st century in technologies of electronic devices and electric vehicles with increasing need. In this context, the valorization of lignocellulosic wastes as biosorbents for potential application in sustainable lithium recovery from water offers a promising solution with several environmental and economic advantages that simultaneously addresses waste management and resource scarcity issues. It reduces the dependency on traditional lithium sources, such as lithium-rich ores, and mitigates the environmental impact associated with mining and extraction processes. Recovering lithium from geothermal waters existing in Türkiye also reduces the dependency on lithium import as raw material needed for energy storage systems such as batteries. Moreover, it contributes to the circular economy by transforming waste materials into valuable resources and promoting a sustainable approach to waste management and lithium recovery.

As a result of comprehensive literature survey, it has been found that there is no study in which lithium capable functional materials have been synthesized from cellulose and lignocellulosic wastes by phosphorylation reaction (solid phase reaction of cellulose with phosphorus acid in molten urea). The outputs of this thesis give an idea about obtaining biosorbents from not only hazelnut shell wastes, but also various biomass wastes which were not evaluated properly in Türkiye and may have high potential for phosphorylation to utilize in lithium recovery from water. To sum up, the valorization of lignocellulosic wastes abundant in Türkiye as biosorbents for potential application in

sustainable lithium recovery from water sources represents an innovative solution. By utilizing the inherent modification properties of them, such as their surface chemistry and structure, effective biosorbents can be synthesized. This integrated approach addresses waste management challenges and contributes to the development of eco-friendly energy storage systems by holding potential in sustainable lithium production.

1.2. Thesis Overview

The main objective of this PhD thesis was to develop novel functional materials by phosphorylation for potential application in sustainable lithium recovery from water such as modified cellulose (phosphorylated functional cellulose, FC), and the valorized lignocellulosic wastes, specifically hazelnut shell wastes (phosphorylated hazelnut shell waste, FHS). The summarized contents of each chapter are as follows:

i. In Chapter 2, pristine cellulose was functionalized by the phosphorylation reaction to make it suitable for lithium sorption from water. After characterization studies of the synthesized adsorbent with SEM, EDX, FTIR, TGA and XPS, the effects of various parameters on the lithium uptake capacity of the adsorbent were examined in detail. The equilibrium data were analyzed by several adsorption models to estimate its maximum sorption capacity and isotherm behavior. As well as thermodynamic and kinetic investigation, desorption studies were also performed with several parameters.

ii. In Chapter 3, hazelnut shell waste was phosphorylated to develop a novel biosorbent based on natural renewable resource for the recovery of lithium from aqueous solution. For the synthesized biosorbent, the surface morphology and mapping by SEM–EDS, chemical properties by FTIR, elemental analysis by XPS, specific surface area by BET, crystallinity by XRD and thermal properties by TGA were elucidated elaborately. The influence of biosorbent dosage, initial concentration, temperature, contact time, pH and coexisting ions were investigated. Thermodynamic parameters were obtained by different isokinetic temperatures. Desorption studies were carried out by NaCl, HCl, and H_2SO_4 at various molarities. A preliminary test on the Li recovery from geothermal water was also done to check its applicability in a real brine.

iii. In Chapter 4, phosphorylated functional cellulose (FC) was cross-linked with epichlorohydrin at different ratios because it is a very hydrophilic substance that instantly swells to form a hydrogel when it encounters water. It was aimed to utilize a packed column to recover lithium from water continuously under varying operating conditions such as flow rate and bed height. The Thomas, Yoon–Nelson, and Modified Dose Response (MDR) models were fitted to experimental data to examine the breakthrough curves.

iv. In Chapter 5, lithium biosorption via phosphorylated functional hazelnut shell waste (FHS) was investigated utilizing a continuous-flow packed-bed column operated under various flow rates and bed heights, with the goal of removing Li to ultra-low levels and then recovering it. Because in batch-scale operations, biosorption employing FHS revealed excellent lithium removal and recovery efficiency therefore, scaling up and implementing packed bed column systems necessitates further optimization of the design and performance. The three conventional breakthrough models of the Thomas, Yoon-Nelson, and MDR were also used to properly estimate the whole breakthrough behavior of the FHS column and to estimate the characteristic model parameters. Some cyclic studies were performed for both FC and FHS. They are also compared under specified conditions in column operations.

v. In Chapter 6, the focus was on exploring the potential of FC and FHS as sustainable and efficient materials for recovering lithium from geothermal water. The aim was to present the results of preliminary studies to determine the sorption capacity and selectivity of these materials towards lithium ions, as well as their performance in real geothermal water samples.

1.3. Contributions to the Literature

To my best knowledge, lithium recovery using low-cost and sustainable lignocellulosic waste sources containing a considerable portion of cellulose is a new field with scant literature. The contributions of this Ph.D. thesis to the literature are explained as follows:

i. Chapter 2: Phosphate groups are known to show excellent chelating properties.

Thus, phosphated polysaccharides were used as metal-chelating polymers, as cation exchange materials and for the treatment of polluted wastewater (Illy et al., 2015). For example, phosphated chitosan and cellulose were used as adsorbents for uranium or for various transition metals and lanthanide ions (Oshima et al., 2008; Sakaguchi et al., 1981). Phosphorylated functional cellulose (FC) was used for the first time in the literature for the recovery of lithium from aqueous solutions which was shown to be a favorable adsorbent. The outputs of this chapter provide an insight into the possibility of obtaining promising low-cost biosorbents from various lignocellulosic biomass waste and open the way to lithium recovery from real water sources such as geothermal water.

ii. Chapter 3: This is the first study to develop an efficient and sustainable Li capable biosorbent from hazelnut shell waste via phosphorylation reaction. Hazelnut shell waste was valorized properly rather than low value application such as hazelnut shell coals for heating purpose. With the promising results in lithium sorption capacity and efficiency, the novel phosphorylated hazelnut shell waste had a great potential for lithium recovery from aqueous solution by being added value as a waste and recovering a strategic element of modern life simultaneously.

iii. Chapter 4: Phosphorylated functional cellulose (FC) was modified via cross-linking with epichlorohydrin to obtain more water stable form and employed in a packed bed column to examine its continuous Li recovery capability for the first time in the literature. As a result of experimental runs and theoretical investigation via Thomas, Yoon–Nelson and MDR models, FC strengthened with crosslinking by epichlorohydrin was discovered to be a potential sorbent for the extraction of Li from aqueous solutions in a dynamic packed bed column.

iv. Chapter 5: In batch-scale operations, biosorption employing phosphorylated hazelnut shell waste (FHS) revealed excellent lithium removal and recovery efficiency. Scaling up and implementing packed bed column systems necessitates further optimization of the design and performance. Lithium biosorption via FHS was investigated for the first time utilizing a continuous-flow packed-bed column operated under various flow rates and bed heights, with the goal of removing Li to ultra-low levels and then recovering it.

v. Chapter 6: Three different geothermal water samples collected from the İzmir, Çanakkale, and Aydın provinces of Türkiye (all located in western Anatolia) as real Li sources were used for the preliminary tests in the recovery of Li for the first time. As data indicates, although other competing ions reduced slightly Li separation efficiency depending on level of concentrations, Li could be concentrated almost two times higher than in the initial geothermal water using phosphorylated functional cellulose and hazelnut shell waste.

CHAPTER 2

SYNTHESIS, CHARACTERIZATION AND ADSORPTION STUDIES OF PHOSPHORYLATED CELLULOSE FOR THE RECOVERY OF LITHIUM FROM AQUEOUS SOLUTIONS*, †

2.1. Introduction

Lithium has been recognized as an important raw material in the last decade due to its wide use in many applications, such as rechargeable batteries (market share: 35%), glasses and ceramics (market share: 32%), light aircraft alloys, medicinal drugs, thermonuclear fusion, air purification, electrode welding paints, additives for lubricating greases and cement (Reichel et al., 2017; Xu et al., 2016). Especially since the 1990s, large battery applications in lithium-ion batteries, such as electric vehicles and stationary storage systems, have gained significance in terms of continuous improvement, cost and energy savings (Singh et al., 2016). Therefore, there is a growing interest in lithium and lithium sources worldwide. Also, it has been noted that the recovery of lithium from several saline waters, such as geothermal water and seawater, which are known to be large sources of lithium, is less costly than its recovery from rocks as a result of mining (Park et al., 2012; Swain, 2017; Q. Yu et al., 2013). Apart from the technologies such as solvent extraction (Dang and Steinberg, 1978; Shi et al., 2017), solar evaporation (Epstein et al., 1981), co-precipitation (Yanagase et al., 1983), and membrane processes (Iizuka et al., 2013; Somrani et al., 2013), adsorption and/or ion exchange methods with lower operating costs can be considered as the most suitable methods for the recovery of lithium from diluted aqueous sources. Some inorganic ion exchange materials with superior physicochemical properties (e.g., large specific surface area, high adsorption and ion exchange capacity, mechanical stability, and layer structure) exhibit extremely high selec-

*This chapter has been published as: Y.K. Recepoğlu, A. Yüksel, Synthesis, Characterization and Adsorption Studies of Phosphorylated Cellulose for the Recovery of Lithium from Aqueous Solutions, Cellulose Chemistry and Technology 55(3-4) (2021) 385-401.
†This chapter was partly presented orally at IEX 2022: Ion Exchange – a continuing success story Conference (virtual), September 07–09, 2022, UK.

tivity for lithium ions. Various studies have been carried out for the recovery of lithium from seawater using different types of inorganic adsorbents (Chitrakar et al., 2001; Kitajou et al., 2006, 2005, 2003; Miyai et al., 1988; Yoshizuka et al., 2002). Among these adsorbents, adsorption by λ-MnO_2 adsorbent is the most studied one (Chitrakar et al., 2002b, 2002a; Kim et al., 2003; Kitajou et al., 2006, 2005, 2003; Li et al., 2014; Nishihama et al., 2011; Recepoğlu et al., 2017a, 2018a; Yoshizuka et al., 2002; Q. Yu et al., 2013).

The synthesis and development of novel functional low-cost adsorbents with large capacity, high selectivity, as well as high adsorption rate, still greatly attract interest for both removal of hazardous materials and the recovery of valuable minerals from water. Specifically, adsorbents derived from a natural polymer are the most preferable ones due to their being environmentally benign materials (Recepoğlu et al., 2018b). Cellulose is the most widely available natural polymer that accounts for about 35-50% of most plant materials in the world (Sengupta and Pike, 2012). It is a linear syndiotactic homopolymer composed of D-anhydroglucopyranose units (AGU), which are linked together by β-(1→4)-glucosidic bonds. The hydroxyl groups at both ends of the cellulose chain behave differently. Bridging and ring oxygen atoms are mainly involved in intermolecular and intra-molecular interactions, such as hydrogen bonding and degradation reactions (Suflet et al., 2006).

Zhou et al., (2014) used glycidyl methacrylate and sulfosalicylic acid to modify cellulose and obtained a new adsorbent CGS (i.e., cellulose modified with glycidyl methacrylate and sulfosalicylic acid) for the removal of crystal violet (CV) (Zhou et al., 2014). So far, Yue et al., (2019) synthesized and characterized a cellulose based adsorbent prepared by grafting amino-terminated hyperbranched polymer (NH_2-HBP) and beta-cyclodextrin (β-CD) onto cotton fibers for the removal of anionic and cationic dyes (Yue et al., 2019). In addition to the removal of textile dyes, cellulose-based adsorbents synthesized by different esterification methods for cellulose modification, using various chemical reagents and pollutant binding groups for the removal of different heavy metals, were also reported in the literature (Belhalfaoui et al., 2009; Gurgel et al., 2008, 2009; Gurgel and Gil, 2009; Hokkanen et al., 2013; Kardam et al., 2014; Low et al., 2004; Melo et al., 2011; Pangeni et al., 2012; Velazquez-Jimenez et al., 2013; Yu et al., 2013; C. H. Zhou et al., 2012; Y. Zhou et al., 2012).

Phosphorylation is one of the modification ways for cellulose. The grafting reaction of phosphorus compounds to cellulose can be carried by several routes: with

trivalent (III) or pentavalent (V) phosphorus reagents, by direct or indirect bonding of phosphorus functions to cellulose, using cellulose or cellulose derivatives as substrates, with or without catalysts, in heterogeneous or homogeneous reaction environment, etc. Phosphorus derivatives, such as $POCl_3$, H_3PO_4, and P_2O_5, are the most utilized phosphorylating agents for pentavalent phosphorus. These reagents, usually leading to anionic cellulose phosphates, show lower esterification reactivity than the similar derivatives of trivalent phosphorus and cause higher degradation of the cellulose substrate. This drawback is partially overcome if urea is introduced in the phosphorylation system as a catalyst (Belosinschi et al., 2012; Shi et al., 2014). Phosphate groups are known to show excellent chelating properties. Thus, phosphated polysaccharides were used as metal-chelating polymers, as cation exchange materials and for the treatment of polluted wastewater (Illy et al., 2015). For example, phosphated chitosan and cellulose were used as adsorbents for uranium or for various transition metals and lanthanide ions (Oshima et al., 2008; Sakaguchi et al., 1981). On the other hand, novel functionalized cellulose microspheres have also been developed by different synthesis routes and functional groups for efficient lithium-ion separation. Chen et al., (2019) recently synthesized cellulose-based microspheres containing crown ethers groups (named as MCM-g-AB15C5) by pre-irradiation-induced emulsion grafting of glycidyl methacrylate (GMA), followed by the chemical reaction between the epoxy group of grafted polymers and 4′-aminobenzo-15-crown-5 (AB15C5), which showed maximum adsorption capacity of 12.9 mg/g (Chen et al., 2019). Another cellulose microsphere adsorbent with sulfonic acid groups (named as CGS) was prepared by the pre-irradiation-induced emulsion graft polymerization of glycidyl methacrylate onto cellulose microspheres through subsequent sulfonation and protonation, which exhibited adsorption capacity of 16.0 mg Li^+/g-adsorbent (Xu et al., 2020). Tang et al., (2020)developed and investigated a renewable and recyclable hydrogen manganese oxide (HMO)-modified cellulose film toward the extraction of lithium from lithium-containing aqueous solutions. They found that the HMO/cellulose film exhibited a higher Li^+ adsorption capacity (21.6 mg/g HMO) than the HMO/polymer (e.g., poly(vinyl chloride) or poly(vinylidene fluoride)) films (Tang et al., 2020).

In this chapter, we aimed to obtain a low-cost and novel lithium selective adsorbent by attaching phosphorous functional groups to pristine cellulose. To our best knowledge, no studies have been reported in the literature regarding the synthesis of lithium selective adsorbents from cellulose. Recently, Çiçek et al., (2018) studied the

lithium selectivity of this functional group using chelating resins containing aminomethylphosphonic acid for lithium removal from water (Çiçek et al., 2018). Moreover, Suflet et al., (2006) pioneered the synthesis and characterization of phosphorylated cellulose by reacting microcrystalline cellulose in molten urea with phosphoric acid (Shi et al., 2014; Suflet et al., 2006). The synthesized functional adsorbent was characterized and evaluated for its potential to recover lithium from aqueous solution in terms of various parameters, such as adsorbent dosage, initial concentration of Li, contact time, temperature, pH, and common ion. The isotherm of the adsorption process was studied using Freundlich, Halsey, Langmuir, Redlich–Peterson and Temkin models. Thermodynamic parameters were calculated, and desorption of lithium was achieved successfully. The adsorbent exhibited quite rapid sorption of lithium.

2.2. Experimental

2.2.1. Materials

Microcrystalline cellulose, di-Ammonium hydrogen phosphate, hydrochloric acid (37%), lithium chloride, ortho-phosphoric acid (85%), potassium chloride, sodium chloride, sodium hydroxide, sulfuric acid (95–97%) and urea were purchased from Merck. Other reagents were all in analytical grade.

2.2.2. Synthesis of the Adsorbent

2.2.2.1. Conditioning of the Cellulose

In order to activate hydroxy groups in cellulose prior to the phosphorylation reaction (that is, the NaOH treatment breaks the van der Waals and hydrogen bonds between cellulose molecules, which causes more hydroxy groups to become exposed to H_3PO_4 in the second step of the process) as reported in the patent (Yabusaki, 2010), 10 M NaOH solution (100 mL) was added to microcrystalline cellulose (10 g) and the

mixture was stirred at room temperature (25°C) for 2 h. Then, 10 M HCl (100 mL) was added to the mixture to neutralize the solution and to precipitate cellulose. After that, the mixture was washed with excess water and filtered to remove the alkali. Finally, the residue was dried at 70°C for 6 h and was ground in a mortar and pestle. The flowsheet of the procedure is depicted in the supplementary information for chapter 2 in Figure B.1.

2.2.2.2. Binding of Functional Groups to Cellulose

The phosphorylating chemical solution prepared by dissolving phosphoric acid (0.15 mol), di-Ammonium hydrogen phosphate (0.2 mol) and urea (1 mol) in water (150 mL) was added to previously NaOH treated cellulose (10 g). After thoroughly mixing the mixture thus prepared, it was allowed to stand at room temperature (25°C) for 1 h, and next, the water content was evaporated, and the residue was completely dried at 105°C for 18 h. The mixture was then heated to 150°C and it was allowed to react at this temperature for 2 h based on the reaction mechanism given below in Figure 2.1. After that, the reaction product was washed with excess water and dried at 70°C for 6 h and finally was ground in a mill to give functionalized cellulose (Yabusaki, 2010). The pristine microcrystalline cellulose and phosphorylated functional cellulose are shown in Figure 2.2 (a) and (b), respectively. In addition, the method applied for the phosphorylation is given as a flowsheet in Figure B.2.

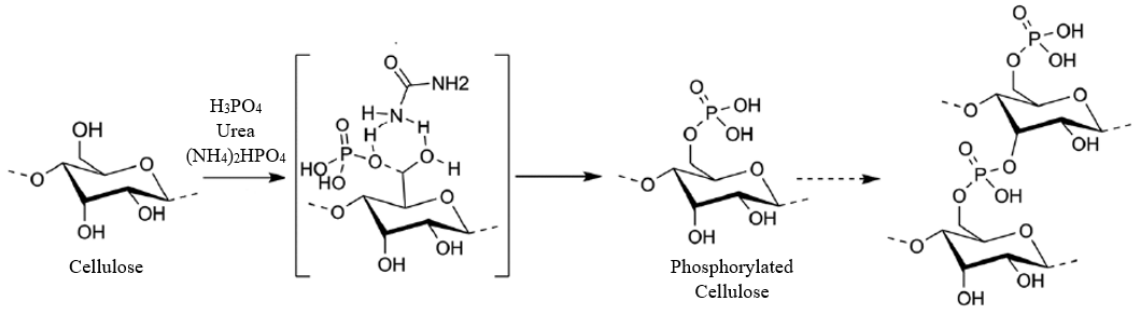

Figure 2.1. Proposed mechanism for cellulose phosphorylation with H_3PO_4 in the presence of urea (Illy et al., 2015)

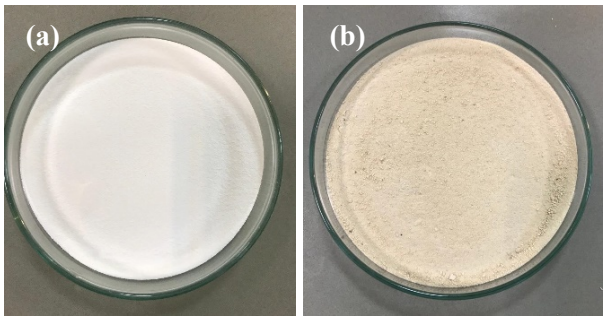

Figure 2.2. **(a)** Pristine microcrystalline cellulose, **(b)** phoshorylated functional cellulose

2.2.3. Characterization of the Synthesized Adsorbent

The surface morphology of the materials was examined by SEM equipment (Quanta 250 SEM). Before taking SEM photomicrographs at an accelerating voltage range of 3.0 – 5.0 kV, the free surfaces of the materials were coated with thin layers of gold. The elemental analysis obtained by EDX combined with the SEM method gave information on whether the expected functional groups were effectively attached to the cellulose matrix, or not.

A Shimadzu FTIR-8400S spectrophotometer was used to record the changes in the bond structures of pristine cellulose and phosphorylated functional cellulose by IR spectra within the range of 4000–400 cm^{-1}, with a resolution of 4 cm^{-1} and 24 scans per sample. The IR spectra were recorded in a solid state using a KBr pellet method, in which pellets of ca. 2 mg of cellulosic samples were prepared by mixing with ca. 150 mg of spectroscopic grade KBr.

The measurable differences in the thermal stability and heat capacity of pristine and phosphorylated materials were determined by TGA equipment (Setaram). Thermograms were obtained by heating the samples from 30°C to 1000°C, in a dynamic heating regime, under nitrogen with a constant heating rate of 5°C/min.

Quantitative elemental analysis was performed by XPS (Thermo Scientific, Nexsa) having 180° hemispherical analyzer-128 channel detector for C, O, P and Li elements based on the changes in the bond energies in the molecule. The elements were scanned in the range of 0.0 – 1350.0 eV, using monochromatic Al Kα X-rays (1486.68 eV), with a pass energy of 30 eV and scan number of 3.

2.2.4. Batch Adsorption Experiments

A series of experiments were performed to determine the lithium adsorption performance of phosphorylated functional cellulose in model Li solution, based on preliminary studies of lithium adsorption, showing that 24 h is adequate to reach adsorption equilibrium for batch treatment. To observe the effect of adsorbent dosage, various amounts (0.1 – 0.5 g) of phosphorylated functional cellulose were placed in plastic bottles that contained 25 mL of LiCl solution (Li^+: 10 mg L^{-1}) at different mass/volume ratios, and the solutions were shaken at ambient temperature (25°C) at 180 rpm. The effects of the initial concentration of lithium ions and temperature on the adsorption process were determined via LiCl solution (25 mL) at various concentrations (10 – 100 mg L^{-1}) and a constant mass of phosphorylated functional cellulose (0.3 g), shaking at various temperatures (25, 35, 45 and 55°C). For the effect of pH, experiments were carried out at various pH values (2 – 6) using LiCl solution (Li^+: 10 mg L^{-1}) and 0.3 g of phosphorylated functional cellulose at 25°C. The selectivity of the phosphorylated functional cellulose was investigated using 25 mL of the adjusted model solution (Li^+, K^+ and Na^+ each 10 mg L^{-1}) at ambient temperature as well. All the experiments were repeated twice, and average values were reported with error bars as standard deviation.

The adsorption capacity and recovery percentage of Li were calculated by the following equations, respectively:

$$q_e = \frac{(C_0 - C_e)V}{m} \tag{2.1}$$

$$R = \frac{C_0 - C_e}{C_0} \times 100 \tag{2.2}$$

where q_e is the unit adsorption capacity at equilibrium (mg g^{-1}), R is the recovery percentage of Li, C_0 and C_e are the initial Li concentration (mg L^{-1}) and Li concentration at equilibrium (mg L^{-1}), respectively. V is the volume of Li solution (L), and m is the dry weight of adsorbent (g).

2.2.5. Adsorption Kinetics

For kinetic tests, the adsorbents with various dosages (3.0 – 5.0 g L^{-1}) were contacted with 750 mL of 10 mg L^{-1} Li containing solution at 25°C. To investigate the effect of contact time on the recovery of lithium, sampling was done periodically in the time interval of 0 – 120 min. The experimental setup is illustrated in Figure B.3.

2.2.6. Desorption and Regeneration of the Phosphorylated Functional Cellulose

Saturated adsorbents obtained from the adsorption experiment via 100 mg L^{-1} Li^+ and 10 g L^{-1} adsorbent dosage were regenerated using 0.5 M, 1.0 M, and 2.0 M of NaCl, HCl and H_2SO_4 as regenerants by 25 mL solvent/0.3 g solid ratio and at 25°C, similarly to the method applied in the batch lithium adsorption experiments. After regeneration, concentrated Li can be recovered by evaporation of the spent solution in Li salt forms and further purification steps can be considered.

2.2.7. Analysis of Li and Other Cations

After each experiment, the adsorbents were separated from the solution by filtration. The filtrate was diluted as necessary and the concentrations of cations in the filtrate were determined by an ICP-OES instrument (Agilent Technologies, 5110).

2.3. Theoretical Background

2.3.1. Adsorption Isotherms

Equilibrium data were analyzed by the Freundlich, Halsey, Langmuir, Redlich–Peterson and Temkin models using the non-linear regression technique.

The Langmuir theory assumes that adsorption occurs at specific homogeneous

sites inside the adsorbent and that once a lithium ion occupies a site, no additional adsorption can occur there. In other words, there is no transmigration of adsorbate in the plane of the surface, resulting in uniform energies of adsorption onto the surface (Hamdaoui and Naffrechoux, 2007; Ismail et al., 2013). The Langmuir model (Langmuir, 1916) is expressed as follows:

$$q_e = \frac{Q_{max} K_L C_e}{1 + K_L C_e} \tag{2.3}$$

where Q_{max} (mg g^{-1}) is the maximum adsorption capacity and K_L (L mg^{-1}) is the Langmuir constant related to the affinity of the binding sites.

The essential characteristics of Langmuir isotherm is also expressed by a dimensionless constant called equilibrium parameter or separation factor, R_L, as (Hameed et al., 2008):

$$R_L = \frac{1}{1 + K_L C_0} \tag{2.4}$$

The parameter R_L describes the shape of the isotherm as follows:

- $R_L = 0$ irreversible,
- $0 < R_L < 1$ favorable,
- $R_L = 1$ linear,
- $R_L > 1$ unfavorable.

The Freundlich model is an exponential equation assuming that as the adsorbate concentration increases, the concentration of the adsorbate on the adsorbent surface also increases. According to this theory, the stronger binding sites are occupied first, and the binding strength decreases with an increasing degree of site occupation, corresponding to sorption on heterogeneous surfaces or surfaces supporting sites of varied affinities (Hamdaoui and Naffrechoux, 2007; Hameed et al., 2008). The Freundlich model is given as follows (Freundlich, 1907):

$$q_e = K_F C_e^{1/n} \tag{2.5}$$

where K_F ((mg g^{-1}) (L $mg^{-1})^{1/n}$) and n are Freundlich constants for adsorption capacity and adsorption intensity of the adsorbent, respectively. The value of n also describes the adsorption characteristics as follows:

- $n < 1$ unfavorable adsorption,
- $n = 1$ no interaction between the adsorbed species means homogenous adsorption,
- $n > 1$ favorable adsorption.

The Redlich–Peterson (R–P) model compromises between the Freundlich and Langmuir systems. This three–parameter model has the advantages of both models (Hameed et al., 2008). R–P model (Redlich and Peterson, 1959) is represented as follows:

$$q_e = \frac{K_{RP} C_e}{1 + (\alpha C_e)^{\beta}} \tag{2.6}$$

where K_{RP} (L mg^{-1}) and α (L mg^{-1})$^{\beta}$ are R–P isotherm constants, whereas β is the exponent which lies between 0 and 1. The R–P model has two limiting cases, when β = 0, the R–P model transforms to Henry's law equation, whereas when β = 1, the Langmuir model results.

The Temkin isotherm considers explicitly the adsorbent–adsorbate interactions by a factor. Due to these interactions, the heat of adsorption of all the molecules in the layer decreases linearly as coverage increases (Hameed et al., 2008). The Temkin model (Tempkin and Pyzhev, 1940) is expressed as follows:

$$q_e = (RT/b_T) ln(AC_e) \tag{2.7}$$

where $B = RT/b_T$, which is the Temkin constant related to the heat of sorption, whereas A (L mg^{-1}) is the equilibrium binding constant related to the maximum binding energy. R (8.314 J mol^{-1} K^{-1}) is the universal gas constant and T (K) is the absolute solution temperature.

The Halsey isotherm is used to evaluate multilayer adsorption at a relatively large distance from the surface and this model verifies the heteroporous nature of the adsorbent (Khambhaty et al., 2009). The Halsey model (Halsey, 1948) can be defined as:

$$q_e = exp\left(\frac{lnK_H - lnC_e}{n_H}\right) \tag{2.8}$$

where K_H and n_H are Halsey isotherm constants.

2.3.2. Adsorption Thermodynamics

The effect of temperature on lithium adsorption with phosphorylated functional adsorbent was also explained in terms of thermodynamic parameters. In this context, adsorption thermodynamics means obtaining thermodynamic parameters, including free energy changes ($\Delta G°$), standard enthalpy changes ($\Delta H°$) and entropy changes ($\Delta S°$) associated with the adsorption process to deduce the adsorption mechanism (Lin et al., 2017).

$\Delta G°$ is the basic criterion of spontaneity. If the value of $\Delta G°$ is negative, the reaction occurs spontaneously at the given temperature. The $\Delta G°$ value can be expressed by Equation (2.9) and the relationship between $\Delta G°$, $\Delta H°$ and $\Delta S°$ by Equation (2.10).

$$\Delta G° = -RTlnK_e \tag{2.9}$$

$$\Delta G° = \Delta H° - T\Delta S° \tag{2.10}$$

Other thermodynamic parameters ($\Delta H°$ and $\Delta S°$) of the adsorption process can be determined from Van't Hoff's Equation (Eq. 2.11) by plotting $1/T$ versus lnK_e for different temperatures (Lin et al., 2017).

$$lnK_e = -\frac{\Delta H°}{RT} + \frac{\Delta S°}{R} \tag{2.11}$$

The equilibrium constant (K_e) obtained in the isotherms (usually in L mg^{-1}) must become dimensionless before applying in the Van't Hoff equation. In this sense, (Lima et al., 2019) recommended a conversion of the best fitted isotherm constant ($K_{isotherm}$) into the dimensionless K_e as in Equation (12) described below:

$$K_e = \frac{(1000K_{isotherm}MW_{adsorbate})[Adsorbate]^0}{\gamma} \tag{2.12}$$

where γ is the coefficient of activity (dimensionless), $[Adsorbate]^0$ is the standard concentration of the adsorbate (1 mol L^{-1}). $MW_{adsorbate}$ is the molecular weight of the adsorbate (g mol^{-1}). 1000 stands for converting L mg^{-1} into L g^{-1}.

2.4. Results and Discussion

2.4.1. Characterization of the Synthesized Adsorbent

Figure 2.3 shows the SEM images of pristine cellulose, NaOH treated cellulose, phosphorylated functional cellulose and lithium-adsorbed phosphorylated functional cellulose, respectively, taken at 5000x magnification to observe the changes in the morphological structure of the materials. The morphological structure of pristine cellulose (Figure 2.3(a)) changes as it is processed, especially when compared to the lithium-capable adsorbent (Figure 2.3(c)) obtained by the phosphorylation reaction. When the same magnification images are compared, it is seen that Li adsorbed functional adsorbent (Figure 2.3(d)) transforms to a more porous structure and pristine cellulose has a more fibrous structure.

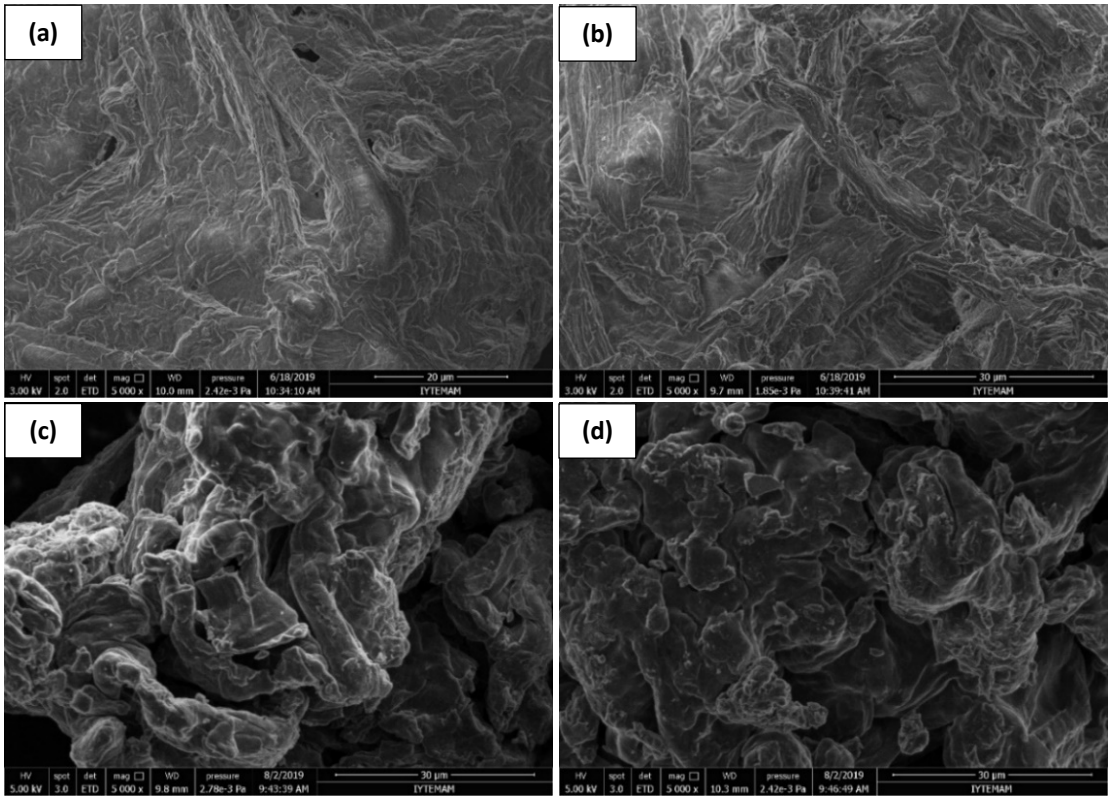

Figure 2.3. SEM surface morphology (magnification 5000x): **(a)** pristine cellulose, **(b)** NaOH treated cellulose, **(c)** phosphorylated cellulose and **(d)** lithium- loaded phosphorylated cellulose.

On the other hand, Figure 2.4 shows the elemental mapping of the phosphorylated functional adsorbent and the results of EDX. As a result of mapping, it was observed that P (blue) element was homogeneously added to the structure of phosphorylated functional cellulose, as well as C (red) and O (green) elements, coming from the structure of pristine cellulose. The presence and distribution of the P element at the scanned point indicates that the functional group is homogeneously located throughout the material. In addition, the weight percentages of atoms (37.98% C, 52.58% O, and 9.44% P) from the elemental analysis with EDX showed that functionalization was also successful.

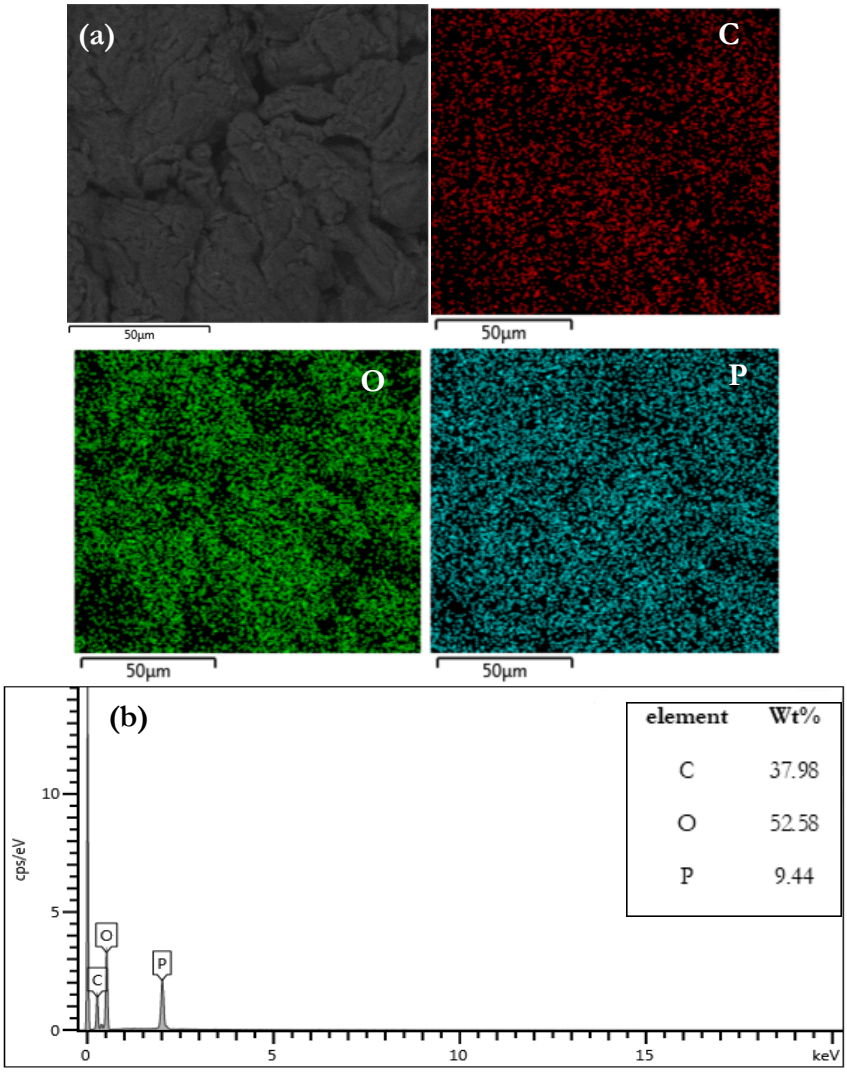

Figure 2.4. **(a)** C, O and P elemental mapping for phosphorylated cellulose; **(b)** EDX results

The FTIR spectra of pristine cellulose and phosphorylated functional cellulose-based adsorbent synthesized in this research are given in Figure 2.5 to compare the changes in the structure. In the literature, it is known that compounds containing P–OH group have a medium to strong wide band at 1040–910 cm^{-1} due to the P–O stretching vibration. Therefore, the wavenumber seen around 1028 cm^{-1} indicates the presence of the P–O bond. The band of P–O–P symmetric stretching vibrations is manifested in the interval 780–850 cm^{-1}, so that the peak around 827 cm^{-1} verified the existence of this structure. However, the peak around 914 cm^{-1} showed the bands of P–O–P antisymmetric stretching vibrations. It is also known that there is a strong P=O bonds in the range of 1350–1150 cm^{-1}. The peak at ca. 1242 cm^{-1} is attributed to the presence of this structure. The 1402 cm^{-1} peak shows the presence of weak –OH acid group. Moreover, in the range 3200–3600 cm^{-1}, the OH stretching vibration band became more asymmetric owing to the introduction of more acidic OH groups of phosphoric acids into the polymer (Luneva and Ezovitova, 2014; Socrates, 2004). Hence, these peaks clearly revealed that the phosphorylated functional adsorbent has been successfully synthesized.

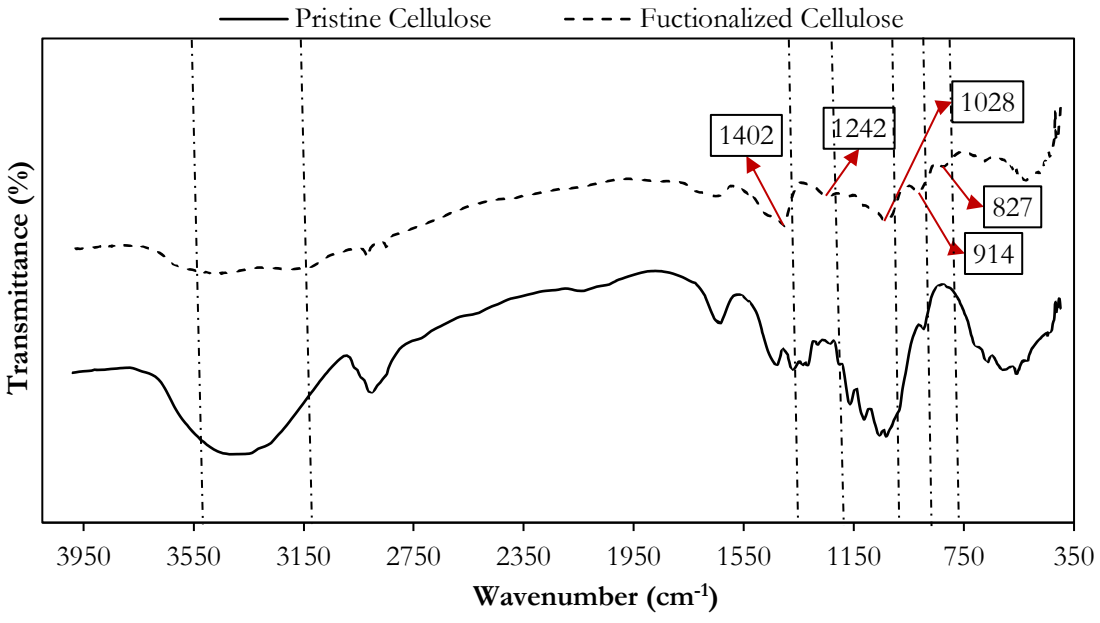

Figure 2.5. FT-IR spectra of pristine cellulose and phosphorylated cellulose

Figure 2.6 shows the thermogravimetric analysis (TGA) thermograms and differential weight loss thermograms (DTG) for pristine cellulose and phosphorylated functional cellulose. A minor weight loss of 1.32% around 100°C in the graph of pristine

cellulose could be attributed to the loss of adsorbed and bound water molecules. On the other hand, the major weight loss was 74.4% due to the decomposition of glycosidic bonds (C–O–C) at about 368ºC. At the final decomposition temperature, *i.e.,* 1000ºC, only 11.67 wt% of char remained. Compared to the unmodified pristine cellulose, the presence of phosphorus in the functional cellulose caused earlier dehydration of cellulose into char formation and a strong reduction in the decomposition temperature of cellulose. The 3.6% weight loss of functional cellulose at about 100ºC could be attributed to water molecules adsorbed by binding, as in the case of pristine cellulose. The initial weight loss thereafter was at around 200–250ºC, and it is evident that the phosphoryl groups have increased the thermal decomposition reaction of the cellulosic polymer (and consequently the heat resistance of the material is reduced), but the carbonization (and hence flame resistance) has significantly increased instead. The weight loss of 38.1% at a temperature of about 870ºC indicates that the phosphorous functional group was decomposed, and it is known in the literature that cellulosic materials containing phosphoryl compounds have flame retardant properties (Aoki and Nishio, 2010). At the final decomposition temperature of the functional cellulose (1000ºC), 55.4% by weight remained.

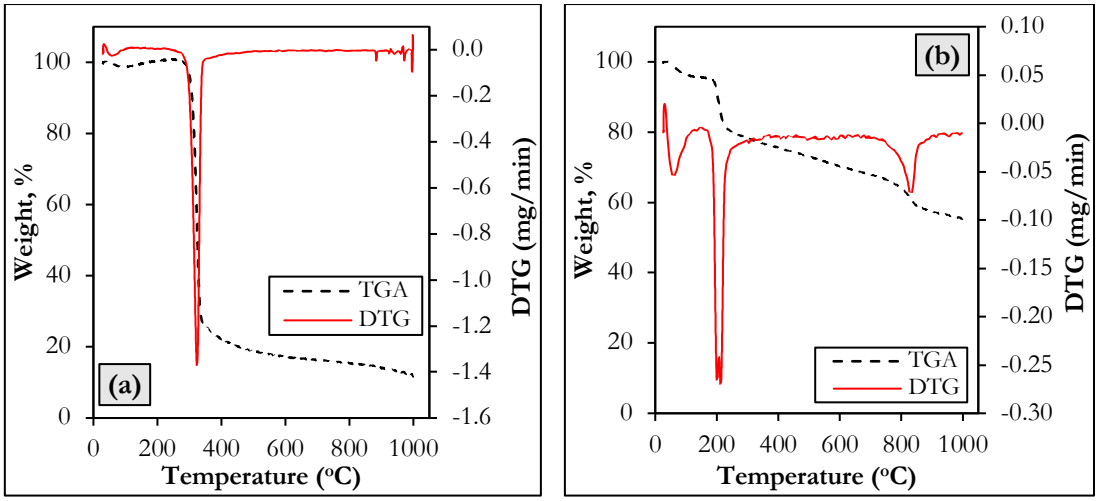

Figure 2.6. TGA and DTG thermograms of **(a)** pristine cellulose, **(b)** phosphorylated functional cellulose.

Figure 2.7 illustrates analyses of survey scan, including the main atoms labelled on it. Since cellulose is a large molecule, C 1s and O 1s spectra were deconvoluted into several peaks. The peak at 134.21 eV, suggesting the new bond involving the atom P, was observed for phosphorylated functional cellulose, in contrast to pristine cellulose.

Estimating the local surface compositions of phosphorylated functional cellulose and the interactions of functional groups with loaded lithium is of high interest for understanding the origins of its interesting separation property. Because the surface heterogeneities related to functionalized cellulose show little to no long-range structural order, diffraction-based techniques are generally not able to distinguish and identify surface functional groups. By comparison, analyses of survey-scan (Figure 2.7) of lithium-loaded adsorbent enable near-surface elemental compositions of C, O, P, and Li moieties to be determined. Detailed XPS information of pristine cellulose, phosphorylated functional cellulose, and lithium loaded phosphorylated functional cellulose can be found in supplementary information for chapter 2 in Table B.1.

There are no lithium secondary peaks to assist in confirmation and the Li 1s peak has very low sensitivity. Therefore, it was difficult to confidently assign the Li 1s peak to low concentrations. Many scans (50) were needed to acquire the Li 1s spectrum. In a survey scan XPS spectrum of lithium loaded adsorbent, the signals at 287, 533, 134, and 55 eV are attributed to the binding energies of C 1s, O 1s, P 2p and Li 1s electrons, which can be better determined by the high resolution XPS spectra depicted in Figure 2.8. Spectral deconvolution of these signals yields near-surface elemental compositions of C, O, P, and Li atoms, which were 43.63, 43.32, 6.63 and 6.41 atom %, respectively.

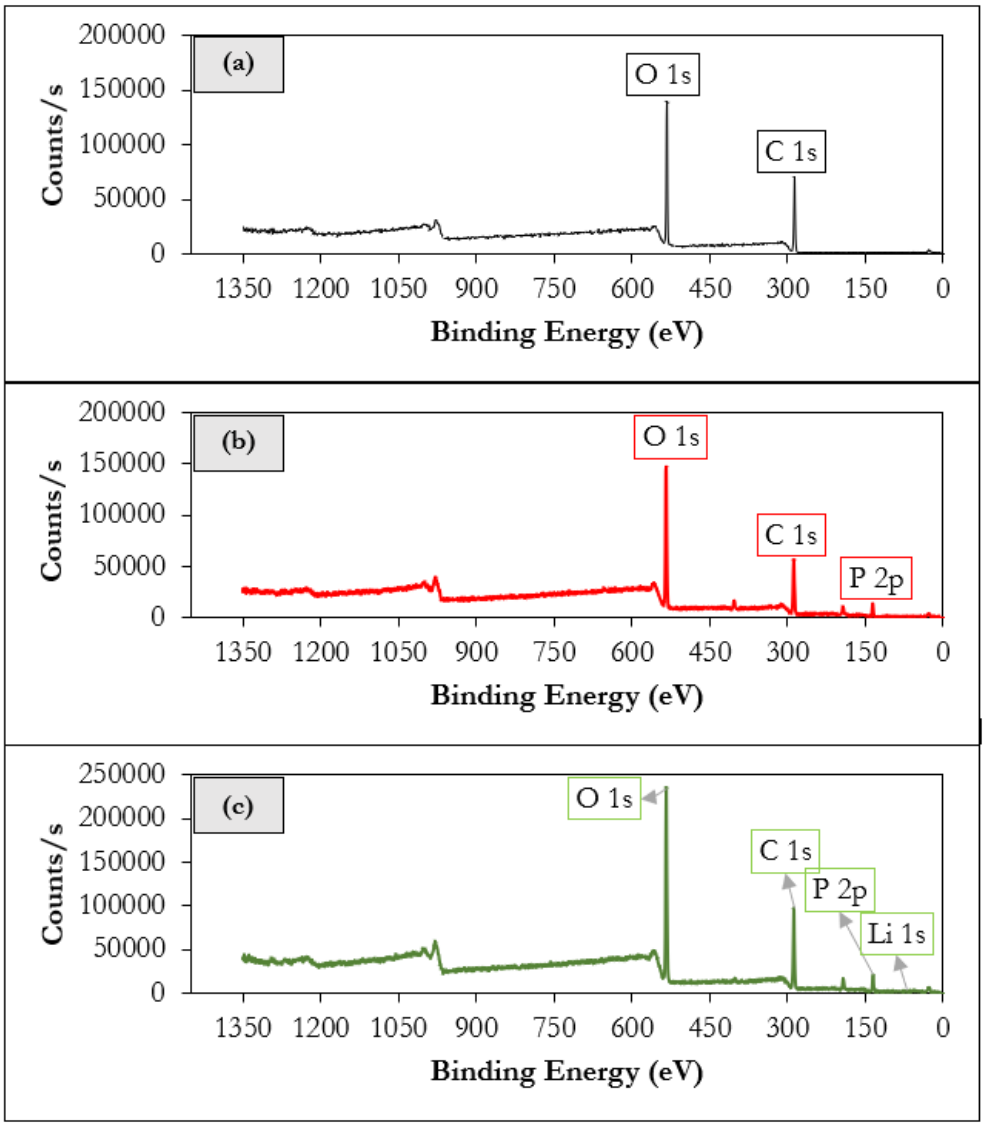

Figure 2.7. Analyses of survey scan for **(a)** pristine, **(b)** phosphorylated functional, and **(c)** lithium-loaded phosphorylated functional cellulose.

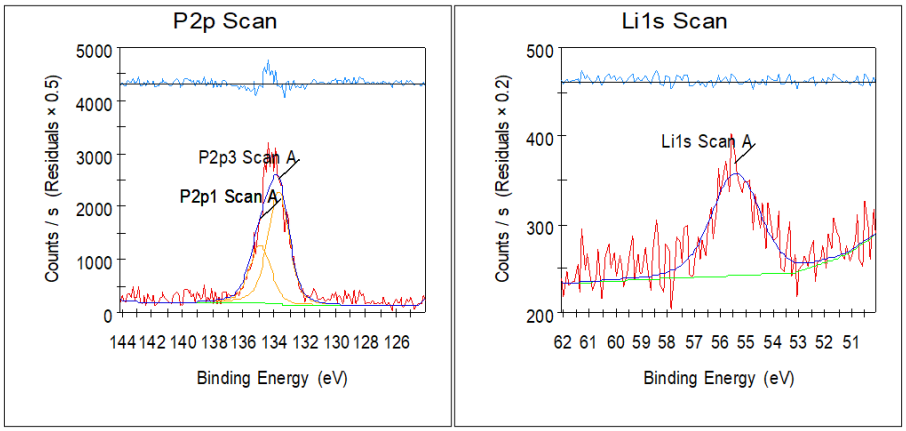

Figure 2.8. High-resolution XPS spectra acquired at room temperature for a lithium-loaded phosphorylated functional cellulose with binding energies (BE, eV) that correspond to P 2p and Li 1s electrons.

According to the crosslinking structure of phosphorylated cellulose and its combined stoichiometry (Figure 2.1), a P/Li atom ratio of approximately 1.03 obtained from XPS measurements is consistent with structure, indicating the presence of these phosphorous moieties on the adsorbent surfaces because one Li^+ is exchanged with H^+ in the functional group and the expected ion exchange mechanism is given in Equation (2.13):

$$Cellulose-O-\underset{\underset{OH^+}{|}}{\overset{\overset{O}{||}}{P}}-Cellulose+Li^+ \leftrightarrow Cellulose-O-\underset{\underset{OLi^+}{|}}{\overset{\overset{O}{||}}{P}}-Cellulose+H^+ \qquad (2.13)$$

2.4.2. Adsorption Studies

2.4.2.1. Effect of Adsorbent Dosage

The adsorbent dosage is an important parameter to estimate the required amount of adsorbent for a specified initial concentration of adsorbate (Ulatowska et al., 2019). The effect of adsorbent dosage on the lithium recovery by phosphorylated functional cellulose is shown in Figure 2.9. The adsorbent dosage varied from 4.0 to 20.0 g L^{-1}. The results showed that the lithium percentage separation increased with increasing adsorbent dosage due to increasing availability of the functional sites.

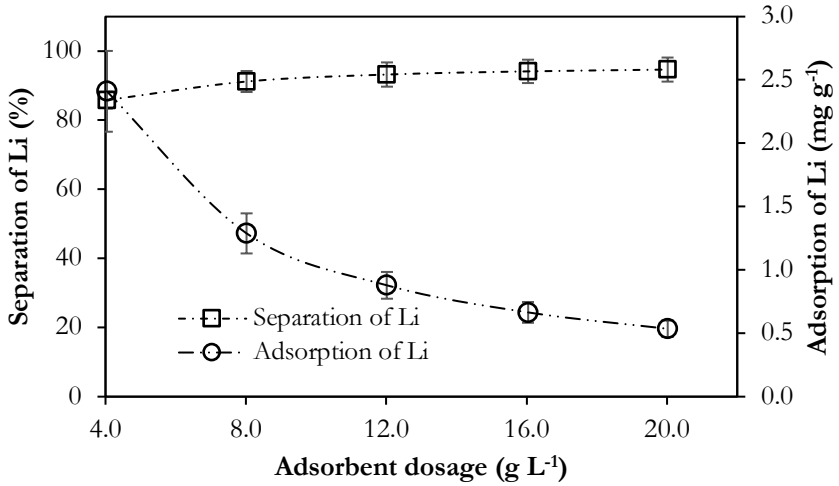

Figure 2.9. Dependence of lithium adsorption on the amount of adsorbent (C_0=10 mg/L, T=25°C, and pH=5 – 6)

The maximum static adsorption of lithium onto phosphorylated functional cellulose was achieved for an adsorbent-to-solution ratio of 4.0 g L^{-1} and was found to be ca. 2.50 mg g^{-1} for 10 mg L^{-1} of initial solution concentration. The optimum adsorbent dosage of 12.0 g L^{-1} was obtained for ca. 94% of lithium separation, in which above 12.0 g L^{-1} adsorbent dosage, the sorption equilibrium for lithium was reached and no further considerable increase was observed beyond this point as maximum removal was achieved. Therefore, the adsorbent dosage of 12.0 g L^{-1} was chosen for subsequent experiments.

2.4.2.2. Effect of pH

pH plays a significant role in the adsorption of any substance depending on both the chemistry of adsorbate and the functional group attached to the matrix. The adsorbent in the present work contains phosphoric acid group, which is triprotic, meaning that it has three acidic protons available to donate, with *pKa* values of 2.16, 7.21 and 12.32, respectively. The separation of lithium from aqueous solution with pH ranging from 2 to 6 by adsorption onto phosphorylated functional cellulose is illustrated in Figure 2.10. Relatively less separation was observed at pH 2 as expected. However, as the initial pH increased up to 6, the separation efficiency of lithium reached about 90% under specified conditions. As the effect of pH on the separation of lithium from aqueous solution by phosphorylated functional cellulose in the investigated pH range was minor, the sorption studies have been performed in the pH range of 5 – 6, which is the original pH of LiCl solution.

Beyond the initial pH of 2, the final pH values were found as ca. 6.6 for all other initial pH (3, 4, 5, 6 and even 8, despite not being reported.) For better understanding the effect of pH on the adsorption of lithium by phosphorylated cellulose, the point of zero charge (PZC) value of this adsorbent was also determined as 6.75, meaning that the adsorbent's surface was positively charged at a solution pH below 6.75 (see Figure B.4). This causes competition between protons and lithium ions for adsorption locations, as well as the repulsion of lithium ions, resulting in the reduction of lithium adsorption. The lower the pH goes below pH_{PZC}, the greater the density of positive ions on the surface of phosphorylated cellulose will be, which in turn allows for less adsorption. This is confirmed by low lithium separation at a highly acidic pH of 2.

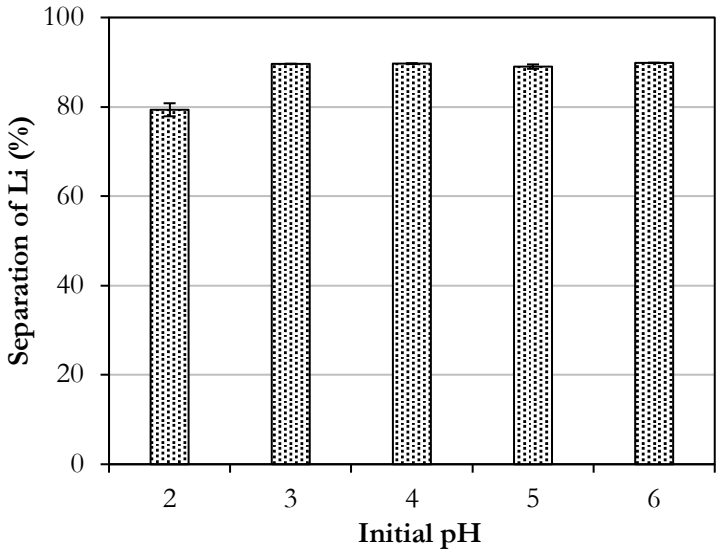

Figure 2.10. Effect of pH on the separation of lithium from aqueous solution by phosphorylated functional cellulose (C_0=10 mg L^{-1}, T=25°C and adsorbent dosage=12 g L^{-1}).

2.4.2.3. Effect of Common Ions

Other cations, such as Na^+ and K^+, present in the aqueous solution can compete with Li^+ for the same adsorption sites, obviously the coexistence of other ions inhibits the lithium adsorption and decreases the adsorption capacity. The effect of common ions is illustrated in Figure 2.11. Although the simultaneous presence of other cations in the solution reduced slightly the separation efficiency of Li from 94% to 87%, compared to the efficiency achieved in the solution with only lithium under the same conditions, the overall adsorption capacity of the phosphorylated functional cellulose was improved. This phenomenon is due to a shift in the equilibrium towards the formation of the adsorbent-adsorbate complex with increasing concentration of the adsorbate.

Selectivity coefficients were calculated as follows (Helfferich, 1962):

$$\alpha_A^B = \frac{[A]^a}{[B]^b}\frac{[\bar{B}]^b}{[\bar{A}]^a} \qquad (2.14)$$

where brackets stand for concentrations in both liquid and solid phases, and the bar indicates the solid phase; α is the selectivity coefficient of B^+ over A^+ for the ion exchange reaction, and a and b are the valency of the ions.

Selectivity coefficients, α_{Li}^{Na} and α_{Li}^{K} of phosphorylated functional cellulose were

calculated as 0.43 and 0.61, respectively. Since those values are smaller than unity, among mono-valent ions, it can be said that the synthesized adsorbent has more affinity towards lithium.

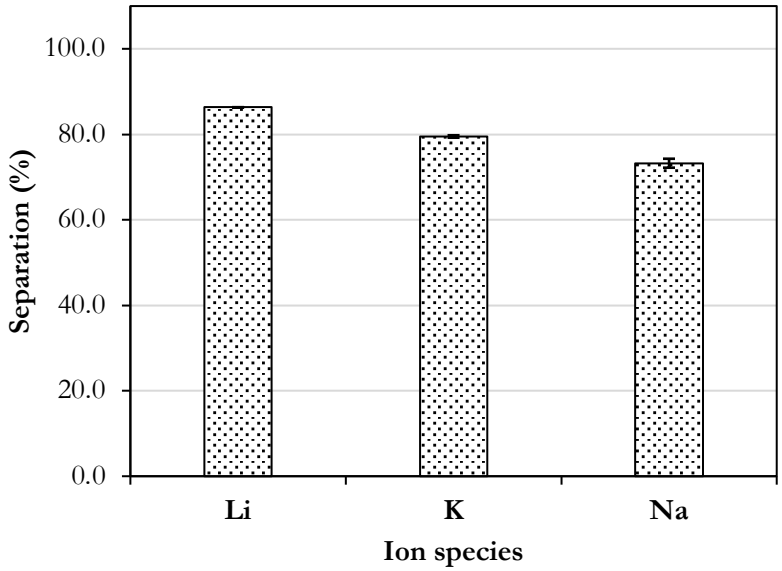

Figure 2.11. Separation efficiencies of coexisting ions by phosphorylated functional cellulose (C_0=10 mg/L for each ion, T=25°C, and adsorbent dosage=12 g/L).

2.4.2.4. Effect of Initial Concentration and Temperature

The effects of the initial lithium concentration and temperature on the uptake of lithium onto phosphorylated functional cellulose are depicted in Figure 2.12. An increase in initial concentration resulted in a corresponding increase in adsorption of lithium on the adsorbent. The rise in adsorption capacity with initial concentration can be conducted with the rise in the possibility of collisions between the adsorbent and the adsorbate. The phenomenon is due to the acceleration of an original driving force, *i.e.*, concentration (basically chemical potential) difference, which may lead to enhanced adsorption. As temperature increased, the adsorption of lithium on phosphorylated functional cellulose decreased. This behavior indicates that the adsorption of lithium onto this adsorbent is an exothermic process, so that higher temperature will worsen the affinity of lithium ions to be adsorbed on the active sites of the adsorbent, as confirmed by the negative value of adsorption energy obtained from Van't Hoff's equation.

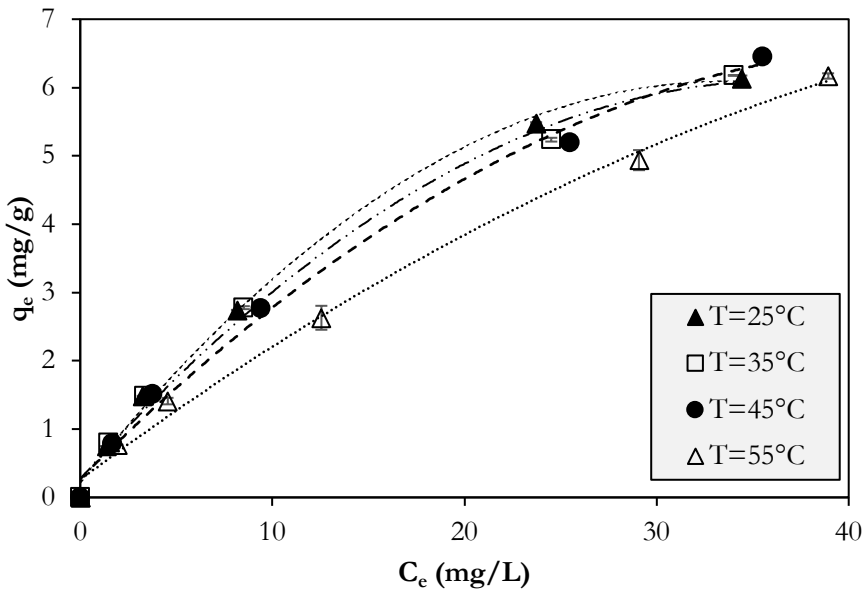

Figure 2.12. Adsorption isotherms of lithium at various temperatures using phosphorylated functional cellulose.

It is important to establish the most suitable correlation for the equilibrium curves to optimize the design of an adsorption system (Yilmaz Ipek, 2014). Several isotherm models, such as Freundlich, Halsey, Langmuir, Redlich–Peterson and Temkin models, were used to describe the adsorption behavior and adsorption process of phosphorylated functional cellulose at various temperatures. Non-linear regression technique was applied by MATLAB® software to determine the parameters and adequacy of these models. All the correlation coefficients, R^2, sum of squares of error (SSE) and the constants obtained for the models are tabulated in Table 2.1.

Although it was difficult to distinguish, at moderately lower temperatures (*i.e.*, 25ºC and 35ºC), the experimental data agreed better with the Langmuir isotherm, with a relatively higher R^2 value of 0.997 and lower SSE value of 0.021. However, as the temperature increased to 45ºC and 55ºC, the adsorption behavior fitted better to the Freundlich isotherm model, according to the higher R^2 of 0.999 and quite lower SSE ranging between 3.91×10^{-3} – 0.0784.

Based on the Langmuir model assumption, monolayer maximum adsorption capacities (Q_{max}) were determined as 9.60, 9.95, 11.26 and 12.60 mg/mg at 25, 35, 45 and 55ºC, respectively. As the temperature increased, the Langmuir constant (K_L) related to the affinity of binding sites decreased. All the dimensionless separation factors (R_L) calculated for phosphorylated functional cellulose at various temperatures and initial

lithium concentration were between 0 and 1, indicating the shape of the isotherm as favorable for lithium adsorption. For example, as the initial concentration increased from 10 to 100 mg L^{-1}, the R_L values decreased from 0.645 to 0.149 and from 0.746 to 0.225 at 25 and 55°C, respectively. These results revealed that adsorption was more favorable at higher concentration and lower temperature.

Table 2.1. Various isotherm model constants and correlation coefficients for adsorption of lithium on prepared phosphorylated cellulose at 25, 35, 45 and 55°C

	25°C	35°C	45°C	55°C
			Langmuir	
Q_{max}	9.60 mg/g	9.95 mg/g	11.26 mg/g	12.60 mg/g
K_L	0.0529 L/mg	0.0466 L/mg	0.0359 L/mg	0.0305 L/mg
R^2	0.997	0.997	0.995	0.993
SSE	0.0210	0.0230	0.0361	0.0630
			Freundlich	
$^*K_F$	0.7728	0.7124	0.6276	0.4498
n	1.6753	1.6216	1.5311	1.4026
R^2	0.990	0.998	0.999	0.999
SSE	0.0784	0.0120	3.91×10^{-3}	8.05×10^{-3}
			Temkin	
A	0.856 L/mg	0.821 L/mg	0.6942 L/mg	0.5868 L/mg
B	1.7426	1.732	1.8425	1.7559
b_T	1.422 kJ/mol	1.479 kJ/mol	1.436 kJ/mol	1.554 kJ/mol
R^2	0.963	0.959	0.952	0.923
SSE	0.2809	0.2980	0.3700	0.5450
			Redlich-Peterson	
K_{RP}	0.505 L/mg	0.834 L/mg	1.1216 L/mg	
α	0.0523 $(L/mg)^{\beta}$	0.254 $(L/mg)^{\beta}$	1.0296 $(L/mg)^{\beta}$	
β	1	0.591	0.458	Not determined
R^2	0.997	1.000	1.000	
SSE	0.0310	2.73×10^{-3}	2.02×10^{-3}	
			Halsey	
K_H	1.5399 L/g	1.733 L/g	2.0408 L/g	3.067 L/g
n_H	-1.6753	-1.6216	-1.5311	-1.4026
R^2	0.990	0.998	0.999	0.999
SSE	0.0784	0.0120	3.91×10^{-3}	8.05×10^{-3}

*The unit of K_F is $mg/g\ (L/mg)^{1/n}$

The Freundlich isotherm was used for encompassing the exponential distribution of active sites and their energies and the surface heterogeneity (Jamil et al., 2011). The value of K_F, which is a constant related to temperature and a measure for adsorption

capacity, decreased from 0.7728 to 0.4498 as the temperature increased. Besides, a decrease in n values from 1.6753 to 1.4026 with the temperature increase suggests a decreasing trend of the adsorption intensity. Because the rise in temperature caused a rise in the kinetic energy of lithium ions in the solution, hence, there occurred sharper competitions for the limited adsorption sites and strong repulsions among the lithium ions resulted in a decrease of adsorption intensity. The magnitude of the exponent n also verifies the favorability of adsorption. The results show that lithium is favorably adsorbed by the phosphorylated functional cellulose due to the values of n being greater than unity at all temperatures, which is in great agreement with the findings regarding to the R_L values.

Despite having relatively lower R^2 values, the Temkin model indicated that positive values of b_T (1.422, 1.479, 1.436 and 1.554 kJ/mol) for all temperatures correspond to exothermic adsorption of lithium onto phosphorylated cellulose, where $b_T = \Delta Q = -\Delta H$. Given that those values are all less than 8 kJ/mol, the interactions between the adsorbate and the adsorbent are weak and therefore the adsorption mechanism taking place here is merely that of ion exchange (Ghogomu, 2013).

At 25°C, the R-P model transformed into the Langmuir isotherm, since β was found to be exactly 1. However, as the temperature increased, the value of β decreased and lied between 0 and 1. Lower β values mean their isotherm curves are milder than those of the Langmuir isotherm equation (Wu et al., 2010), as can be seen in Figure 2.12.

The Halsey isotherm is valid for multilayer adsorption and the fitting of the experimental data to this model attest the heteroporous nature of the adsorbent (Ayawei et al., 2017). The high correlation coefficients for this model can be attributed to the heteroporous nature of phosphorylated cellulose, parallel to fitting more the Freundlich isotherm.

2.4.3. Adsorption Thermodynamics

The thermodynamic parameters for phosphorylated functional cellulose at 298, 308, 318 and 328 K are listed in Table 2.2, indicating the effect of the temperature on the adsorption process. The negative values of ΔG^o at all temperatures show that the adsorption of lithium onto the adsorbent was spontaneous and thermodynamically favorable, indicating increased randomness at the adsorbent-solution interface during the

diffusion of the lithium on the functional groups of the cellulose. Therefore, the adsorbates have the tendency to stay in the stationary phase rather than in the mobile phase. The values of ΔH^o and ΔS^o were obtained from the slope and the intercept of the linear plot of lnK_e *vs.* $1/T$ respectively, as in Figure 2.13. ΔH^o was found to be -15.532 kJ/mol and the negative value verified the exothermic nature of adsorption, which was also supported by the result that the adsorption of lithium decreased with the increase in temperature. The absolute value of ΔH^o less than 40 kJ/mol (Yilmaz Ipek, 2014) showed that there is an ionic interaction between the phosphate moiety and the Li ion. A negative value of ΔS^o was attributed to a decrease in randomness at the solid-liquid interface during the adsorption of lithium.

Table 2.2. Thermodynamic parameters for adsorption of lithium on phosphorylated functional cellulose

T(K)	$\Delta G°$ (kJ/mol)	ΔH° (kJ/mol)	ΔS° (J/mol.K)
298	-14.640	-15.532	-2.776
308	-14.806		
318	-14.596		
328	-14.610		

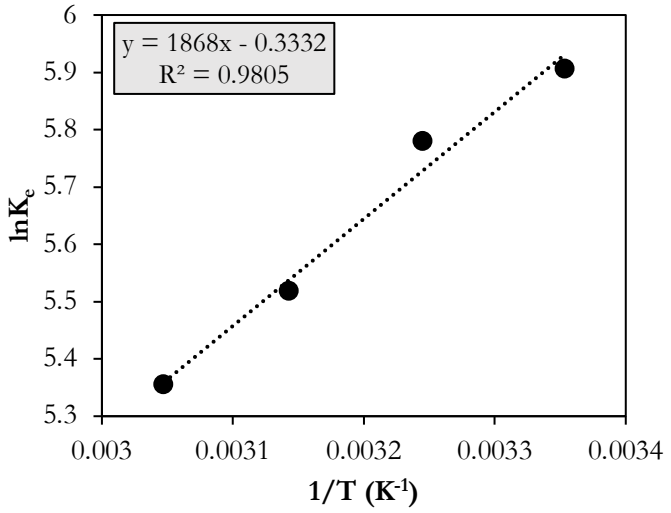

Figure 2.13. Plot of lnK_e vs. $1/T$ for the sorption of lithium on phosphorylated functional cellulose.

2.4.4. Adsorption Kinetics

Adsorption kinetic is useful to describe the rate of lithium uptake on the phosphorylated functional cellulose, which reveals the equilibrium time by means of the effect of contact time. The adsorption kinetic behavior of this adsorbent at various adsorbent dosage is depicted in Figure 2.14. The adsorption rate was found to be quite rapid initially, immediately slowing down and then reaching the equilibrium for lithium adsorption onto this adsorbent. 80% of lithium adsorption within 3 minutes with 5 g/L of adsorbent dosage proved the quite fast kinetic nature of the adsorbent. Therefore, the adsorption kinetics analysis by some empirical kinetic models, such as pseudo-first order, pseudo-second order, intraparticle diffusion or Elovich model, could not be done because of difficulties in sampling less than 1 minute. Hence, observable data could not be collected to find the related rate constants or rate determining step proposed by Weber and Morris (Weber and Morris, 1963).

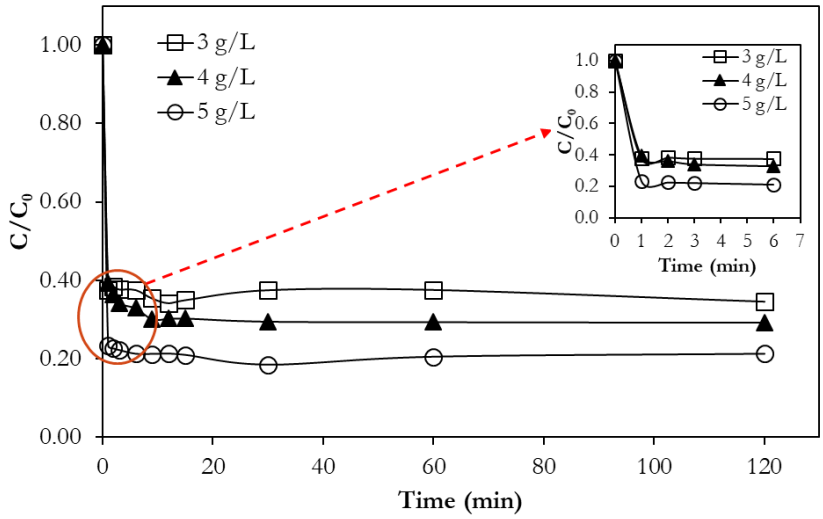

Figure 2.14. Effect of adsorbent dosage on adsorption kinetics using phosphorylated functional cellulose.

2.4.5. Desorption of Lithium and Regeneration of the Adsorbent

Desorption of Li from phosphorylated functional cellulose using HCl, NaCl and H_2SO_4 at different concentrations (0.5–2.0 M) is shown in Figure 2.15. The lowest

desorption efficiency was observed as ca. 76% when 2.0 M NaCl solution was used, whereas a 99.5% desorption efficiency of lithium was achieved with 0.5 M H_2SO_4. On the other hand, the desorption of lithium was almost in close proximity and above 90% at all concentrations of HCl. These results indicated that elution of lithium and the regeneration of the adsorbent can be easily done using acid solutions, especially with low concentration diprotic acids.

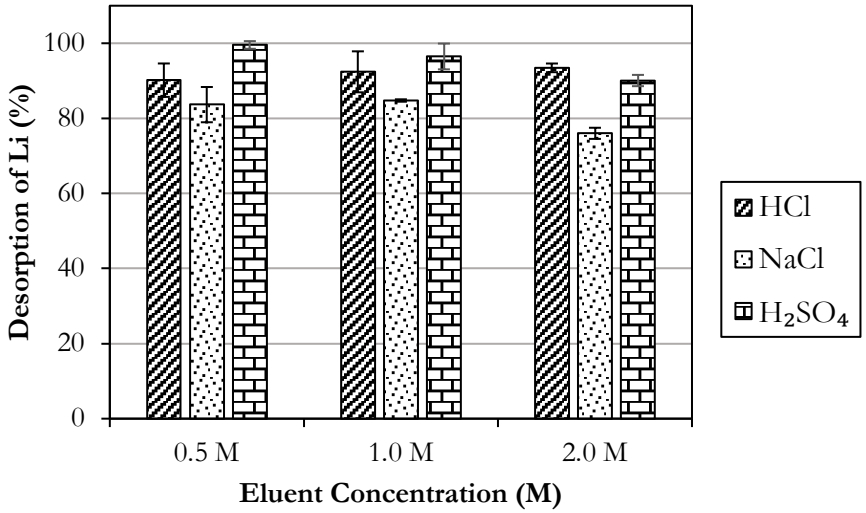

Figure 2.15. Desorption of Li from phosphorylated functional cellulose using different eluents at different concentrations.

2.5. Conclusion

The present study showed that the synthesized cellulose-based phosphorylated functional material is a promising low-cost adsorbent to be utilized in the recovery of lithium from aqueous solutions. The adsorbent was synthesized by the reaction of cellulose with phosphorus acid in molten urea and characterized by SEM, EDX, FTIR, TGA and XPS to confirm its functionality. The results for the adsorption behavior of lithium on phosphorylated functional cellulose showed that the optimum adsorbent dosage to recover lithium from an initial concentration of 10 mg L^{-1} was 12.0 g adsorbent/L-solution, with a removal efficiency of ca. 94%. There was no considerable influence of pH on the adsorption of lithium over the pH range studied. The simultaneous presence of other cations, such as Na^+ and K^+, in the solution reduced slightly the

separation efficiency of Li from 94% to 87%, compared to the efficiency in the solution with only lithium under the same conditions. However, the adsorbent exhibited higher affinity towards lithium among others. The adsorption of lithium was found to increase with increasing initial concentration, but it decreased as the temperature increased due to the exothermic nature of lithium adsorption on this adsorbent.

A few isotherm models were applied. The results indicated that the adsorption isotherm models fitted the data in the order: Langmuir≈Freundlich>Halsey>Redlich-Peterson>Temkin. The maximum lithium uptake capacity was estimated as 9.60 mg g^{-1} at 25^{o}C, which was higher than that of magnetic lithium-ion imprinted polymer (4.07 mg g^{-1}) (Luo et al., 2015) and ion-sieve manganese oxide (8.5 mg g^{-1}) (Miyai et al., 1988), but comparable with commercially available Lewatit TP 260 resin (13.65 mg g^{-1}) (Çiçek et al., 2018). Thermodynamic analysis revealed that the adsorption of lithium on phosphorylated functional cellulose was spontaneous, exothermic, and with the tendency of decreased randomness. The kinetics of Li separation is quite fast and in three minutes it reached equilibrium. Moreover, the Li loaded phosphorylated functional cellulose can be easily regenerated with 0.5 M H_2SO_4 solution and the spent solution can be further evaporated to recover lithium from it.

As future perspective, the output of the study provided an insight into the possibility of obtaining promising low-cost adsorbents from various lignocellulosic biomass wastes, which may have high cellulose content, and opens the way to lithium recovery from real water sources, such as geothermal water.

CHAPTER 3

PHOSPHORYLATED HAZELNUT SHELL WASTE FOR SUSTAINABLE LITHIUM RECOVERY APPLICATION AS BIOSORBENT*, †

3.1. Introduction

A million tons of waste and by-products are produced by modern agricultural facilities every year that have potential as useful resources (Sarker et al., 2017). These agro-industrial residues obtained from harvesting and industrial processing of agricultural crops can be a promising alternative to traditional adsorbents, since they are readily available, cheap, highly sorptive and easily modifiable (Ngo et al., 2015). A plenty of agricultural wastes which have lignocellulosic structures such as peanut shell (Witek-Krowiak et al., 2011), walnut shell (Segovia-Sandoval et al., 2018), cotton stalk/wheat stalk (Xu et al., 2011), rice husk (Chuah et al., 2005), orange peels (Romero-Cano et al., 2016), sugar cane bagasse and olive stones (Moubarik and Grimi, 2015) have been extensively modified and used for bioremediation particularly in heavy metal and textile dye removal from water. Recently, hazelnut processing plant wastes, hazelnut shell and hazelnut skin, were used without further chemical modification for the simultaneous removal of multi-elements (Al, As, Cd, Cr, Cu, Fe and Pb) from water (Özlem, 2019).

One of lignocellulosic biomass, hazelnut, is an agricultural product grown in significant quantities in Türkiye due to its climatological and ecological conditions and land property. Therefore, Türkiye is the leader in the production of shelled hazelnuts (*Corylus Avellana L.*) in the world by supplying namely, 70% of the total production (650,000 tons/year), followed by Italy (13%), the USA (4%), Azerbaijan (3%), Spain (3%) and Georgia (3%) in 2017 with a huge gap in terms of the production capacity as

*This chapter has been published as: Y. K. Recepoğlu, A. Yüksel, Phosphorylated Hazelnut Shell Waste for Sustainable Lithium Recovery Application as Biosorbent, Cellulose, 28(15) (2021) 9837-9855.

†The study in this chapter was awarded for the PhD research during Activity B of the 2nd edition of the Mediterranean PhD School on «EUROPEAN GREEN DEAL. THE CONTRIBUTION FROM CIVIL, ARCHITECTURAL AND ENVIRONMENTAL ENGINEERING», University of Naples Federico II, 11-16 October 2021.

shown in the supplementary material for chapter 3 in Figure C.1 (Alasalvar et al., 2009; Guney, 2013). It has been reported that 70 wt% of the product is shell and pruning waste is produced as 2.7 times of the product after harvesting (Alkaya et al., 2010). Although hazelnut shell found use in plywood, linoleum and paint industry in the USA, Italy, and Germany, which have advanced technologies, it is mostly used for heating purposes as hazelnut coals in Türkiye. Currently, hazelnut bark and pruning wastes are used as fuel, while the slag is left in the soil as a fertilizer or directly burned after the harvest (Çöpür et al., 2008; Özlem, 2019; Şenol, 2019). Considering those wastes arising out of high production rate, converting such a large amount of lignocellulosic material into valuable products instead of low value applications is of great importance for our country's economy and environment. Over the last decade, sustainability and green chemistry has been important for the development of the next generation of materials in which the use of bio-based polymer matrices might allow the reduction of environmental impacts by using renewable carbon and by achieving more easily biodegradable or reusable materials (Illy et al., 2015). Among several strategies for the modification of biomass, introduction of phosphorous moieties to bio-based compounds have been widely studied due to their fire resistance, excellent chelating, and metal-adhesion properties. The grafting reaction of phosphorus compounds to cellulose can undergo in several routes: with tervalent (III) or pentavalent (V) phosphorus reagents, by direct or indirect bonding of phosphorus functions to cellulose, using cellulose or cellulose derivatives as substrates, with or without catalysts, in heterogeneous or homogeneous reaction environment, etc. Although phosphorus derivatives such as $POCl_3$, H_3PO_4 and P_2O_5 are the most common phosphorylating agents for pentavalent phosphorus, these reagents, usually leading to anionic cellulose phosphates, show a lower esterification reactivity than the similar derivatives of trivalent phosphorus and cause a higher degradation of the cellulose substrate. This drawback is partially overcome if urea is introduced in the phosphorylation system as a catalyst (Illy et al., 2015; Kokol et al., 2015; Shi et al., 2014). On the other hand, lignocellulosic biomasses are rich in polysaccharides (cellulose and hemicellulose) and lignin. Before going through the modification hemicellulose and lignin should be removed from the lignocellulose that inhibit cellulose utilization in the biomass. A range of chemical, physical, physicochemical, and biological pretreatment techniques have been developed to improve the accessibility to cellulosic fibers in the biomass. Among these methods alkaline pretreatment is widely preferred for the delignification (removal of lignin) of lignocellulosic biomass which enhances the reactivity of the remaining

carbohydrates. NaOH pretreatment of several lignocellulosic materials has been reported to increase the processability of the biomass by decreasing the degree of polymerization, increasing the surface area, and cutting down on lignin content (Hoşgün and Bozan, 2019). Moreover, the NaOH treatment specifically breaks the van der Waals and hydrogen bonds between cellulose molecules and brings about more hydroxy groups to become exposed to H_3PO_4 in the second step of the process that activates hydroxy groups in cellulosic portion of hazelnut shell waste before undergoing phosphorylation reaction (Illy et al., 2015).

The main scope of this chapter is to obtain low cost biosorbent from waste biomass for the recovery of lithium by attaching phosphoric functional groups as lithium is the strategic element of the 21st century. To meet the dramatic rise in the global lithium consumption due to the steep increase in the use of electric vehicles and mobile electronics, the attention has been turned to search for alternative lithium sources (Kim et al., 2019). Because a shortage of lithium is expected soon due to an uneven global distribution of lithium reserves as demand for lithium soars (Grosjean et al., 2012). Biosorption is highly effective in separation of organic and inorganic substances in soluble or insoluble forms from an aqueous solution through the utilization of low-cost biosorbent materials among other methods (Fomina and Gadd, 2014). Most of the studies on lithium recovery from a mixture of diverse cations with high concentrations have been conducted by inorganic adsorbents such as $H_4Mn_5O_{12}$ nanotubes lithium ion sieve (Xu et al., 2019), iron-doped lithium titanium oxides (Wang et al., 2018), titanium type ion sieve (H_xTiO_3) (Wang et al., 2017), λ-MnO_2 (Kitajou et al., 2006; Park et al., 2012; Recepoğlu et al., 2017a, 2018a; Yoshizuka et al., 2002). To our best knowledge, no studies have been found in the literature regarding the synthesis of lithium sorption-capable biosorbents from lignocellulosic wastes. In this context, the reaction of cellulose with phosphorous acid in molten urea by Inagaki et al. (Inagaki et al., 1976) and Suflet et al. (Suflet et al., 2006) were pioneered the synthesis and characterization of phosphorylated hazelnut shell waste. By doing this, hazelnut shell waste, which is a real cellulose resource, cheap, abundant, and easily accessible in Türkiye was evaluated properly by adding a value to a waste and used for the recovery of lithium from aqueous solution simultaneously. Moreover, the spent biosorbent can be converted into a fertilizer under suitable conditions via pyrolysis since it contains phosphorous and nitrogen for further use. In this way, the further use of this bio-sorbent for adsorption-desorption of Li is environmentally friendly and cost-effective.

3.2. Experimental

3.2.1. Materials

Hazelnut shell wastes as biomass used in this study were supplied from Ordu province, Türkiye where hazelnut trees were commonly cultivated. Before using, they were washed extensively with tap water to remove the dust and soil, sprayed with distilled water, and dried in an oven at 60ºC. After that, they were ground into small pieces by a laboratory type grinder and sieved. Samples having particle size range of 150–300 µm were phosphorylated. The characteristics of hazelnut shell as proximate, structural and ultimate analysis identified in the previous study (Gozaydin and Yuksel, 2017) are given in Table C.1.

di-Ammonium hydrogen phosphate, hydrochloric acid (37%), lithium chloride, ortho-phosphoric acid (85%), potassium chloride, sodium chloride, sodium hydroxide, sulfuric acid (95–97%) and urea were purchased from Merck.

3.2.2. Methods

3.2.2.1. Synthesis of the Biosorbent

High alkali treatment of hazelnut shell waste

The procedure applied is given as follows:

(1) 10 g of hazelnut shell waste was added into 10 M NaOH solution (100 mL) and the mixture was stirred at room temperature (25°C) for 2 h.
(2) Then, to precipitate hazelnut shell waste dissolved in the alkali solution, 10 M HCl (100 mL) was added to the mixture.
(3) Next, the mixture was washed with excess water and filtered to remove the alkaline.
(4) Finally, the residue dried at 70°C for 6 h was ground using coffee grinder.

Chemical modification of hazelnut shell waste (Phosphorylation reaction)

Chemical modification of hazelnut shell waste for attaching phosphorous

functional groups to its cellulosic constituents was carried out based on the patent proposed by (Yabusaki, 2010) as follows:

(1) 0.15 mol phosphoric acid, 0.2 mol di-ammonium hydrogen phosphate and 1 mol urea was dissolved in 150 mL water to prepare the phosphorylating chemical solution.

(2) Then, 10 g previously NaOH treated hazelnut shell waste was added into this solution and thoroughly mixed.

(3) Next, the mixture was left at room temperature (25°C) for 1 h before its water content was evaporated and the residue was completely dried at 105°C for 18 h.

(4) After that, the mixture was heated to 150°C and it was left to react at this temperature for 2 h.

(5) Finally, the reaction product was washed with excess water and dried at 70°C for 6 h. The solid product was ground using a coffee grinder to give phosphorylated functional hazelnut shell waste as biosorbent.

The pristine, NaOH treated and phosphorylated functional hazelnut shell waste are shown in Figure 3.1 (a), (b) and (c), respectively.

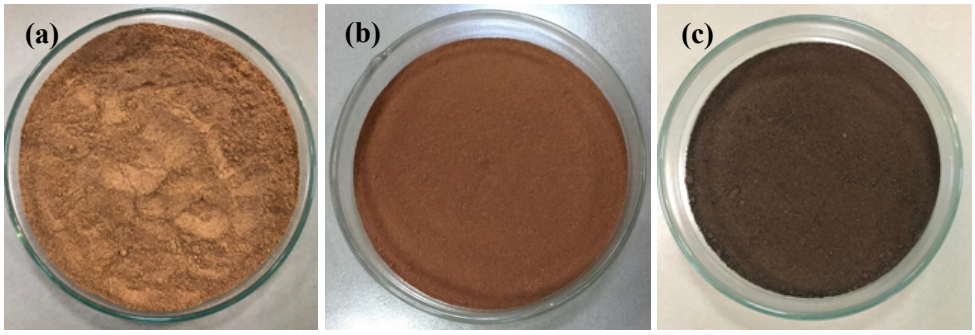

Figure 3.1. **(a)** Pristine hazelnut shell waste, **(b)** NaOH treated hazelnut shell waste and **(c)** phoshorylated functional hazelnut shell waste.

3.2.2.2. Characterization of the Synthesized Biosorbent

The photomicrography was obtained using Scanning Electron Microscopy (Quanta 250 SEM) by coating free surfaces of the materials with thin layers of gold (Emitech K550X) at an accelerating voltage range of 3.0 – 5.0 kV. The chemical compositions of pristine and modified materials were determined by Energy Dispersive

Spectrometer (EDS) combined with SEM.

Fourier Transform Infrared Analysis (FTIR) was conducted on FTIR-8400S spectrophotometer (Shimadzu, Japan) to provide insights into the structure change between pristine and modified hazelnut shell wastes. Infrared spectra were recorded over a wavenumber range from 400 to 4000 cm^{-1}. A total of 24 scans was averaged at a resolution of 4 cm^{-1}.

Quantitative elemental analysis was performed by XPS (Thermo Scientific, Nexsa) having 180° hemispherical analyzer-128 channel detector for C, O, P, N and Li elements based on the change in the bond energies in the molecule. The elements were scanned in the range of 0.0–1350.0 eV using monochromatic Al Kα X-rays (1486.68 eV) with a pass energy of 30 eV and scan number of 3.

The BET surface area, pore size and pore size distribution were measured using a surface area and porosity analyzer (Micromeritics Gemini V) equipped with Micromeritics VacPrep 061 Sample Degas System using N_2-adsorption technique.

XRD measurements were taken with Philips X'Pert Pro equipment using Cu-Kα radiation as X-ray source having generator voltage of 45 kV and tube current of 40 mA. Scanning was done in the range of $10^{o}<2\theta<30^{o}$ with a wavelength of 1.54 A°.

The measurable differences in the heat capacity and thermal stability of pristine and phosphorylated materials were determined by TGA equipment (Setaram). Thermograms were obtained by heating the samples from 30°C to 1000°C in a dynamic heating regime under nitrogen with a constant heating rate of 5°C/min.

3.2.2.3. Lithium Sorption Experiments

The sorbent dosage experiments were performed by mixing various amounts (0.1 – 0.5 g) of phosphorylated hazelnut shell waste with 25 mL of LiCl test solution (Li^+: 10 mg/L) in plastic bottles and shaking in a shaker (Grant OLS200) at 25°C, 180 rpm. To investigate the effects of initial solution concentration and temperature on sorption performance, various initial concentrations, ranging from 10 to 100 mg/L and various temperatures (25°C–45°C) were carried out with a constant mass of phosphorylated functional hazelnut shell waste (0.35 g). In addition, pH effect was studied using 10 mg/L of Li^+ solution having different pH values ranging from 2 to 8. The effect of contact time was observed by sorption kinetics experiment at specified time interval (0–60 min) and

the effect of competitive ions was studied by adding Li^+, K^+, Na^+, Ca^{2+} and Mg^{2+} (10 mg/L) at ambient temperature as well. The corresponding Li^+ and the other ion concentrations were determined using an ICP-OES instrument (Agilent Technologies, 5110). All the experiments were repeated twice, and average values were reported with error bars as standard deviation.

The sorption capacity and recovery percentage of Li were calculated by the following equations, respectively:

$$q_e = \frac{(C_0 - C_e)V}{m} \tag{3.1}$$

$$R = \frac{C_0 - C_e}{C_0} \times 100 \tag{3.2}$$

where q_e is the unit sorption capacity at equilibrium (mg/g), R is the recovery percentage of Li, C_0 and C_e are the initial Li concentration (mg/L) and Li concentration at equilibrium (mg/L), respectively. V is the volume of Li solution (L), and m is the dry weight of biosorbent (g).

Freundlich, Langmuir and Temkin isotherm models were used to analyze the sorption behavior of the synthesized biosorbent. The Langmuir model (Langmuir, 1916) is expressed as follows:

$$q_e = \frac{Q_{max} K_L C_e}{1 + K_L C_e} \tag{3.3}$$

where Q_{max} (mg/g) is the maximum sorption capacity and K_L (L/mg) is the Langmuir constant related to the affinity of the binding sites.

The Freundlich model (Freundlich, 1907) is given as follows:

$$q_e = K_F C_e^{1/n} \tag{3.4}$$

where K_F ((mg/g) $(L/mg)^{1/n}$) and n are Freundlich constants for sorption capacity and sorption intensity of the biosorbent, respectively.

Temkin model (Tempkin and Pyzhev, 1940) is described as follows:

$$q_e = (RT/b_T) ln(AC_e) \tag{3.5}$$

where $B = RT/b_T$, which is the Temkin constant related to heat of sorption whereas A

(L/mg) is the equilibrium binding constant related to the maximum binding energy. R (8.314 J/mol K) is the universal gas constant and T (K) is the absolute solution temperature.

3.2.2.4. Desorption and Regeneration of the Phosphorylated Functional Hazelnut Shell Waste

Li was desorbed from saturated biosorbent by sorption experiment via 100 mg L^{-1} Li^{+} and 12 g/L biosorbent dosage using 0.25 M, 0.5 M, and 1.0 M of NaCl, HCl and H_2SO_4 as eluents. After regeneration, concentrated Li can be recovered by evaporation of spent solution in Li salt forms and further purification steps can be considered.

3.3. Results and Discussion

3.3.1. Characteristics of the Biosorbent

3.3.1.1. SEM and EDS Analysis

The surface morphologies of the samples at 5,000 times magnification are shown in Figure 3.2. While the surfaces of both pristine hazelnut shell waste (Figure 3.2(a)) and NaOH treated one (Figure 3.2(b)) in powdery form were smoother with less burrs on the surface, the surface of phosphorylated hazelnut shell (Figure 3.2(c)) became folded and rough that can be attributed to the phosphorylation reaction of active hydroxy groups in pristine hazelnut shell waste. In addition, several small particles seen on the surface of phosphorylated hazelnut shell waste and between layers suggested that the phosphoric functional group associated with the pristine material successfully. Furthermore, spots appeared on phosphorylated hazelnut shell confirmed its specific surface area having active biosorption sites for Li to be attached from aqueous solutions. Figure 3.2(d) was the apparent morphology of Li-loaded phosphorylated hazelnut shell waste. Compared with phosphorylated hazelnut shell waste before biosorption, the surface of its Li-loaded form had more irregularity and the fibrous structure was more obvious. That could be

explained by the fact that H^+ ions in the phoshporous functional group were exchanged by Li^+ ions in the aqueous solution hence reductive spots have appeared on Li-loaded phosphorylated hazelnut shell waste in acid medium. This difference can also be clearly distinguished in SEM images at 10,000 times maginification given in Figure 3.3.

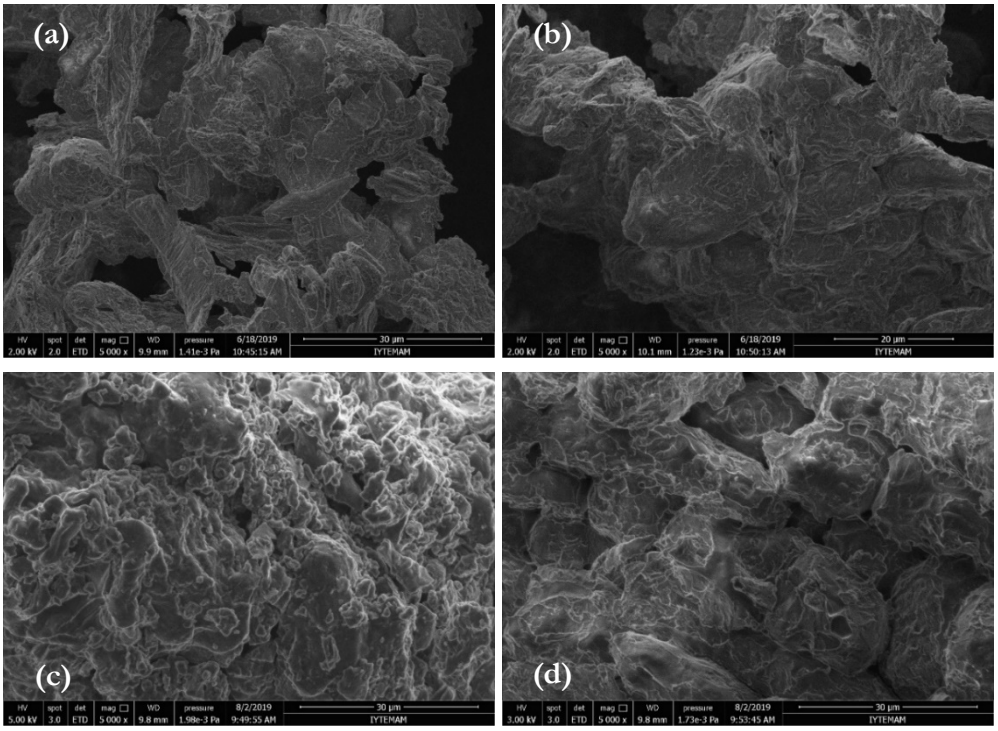

Figure 3.2. SEM surface morphology (magnification 5,000x): **(a)** pristine hazelnut shell waste, **(b)** NaOH treated hazelnut shell waste, **(c)** phosphorylated hazelnut shell waste and **(d)** lithium-loaded phosphorylated hazelnut shell waste

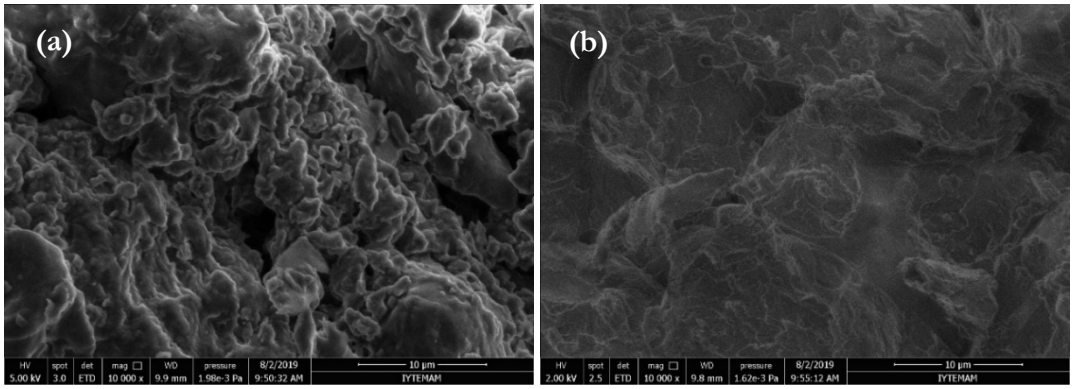

Figure 3.3. SEM surface morphology (magnification 10,000x): **(a)** Phoshorylated hazelnut shell waste, **(b)** Li-loaded phoshorylated functional hazelnut shell waste

Elemental mapping and energy dispersive spectra of phosphorylated hazelnut shell waste are shown in Figure 3.4(a) and 3.4(b), respectively. Highly exposed phosphoric functional group were well distributed in the cellulosic portion of the hazelnut shell waste as revealed by P EDS map. The peaks pertained to phosphorylated hazelnut shell waste regarding precise elemental composition of its surface from EDS analysis gives C (41.98 wt%), O (40.70 wt%), N (11.66 wt%) and P (5.67 wt%). Although carbon, oxygen and nitrogen contribute most to the elemental composition of the synthesized biosorbent, which is attributed to the organic nature of lignocellulosic residues, the considerable presence of phoshorous element suggests that the high exposure of phosporic groups on the surface of the cellulosic portion of hazelnut shell waste.

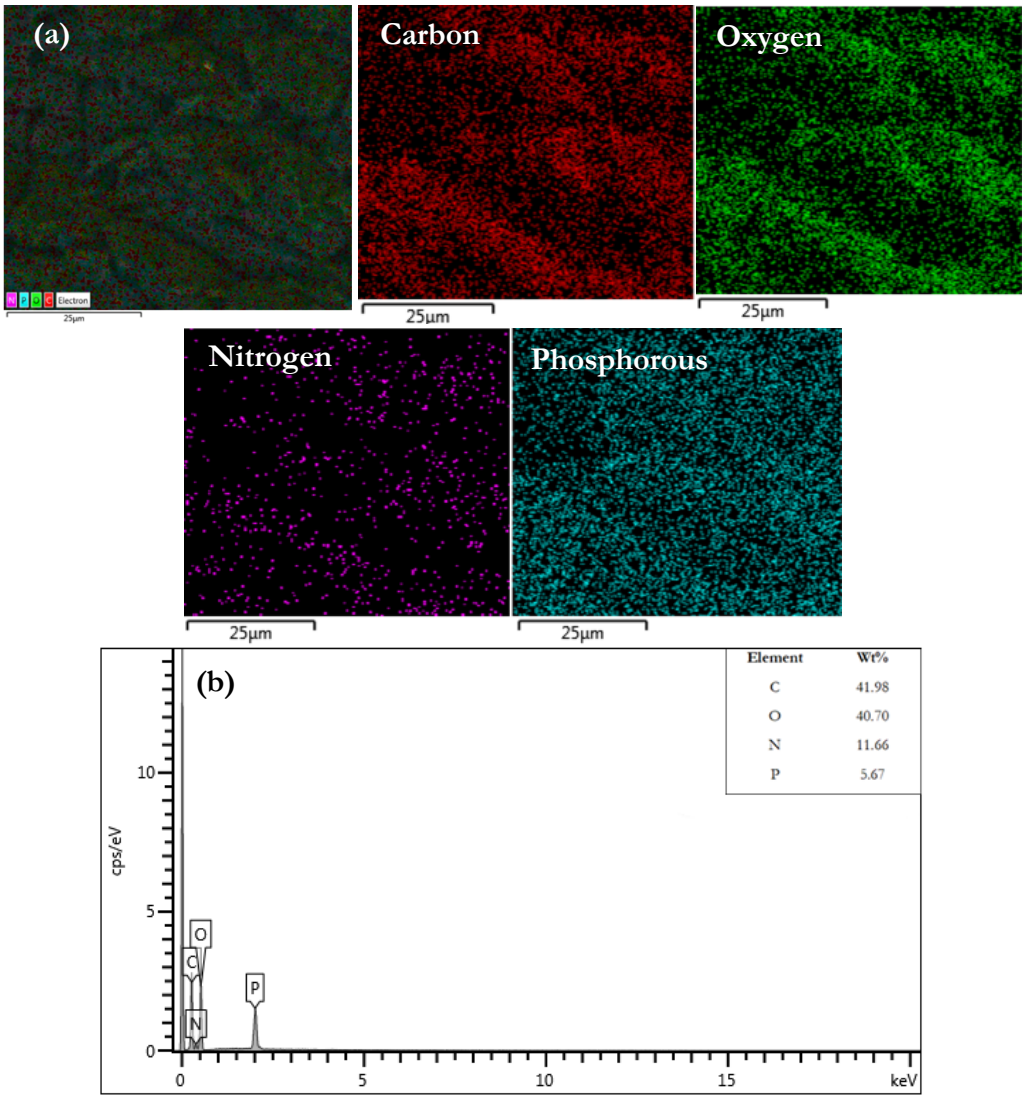

Figure 3.4. **(a)** C, O, N and P elemental mapping for phosphorylated hazelnut shell waste, **(b)** EDS results

3.3.1.2. FTIR Analysis

The micro-FTIR spectra of the pristine hazelnut shell and phosphorylated hazelnut shell waste are shown in Figure 3.5. After phosphorylation of hazelnut shell, a peak at wave number 1039 cm^{-1} in the phosphorylated hazelnut shell was found that corresponded to the characteristic absorption peak of a P–O stretching vibration belonging a medium to strong wide band at 1040–910 cm^{-1} for the compounds containing P–OH group. Moreover, the bands at 823 cm^{-1} and 922 cm^{-1} were attributed to the P–O–P symmetric and antisymmetric stretching vibrations, respectively. For the phosphorylated hazelnut shell, a new peak at 1238 cm^{-1} appeared that was assigned to the strong P=O bond. Absorbance of the peak at 1315 cm^{-1} ascribed to CH_2 coupled with OH deformation disappeared due to the phosphorylation of hydroxyl groups (Shi et al., 2014). The peak around 1402 cm^{-1} presents weak –OH acid group so that the OH stretching vibration band became more asymmetric owing to introduction of more acidic OH groups of phosphoric acids into the polymer in the range 3200–3600 cm^{-1} (Luneva and Ezovitova, 2014; Socrates, 2004). Micro-FTIR results confirmed a successful synthesis of phosphorylated functional biosorbent from hazelnut shell waste.

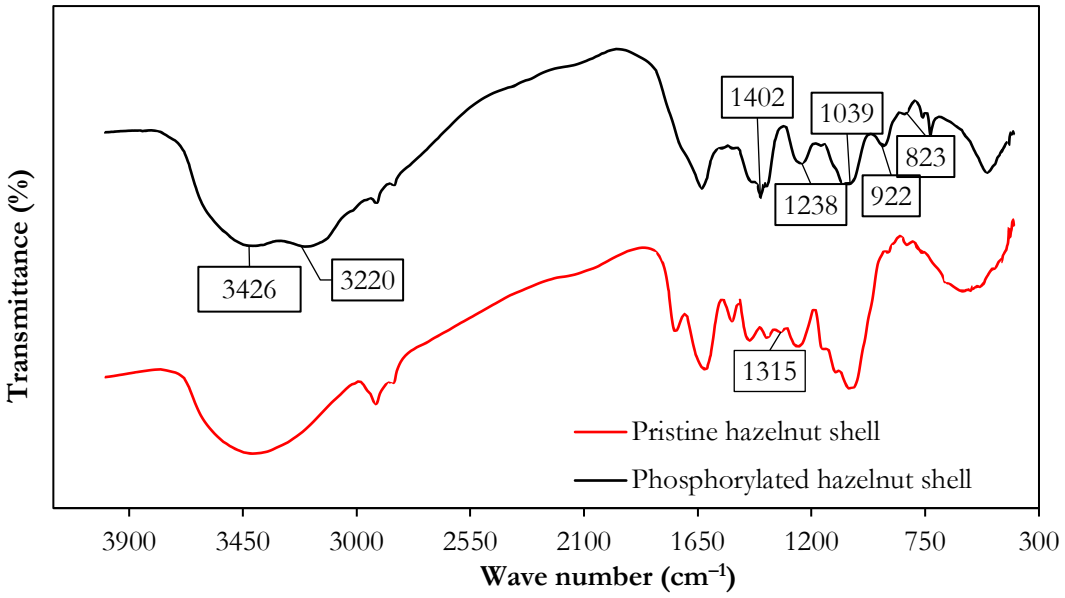

Figure 3.5. Micro-FTIR spectra of both pristine and phosphorylated hazelnut shell waste

3.3.1.3. XPS Analysis

XPS is another useful technique to analyze and confirm the functional groups on surface of materials semi-quantitatively. Broad scan XPS patterns of the pristine, phosphorylated and Li-loaded phosphorylated hazelnut shell are shown in Figure 3.6. For the pristine hazelnut shell, only characteristics peaks of C 1s, N 1s and O 1 s could be observed in XPS at 285 eV, 400 eV and 533 eV, respectively. In contrast, after phosphorylation, new peaks of P 2s and P 2p at 190 eV and 134 eV, respectively, appeared for the phosphorylated hazelnut shell and it further identified the successful phosphorylation that agreed well with the micro-FTIR results. Although the detection of lithium is difficult due to the low photon energy of this element which emits low energy peaks close to the electronic noise of the detection system, large number (50) of scans were done to acquire Li 1s spectrum for the Li-loaded phosphorylated hazelnut shell. Hence, the signal observed at 55 eV was attributed to binding energy of Li 1s which could be better determined by high resolution XPS spectra given in Figure C.2.

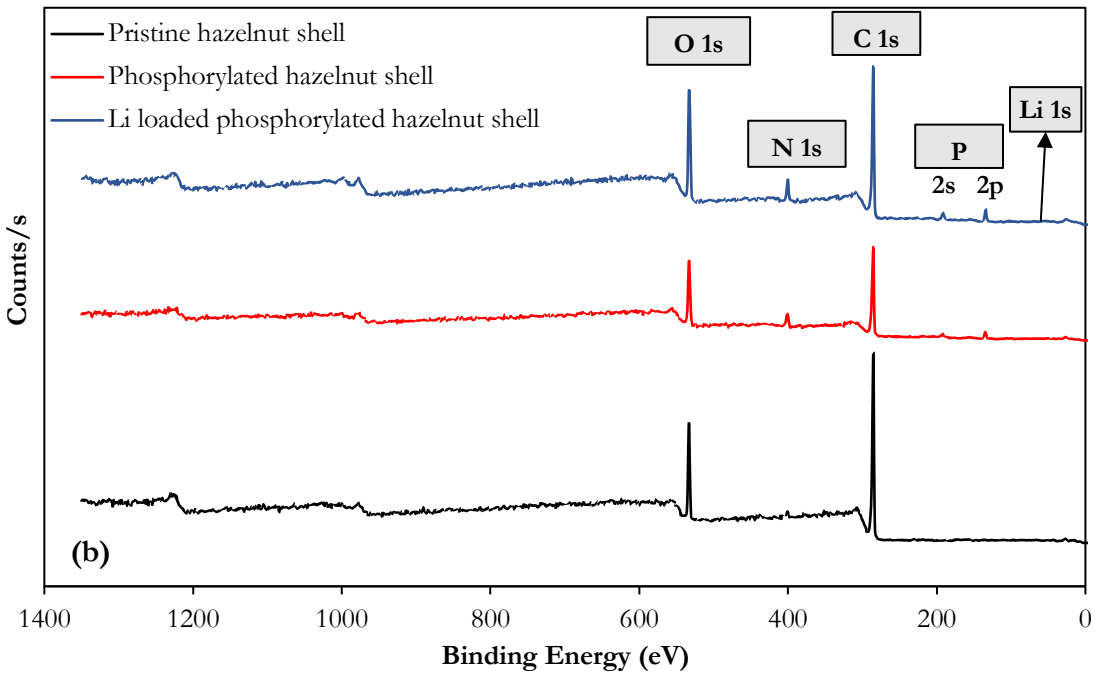

Figure 3.6. XPS diagram of pristine, phosphorylated and Li-loaded phosphorylated hazelnut shell waste.

The atomic concentrations of all present elements for pristine, phosphorylated and Li-loaded phosphorylated hazelnut shell are listed in Table 3.1. After NaOH treatment ca. 4% increase in O and ca. 4% decrease in C content were observed due to removal another carbonaceous portion of the biomass. Phosphorylated hazelnut shell after grafting of phosphorous group contains 3.27% P in the surface. Data confirmed that phosphorylation occurred preferentially at the surface where the hydroxyl functional groups are more accessible. In addition, the O 1s peak for modified hazelnut shell showed an increase in intensity and a slight chemical shift to a higher BE value compared to unmodified hazelnut shell corresponding to 17.89% and 21.32% of O content, respectively. These changes can be attributed to non-bridging oxygen in the phosphate group (O=P) and oxygen double bonded to carbon (O=C) from carbamates. It seemed that the O=P bond was responsible for O 1s evolution since the carbamate moiety came from the less favored side reaction between cellulose and urea. N content increased from 3.24% to 9.49% after phosphorylation of hazelnut shell which assigned to nitrogen covalent bonds in the carbamate moiety (N–C=O and NH_2) in the surface. 5.95% Li proved lithium sorption capability of phosphorylated hazelnut shell.

Table 3.1. Surface composition (atom fraction, %) of pristine, NAOH treated, phosphorylated and Li-loaded phosphorylated hazelnut shell wastes.

Elements	**PHS**[1] (Atom fraction, %)	**NHS**[2] (Atom fraction, %)	**FHS**[3] (Atom fraction, %)	**Li-FHS**[4] (Atom fraction, %)
C 1s	78.92	74.51	65.93	62.27
O 1s	17.86	22.32	21.32	21.57
N 1s	3.24	3.19	9.49	6.50
P 2p	-	-	3.27	3.72
Li 1s	-	-	-	5.95

[1] PHS: Pristine hazelnut shell waste

[2] NHS: NaOH treated hazelnut shell waste

[3] FHS: Phosphorylated functional hazelnut shell waste

[4] Li-FHS: Li-loaded phosphorylated functional hazelnut shell waste

3.3.1.4. BET Analysis

BET surface areas and pore structures of pristine (PHS), NaOH treated (NHS) and phosphorylated functional hazelnut shell waste (FHS) are provided in Table 3.2. It was found that the NaOH treatment increased BET surface area threefold and total pore volume fivefold due to removal of lignin that is also a barrier to access the cellulose. However, further phosphorylation process decreased the BET surface areas and the pore volumes of NHS as intermediate due to the blockage of internal porosity by incorporated phosphorous functional group. In addition, the percentage of micropore of sample decreased from ~8% to ~3% and macropore increased from ~50% to 70% at the end of total modification, thus the micropores might have been enlarged and converted into macropores leading to a decrease in specific surface area. Moreover, the total pore volume was also greatly reduced after phosphorylation.

3.3.1.5. XRD Analysis

The X-ray diffractograms of pristine, NaOH treated and functionalized hazelnut shell waste samples are shown in Figure 3.7. In general, the diffractogram characteristic of hazelnut shell waste showed cellulose identifier as strongly justified by the presence of a peak at 2θ angle values around 16.5º and 22.6º whose patterns look like those from amorphous samples reported in the literature (French, 2020; French and Santiago Cintrón, 2013; Poletto et al., 2012). Cellulose is composed of glucose monomer units in the form of linear chains making up the crystalline structure that is essentially attributed to hydrogen bonding interactions and Van der Waals forces among adjacent molecules (Tomul et al., 2019). In contrast, hemicellulose (with branched as well as straight polymer chains) and lignin (with three-dimensional polymer) are amorphous (Cagnon et al., 2009).

Crystallinity index (CrI %) values were calculated by using Segal equation (Eq. (6)) (French, 2014; Segal et al., 1959):

$$CrI(\%) = \frac{I_{200} - I_{am}}{I_{200}} \times 100 \qquad (3.6)$$

where CrI is the relative degree of crystallinity, I_{200} is the maximum intensity (in arbitrary

units) of the 200-lattice diffraction and I_{am} is the intensity of diffraction in the same units at 2θ=18°. The calculated CrI % values are given in Table 3.2. After pretreatment by NaOH crystallinity index increased from 19.76% to 27.55% as expected since amorphous contributors i.e., hemicellulose and lignin were removed. However, then the crystallinity index decreased to 17.88% because modification by phosphorylation led to the diffraction peak located at 200-lattice plane becoming flatter, also indicating a decrease in crystallinity. Nonetheless, it was believed that the improved crystallinity of cellulose increases its rigidity, which can lead to an increase in the mechanical properties (higher tensile strength) of cellulose-based composite.

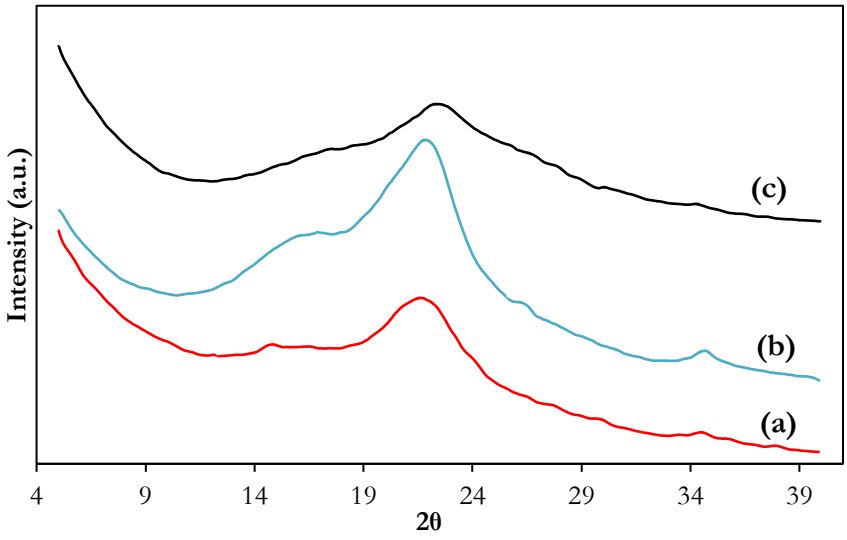

Figure 3.7. X-ray diffraction patterns of **(a)** pristine, **(b)** NaOH treated and **(c)** phosphorylated functional hazelnut shell waste.

Table 3.2. Pore size analysis, BET surface area and crystallinity index value of pristine, NaOH treated, and phosphorylated functional hazelnut shell waste.

Material	**Pore volume (%)**			**Total pore volume (cm^3/g)**	**BET Surface Area (m^2/g)**	**CrI (%)**
	Micropore (< 2 nm)	**Mesopore (2–50 nm)**	**Macropore (>50 nm)**			
*PHS	7.89	42.00	50.11	0.001407	1.7367	19.76
**NHS	4.07	21.04	74.89	0.007496	5.6877	27.55
***FHS	3.30	27.00	69.70	0.000637	0.8193	17.88

*PHS: Pristine hazelnut shell waste, **NHS: NaOH treated hazelnut shell waste, ***FHS: Phosphorylated functional hazelnut shell waste

3.3.1.6. TGA Analysis

Figure 3.8 illustrates thermal profiles of pristine, NaOH treated and phosphorylated functional hazelnut shell waste by pyrolysis. As pronounced in the differential thermogravimetric curve (DTG) of pristine hazelnut shell waste (Figure 3.8(a)) three peaks at 70°C, 260ºC and 338ºC were observed corresponding to moisture evaporation, hemicellulose, and cellulose thermal decomposition, respectively. Specifically, a minor weight loss of 5% at 70ºC seen in the thermo-gravimetric analysis (TGA) curve is explained with the adsorbed and bound water molecules. In addition, thermal biomass degradation of hemicellulose and cellulose occurred by 9.36% weight loss and 30.07% weight loss due to decomposition of glycosidic bonds (C–O–C). Meanwhile, lignin decomposition could not be observed since the lignin is commonly known as the most difficult main structural component in the biomass for thermal decomposition (often ranging from 160°C to elevated temperatures) (Tran et al., 2017). The complete carbonization of hazelnut shell waste required the minimum temperature of 363ºC and at the final decomposition temperature in the studied temperature range, i.e., 1000°C, only 25% of the char remained.

Compared to the unmodified pristine hazelnut shell waste, an almost similar nature of degradation curve (Figure 3.8(b)) with microcrystalline cellulose, having the onset of degradation at 285°C and with the degradation peak around 330°C (Das et al., 2010) was obtained for NaOH treated hazelnut shell waste. Since alkali pretreatment was applied to remove lignin and a part of the hemicellulose, this result was in line with the literature (Kim et al., 2016).

On the other hand, the thermal analysis of the phosphorylated functional hazelnut shell waste indicated a relatively complex pyrolysis process (Figure 3.8(c)) since the grafting of phosphorous groups on the surface of cellulose particles modifies the thermal degradation pathway of cellulose by decreasing its onset degradation temperature and by improving the formation of high amount of char residues (Costes et al., 2016). A similar minor weight loss (ca. 7%) was observed at 73.5ºC due to evaporation of water molecules adsorbed on the phosphorylated functional cellulose. Thereafter, the initial prominent major weight loss by 18.7% was at 200–250°C, and it verified that the phosphorous groups increased the thermal decomposition reaction of the cellulosic polymer (and hence the heat resistance of the material was reduced), but the carbonization

(and hence the flame resistance) increased significantly instead. The final observed peak at 828ºC with another major weight loss of 26.27% indicates that the phosphorous functional group was decomposed. It is widely known in the literature that cellulosic materials containing phosphorous group have flame retardant properties (Aoki and Nishio, 2010; Ghanadpour et al., 2015; Rol et al., 2019). At the final decomposition temperature (1000ºC) of the phosphorylated functional hazelnut shell waste the char residue was 33% which is in good agreement with the improvement in the char formation after phosphorylation.

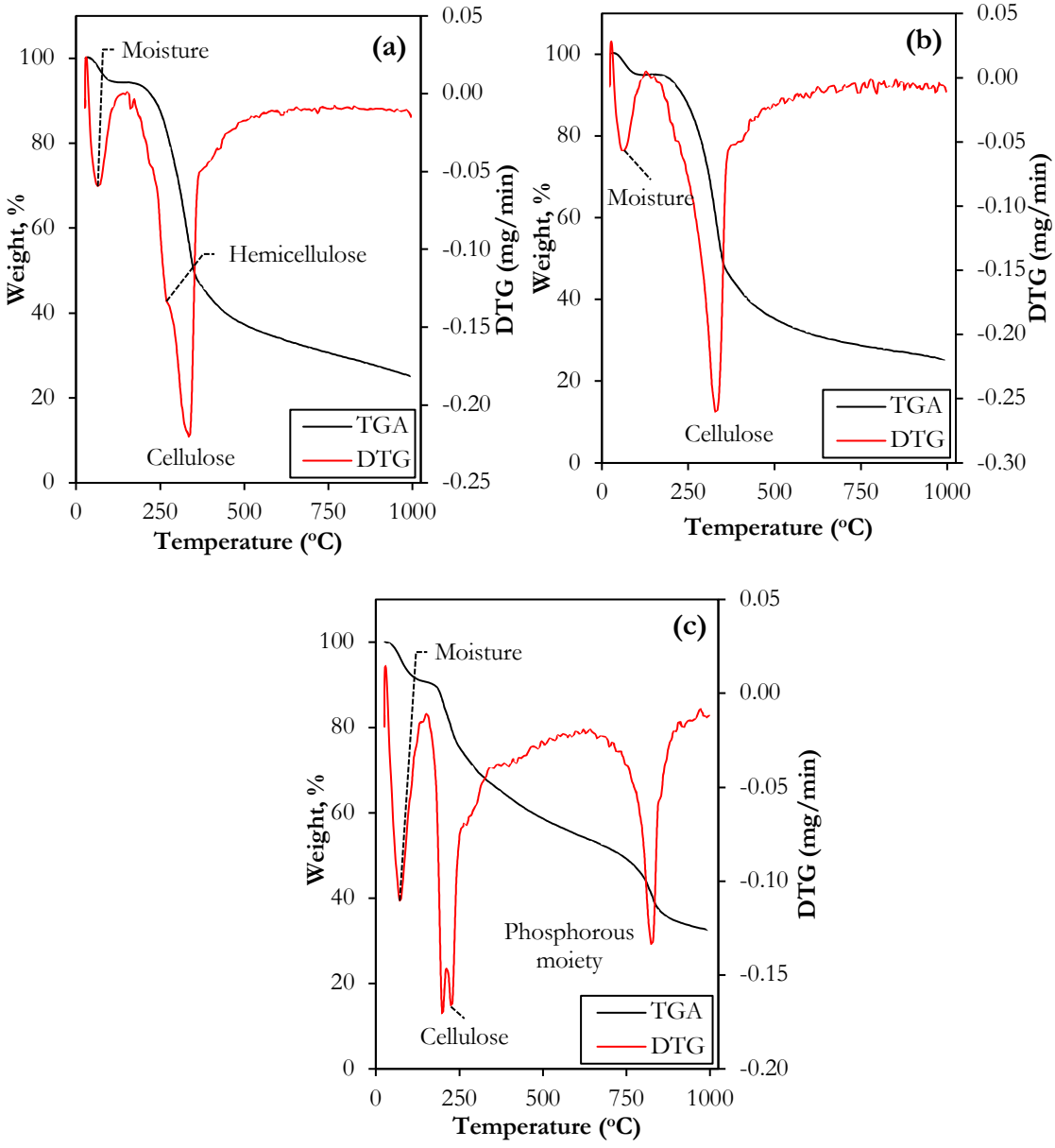

Figure 3.8. Thermal profiles of **(a)** pristine, **(b)** NaOH treated and **(c)** phosphorylated functional hazelnut shell waste.

3.3.2. Lithium Sorption Performance of the Biosorbent

3.3.2.1. The Effect of Biosorbent Dosage

The sorbent dosage is of great importance with respect to the sorption studies as it determines the potential of material to uptake metal ions for a given initial concentration of the sorbent (Panda et al., 2011). The effect of biosorbent dosage is presented in Figure 3.9(a). Experimental results revealed that the percentage of sorption increased with an increase in biosorbent dosages. This was in fact expected since increasing the biosorbent dosage provides greater surface area or higher sorption sites for a constant metal ion concentration. A maximum lithium sorption of 92% was achieved at biosorbent dosage of between 12 g/L and 16 g/L and sorption for any biosorbent dosage beyond it gave almost the same uptake. Therefore, the use of 14 g/L biosorbent dosage is justified from an economic point of view for the recovery of lithium from aqueous solutions.

3.3.2.2. The Effect of pH

The solution pH is one of the factors that must be considered in sorption studies, as it can affect the structure of sorbent depending on the functional group it carries (especially if weak base or weak acidic) (Çiçek et al., 2018). The data presented in Figure 3.9(b) indicates the sorption efficiency of phosphorylated functional hazelnut shell waste from pH 2 to pH 8. Relatively lower sorption of Li (82.15%) was observed at pH 2 but sorption behavior was similar within the range pH 3–8 by around 92% of lithium sorption efficiency. Since the biosorbent contains phosphoric acid derived functional group *pKa* values are 2.16, 7.21 and 12.32. Therefore, at pH 2, the functional group of the sorbent tends to stay in the molecular form, thus sorption of lithium was relatively low. Nonetheless, when the pH of solution was increased from 2 to 8, the functional group of the sorbent ionized, and sorption of lithium was enhanced as the next *pKa* value is 7.21.On the other hand, point of zero charge (PZC) value of this biosorbent was also determined as 6.95 (see Figure C.3) which means the biosorbent's surface was positively charged at solution pH below 6.95 resulting in the decrease of lithium sorption due to competition between lithium and protons ions for sorption active sites along with the repulsion of

lithium ions. So, the lower the pH goes below pH_{PZC}, the greater the density of positive ions on the surface of phosphorylated functional hazelnut shell waste will be. As a result, except pH 2, no remarkable change was observed for the other pH values studied.

3.3.2.3. The Effect of Contact Time

The effect of contact time on lithium sorption efficiency is depicted in Figure 3.9(c). As it is exhibited, sorption rate immediately increased, followed by a relatively slow process and then the optimal efficiency was reached within about 3 min. No obvious changes were observed from 3 to 60 min. Hence, the sorption process appeared to proceed very fast when the number of lithium ions to be transported from the medium is much larger than the numbers of available sites. This result also suggested that phosphorylated functional hazelnut shell waste has a high affinity toward lithium ions in aqueous solutions. On the other hand, it is truly surprising that the biosorbent possess high a lithium ions sorption efficiency and reach sorption equilibrium quickly so that observable data could not be collected (i.e., sampling $< 1\ min$ was highly difficult) to find related rate constants and rate determining step from proposed any of empirical models in the literature. In addition, cellulose based sorbents also reported in the literature performed quite rapid kinetics for different solutes (Arar, 2019; Tomul et al., 2019; Xu et al., 2020; Zhang et al., 2020).

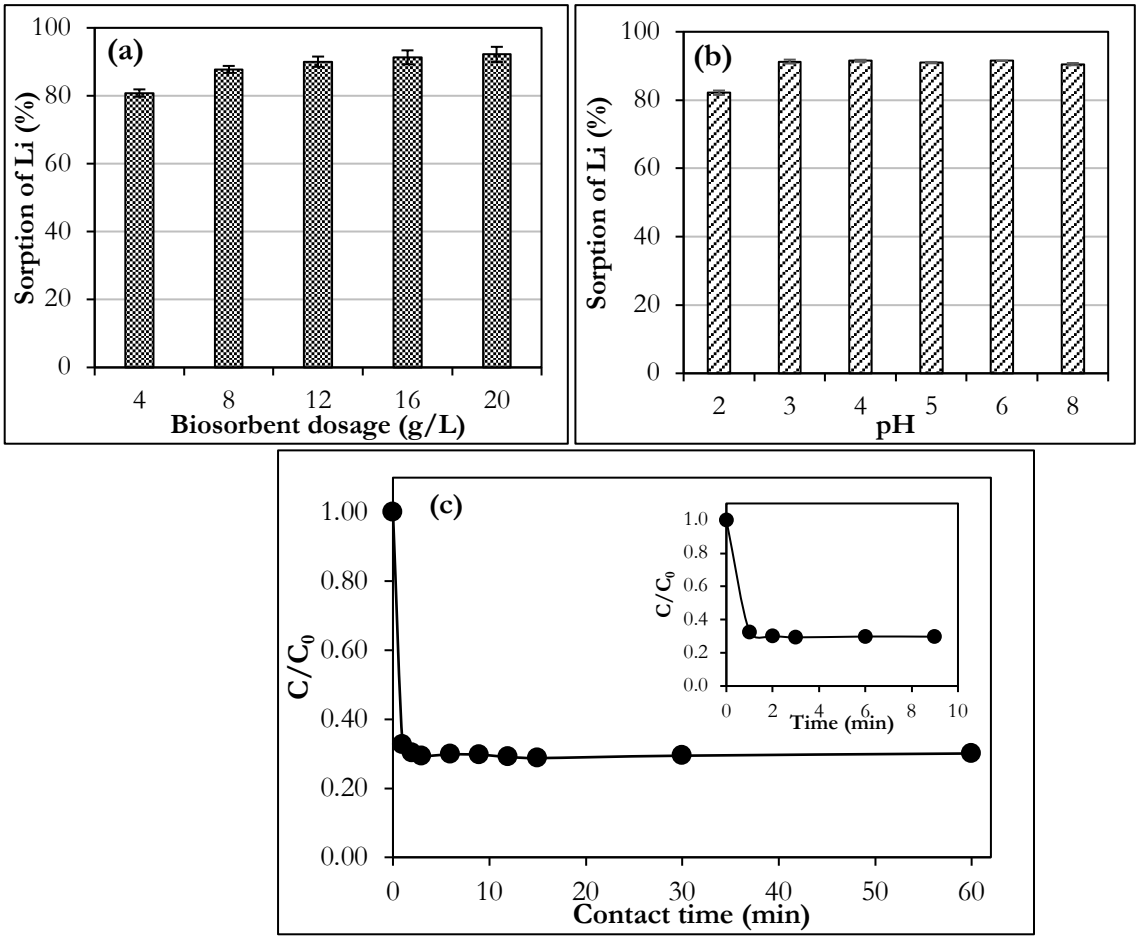

Figure 3.9. **(a)** Effect of biosorbent dosage on lithium sorption efficiency (t: 24 h, C_0: 10 mg/L, pH 5–6 , speed 180 rpm, T: 25ºC) **(b)** effect of solution pH on extent of lithium sorption (t: 24 h, biosorbent dosage: 14 g/L, C_0: 10 mg/L, pH 2–8, speed 180 rpm, T: 25ºC) **(c)** effect of contact time on lithium sorption on phoshorylated hazelnut shell waste (t: 0–60 min, biosorbent dosage: 12 g/L, C_0: 100 mg/L, pH 5–6 , speed 180 rpm, T: 25ºC)

3.3.2.4. The Effects of Initial Concentration and Temperature

The effect of temperature dependence of lithium sorption by phosphorylated functional hazelnut shell waste with various initial ion concentration for different temperatures is presented in Figure 3.10(a). It is clearer for the solution having 100 mg/L initial lithium concentration that the equilibrium sorption capacity of phosphorylated hazelnut shell waste was considerably lower (4.97 mg/g) at the temperature of 45°C than that at 35°C (5.20 mg/g) and 25°C (5.48 mg/g). Since the equilibrium sorption capacity of the biosorbent decreased from 5.48 to 4.97 mg/g when the temperature was increased from 25°C to 45°C, it can be said that an exothermic reaction is controlling the sorption

of lithium onto phosphorylated functional hazelnut shell in this temperature range. It can be attributed to high surface coverage depending on activation of reactive sites at lower temperature. On the other hand, the initial lithium concentration creates an important driving gradient force to overcome the mass transfer resistance to lithium ions between the aqueous and solid phases. The data for the lower temperature (25ºC) showed that lithium sorption capacity of phosphorylated hazelnut shell was increased from 0.67 to 5.48 mg/g with lithium concentration increasing from 10 to 100 mg/L due to a high driving force in terms of mass transfer, although the lithium percent sorption decreased from 92 to 67 due to the saturation of binding sites onto the biosorbent.

Sorption isotherms

The sorption isotherms of lithium onto phosphorylated functional hazelnut shell waste at different operation temperatures (25°C, 35°C and 45°C) are given in Figure 3.10(b). According to the isotherm shape's classification, the biosorbent exhibited the F-type (Freundlich) isotherm, which is characterized by an indefinite multi-layer formation after completion of the monolayer and is found in sorbents with a wide distribution of pore sizes. Near to the point of inflexion a monolayer is completed, following which sorption occurs in successive layers (Ruthven, 1984). As noted earlier, the process of lithium sorption onto the biosorbent occurred favorably at low solution temperature and high solution concentration.

Table 3.3 provides the corresponding parameters of the investigated sorption isotherms that were determined by the help of MATLAB® Software from the nonlinear regression technique. The correlation coefficient (R^2) and sum of squares of error (SSE) revealed that the experimental data of sorption equilibrium were satisfactorily described by the Freundlich model (0.996–0.999 and 0.0175–0.0607) than the Langmuir (0.991–0.998 and 0.0232–0.1572) and Temkin (0.953–0.959 and 0.6367–0.7221) models, respectively.

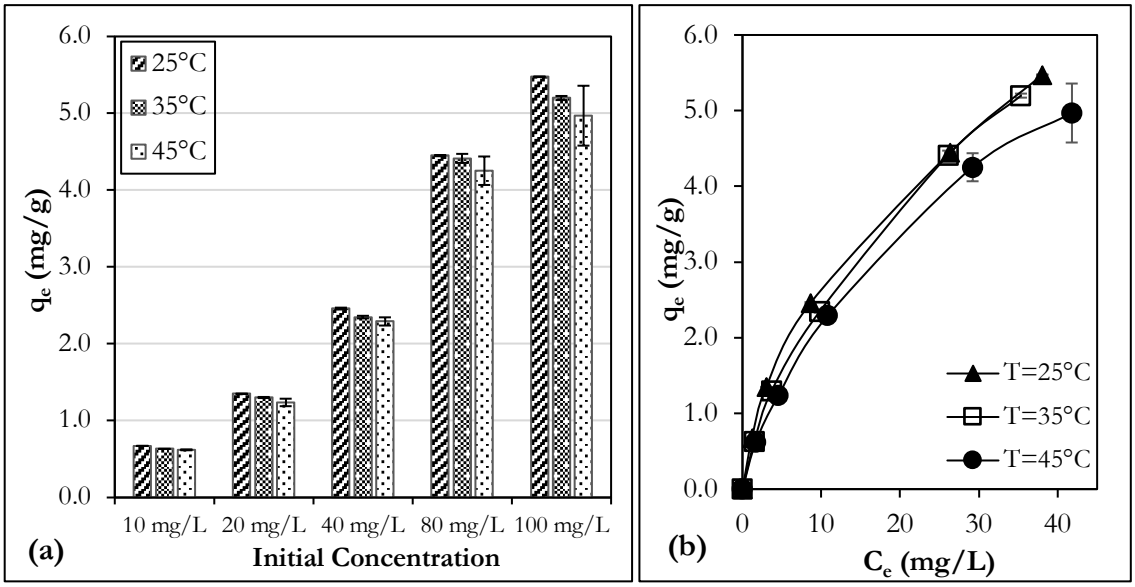

Figure 3.10. **(a)** Effect of temperature on lithium uptake capacity of phosphorylated functional hazelnut shell waste at different initial concentrations **(b)** sorption isotherms of phosphorylated functional hazelnut shell waste (t: 24 h, biosorbent dosage: 14 g/L, C_0: 10–100 mg/L, pH 5–6, speed 180 rpm, T: 25–45°C)

According to Langmuir model Q_{max} seems to increase first from 7.71 mg/g to 8.71 mg/g and then decrease to 8.04 mg/g as temperature increased from 25°C to 45°C which is quite comparable with some reported sorbents for lithium in Table 3.4. Although the nature of sorption is exothermic, this fluctuation may stem from relatively lower model fitting compared to expected fitting for Freundlich model. However, decrease in the K_L value from 0.0579 L/mg to 0.0385 L/mg as temperature increased clarifies that binding affinity of the biosorbent to lithium ions in the solution was reduced as temperature was raised. This finding also justified that the contribution of pore filling to the sorption mechanism was not as substantial as the other surface interactions, such as hydrogen bonding and electrostatic attraction. For the Freundlich model, larger value of n_F (smaller value of $1/n_F$) implies stronger interaction between sorbent and solute. The values of $0.1<(1/n_F)<1.0$ for all temperatures shows that sorption of lithium is favorable (Ruthven, 1984). Besides, Temkin isotherm considers explicitly the sorbent–solute interactions by a factor. Due to these interactions, the heat of sorption of all the molecules in the layer decreases linearly as coverage increases (Hameed et al., 2008).

Table 3.3. Parameters of the sorption isotherm lithium onto phosphorylated functional hazelnut shell waste.

Model	25°C	35°C	45°C
Langmuir	$Q_{max} = 7.71\ mg/g$ $K_L = 0.0579\ L/mg$ $R^2 = 0.991$ $SSE = 0.0524$	$Q_{max} = 8.71\ mg/g$ $K_L = 0.0406\ L/mg$ $R^2 = 0.996$ $SSE = 0.0228$	$Q_{max} = 8.04\ mg/g$ $K_L = 0.0385\ L/mg$ $R^2 = 0.998$ $SSE = 7.744 \times 10^{-3}$
Freundlich	$^*K_F = 0.7129$ $n_F = 1.7834$ $R^2 = 0.999$ $SSE = 6.790 \times 10^{-3}$	$^*K_F = 0.5553$ $n_F = 1.6321$ $R^2 = 0.999$ $SSE = 5.852 \times 10^{-3}$	$^*K_F = 0.5176$ $n_F = 1.5861$ $R^2 = 0.996$ $SSE = 0.0202$
Temkin	$A = 1.0237\ L/g$ $B = 1.3761\ J/mol$ $R^2 = 0.959$ $SSE = 0.2256$	$A = 0.7702\ L/g$ $B = 1.4575\ J/mol$ $R^2 = 0.953$ $SSE = 0.2411$	$A = 0.6781\ L/g$ $B = 1.3943\ J/mol$ $R^2 = 0.955$ $SSE = 0.2125$

*The unit of K_F is $mg/g\ (L/mg)^{1/n_F}$

Table 3.4. Comparison of sorption capacity of phosphorylated hazelnut shell waste with some published sorbents for lithium.

Sorbent	Functional group	Maximum sorption capacity ($mg.g^{-1}$)	Reference
HMO-modified cellulose film	Hydrogen manganese oxide	21.6	(Tang et al., 2020)
Arthrospira platensis biomass	OH, –COOH, –NH, $–NH_2$, and $–NH_3$	1.75	(Zinicovscaia et al., 2020)
Cellulose microsphere adsorbent with sulfonic acid groups (CGS)	Sulfonic acid	16.0	(Xu et al., 2020)
Cellulose-based microsphere containing crown ethers groups (MCM-g-AB15C5)	4'-aminobenzo-15-crown-5 (AB15C5)	12.9	(Chen et al., 2019)
Lewatit TP 260 chelating resin	Aminomethylphosphonic acid	13.65	(Çiçek et al., 2018)
Magnetic lithium ion-imprinted polymer (Fe_3O_4@SiO_2@IIP)	2-(allyloxy) methyl-12-crown-4	4.07	(Luo et al., 2015)
Macroporous cellulose gel beads-based hybrid-type ion-exchanger (HIE)	Microcrystalline λ-MnO_2	9.72	(Sagara et al., 1989)
Phosphorylated hazelnut shell waste	Phosphorous group	7.71	This work

Sorption thermodynamics

Thermodynamic parameters ($\Delta G°$, $\Delta H°$ and $\Delta S°$) of the lithium sorption can be essentially predicted by using following equation and van't Hoff approach, respectively:

$$\Delta G° = -RTlnK_e \tag{3.7}$$

$$lnK_e = -\frac{\Delta H°}{RT} + \frac{\Delta S°}{R} \tag{3.8}$$

where $\Delta G°$ is Gibbs free energy change (kJ/mol), $\Delta H°$ is enthalpy change (kJ/mol) and $\Delta S°$ is entropy change (kJ/mol.K). Equilibrium constant (K_e, dimensionless) can be obtained from the modification of Freundlich constant ($K_F, mg/g\ (L/mg)^{1/n_F}$), related with the thermodynamics of heterogeneous sorption, by the equation given below (Tran et al., 2016):

$$K_e = K_F \rho \left(\frac{10^6}{\rho}\right)^{\left(1-\frac{1}{n_F}\right)} \tag{3.9}$$

where ρ (g/mL) is the density of the aqueous solution but it can be simply approximated to density of water at the temperature of interest.

Thermodynamic parameters for the sorption of lithium by phosphorylated functional hazelnut shell waste were listed in Table 3.5. Gibbs free energy change, the basic principle for sorption spontaneity, must be negative for a feasible adsorption to occur so that negative $\Delta G°$ values confirm spontaneity of the sorption of lithium ions on biosorbent. Meanwhile, an increase in temperature caused less favorable sorption condition since greater (less negative) $\Delta G°$ values obtained at higher temperatures. This can also be supported by the exothermic nature of the sorption corresponding to the negative $\Delta H°$ value (−51.07 kJ/mol). In addition, negative $\Delta S°$ value (−0.125 kJ/kmol. K) indicated that the lithium sorption onto phosphorylated functional hazelnut shell become less random at the solid/solution interface during the sorption process. Another helpful outcome of the thermodynamic analysis is to estimate the physical nature of the ion sorption on the biosorbent. As an order of magnitude, $\Delta G°$ is in the range of 0 to −20 kJ/mol for physical sorption and in the range of −80 to −400 kJ/mol for chemisorption (Salehi et al., 2012). Therefore, the mechanism of lithium sorption on phosphorylated functional hazelnut shell waste can be described as physical sorption based on $\Delta G°$ values that lie between 0 to −20 kJ/mol. Most likely, rather than chemical bonds, weak physical

electrostatic and van der Waals interactions attached lithium ions to the functional vacant sites of the biosorbent.

Table 3.5. Thermodynamic parameters for the sorption of lithium by phosphorylated functional hazelnut shell waste.

Temperature (°C)	$\Delta G°$ (kJ/mol)	$\Delta H°$ (kJ/mol)	$\Delta S°$ (kJ/mol.K)
25	−13.957		
35	−12.712	−51.070	−0.125
45	−11.467		

3.3.2.5. The Effect of Competitive Ions

The effect of competitive ions was investigated in the existence of both other similar cations such as Na^+ and K^+ and Ca^{2+} and Mg^{2+} in the aqueous solution. As illustrated in Figure 3.11(a)., these ions competed with Li^+ for the same sorption sites, therefore apparently the coexistence of the ions inhibited lithium sorption efficiency. Even though the presence of other cations in the solution simultaneously reduced slightly the separation efficiency of lithium from 92% to 85.54% when solution contains only lithium under the same conditions, overall sorption capacity of the phosphorylated functional hazelnut shell was improved. So that, Na^+, K^+, Ca^{2+} and Mg^{2+} separation percentages were also obtained as 58.47% 76.72%, 91.53% and 98.87%, respectively. This phenomenon is due to a shift in the equilibrium toward the formation of sorbent-solute complex with raising concentration of solute. On the other hand, the results showed that Ca^{2+} and Mg^{2+} highly competed with monovalent ions since they have higher valence and atomic radius as expected but the material still possessed a considerable lithium uptake capacity.

Moreover, as a preliminary study, this biosorbent was also tested with a geothermal water sample obtained from a well located in Seferihisar, İzmir region of which some physicochemical properties are given in Table 3.6 to check its lithium uptake performance in a real medium. As seen in Figure 3.11(b), lithium sorption efficiency decreased from 90% to 50% at optimum sorbent dosage when used in geothermal water compared to Li aqueous solution as expected. However, such performance comparison

does not give precise idea since sorption efficiency is also highly dependent on initial Li concentration along with other competitor ions. Here in this preliminary test, the lithium concentration of the geothermal water used is 7.13 ppm and it also contains other quite high concentration of other ions, but the model solution contains only 10 ppm of Li. Despite relatively lower lithium sorption efficiency, the material proved its lithium capability in a real brine. By further modification of the material or applying pretreatment such as softening by hybrid methods the lithium sorption efficiency of this biosorbent can be improved.

Table 3.6. Some physicochemical properties of the geothermal water sample obtained from a well in Seferihisar, İzmir region.

Cations	**Concentration (mg/L)**	**Anions**	**Concentration (mg/L)**
Li^+	7.13	**HCO_3^-**	504.44
Na^+	6624.2	**Cl^-**	12478.8
K^+	744.156	**SO_4^{2-}**	569.04
Ca^{2+}	850.036		
Mg^{2+}	180.326		
	pH		6.6
	EC (mS/cm)		39
	SiO_2 (mg/L)		90

3.3.2.6. Desorption of Lithium and Regeneration of the Biosorbent

The desorption study is of great importance to recycle the sorbent and to recover the lithium simultaneously. As depicted in Figure 3.11(c), according to desorption experiments conducted with NaCl, HCl and H_2SO_4, it was observed that the desorption ratio of lithium with 0.25 M NaCl was the lowest by 82% but this value was 93.8% and 92.7% for 0.25 M HCl and H_2SO_4, respectively. In contrast, for both 0.5 M and 1.0 M NaCl regenerant solution almost 93% desorption was recorded. Although the highest

desorption efficiency was obtained with 1.0 M H_2SO_4 by 97.4%, using 1.0 M HCl resulted in considerable desorption ratio by 94.6%. In general, these results indicated that elution of lithium and regeneration of the biosorbent can easily be done using either of solutions at appropriate concentrations.

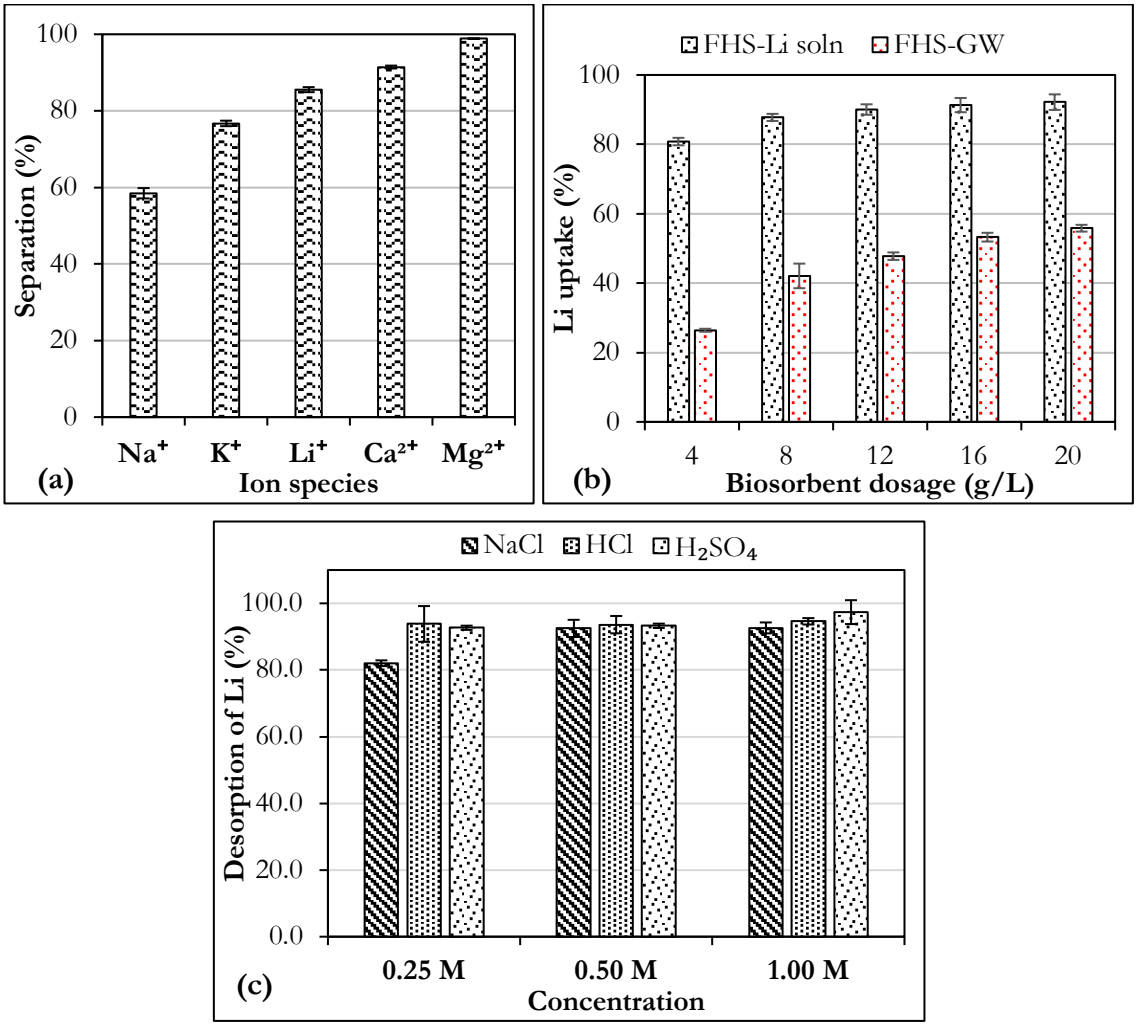

Figure 3.11. **(a)** Effect of competitive ions on lithium sorption by phoshorylated functional hazelnut shell waste (t: 24 h, biosorbent dosage: 14 g/L, C_0: 10 mg/L for all species, pH 5–6 , speed 180 rpm, T: 25°C), **(b)** comparison of lithium uptake percentage by phosphorylated hazelnut shell waste (FHS) at different biosorbent dosage both in Li solution (Li-soln) and real geothermal water (GW) and, **(c)** comparison of desorption efficiency for phosphorylated functional hazelnut shell waste (t: 24 h, speed 180 rpm, T: 25°C).

3.4. Conclusions and Future Perspectives

In the buildup of sustainable separation technologies for the recovery of valuable metals such as lithium, biosorption can be a facile route. A breakthrough in sorbents development is needed to solve the critical problem of recovery of strategic metal ions to promote circular (bio) economy. In this study, by applying recycling based (bio) technologies to recover valuable materials approach a novel biosorbent was developed from hazelnut shell wastes by grafting phosphorous functional groups. Characterization studies showed that hazelnut shell waste was functionalized by phosphorylation reaction successfully. Optimum sorbent dose was found to be 14 g/L. Thermodynamic analysis revealed that the sorption of lithium on phosphorylated functional hazelnut shell waste was spontaneous, exothermic, and more random. As temperature increased sorption of lithium decreased due to exothermic nature of the biosorbent which is advantageous for metal recovery. Although as initial concentration increased sorption of lithium enhanced, no considerable effect is observed for the solution pH except pH 2. Sorption behavior of phosphorylated functional hazelnut shell waste was well described by Freundlich isotherm, but maximum sorption of lithium was estimated as 7.71 mg/g at 25^{o}C by Langmuir model. The rate of sorption was quite rapid therefore kinetic trials were out of range in terms of duration which can be one of superior properties of this biosorbent. Even though coexistence of other cations such as Na^{+}, K^{+}, Ca^{2+} and Mg^{2+} in the solution reduced slightly sorption efficiency of Li from 92% to 85.54% under the same condition when only Li^{+} exists, the biosorbent still exhibited a considerable lithium capability. Moreover, the Li loaded phosphorylated functional hazelnut shell waste can easily be regenerated with 1.0 M HCl or H_2SO_4 with high desorption efficiencies. It can be concluded through experimental results for its significant and fast lithium sorption capacity, low-cost and easily obtained properties, phosphorylated hazelnut shell waste could be considered a promising sorbent for lithium recovery from natural sources such as geothermal water for which a preliminary study was performed. By doing this, goals of the conversion of abundant waste, a renewable raw material, into value-added products and the recovery of valuable minerals to promote renewable energy will be met simultaneously. However, since the biosorbent is at a very early stage of its development, a further modification step for either the material or the biosorption process is under consideration to increase its lithium sorption efficiency. Since the phosphorylated

biosorbent can be used in the forms of proton as counter ions if the solution is alkaline or it can be used in the forms of sodium as counter ions if the solution is acidic. On the other hand, chromatographic separation of Li from aqueous solutions will be carried out by cross-linked phosphorylated biosorbent and will be published in the literature available to the public.

CHAPTER 4

CROSS-LINKED PHOSPHORYLATED CELLULOSE AS A POTENTIAL SORBENT FOR LITHIUM EXTRACTION FROM WATER: DYNAMIC COLUMN STUDIES AND MODELING*

4.1. Introduction

As new renewable energy technologies, such as electric vehicles and energy storage systems, emerge, the need for lithium salts is also expected to rise dramatically (Recepoğlu and Yüksel, 2021a; Stringfellow and Dobson, 2021). The use of lithium as an electrode material in rechargeable batteries has been a significant market opportunity since the 1990s (Swain, 2017). Lithium is obtained primarily from rocks as a mineral and liquid resources; however, the quality of lithium ores has deteriorated due to over-mining. Thus, lithium recovery from aqueous sources, such as seawater, geothermal water, and salt-lake brines, has become an essential option for lithium salt production (Can et al., 2021; Zhang et al., 2021). The solar evaporation process is the most widely used industrial method for recovering Li from brines (Flexer et al., 2018). Several potential strategies, including adsorption (Kamran et al., 2019; J. Liu et al., 2021; Xu et al., 2020), solvent extraction (Masmoudi et al., 2021; Wesselborg et al., 2021; Yang et al., 2019; Zhang et al., 2018), and membrane-related technologies (Cha-umpong et al., 2021; Peng and Zhao, 2021; Wang et al., 2021), for Li recovery from brines, have been reported to replace solar evaporation because it needs a long time to concentrate considerable amounts of Li. Adsorption is the most promising strategy for recovering Li from aqueous resources because it is more climate-friendly and more effective in an industrial application (Yoshizuka et al., 2021). Although there are many studies reported in the literature regarding metal ion extraction based on different functionalized composite materials (Awual, 2019, 2016a, 2016b, 2016c, 2015; Awual et al., 2020a, 2020b, 2015, 2013), alu-

*This chapter has been published as: Y. K. Recepoğlu, A. Yüksel, Cross-Linked Phosphorylated Cellulose as a Potential Sorbent for Lithium Extraction from Water: Dynamic Column Studies and Modeling, ACS Omega 7(43) (2022) 38957–38968.

minum hydroxides (AlOH) (Heidari and Momeni, 2017; Lee et al., 2021), aluminum oxides (AlO_x) (Kitamura and Wada, 1978), manganese oxides (MnO_x) (Gao et al., 2021; Marthi and Smith, 2019; Ohashi and Tai, 2019; Qian et al., 2021; Recepoğlu et al., 2018a), and titanium oxides (TiO_x) (Marthi et al., 2021; Zhang et al., 2021; Zhao et al., 2021, 2022) have been known to be the most selective lithium adsorbents until now. They are classified as inorganic crystalline solids either being studied for direct lithium extraction from brines or employed as cathode materials in lithium-ion batteries. Furthermore, researchers have been looking at using selective cation-exchange resins as organic sorbents in the form of a strong acid to recover lithium from lithium-containing fluids. Lewatit K2629, TP 207, TP 208 (Arroyo et al., 2019), and Lewatit TP 260 (Çiçek et al., 2018) are some organic sorbents exhibiting low selectivity of lithium because they only become efficient when impregnated with inorganic ones that have just been aforementioned. Ion-imprinted polymers are developed as organic sorbents to separate lithium selectively from an aqueous medium (Luo et al., 2015). To our best knowledge, lithium recovery using low-cost and sustainable sources containing a considerable portion of cellulose is a new field with scant literature. Since the development of the next generation of materials has been critical in terms of sustainability and green chemistry over the last decade, bio-based polymer matrices potentially allow for lower environmental impacts through the use of renewable biomass and biodegradable or reusable materials are of great interest (Günan Yücel et al., 2021; Illy et al., 2015). Moreover, the synthesis and development of innovative functional low-cost adsorbents with large capacity, high selectivity, and high adsorption rate continue to pique attention for both hazardous substance removal and mineral recovery from water (Recepoğlu et al., 2018b). Cellulose is the most common natural polymer, accounting for 35-50% of all plant materials on the planet (Sengupta and Pike, 2012). It is a linear syndiotactic photopolymer made up of D-anhydroglucopyranose units (AGU) connected by β-(1→4)-glucosidic linkages. At both ends of the cellulose chain, the hydroxyl groups function differently. Intermolecular and intramolecular interactions such as hydrogen bonding and degradation processes mainly include bridging and ring oxygen atoms (Suflet et al., 2006). The presence of hydroxyl groups on cellulose enables several modification processes to create new sorbents with varied functional groups (Yetgin et al., 2022). Phosphorylation is one approach to modifying cellulose. The chelating properties of phosphate groups are well recognized. As a result, phosphorylated polysaccharides have been exploited as metal-chelating polymers and cation exchange materials for pollution

remediation (Illy et al., 2015). Recently, microcrystalline cellulose along with hazelnut shell waste and olive pruning waste as natural cellulose resources has been phosphorylated to synthesize lithium-capable low-cost and sustainable sorbents and tested via batch mode sorption studies in our research group (Nampeera et al., 2022; Recepoğlu and Yüksel, 2021a, 2021b).

A batch mode, known as static adsorption, or a continuous flow mode, known as dynamic adsorption in packed bed columns, can be used to design and operate an adsorption system. The material itself merely acts as an adsorbent in batch tests, and metal ions are adsorbed mainly by the surface area of its outer layers, reducing the adsorbent's efficacy (Zhang et al., 2019). However, the material performs both filtration and adsorption in dynamic adsorption. Low adsorption rates due to the bulk of binding sites situated inside the pores of the adsorbents and high-pressure drops caused by tightly packed small particles in a column are common difficulties for the traditionally packed bed column. However, column adsorption is still more suitable in large-scale operations in the industry than batch adsorption because it is more straightforward, requiring no additional operations such as filtration or centrifugation (Li et al., 2016; Recepoğlu et al., 2018a, 2018b) Therefore, in this study, phosphorylated functional cellulose (FC) was used for the first time in a dynamic packed bed column to recover lithium from water under varying operating conditions such as bed height and flow rate. However, before utilization, it was first cross-linked with epichlorohydrin (ECH) at different ratios (0.02, 0.04, and 0.08 mL ECH/g FC) because it is a very hydrophilic substance that instantly swells to form a hydrogel when it comes into contact with water. The synthesized material's textural, structural, and thermal properties were investigated. The effects of the flow rate and bed height on breakthrough curves and the saturated column's reusability by packed bed dynamic studies were studied extensively. After all, the breakthrough curves were fitted to commonly used models for a fixed-bed column such as Thomas, Yoon-Nelson, and Modified Dose-Response (MDR) models to estimate relative factors like the breakthrough time and adsorption capacity.

4.2. Experimental Section

4.2.1. Materials

Chemicals used in this study included sodium chloride (NaCl, CP, 99.5%), lithium chloride (LiCl, AR, 99%), potassium chloride (KCl, AR, 99%), ECH (C_3H_5ClO), sulfuric acid (H_2SO_4, 95– 97%), and potassium hydroxide (KOH) were purchased from Merck.

4.2.2. Methods

4.2.2.1. Synthesis of the Cross-Linked Phosphorylated Functional Cellulose

Phosphorylated FC was synthesized according to the procedure described elaborately in our previous studies (Recepoğlu and Yüksel, 2021a, 2021b). Nonetheless, due to the phosphorous groups in its structure, phosphorylated FC is a very hydrophilic substance that instantly swells to form a hydrogel when it comes into contact with water. Before using the phosphorylated FC in the column, the material was cross-linked with ECH to eliminate the hydrophilicity of the material, as it becomes hydrogel when filled into the column. To do this, the method applied directly for cellulose was given as follows:

Phosphorylated FC (10 g) was slurried in water (75 mL) containing sodium chloride (0.15 g) and ECH (0.2 mL, 0.4 mL, or 0.8 mL) in a glass beaker. Then, potassium hydroxide (0.6 g) dissolved in water (4 mL) was added slowly over 15 min to this slurry, and the mixture was stirred at 25°C for 16 h. Afterward, the mixture was filtered, and the residue obtained was dried at 70°C overnight (Chan, 1993). The reaction inputs of the applied method according to the desired degree of crosslinking are summarized in the supplementary for chapter 4 in Table D.1.

4.2.2.2. Characterization of the Cellulose-Based Polymers

SEM was used to explore the textural properties of polymer materials with a Quanta 250 SEM equipment. The SEM photomicrographs of the materials whose free surfaces were coated with thin gold layers were taken in the 3.0-5.0 kV accelerating voltage range.

To determine the change in phosphorylated FC bond structures with and without crosslinking, a Shimazdzu FTIR-8400S spectrophotometer equipment was used to acquire IR spectra of 4000-400 cm^{-1} with a resolution of 4 cm^{-1} and 24 scans per sample. The KBr pellet approach was used to obtain IR spectra by scanning solid pellets containing roughly 2 mg of cellulosic material and 148 mg of spectroscopically pure KBr.

The samples' Brunauer–Emmett–Teller (BET) surface area and pore size were evaluated using the Micromeritics Gemini V analyzer and the N_2 adsorption–desorption method at 77 K. Analysis chamber containing samples was vacuumed up to a pressure of 20 mTorr for the first 2 h at 70°C and then at 90°C for 12 h.

A thermogravimetric analyzer (Shimadzu, TGA-51) was used to determine detectable thermal stability and heat capacity variations. Thermograms were acquired by dynamic heating under a nitrogen environment from 20 to 1000°C with a heating rate of 5°C/min.

4.2.2.3. Equilibrium Swelling Test

Approximately 50 mg of phosphorylated FC and its cross-linked forms were equilibrated in 12 mL of distilled water at 25°C for 72 h to investigate the swelling property. The hydrated polymer was obtained by centrifuging three times at 8°C at 7000 rpm for 15 min and completely withdrawing the remaining water until it reached a constant weight. The swelling rate (S_w) was calculated using Eq. (4.1), which includes the weight of the hydrated polymer (W_s) and the dry weight of the polymer (W_d):

$$S_w\ (\%) = \frac{W_s - W_d}{W_d} \times 100 \qquad (4.1)$$

4.2.2.4. Batch Studies for the Effect of Crosslinking on Lithium Sorption Efficiency

To investigate the effect of crosslinking on lithium sorption efficiency, the synthesized phosphorylated FC and its cross-linked forms with ECH at different ratios of 2-ECH (0.02 mL ECH/g FC), 4-ECH (0.04 mL ECH/g FC) and 8-ECH (0.08 mL ECH/g FC) were tested with a 12 g L^{-1} sorbent dose, a solution having 10 mg L^{-1} initial concentration of Li, via shaking at 30°C for 24 h in a batch-mode operation. Li concentrations were determined with the ICP-OES equipment.

4.2.2.5. Lithium Sorption–Desorption Studies in the Packed Bed Dynamic Column

A 0.7 cm diameter and 12 cm high glass column filled with cross-linked phosphorylated FC at a ratio of 0.04 mL ECH/g FC was used for the chromatographic separation of lithium from the aqueous solution. The schematic drawing of the experimental setup is given in Figure 4.1. First, the effect of the flow rate on lithium sorp-

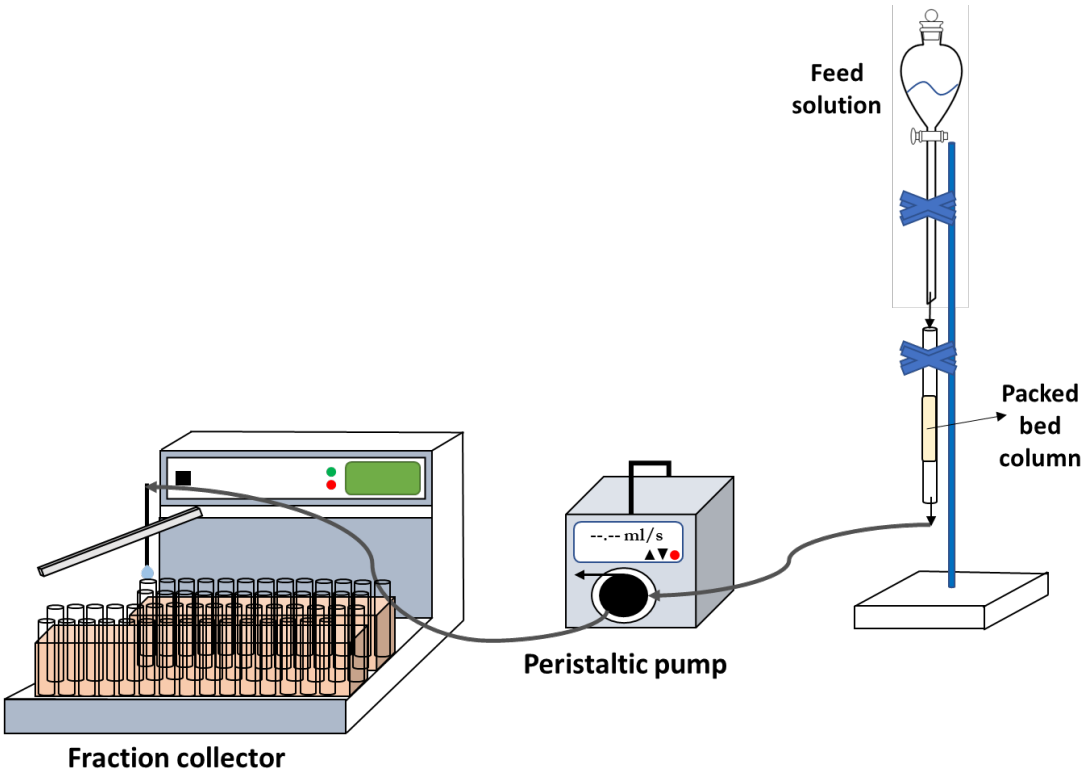

Figure 4.1. Schematic experimental setup representation of the column study

tion was investigated by feeding the solution with an initial lithium concentration of 10 mg L^{-1} at different flow rates (0.25, 0.5-, and 1.0-mL min^{-1}) in a 1.5 cm bed height column from the top to bottom. In addition, the effect of bed height on lithium sorption was investigated with a flow rate of 0.5 mL min^{-1} at different bed heights (1.0, 1.5, and 2.0 cm). Samples (3 mL) were collected by time in lithium sorption experiments. Lithium desorption experiments were performed with a 5% by volume (0.51 M) H_2SO_4 solution at a flow rate of 0.12 mL min^{-1} by collecting a 2 mL fraction with the setup consisting of a peristaltic pump (SHENCHEN) and a fraction collector (BÜCHI C-660). The lithium concentration of the samples was determined with the help of a flame photometer (JENWAY PFP7) equipment.

Breakthrough curves showing the performance of fixed-bed column sorption were plotted as bed volume (BV) versus normalized concentration (C/C_0), defined as the ratio of the effluent lithium concentration (C, mg L^{-1}) to inlet lithium concentration (C_0, mg L^{-1}). BV (mL solution/mL sorbent) was calculated by Eq. (4.2):

$$BV = \frac{Q.t}{V} \tag{4.2}$$

where t is the operating time (min), Q is the flow rate of feed solution (mL/min), and V is the wet volume of sorbent packed in the column (mL).

4.3. Modeling of Packed Bed Column Dynamic Behavior

Modeling of experimental data is used to successfully design a column adsorption process and provide mathematical and quantitative approaches. Breakthrough curves for the adsorption of both inorganic ions and organic compounds in a fixed bed column are simulated with the frequently used models such as the Thomas model, the Yoon–Nelson model, and the MDR model to describe the dynamic behavior (Zhang et al., 2019). In this study, these three models were also evaluated to predict the rate and capacity parameters from breakthrough curves of Li sorption onto cross-linked phosphorylated FC.

4.3.1. Thomas Model

The Thomas model assumes the second-order reversible reaction kinetics, and the Langmuir isotherm is one of the most commonly used models to describe breakthrough curves. Specifically, it is convenient to predict the adsorption process in which internal and external diffusion are not rate-limiting steps (Thomas, 1948; Wang et al., 2016). The Thomas model can be expressed as in Eq. (4.3) below:

$$\frac{C}{C_0} = \frac{1}{1 + \exp\left(K_T(q_o m - C_0 \vartheta)/Q\right)} \tag{4.3}$$

where K_T [mL/(min mg)] is the Thomas rate constant and ϑ (mL) is the total volume of solution passing through the column at any given time. q_o is the sorption capacity (mg g^{-1}), and m is the dry weight of the sorbent filled in the column. Other parameters have been defined previously.

The linearized form of the Thomas model can be written as in Eq. (4.4). K_T and adsorption capacity q_o values can be found from the slope and intercept of the graph between ln((C_0/C)-1) and time (ϑ/Q), respectively.

$$ln\left(\frac{C_0}{C} - 1\right) = \frac{K_T q_o m}{Q} - \frac{K_T C_0}{Q}\vartheta \tag{4.4}$$

4.3.2. Yoon–Nelson Model

A relatively simple model focusing on the adsorption of gases or vapors on activated carbon was developed by Yoon–Nelson. The basic assumption made for this model to be applicable is the rate of decrease in the adsorption probability for each adsorbed molecule is proportional to the sorption probability of the adsorbed molecule and the probability of the molecule being adsorbed on the adsorbent (Liu et al., 2020; Yoon and Nelson, 1984). The Yoon–Nelson equation is given as follows:

$$\frac{C}{C_o} = \frac{\exp\left(K_{YN}t - \tau K_{YN}\right)}{1 + \exp\left(K_{YN}t - \tau K_{YN}\right)} \tag{4.5}$$

where K_{YN} is the rate constant (min^{-1}), and τ (min) is the time required for 50% of the

molecule to be adsorbed to pass when the concentration (C, mg L^{-1}) is half of the initial concentration (C_0, mg L^{-1}). K_{YN} and τ can be found from the slope and intercept of the graph (ln(C/(C_0-C)) versus t) plotted for the linearized form of the Yoon–Nelson model given in Eq. (4.6):

$$\ln \frac{C}{C_o - C} = K_{YN} t - \tau K_{YN} \tag{4.6}$$

According to the Yoon–Nelson model, the adsorption capacity (q_0, mg/g) can be calculated using Eq. (4.7). The model claims that the amount of lithium adsorbed by the sorbent is half of the initial lithium concentration passing through the packed column in the 2τ period (İpek et al., 2013).

$$q_o = \frac{1}{2}\frac{(C_o Q 2\tau)}{m} = \frac{(C_o Q \tau)}{m} \tag{4.7}$$

4.3.3. Modified Dose–Response Model

The MDR model is another simplified mathematical model used to evaluate the dynamic behavior of packed bed column adsorption data. This model reduces the error caused by using the Thomas model, especially at lower or higher periods of the breakthrough curve (Ting et al., 2021). The mathematical model is expressed in Eq. (4.8):

$$\frac{C}{C_0} = 1 - \frac{1}{1 + \left(\frac{\vartheta}{b}\right)^a} \tag{4.8}$$

a and b are model constants, b specifies the output volume producing a half-maximum response, and a determines the slope of the regression function. From the b value, the value of the maximum solid-phase concentration of the solute (q_0) can be calculated using Eq. (4.9):

$$q_0 = \frac{bC_o}{m} \tag{4.9}$$

The model parameters were determined by fitting the experimentally obtained data with the help of MATLAB software using the nonlinear regression technique for the

MDR model given in Eq. (4.8). The sum of the squares of the differences between the experimental data and the theoretical data (calculated from the models) was taken into account in error analysis to find the best-fitted model. The sum of squares of error (SSE) can be obtained from the following equation:

$$SSE = \frac{\Sigma\left(\left(\frac{C}{C_o}\right)_{theo} - \left(\frac{C}{C_o}\right)_{exp}\right)^2}{N} \quad (4.10)$$

$(C/C_0)_{theo}$ is the ratio of the outlet and inlet lithium concentration obtained from the model, $(C/C_0)_{exp}$ is the ratio of lithium concentration in the outlet and inlet water obtained from the experiment, and N is the total number of experimental points.

4.4. Results and Discussion

4.4.1. Characterization of Synthesized Cross-Linked Phosphorylated Functional Cellulose

4.4.1.1. SEM Analysis

Figure 4.2 shows the surface morphology of phosphorylated FC materials, where Figure 4.2(a) belongs to only phosphorylated FC fibers (without cross-linking). In contrast, Figure 4.2(b)–(d) belongs to cross-linked phosphorylated FC with a different cross-linking agent, ECH, with ratios of 0.02 mL, 0.04 mL, and 0.08 mL ECH/g, respectively. As the ratio of ECH increased, more porous structures were formed, although the network tended to agglomerate based on the formation of more crosslinks. SEM images support the formation of interconnected pores and capillary channels because it is known that at a higher ECH ratio, higher branching polymer chains are produced and an additional network is formed (Winarti et al., 2018). In addition, ECH crosslinking in cellulose results in a macroporous interior, as evidenced by the BET analysis, the findings of which will be discussed elaborately later. The high ECH ratio increased the pore size, which can be explained by the slow cross-linking process at low temperatures with strong self-assembly of the free hydroxyl groups between cellulose chains.

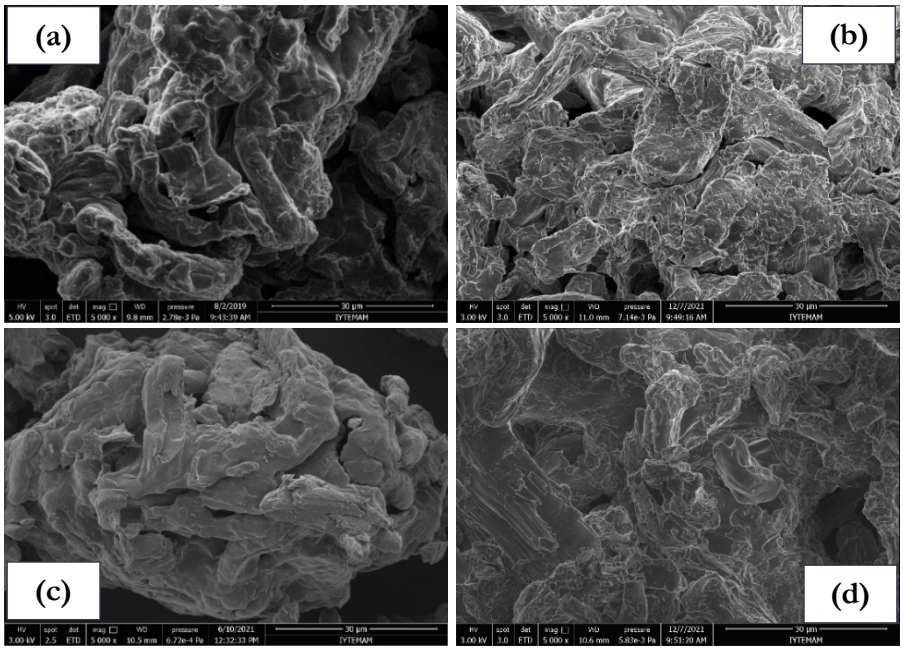

Figure 4.2. SEM surface morphology (magnification 5,000x): **(a)** only phosphorylated, crosslinked with the ratio of **(b)** 0.02 mL ECH/g FC, **(c)** 0.04 mL ECH/g FC and **(d)** 0.08 mL ECH/g FC phosphorylated functional cellulose

4.4.1.2. FTIR Analysis

The Fourier transform infrared (FTIR) spectroscopy is one of the characterization techniques used to verify cross-linked structures as it gives spectral properties from the formation of new binding arrangements or functional groups. Figure 4.3 illustrates FTIR spectra of phosphorylated FC alone and phosphorylated FC cross-linked with ECH at different ratios (0.02 mL, 0.04 mL and 0.08 mL/g FC). The spectrum shows broadband attributable to intermolecular bonds such as hydroxyl (–OH) groups at 3000–3600 cm^{-1}, C–H stretching at 2800–3000 cm^{-1}, O–H and C–H bending and C–O–H and C–O–C asymmetric stretching at 1400–1300 cm^{-1} and 1000–1200 cm^{-1}, respectively. Besides the relative signal intensities that grow and sharpen with higher ECH content, these bands are nearly identical to the various phosphorylated cellulose materials. Meanwhile, due to the stoichiometric excess of the crosslinker, self-crosslinking of the –OH group of ECH at the C2 position and hydrolysis of ECH may cause weakening of these bands in places. In general, ECH is more likely to self-crosslink when the present –OH groups of the cellulose react or become sterically unavailable due to crosslinking and/or the fibrous character of the cellulose (Udoetok et al., 2016). This stepwise crosslinking process explains the lower density of the –OH band (3000-3600 cm^{-1}) for

this polymer compared to FC cross-linked with 0.08 mL ECH/g compared to other peak densities. Also, the C–O band at 1050–1200 cm^{-1}, where new peaks appear due to the formation of new C–O bonds, is a marker for confirmation of successful crosslinking.

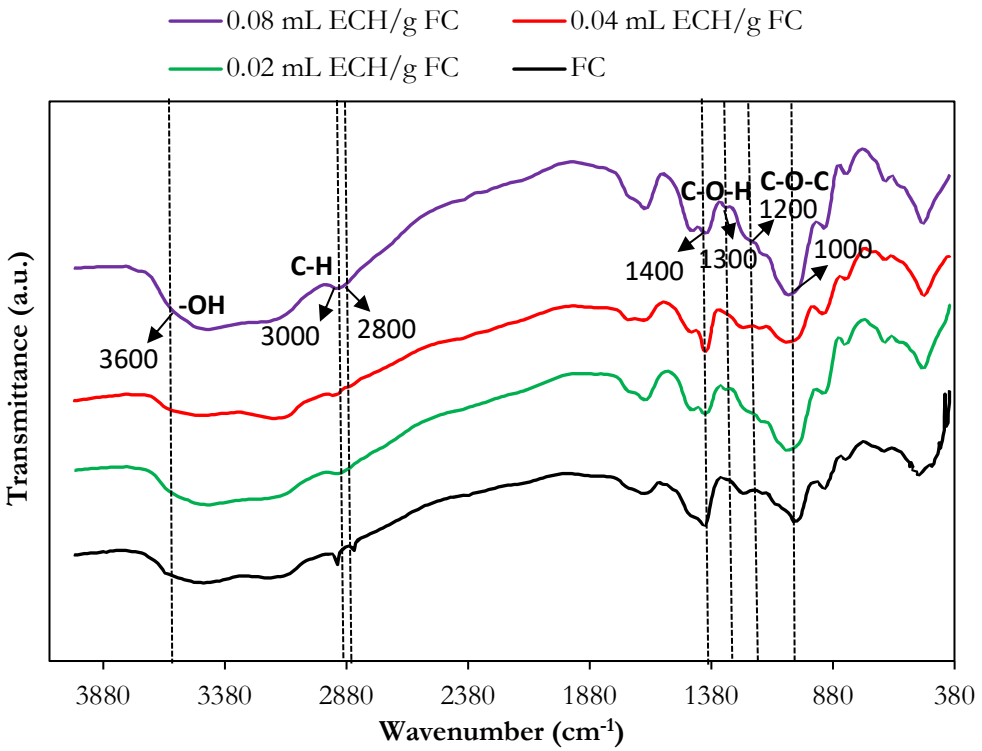

Figure 4.3. Micro-FTIR spectra of phosphorylated functional cellulose (FC) alone and its cross-linked forms with epichlorohydrin (ECH) at different rates (0.02 mL, 0.04 mL, and 0.08 mL/g FC)

4.4.1.3. BET Analysis

BET surface areas and Barrett–Joyner–Halenda (BJH) cumulative pore volume percentages for phosphorylated FC and its cross-linked forms at different ratios are listed in Table 4.1. In general, BET surface area values of less than 1 m^2 g^{-1} were observed to decrease with the increasing crosslinking ratio for all modified materials. Because functional groups are attached to the surface of the material, FC and its cross-linked form in different proportions commonly have macropores. While the macropore volume in phosphorylated FC was 49.01% when the crosslinking ratio was increased from 2-ECH to 8-ECH, the percentage of macropores in the structure of the material increased from

58.80 to 73.25%. Relatively decreasing surface area and increasing macropores can be explained by the fact that the two free hydroxyl groups of the cellulose molecule bond with each other, as well as the hydrogen bonding effects of the phosphorous functional groups in the structure of the material with each other, and thus, that may also cause to decrease in the active sites where lithium can be retained.

Table 4.1. Pore structure parameters and BET surface areas for phosphorylated functional cellulose (FC) alone and its cross-linked forms with epichlorohydrin (ECH) at different rates (0.02 mL, 0.04 mL, and 0.08 mL/g FC).

	pore volume (%)			BET surface area (m^2/g)	total pore volume (cm^3/g)
material	micropore (< 2 nm)	mesopore (2–50 nm)	macropore (>50 nm)		
FC	17.75	33.24	49.01	0.95	0.0004
2-ECH	22.89	18.31	58.80	0.79	0.0003
4-ECH	6.23	25.09	68.68	0.76	0.0006
8-ECH	7.44	19.31	73.25	0.73	0.0005

4.4.1.4. TGA Analysis

TGA is one of the sensitive characterization methods for observing crosslinking reactions due to measurable differences in thermal stability and heat capacity of pure and cross-linked materials (Mohamed et al., 2015). The TGA results of phosphorylated FC that is not cross-linked and cross-linked with ECH at different ratios and the thermal stability profile of thermal degradation events between 20 and 1000°C are shown in Figure 4.4. Basically, one minor and two major weight losses are observed for all materials. Data on these findings are given in Table 4.2. Minor weight losses of approximately 2–3% observed in raw and cross-linked phosphorylated FC materials in the temperature range of 86–95°C are due to the evaporation of water molecules adsorbed by the materials. Depending on the primary major weight losses, thermal degradation events were recorded between 200 and 250°C. Non-crosslinked phosphorylated cellulose decomposed at ~200 to 213°C, while the cross-linked polymers showed offset values: 2-ECH (~245°C), 4-ECH (~236°C), and 8-ECH (~250°C). These results indicate that the main degradation events for cross-linked polymers occur at higher temperatures than for non-cross-linked phosphorylated cellulose. The situation at temperatures where primary

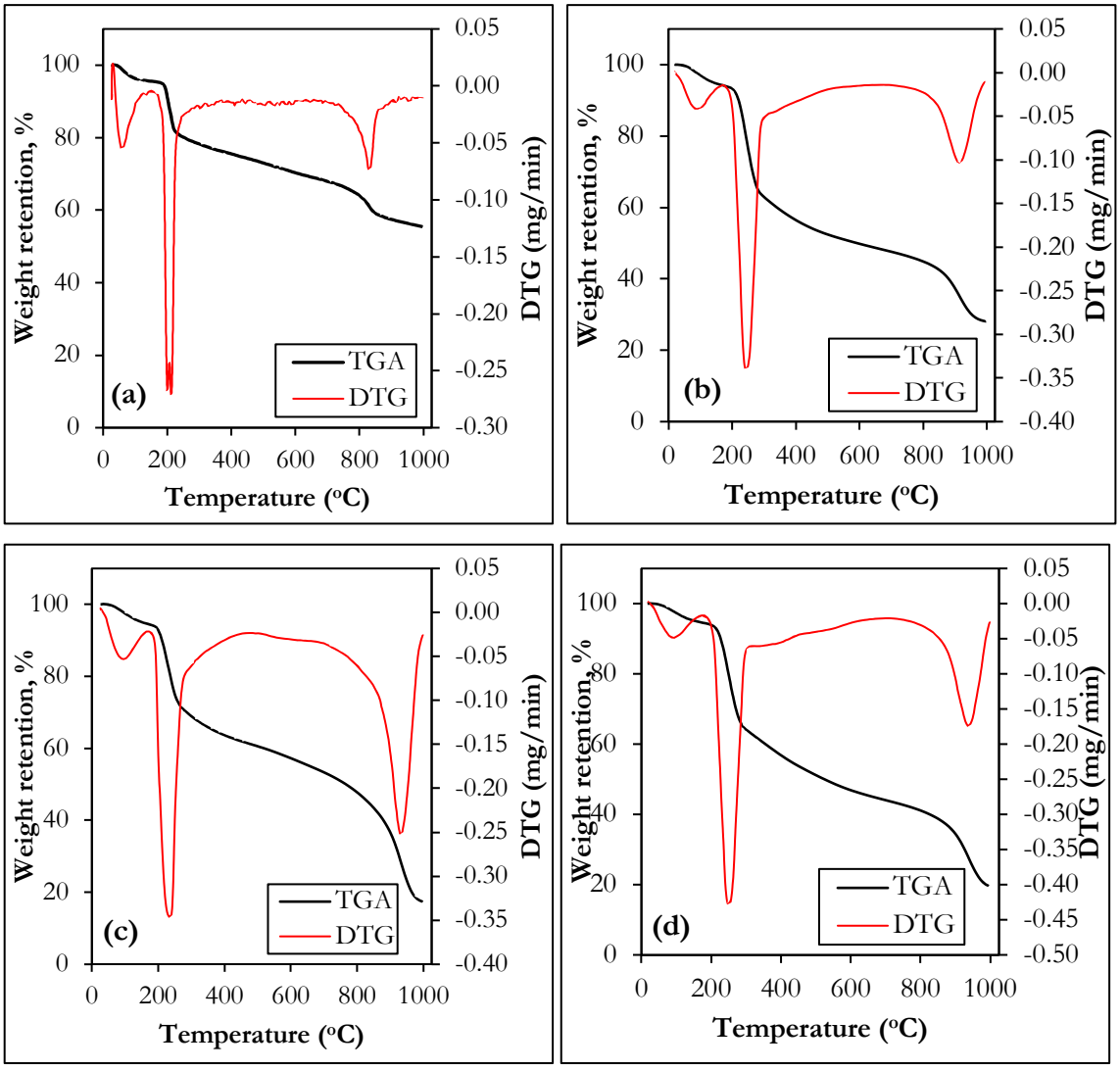

Figure 4.4. Thermogravimetric analysis curves of functional cellulose **(a)** phosphorylated only, cross-linked at **(b)** 0.02 mL ECH/g FC, **(c)** 0.04 mL ECH/g FC, and **(d)** 0.08 mL ECH/g FC ratios.

major weight loss is observed indicates that the glycosidic bonds in the cellulose structure are degraded. On the other hand, phosphorus-containing functional groups are known to increase the thermal degradation reaction of the cellulosic polymer (and thus decrease the heat resistance of the material) but instead significantly increase the carbonization (and, therefore, the flame resistance) (Kokol et al., 2015). Furthermore, cellulosic polymers containing phosphoryl compounds exhibit flame retardant qualities, according to the literature (Aoki and Nishio, 2010; Belosinschi et al., 2012; Shi et al., 2014). Based on this, the secondary major weight losses observed in all materials in the temperature range of 830–940°C are the temperatures at which phosphorous functional groups decompose. As the crosslinking ratio increased, the weight losses of the materials increased, but the

maximum decomposition temperature shifted from 832 to 937°C. 8-ECH was higher thermal durability due to the higher crosslinking ratio. The lower temperatures where primary major weight losses were observed are attributed to the covalent bond interaction of the polymer framework. In contrast, the higher temperature event secondary to major weight losses can be explained by the reduction in heat capacity and hydrogen bond interactions between the cellulose chains. This trend also coincides with structural effects from crosslinking, such as the macropore formation and related changes in heat capacity observed for similar types of cross-linked materials (Udoetok et al., 2016).

Table 4.2. TGA findings of crude and cross-linked phosphorylated functional cellulose

material	minor weight loss		primary major weight loss		Secondary major weight loss		The mass remained at the end of 1000°C (%)
	Temperature (°C)	Weight loss (%)	Temperature (°C)	Weight loss (%)	Temperature (°C)	Weight loss (%)	
FC	91	3.32	200-213	11.37	832	24.52	55.40
2-ECH	86	2.10	245	18.76	912	43.76	28.04
4-ECH	95	2.20	236	17.50	933	52.20	17.30
8-ECH	91	2.15	250	17.97	937	52.08	19.52

4.4.1.5. Equilibrium Swelling Properties of Hydrophilic and Cellulosic Materials

Lists of the findings of equilibrium swelling tests of phosphorylated FC and its cross-linked forms are listed in Table D.2. The results show that phosphorylated FC has a higher swelling ratio than cross-linked polymers, which is consistent with independent expectations. As the ECH increased, the material turned into a more rigid structure and the swelling ratio decreased. This decreasing trend can be explained by less passage of water into the fiber domains of cellulose. It has been observed that the change in the swelling ratio is more minor when the cross-linker ratio is increased from 4-ECH to 8-ECH, compared to the variation in the swelling ratio from 0 to 2-ECH and from 2-ECH to 4-ECH. Based on this, the optimum crosslinking rate was determined as 4-ECH (0.04 mL ECH/g FC). Then, the effect of crosslinking on lithium sorption was also investigated to strengthen the selection of the optimum crosslinking ratio.

4.4.2. Effect of Cross-Linking on Lithium Sorption Efficiency

Removing contaminants from wastewater at a large scale economically would open up new technological frontiers, and natural carbohydrate polymeric materials and tunable and sensitive materials are in great demand (Hasan et al., 2021; Munjur et al., 2020). In Figure 4.5, the lithium sorption percentages of phosphorylated FC without crosslinking and crosslinking at different ratios were compared via a batch-mode operation. According to the findings, the lithium sorption of phosphorylated FC without crosslinking was 92.59%, and the yield decreased gradually as the cross-linker ratio increased. Lithium sorption efficiency was 85.25% at the highest cross-linker ratio (0.08 mL ECH/g FC). This situation can be explained by the fact that the two free hydroxyl groups of cellulose are bonded to each other, as well as the decrease in the active sites where lithium can be retained due to the hydrogen bonding effects of the phosphorous functional groups in the structure of the material with each other. As reported in our pre-

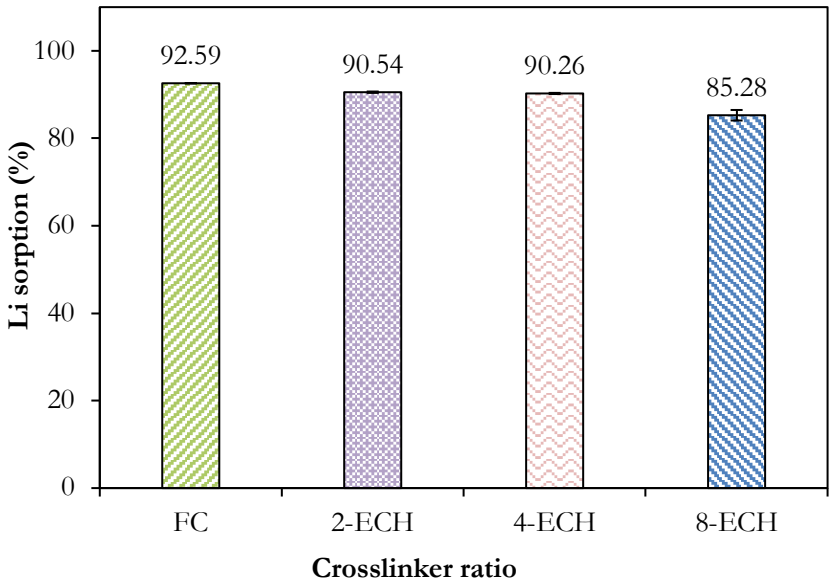

Figure 4.5. Comparison of lithium sorption efficiencies of phosphorylated functional celluloses without crosslinking and with crosslinking via epichlorohydrin at different ratios.

vious study (Recepoğlu and Yüksel, 2021a), according to the crosslinking structure of phosphorylated cellulose and its combined stoichiometry, a P/Li atom ratio was obtained at approximately 1.03 from XPS measurements, indicating the presence of these phosphorous moieties on the adsorbent surfaces because one Li^+ is exchanged with H^+ in

the functional group and the expected ion exchange mechanism is given in Eq. (4.11).

$$Cellulose-O-\underset{\underset{OH^+}{|}}{\overset{\overset{O}{||}}{P}}-Cellulose+Li^+ \leftrightarrow Cellulose-O-\underset{\underset{OLi^+}{|}}{\overset{\overset{O}{||}}{P}}-Cellulose+H^+ \qquad (4.11)$$

Hence, considering both the swelling ratio and lithium sorption efficiency of the material, the optimum cross-linker ratio was determined as 0.04 mL ECH/g FC and phosphorylated FC cross-linked at this ratio was used in further column studies.

4.4.3. Packed Bed Column Studies of Cross-Linked Phosphorylated Functional Cellulose

The breakthrough time that gives the operating life of the adsorbent in a single adsorption process and breakthrough capacity are significant parameters that entirely affect the performance of the column adsorption process. The breakthrough time is directly related to the ratio of the outlet concentration to the inlet concentration. Namely, the value of 0.05 as the breakthrough time is taken as the ratio between the effluent and the feed concentrations for the removal of heavy metal ions from water in fixed bed operations. However, because it was aimed to recover a valuable metal in this study, based on the literature, the breakthrough time (t_b, min) was defined as the time required for the lithium extraction rate to decrease to 0.6 and is expressed by Eq. (4.12) (Jiang et al., 2020b). In other words, the time when the solution with an initial concentration of 10 mg L^{-1} is obtained as approximately 4 mg/L at the effluent was accepted as the breakthrough time. The breakthrough capacity and column utilization degree were calculated according to this assumption:

$$1-\frac{\int_0^{t_b} C/C_0\,dt}{t_b}=0.6 \qquad (4.12)$$

4.4.3.1. Effect of Flow Rate on Lithium Sorption Capacity in a Packed Bed Column

Flow rate is an important parameter to determine the effectiveness of sorbents in the continuous treatment of wastewater. The breakthrough curves of lithium sorption obtained with varying flow rates at constant inlet lithium concentration (10 mg L^{-1}) and bed height (1.5 cm; 0.58 mL sorbent) are given in Figure 4.6(a). The trend of the breakthrough curves has been obtained as commonly observed in liquid phase adsorption, where intraparticle diffusion is the rate-limiting transport process (Kofa et al., 2015; Srivastava et al., 2008; Yagub et al., 2015). The effect of the feed flow rate on the breakthrough point was particularly pronounced when it decreased from 1.0 to 0.25 mL min^{-1}, with an increase in the flow rate found to increase the sharpness of the breakthrough curve. Also, increasing the flow rate shifted the breakthrough curves significantly from right to left, indicating that the service time of the fixed bed is reduced. The higher the flow rate, the earlier the release. Table 4.3 compares and summarizes the study results such as capacity, elution efficiency, and column utilization degree obtained using cross-linked phosphorylated FC at different flow rates. As the flow rate increases from 0.25 to 1.0 mL min^{-1}, the BV required for release has fallen from 477 mL solution/mL sorbent to 386 mL solution/mL sorbent, as there is a decrease in mass transfer rate and faster lithium passes through the column. The breakthrough capacities at the three flow rates (0.25, 0.5-, and 1.0-mL min^{-1}) were 25.82, 23.60, and 18.81 mg g^{-1}, respectively, while the total capacities were 33.56, 30.15, and 25.54 mg g^{-1}. The decrease in capacity as the flow rate increases can be explained by the insufficient residence time of lithium ions in the column and the intraparticle diffusion to the reaction sites, which limited the mass transfer rate at a high flow rate (Goshadrou and Moheb, 2011; Malkoc et al., 2006). Operating at a flow rate of 0.25 mL min^{-1}, the BV for the total capacity was 1260, i.e., 730 mL of a solution containing 10 mg L^{-1} Li took approximately 2900 minutes (48 h) to saturate the material. Compared to the previously published capacity of phosphorylated FC, the material exhibited a much higher lithium uptake capacity when used in the column, despite its cross-linking structure. As a result of batch sorption studies, the maximum lithium retention capacity was determined as 9.60 mg/g (Recepoğlu and Yüksel, 2021a). In addition, lithium elution curves for all sorption tests carried out at different flow rates are plotted in Figure 4.6(b). The desorption rate was fast and slowed down with a decrease in the effluent Li concentration from higher than 625 mg L^{-1} to lower than 1 mg L^{-1} and,

subsequently, zero in a few fractions and time, resulting in ca.100% elution efficiencies at all studied flowrates. Only 15.75 mL of 5% H_2SO_4 solution (0.51 M) was required to desorb approximately 100% of Li from the saturated sorbent to do the desorption. This shows that the lithium retained by the material can be easily and completely recovered Li in the concentrated acid can be purified and precipitated for further use.

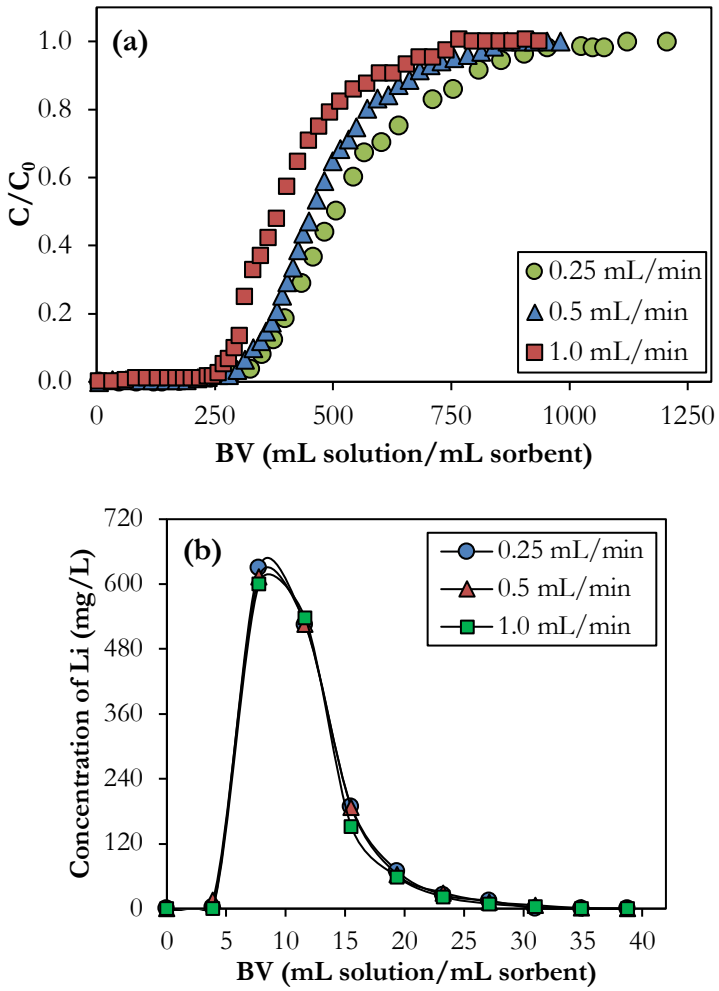

Figure 4.6. **(a)** Breakthrough curves **(b)** elution curves of the column filled with cross-linked phosphorylated functional cellulose at 0.04 mL ECH/g FC at different flow rates (C_0=10 mg L^{-1}, T=25°C, bed height=1.5 cm, ϑ=0.25 – 1.0 mL/min)

Table 4.3. Comparison of fixed bed performance at different flow rates

	0.25 mL min^{-1}	0.5 mL min^{-1}	1.0 mL min^{-1}
Breakthrough capacity, mg Li/mL sorbent	4.8	4.4	3.5
Breakthrough capacity, mg Li/g-sorbent	25.8	23.6	18.8
BV at breakthrough point, mL solution/mL sorbent	477	459	386
Total capacity, mg Li/mL sorbent	6.3	5.7	4.8
Total capacity, mg Li/g-sorbent	33.6	30.2	25.5
BV at total capacity, mL solution/mL sorbent	1260	935	857
Degree of column utilization, %	76.9	78.3	73.7
Elution efficiency, %	~100	~100	~100

4.4.3.2. Effect of Bed Height on Lithium Sorption Capacity in a Packed Bed Column

At a constant flow rate of 0.5 mL min^{-1} and a constant feed concentration of 10 mg L^{-1}, the effect of bed height on breakthrough curves, C/C_0 versus time, is demonstrated in Figure 4.7(a). Phosphorylated FC was filled in the column at three different heights, 1.0, 1.5, and 2.0 cm, equivalent to wet sorbent volumes of 0.38, 0.58, and 0.77 cm^3, respectively. A higher bed height altered the breakthrough curve to the right, lengthening the period between breakthrough and saturation. This result could be explained by the increased sorbent mass providing more accessible active sites for sorption at the higher bed height. As the bed height increased from 1.0 to 2.0 cm, the solution that passed through the column at the breakthrough time increased from 196 to 385 mL. As shown in Figure 4.7(b), the three curves closely overlapped when the breakthrough curves were replotted using the number of BVs to abscissa, revealing that the increase in bed height or sorbent volume had almost no effect on the dynamic sorption of Li. As given in Table 4.4, the similar sorption capacity at the breakthrough and total saturation points and the similar degree of column utilization further supported this evidence. The breakthrough times at the three different bed heights (1.0, 1.5, and 2.0 cm) were 362, 491, and 710 min, respectively, and the total capacities were 30.9, 30.2, and 31.7 mg g^{-1}. Moreover, the degree of column utilization for each bed height was 83.8, 78.3, and 81.1%, respectively. Recently, the effect of bed height on lead removal efficiency was investigated and no impact was observed on sorption capacity with different bed heights (Zhang et al., 2019).

Overall, these findings proved that increasing the bed height enhanced the treated water volume for lithium recovery without affecting sorption capacity, paving the way for the widespread use of phosphorylated FC in dynamic column systems. On the other hand, elution curves of the column filled with cross-linked phosphorylated cellulose obtained by plotting the concentration of Li in effluent 5% H_2SO_4 against the BVs at the studied bed heights are illustrated in Figure 4.7(c). The concentrated lithium was the highest for 2.0 cm bed height, depending on the highest total sorption capacity. Because the sorbent is easily regenerated with the acid, almost 100% elution efficiencies were also obtained for each bed height.

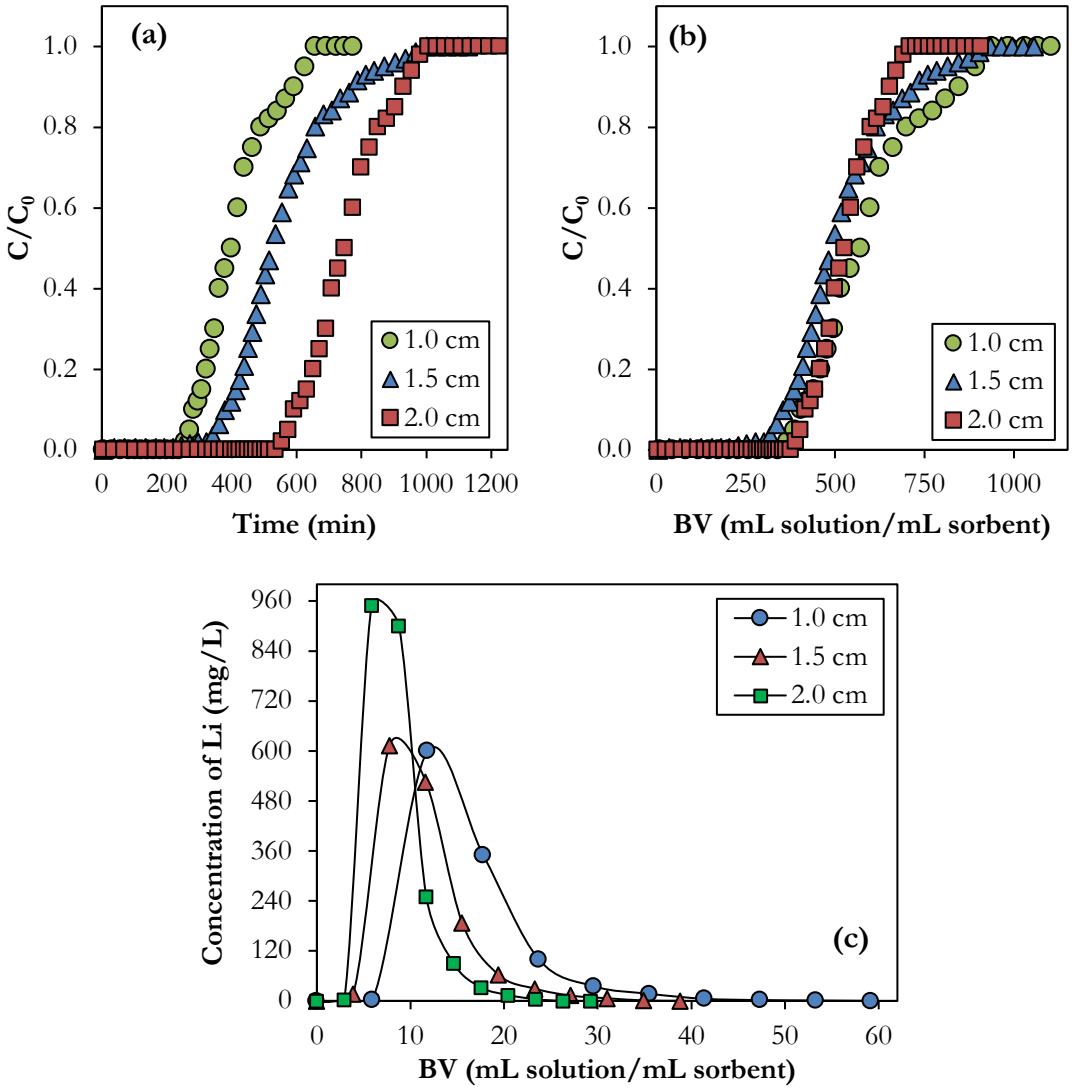

Figure 4.7. **(a)** Breakthrough curves; C/C_0 vs. time, **(b)** Breakthrough curves; C/C_0 vs. bed volumes, **(c)** elution curves of the column filled with cross-linked phosphorylated functional cellulose at 0.04 mL ECH/g FC at different bed heights (C_0=10 mg L^{-1}, T=25°C, ϑ=0.5 mL min^{-1}, bed height=1.0 – 2.0 cm)

Table 4.4. Comparison of fixed bed performance at different bed heights

	1.0 cm	1.5 cm	2.0 cm
Breakthrough capacity, mg Li/mL sorbent	4.8	4.4	4.8
Breakthrough capacity, mg Li/g-sorbent	25.9	23.7	25.7
Breakthrough time, min	362	491	710
Total capacity, mg Li/mL sorbent	5.8	5.7	5.9
Total capacity, mg Li/g-sorbent	30.9	30.2	31.7
Total saturation time, min	659	1001	1007
Degree of column utilization, %	83.8	78.3	81.1
Elution efficiency, %	~100	~100	~100

4.4.4. Modeling of Breakthrough Curves

The breakthrough curves of Li at different flow rates and bed heights were investigated with three commonly used models, Thomas, Yoon–Nelson, and MDR, whose parameters and correlation coefficients (R^2) and SSE values are tabulated in Table 4.5 and Table D.3, respectively, and the figures representing theoretical and experimental data plots for each model at different flow rate and bed height are given in Figure D.1. According to lower SSE values (0.0002–0.0007) and higher correlation coefficient, R^2 (0.996–0.999), reproducing better fitting of experimental data with the theoretical ones, the MDR model has better described the dynamic behavior of Li sorption using phosphorylated FC in a packed bed column.

4.4.4.1. Thomas Model Analysis

Thomas model analysis reveals that the high mass transfer rate led to the values of K_T increasing from 0.458 to 2.018 mL min^{-1} mg^{-1} as the flow rate increased from 0.25 to 1.0 mL min^{-1}. While increasing the flow rate reduced the value of q_0 up to 20.1 mg/g, this was primarily due to the insufficient time for Li diffusion and adsorption. In terms of bed depth, the results showed that the value of K_T decreased from 1.880 to 1.330 mL min^{-1} mg^{-1} as bed depth increased from 1.0 to 2.0 cm, which can be attributed to the longer contact time at greater bed depths. The value of q_0, on the other hand, was observed to increase as the bed depth was increased because the adsorption sites increased. This

suggested that the adsorption rate would be faster at a higher flow rate and lower bed height. Besides, these findings are consistent with those found in the literature (Lu et al., 2019; Metwally et al., 2020). Nonetheless, the model cannot precisely trace the sorption of Li in the column or estimate the minimum height of the adsorption front, allowing for a better understanding of performance. The application of the MDR approach can overcome such a flaw.

4.4.4.2. Yoon–Nelson Model Analysis

Previous studies have effectively employed the Yoon–Nelson model to describe pollutant adsorption in a fixed-bed design (Khalfa et al., 2021). When the Yoon–Nelson model was applied to the experiment data, K_{YN} and τ values were obtained that accurately characterized the packed bed sorption of Li onto the phosphorylated FC. Decreasing the flow rate from 1.0 to 0.25 mL min^{-1} with the same column height resulted in an increase of τ as a longer time is clearly required to saturate the material with Li due to providing sufficient contact time at lower flow rates. However, for 1.0 mL min^{-1} τ fell to 206 min, owing to the fact that a higher flow worsens the mass transfer process (e.g., kinetics and capacity), reducing the time required to recover 50% of Li. When the column height was increased from 1.0 to 2.0 cm, the time to obtain 50% of retention for Li increased from 398.7 to 753.3 min, which is appropriate because the accessible sorbent sites increased correspondingly with column height, which is also supported by the results of previous studies (Dawood et al., 2018; F. Liu et al., 2021).

4.4.4.3. Modified Dose–Response (MDR) Model Analysis

The MDR model shows that as the flow rate increased from 0.25 to 1.0 mL/min, the sorption capacity per unit mass of phosphorylated FC (q_0) decreased from 29.88 to 20.33 mg g^{-1}. When the area of the breakthrough curve of Li for 1.0 and 2.0 cm bed heights at 0.5 mL min^{-1} is similar, the column capacity appears to have a trend opposite to values of q_0 in the MDR model because the column capacity considers the area of the breakthrough curve that is dominated by saturation time. In addition, the values of b

decreased with the increase in the flow rate and increased with an increase in the bed height.

To sum up, the SSE produced from the MDR model was much lower than that obtained from the Yoon–Nelson and Thomas models. As a result, the MDR model outperforms the Yoon–Nelson and Thomas models in predicting the adsorption behavior of phosphorylated FC for lithium sorption from water by chromatographic separation.

Table 4.5. Breakthrough model parameters of Li sorption on phosphorylated functional cellulose.

exp. no.	parameters		model							
	flow rate (mL/min)	bed height (cm)	Thomas		Yoon–Nelson			MDR		
			K_T	q_0	K_{YN}	τ	q_0	a	b	q_0
1	0.25	1.5	0.458	32.5	0.008	998.1	29.3	5.54	0.30	29.88
2	0.5	1.5	1.782	25.0	0.015	495.9	25.4	6.52	0.27	25.31
3	1.0	1.5	2.018	20.1	0.021	206.0	20.1	6.05	0.23	20.33
4	0.5	1.0	1.880	31.0	0.018	398.7	30.4	6.59	0.21	30.25
5	0.5	2.0	1.330	28.4	0.013	753.3	28.4	10.7	0.40	28.05

4.5. Conclusions

Natural carbohydrate polymeric materials and tunable and sensitive materials are in great demand for removing contaminants and recovering valuable minerals economically at large-scale operations such as dynamic column processes. Phosphorylated FC-ECH polymers were synthesized with variable crosslinking ratios (0.02, 0.04, and 0.08 mL ECH/g FC) and characterized via SEM, FTIR, BET, and TGA. Phosphorylated FC was modified via crosslinking with ECH to obtain more water stable and thermally more robust form and employed in a packed bed column to examine its continuous Li recovery capability. The feed flow rate influenced the dynamic recovery of Li by phosphorylated FC, and a lower flow rate was preferred for greater sorption capacity and a better degree of column utilization. As the flow rate increases from 0.25 to 1.0 mL min^{-1}, the BV required for release has fallen from 477 mL solution/mL sorbent to 386 mL solution/mL sorbent, as there is a decrease in mass transfer rate and faster lithium passes through the column. The breakthrough capacities at the three flow rates (0.25, 0.5, and

1.0-mL min^{-1}) were 25.82, 23.60, and 18.81 mg g^{-1}, respectively, while the total capacities were 33.56, 30.15, and 25.54 mg g^{-1}. Meanwhile, (Park et al., 2015) evaluated the applicability of HMO as a sorbent for lithium recovery from seawater having 0.17 mg/L of Li in a fixed bed column and found 3.12 mg/g of total capacity with sorbent dose 5.0 g, superficial velocity 0.15 cm/s for 3 days of operation. The change in the bed height demonstrated almost no effect on sorption capacity. Increasing the bed height enhanced the treated water volume for lithium recovery without affecting sorption capacity. Although the breakthrough times at the three different bed heights (1.0, 1.5, and 2.0 cm) were 362, 491, and 710 min, respectively, and the total capacities were 30.85, 30.15, and 31.68 mg g^{-1}. Thus, the widespread use of phosphorylated FC in dynamic column systems was clarified. The Thomas, Yoon–Nelson, and MDR models were used to examine the breakthrough curves, and the experimental data fitted in the order: MDR>Yoon–Nelson>Thomas. It was discovered that both the Thomas and Yoon–Nelson models might be utilized to forecast the lithium recovery process by comparing the correlation coefficients (R^2) and SSE values under different operating conditions. However, the MDR model best estimates how effluent concentration changes over time during lithium sorption. As a result, due to its adaptability for a continuous system, phosphorylated FC strengthened with crosslinking via ECH was discovered to be a potential sorbent for the extraction of lithium from aqueous solutions in a dynamic packed bed column. Indeed, the cross-linked phosphorylated cellulose-based adsorbent is an improvement because the study's findings suggested that prospective low-cost adsorbents might be made from various lignocellulosic biomass wastes with a high cellulose content and also paved the door for lithium recovery from natural water sources such as geothermal water by continuous processes because the Li sorption capacity in the presence of Na^+, K^+, Ca^{2+}, and Mg^{2+} ions were investigated additionally in our previous batch mode of operation studies (Recepoğlu and Yüksel, 2021a, 2021b). The results showed that the functional group attached to the material exhibited more affinity towards Li among other monovalent cations. On the other hand, in the presence of Ca^{2+} and Mg^{2+}, they highly competed with monovalent ions since they have higher valence and atomic radius as expected, but the material still showed a considerable lithium sorption capacity.

CHAPTER 5

BREAKTHROUGH CURVE ANALYSIS OF PHOSPHORYLATED HAZELNUT SHELL WASTE IN COLUMN OPERATION FOR CONTINUOUS HARVESTING OF LITHIUM FROM WATER*, †

5.1. Introduction

Lithium, a valuable and widely used alkali metal, plays a crucial role in various industrial applications, including the manufacturing batteries for electric vehicles and renewable energy storage systems (Harper et al., 2019). Limited mineral rocks and the increasing demand for lithium have led to a pressing need for efficient and environmentally friendly methods to extract and recover this strategic metal from various aqueous sources such as seawater, geothermal water, and salt-lake brines (Swain, 2017). One promising approach is using biosorbents derived from agricultural waste, which offer an eco-friendly and cost-effective solution for lithium sorption (Yelatontsev, 2023).

Green composites focus on utilizing renewable materials to enhance economic sustainability using biomass resources. For example, an affordable composite biosrorbent was developed by modifying eggshell material with heteropoly acid to eliminate strontium ions from aqueous solutions (Metwally et al., 2017). Almond, cocnut, walnut, and hazelnut shells, along with apricot, olive, and cherry stones, as well as rice husk and sawdust, are excellent starting materials due to their widespread availability, low cost, and favorable physical and chemical attributes for crafting carbon-based adsorbents from agricultural byproducts (Kaya et al., 2018). In particular, hazelnut shells, abundant agricultural waste produced in large quantities worldwide, have gained attention as a potential biosorbent due to their plentiful availability, low cost, and high lignocellulosic content (Puliga et al., 2022; Stjepanović et al., 2022). Also, the modification of hazelnut

*This chapter has been published as: Y. K. Recepoğlu, Ö. Arar, A. Yüksel, Breakthrough curve analysis of phosphorylated hazelnut shell waste in column operation for continuous harvesting of lithium from water, Journal of Chromatography A, 1713 (2024) 464510.

†This chapter was partly presented orally at 5th INTERNATIONAL ENVIRONMENTAL CHEMISTRY CONGRESS **(EnviroChem)**, 30 October – 2 November 2023, Antalya, Türkiye.

shell waste has shown significant potential in enhancing its sorption capabilities for various contaminants such as dyes, organic pollutants, heavy metals, and metalloids (Al-Ajji and Al-Ghouti, 2021; Altun et al., 2021; Chen et al., 2020; Guler and Solmaz, 2022; Guo et al., 2023; Turan and Turan, 2022). As discussed elaborately in our previous study, the phosphorylation process introduces functional groups onto the hazelnut shell surface, increasing its affinity for metal ions, including lithium (Recepoğlu and Yüksel, 2021b).

The utilization of a biosorbent in the column under dynamic flow has several advantages over traditional batch sorption methods. Column operations allow for better understanding of the sorption kinetics, breakthrough curves, and performance of the biosorbent under continuous flow conditions, mimicking real-world applications. Moreover, column studies provide valuable insights into the sorption capacity, efficiency, and the potential for regenerating and reusing the biosorbent, which are critical considerations for large-scale applications (Patel, 2019). Indeed, while high pressure drops from tightly packed small particles in a long bed and low adsorption rates because the majority of binding sites are located inside the pores of the adsorbents, requiring intra-particle diffusion, are common challenges for the traditionally packed bed column, column adsorption is more convenient in industrial applications than batch adsorption because it is more straightforward, requiring no additional operations such as filtration or separation (Li et al., 2016; Recepoğlu et al., 2018a, 2018b).

In batch-scale operations, biosorption employing phosphorylated hazelnut shell waste (FHS) revealed excellent lithium removal and recovery efficiency. This study aims to investigate the sorption behavior of lithium onto FHS biosorbent in a column setup. The specific objectives include evaluating the sorption capacity, breakthrough characteristics, and the influence of operating parameters such as flow rate, and column bed height on the sorption performance. The results obtained from this research will contribute to a deeper understanding of the potential application of FHS as a sustainable and efficient biosorbent for lithium recovery. The three conventional breakthrough models of the Thomas, Yoon-Nelson, and Modified Dose-Response (MDR) were used to properly estimate the whole breakthrough behavior of the FHS column and to estimate the characteristic model parameters. Overall, the utilization of FHS biosorbent in column studies for lithium sorption presents a promising avenue for sustainable resource recovery. This research endeavors to shed light on the sorption behavior and performance of this biosorbent, paving the way for its potential implementation in large-scale lithium extraction and recovery processes.

5.2. Experimental Section

5.2.1. Materials

FHS synthesized as described in our previous work (Recepoğlu and Yüksel, 2021b) was used without further modification. Lithium chloride (LiCl, AR, 99%), and sulfuric acid (H_2SO_4, 95– 97%) were purchased from Merck. Deionized water was used for the preparation of all aqueous solutions. All chemical reagents were used as received.

5.2.2. Methods

5.2.2.1. Lithium Sorption-Desorption Studies in Packed Bed Dynamic Column

Like the case for cross-linked phosphorylated FC (see Chapter 3) for the chromatographic separation of lithium from the aqueous solution, a 0.7 cm diameter and 12 cm height glass column filled with FHS was utilized. Figure 5.1 depicts the experimental setup. First, the influence of flow rate on lithium sorption was examined by feeding a solution with an initial lithium content of 10 mg L^{-1} at varied flow rates (0.25, 0.5-, and 1.0-mL min^{-1}) from top to bottom in a 1.5 cm bed height column. Furthermore, the influence of bed height on lithium sorption was studied using a flow rate of 0.5 mL min^{-1} at various bed heights (1.0, 1.5, and 2.0 cm). In lithium sorption studies, 3 mL of samples were collected by time using a peristaltic pump (SHENCHEN model) and a fraction collector (BÜCHI C-660). Lithium desorption studies were carried out using a 5% by volume (0.51 M) H_2SO_4 solution at a flow rate of 0.12 mL min^{-1} and a 2 mL fraction collected. The lithium concentration in the samples was tested using a flame photometer (JENWAY PFP7).

Breakthrough curves showing the performance of fixed-bed column sorption were plotted as bed volume versus normalized concentration (C/C_0), defined as the ratio of effluent lithium concentration (C, mg/L) to inlet lithium concentration (C_0, mg L^{-1}). Bed volume (BV, mL solution/mL sorbent) was calculated by Eq. (5.1):

$$BV = \frac{Q.t}{V} \tag{5.1}$$

where Q is the feed solution flow rate (mL/min), t is the operating time (min), and V is the sorbent wet volume (mL).

The breakthrough time and capacity are important parameters in the column adsorption process, with the breakthrough time representing the adsorbent's operating life in a single adsorption phase. In general, the breakthrough time is determined by the ratio of the output concentration to the input concentration. For example, in the removal of heavy metal ions, the ratio of the output concentration to the input concentration is considered as 0.05 for the breakthrough time. However, because the goal of this work was to recover a valuable metal, the breakthrough time (t_b, min) was set as the time necessary for the lithium extraction rate to drop to 0.6, as indicated by Eq. (5.2) below (Jiang et al., 2020). In other words, the breakthrough time was accepted as the period when a solution with an initial concentration of 10 mg L^{-1} was acquired as about 4 mg L^{-1} in the effluent.

$$1 - \frac{\int_0^{t_b} C/C_0 \, dt}{t_b} = 0.6 \tag{5.2}$$

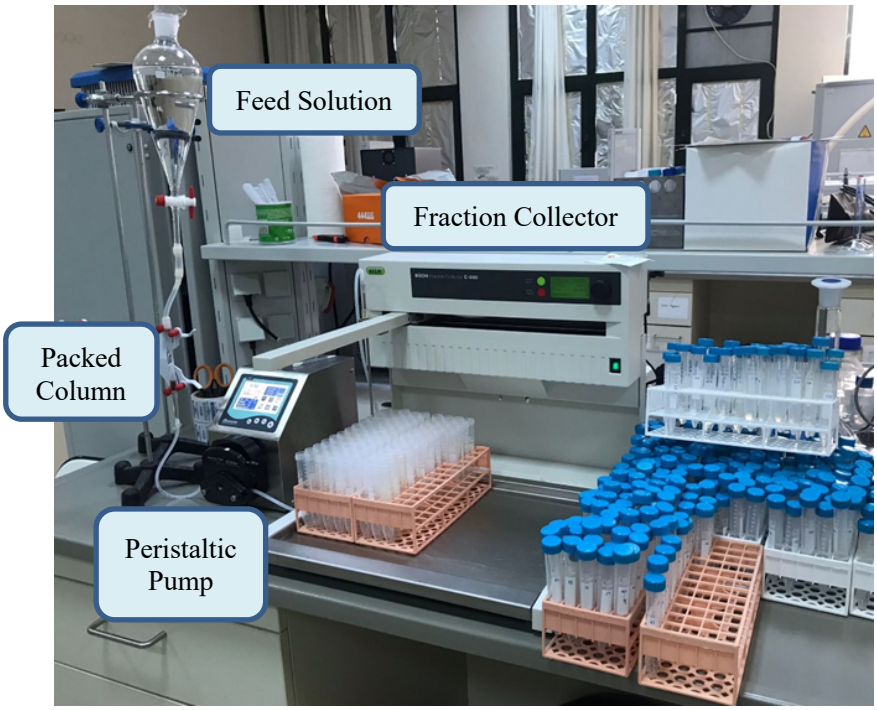

Figure 5.1. The experimental set up for Li sorption from a continuously fed solution consisting of a column filled with FHS, a peristaltic pump and a fraction collector.

5.2.2.2. Regeneration and Reusability Studies of Functional Cellulose and Hazelnut Shell Waste

Lithium sorption/desorption studies were carried out in a continuous-flow packed column with a series of sorption-washing-desorption-washing cycles to test the reusability of phosphorylated functional cellulose and hazelnut shell waste. The sorption conditions were determined as 1.0 mL min^{-1} flow rate, 10 mg L^{-1} lithium initial concentration, 1.0 cm bed height, and 3 mL samples were collected with the help of a peristaltic pump and fraction collector. After the sorption process was completed, the sorbent was washed by passing excess deionized water through the column with a flow rate of 0.5 mL min^{-1}. Then, the desorption study was carried out by collecting 2 mL samples with 5% H_2SO_4 (0.51 M) at a flow rate of 0.12 mL min^{-1}. After the desorption study, the sorbent was again washed with plenty of deionized water with a flow rate of 0.5 mL/min, and thus one cycle was completed. This cycle was repeated 5 times.

5.3. Modeling of Packed Bed Column Dynamic Behavior

Experimental data modeling is utilized to successfully develop a column adsorption process and give mathematical and quantitative solutions. To explain the breakthrough curves for the adsorption of both organic molecules and inorganic ions in a fixed bed column, models such as the Thomas model, the Yoon-Nelson model, and the modified dose-response model (MDR) are widely employed (Recepoğlu et al., 2018b; Zhang et al., 2019). In this study, these three models were used and evaluated to predict the breakthrough curves of Li sorption onto FHS.

5.3.1. Thomas Model

The Thomas model, which assumes the Langmuir isotherm and second-order reversible reaction kinetics, is one of the most often used models to characterize breakthrough curves. It is particularly easy to anticipate the adsorption process when external and internal diffusion are not rate-limiting processes (Thomas, 1948; Wang et al., 2016). Eq. (5.3) below expresses the Thomas model:

$$\frac{C}{C_0} = \frac{1}{1 + \exp\left(K_T(q_o m - C_0 \vartheta)/Q\right)} \tag{5.3}$$

where K_T (mL/(min mg)) is the Thomas rate constant and ϑ (mL) is the total volume of solution passing through the column at any given time. q_o is the sorption capacity (mg g^{-1}) and m is the dry weight of the sorbent filled in the column. Other parameters have been defined previously.

The linearized form of the Thomas model can be written as in Eq. (5.4). K_T and adsorption capacity q_o values can be found from the slope and intercept of the graph between ln((C_0/C)-1) and time (ϑ/Q), respectively.

$$ln\left(\frac{C_0}{C} - 1\right) = \frac{K_T q_o m}{Q} - \frac{K_T C_0}{Q}\vartheta \tag{5.4}$$

5.3.2. Yoon–Nelson Model

Yoon–Nelson suggested a basic model that focuses on the adsorption of gases or vapors on activated carbon. This model implies that the rate of reduction in adsorption probability for each adsorbed molecule is proportional to the adsorbed molecule's sorption probability and the molecule's likelihood of being adsorbed on the adsorbent (Liu et al., 2020; Yoon and Nelson, 1984). The Yoon–Nelson equation is as follows:

$$\frac{C}{C_o} = \frac{\exp\left(K_{YN}t - \tau K_{YN}\right)}{1 + \exp\left(K_{YN}t - \tau K_{YN}\right)} \tag{5.5}$$

where K_{YN} is the rate constant (min^{-1}); and τ (min) is the time required for 50% of the molecule to be adsorbed to pass when the concentration (C, mg L^{-1}) is half of the initial concentration (C_0, mg L^{-1}). K_{YN} and τ can be found from the slope and intercept of the graph (ln(C/(C_0-C)) versus t) plotted for the linearized form of the Yoon-Nelson model given in Eq. (5.6):

$$\ln\frac{C}{C_o - C} = K_{YN}t - \tau K_{YN} \tag{5.6}$$

According to the Yoon-Nelson model, the adsorption capacity (q_0, mg/g) can be calculated using Eq. (5.7) since the model claims that the amount of lithium adsorbed by the sorbent is half of the initial lithium concentration passing through the packed column

in the 2τ period (İpek et al., 2013).

$$q_o = \frac{1}{2}\frac{(C_o Q 2\tau)}{m} = \frac{(C_o Q \tau)}{m} \tag{5.7}$$

5.3.3. Modified Dose–Response (MDR) Model

The Modified dose-response (MDR) model is another simple mathematical model used to examine the dynamic behavior of packed bed column adsorption data. This model lowers the inaccuracy introduced by the Thomas model, particularly at lower and higher points on the breakthrough curve (Ting et al., 2021). The mathematical model is expressed in Eq. (5.8):

$$\frac{C}{C_0} = 1 - \frac{1}{1 + \left(\frac{\vartheta}{b}\right)^a} \tag{5.8}$$

a and b are model constants, b specifies the output volume producing half-maximum response, and a specifies the slope of the regression function. From the b value, the value of the maximum solid phase concentration of the solute (q_0) can be calculated using Eq. (5.9):

$$q_0 = \frac{bC_o}{m} \tag{5.9}$$

The model parameters were determined by fitting the experimentally obtained data with the help of MATLAB® software using the nonlinear regression technique for the MDR model given in Eq. (8). To find the most suitable model, error analysis was performed by considering the sum of the squares of the differences between the experimental data and the theoretical data (calculated from the models). The Sum of Squares of Error (SSE) can be obtained from the following equation:

$$SSE = \frac{\Sigma\left(\left(\frac{C}{C_o}\right)_{theo} - \left(\frac{C}{C_o}\right)_{exp}\right)^2}{N} \tag{5.10}$$

$(C/C_0)_{theo}$ is the ratio of effluent and inlet lithium concentration from the model calculation, $(C/C_0)_{exp}$ is the ratio of lithium concentration in the effluent and inlet water

from the experiment, and N is the total number of experimental points.

5.4. Results and Discussion

5.4.1. Column Sorption Studies of Phosphorylated Hazelnut Shell Waste

5.4.1.1. Effect of Flow Rate

The residence period of lithium in the packed bed column and the sufficient degree of lithium-biosorbent reaction are determined by the flow rate of the dynamic process (Bai et al., 2022). The effect of flow rate was studied, as described earlier, at 0.25, 0.5 and 1.0 mL min^{-1}. The breakthrough curves of the lithium adsorption obtained with varying flow rates at the constant inlet lithium concentration and bed height, and the breakthrough and elution curves were plotted in Figure 5.2(a) and Figure 5.2(b), respectively. In addition, the comparison of the fixed bed (1.5 cm) performance of the column filled with phosphorylated hazelnut shell waste at these flow rates is given in Table 5.1. Despite various flow rates, all breakthrough curves started with zero lithium concentrations in effluent, demonstrating that the adsorption column with a height of 1.5 cm is sufficient to remove litihum in a short time. The sharpness of the breakthrough curve appeared to grow when the flow rate was increased. The curves have a board tailing edge and a sharp leading edge. In liquid-phase sorption, when intraparticle diffusion is the rate-limiting transport mechanism, the tailing of a breakthrough curve is prevalent (Jiang et al., 2020).The breakthrough curves changed dramatically from right to left when the flow rate was increased from 0.25 to 1.0 mL min^{-1}, indicating a reduction in fixed bed service time. As the entering Li flow rate increased, the breakthrough time was earlier. Bed volumes (BVs) at the breakthrough point were found to be 477, 369, and 347 at flow rates of 0.25, 0.5, and 1.0 mL min^{-1}, respectively. The bed volumes required for total saturation were 941, 911 and 829, respectively, while the total capacity was calculated as 22.29, 20.07 and 17.69 mg Li/g sorbent. The breakthrough and saturation times are shortened as the available Li binding sites are rapidly occupied when Li^+ ions enter the column at higher velocities. Furthermore, given the foregoing, a high flow rate appears

to be infovaroble to sorption efficiency. The degree of column utilization at three different flow rates varied between approximately 60% and 80%, and the breakthrough curves formed a smooth S shape with these rates, supporting the usability of the synthesized material in the column. Moreover, ca. 100% desorption efficiency indicates that this material can be easily regenerated and lithium can be recovered at very high rates. Other researchers also reported similar observations (Attia et al., 2022; Charola et al., 2018; Hussein and Mayer, 2022; Khalfa et al., 2021).

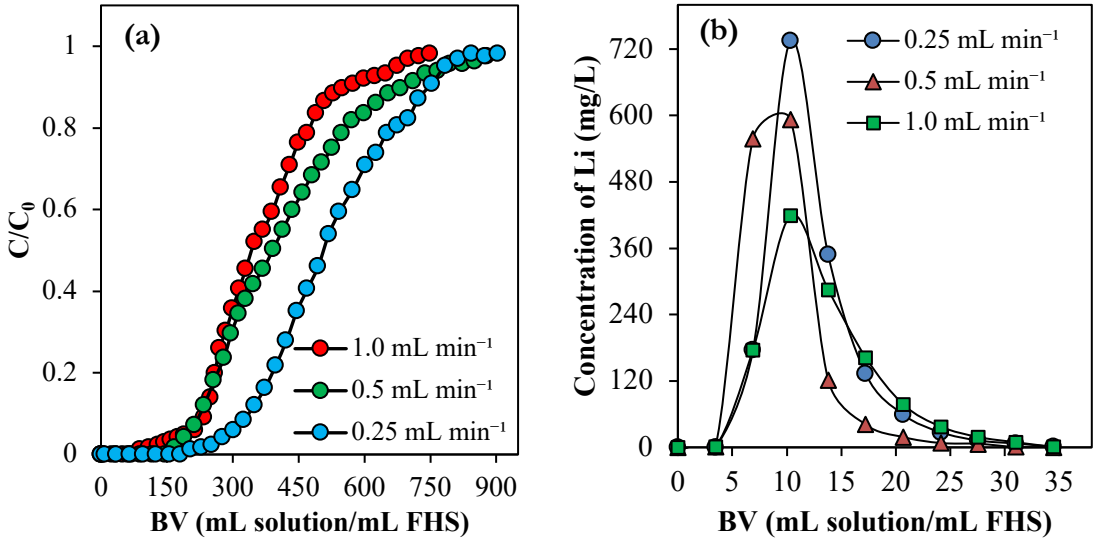

Figure 5.2. **(a)** breakthrough curves (C_0=10 mg/L, T=25°C, bed height=1.5 cm, ϑ=0.25 – 1.0 mL/min) **(b)** elution curves (5% H_2SO_4, ϑ=0.12 mL min^{-1}, T=25°C, bed height=1.5 cm) of the column loaded with phosphorylated functional hazelnut shell waste at different flow rates

Table 5.1. Comparison of packed bed (1.5 cm) performance of column loaded with phosphorylated hazelnut shell waste at different flow rates.

	Flow rate (mL min^{-1})		
	0.25	**0.5**	**1.0**
Breakthrough capacity, mg Li/mL sorbent	4.20	3.22	3.09
Breakthrough capacity, mg Li/g-sorbent	18.10	13.87	13.33
BV at breakthrough point, mL solution/mL sorbent	477	369	347
Total capacity, mg Li/mL sorbent	5.17	4.66	4.10
Total capacity, mg Li/g-sorbent	22.29	20.07	17.69
BV at saturation point, mL solution/mL sorbent	941	911	829
Degree of column utilization, %	81.20	69.11	75.38
Elution efficiency, %	~100.00	~100.00	~100.00

5.4.1.2. Effect of Bed Height

On an industrial scale, the bed height is used to evaluate adsorbent materials for a continuous flow of liquid stream (Attia et al., 2022). The amount of adsorbent inside the fixed bed column determines how much lithium ions accumulate in the column (Jiang et al., 2020). The effect of bed volume (controlled by bed height) on the breakthrough curves of phosphorylated functional hazelnut shell waste plotted C/C_0 versus BV and C/C_0 versus time is illustrated in Figure 5.3(a) and Figure 5.3(b), respectively. Also, the elution curves obtained with different bed heights of column loaded with phosphorylated hazelnut shell waste are given in Figure 5.3(c). A comparison of the constant flow (0.5 mL min^{-1}) performance of the column loaded with phosphorylated functional hazelnut shell waste at different bed heights is tabulated in Table 5.2. The breakthrough curves outline that the breakthrough time increases remarkably with the increase of bed height; a similar raising pattern is observed for the saturation time as well. The breakthrough times were 282, 366, and 433 minutes, respectively, while the times required for saturation were 781, 897, and 1033 minutes in the 1.0, 1.5, and 2.0 cm height columns filled with phosphorylated hazelnut shell waste. It took a long time to reach full saturation (column exhaustion) as increasing bed volume provides more active binding sites in the column to capture lithium. When the bed height was doubled, the number of treated bed volumes doubled, indicating that the sorption of Li onto phosphorylated functional hazelnut shell waste took place with a uniform distribution. Furthermore, at the maximum bed depth, a huge mass transfer zone is produced, making the breakthrough curves significantly steeper, and the diffusion mass transfer phenomena predominates over the axial dispersion phenomenon (F. Liu et al., 2021; Metwally et al., 2020). For the conditions (0.5 mL min^{-1} flow rate) examining the effect of bed height varying from 1.0 to 2.0 cm, the capacity of the material was found to be 20 mg Li/g sorbent on average. The breakthrough curve data obtained at this laboratory-scale have shown that it can be used to advance scaled design with large-scale column applications (continuous feed). In addition, due to the presence of functional groups on the surface of the material, an elution efficiency of ca. 100% was obtained under all conditions, and such a high elution efficiency showed that lithium could be easily recovered.

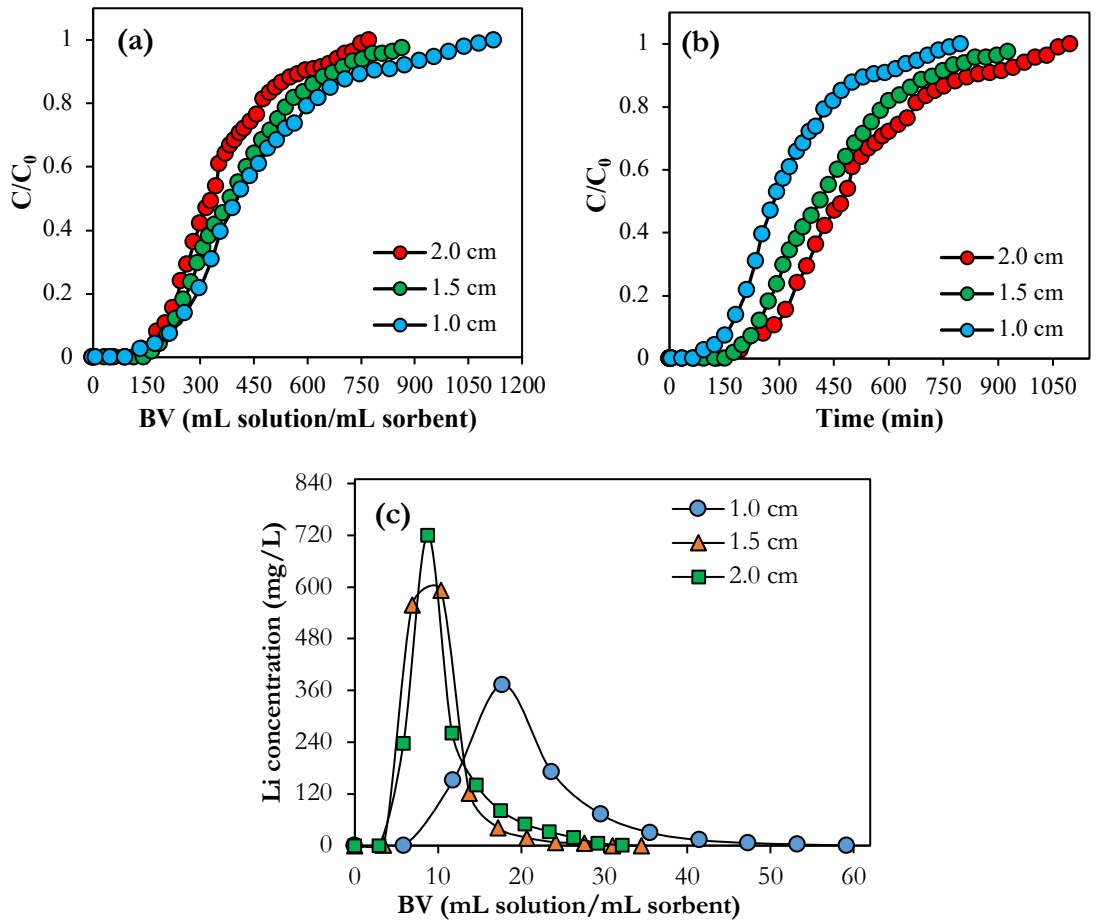

Figure 5.3. Breakthrough curves of phosphorylated functional hazelnut shell waste plotted with **(a)** C/C_0 versus BV, **(b)** C/C_0 versus time (C_0=10 mg L^{-1}, T=25°C, ϑ=0.5 mL min^{-1}, bed height=1.0–2.0 cm), **(c)** Elution curves obtained with different bed heights of the packed column with phosphorylated functional hazelnut shell waste (5% H_2SO_4, ϑ=0.12 mL/min, T=25°C, bed height=1.0–2.0 cm)

Table 5.2. Comparison of constant flow (0.5 mL/min) performance of column filled with phosphorylated functional hazelnut shell waste at different bed heights.

	Bed height		
	1.0 cm	**1.5 cm**	**2.0 cm**
Breakthrough capacity, mg Li/mL sorbent	3.43	3.22	2.92
Breakthrough capacity, mg Li/g-sorbent	14.80	13.87	9.68
Breakthrough time, min	282	366	433
Total capacity, mg Li/mL sorbent	4.81	4.66	4.53
Total capacity, mg Li/g-sorbent	20.71	20.07	19.54
Total saturation time, min	781	897	1033
Degree of column utilization, %	71.46	69.11	64.36
Elution efficiency, %	~100.00	~100.00	~100.00

5.4.2. Modeling of Breakthrough Curves

The breakthrough curves of Li at different flow rates and bed heights were investigated with three commonly used models, Thomas, Yoon-Nelson, and Modified Dose-Response (MDR), whose parameters, correlation coefficients (R^2) and SSE values are tabulated in Table 5.3 and Table 5.4, respectively, and the illustrations representing theoretical and experimental data plots for each model at different flow rate and bed height are given in Figure 5.4. According to lower SSE values (0.0002–0.0004) along with a higher correlation coefficient, R^2 (0.998–0.999), reproducing better fitting of experimental data with the theoretical ones, the MDR model was better described the dynamic behavior of Li sorption using phosphorylated functional hazelnut shell waste in a packed bed column.

5.4.2.1. Thomas Model Analysis

Thomas model analysis reveals that high mass transfer rate led to the values of K_T increasing from 0.687 mL min^{-1} mg^{-1} to 1.739 mL min^{-1} mg^{-1} as flow rate increased from 0.25 mL min^{-1} to 1.0 mL min^{-1}. While increasing the flow rate reduced the value of q_0 up to 16.73 mg g^{-1}, this was primarily due to insufficient time for Li diffusion and adsorption. In terms of bed depth, the results showed that the value of K_T decreased from 0.866 mL min^{-1} mg^{-1} to 0.637 mL min^{-1} mg^{-1} as bed depth increased from 1.0 cm to 2.0 cm, which can be attributed to the longer contact time at greater bed depths. The value of q_0, on the other hand, was observed to increase as the bed depth was increased because the adsorption sites increased. This suggested that at a higher flow rate and lower bed height, the adsorption rate would be faster. Besides, these findings are consistent with those found in the literature (Lu et al., 2019; Metwally et al., 2020). Nonetheless, the model cannot precisely trace the sorption of Li in the column or estimate the minimum height of the adsorption front, allowing for a better understanding of performance. The application of the MDR approach can overcome such a flaw.

5.4.2.2. Yoon–Nelson Model Analysis

The Yoon–Nelson model has been effectively employed in previous studies to describe pollutant adsorption in a packed bed design (Khalfa et al., 2021). When the Yoon and Nelson model was applied to the experiment data, K_{YN} and τ values were obtained that accurately characterized the packed bed sorption of Li onto the phosphorylated functional hazelnut shell waste. Decreasing the flow rate from 1.0 mL min^{-1} to 0.25 mL min^{-1} with the same column height resulted in an increase of τ as a longer time is clearly required to saturate the material with Li due to providing sufficient contact time at lower flow rates. However, for 1.0 mL min^{-1} τ fell to 218 min, because a higher flow worsens the mass transfer process (e.g., kinetics and capacity), reducing the time required to recover 50% of Li. When the column height was increased from 1.0 cm to 2.0 cm, (the time to obtain 50% of retention for Li) increased from 277.3 min to 450.9 min, which is appropriate because the accessible sorbent sites increased correspondingly with column height which is also supported by the results of previous studies (Dawood et al., 2018; F. Liu et al., 2021).

5.4.2.3. Modified Dose–Response (MDR) Model Analysis

The MDR model shows that as the flow rate increased from 0.25 mL min^{-1} to 1.0 mL min^{-1}, the sorption capacity per unit mass of phosphorylated functional hazelnut shell waste (q_0) decreased from 20.96 mg g^{-1} to 16.97 mg g^{-1}. When the area of the breakthrough curve of Li for 1.0 cm and 2.0 cm bed heights at 0.5 mL min^{-1} is similar, the column capacity appears to have a trend opposite to values of q_0 in the MDR model, because the column capacity considers the area of the breakthrough curve that is dominated by saturation time. In addition, the values of b decreased with the increase in the flow rate and increased with the increase in the bed height.

To summarize, the SSE generated by the MDR model was significantly smaller than that created by the Yoon–Nelson and Thomas models. Consequently, when it comes to forecasting the adsorption behavior of phosphorylated functional hazelnut shell waste for lithium sorption from water by chromatographic separation, the MDR model outperforms the Yoon–Nelson and Thomas models.

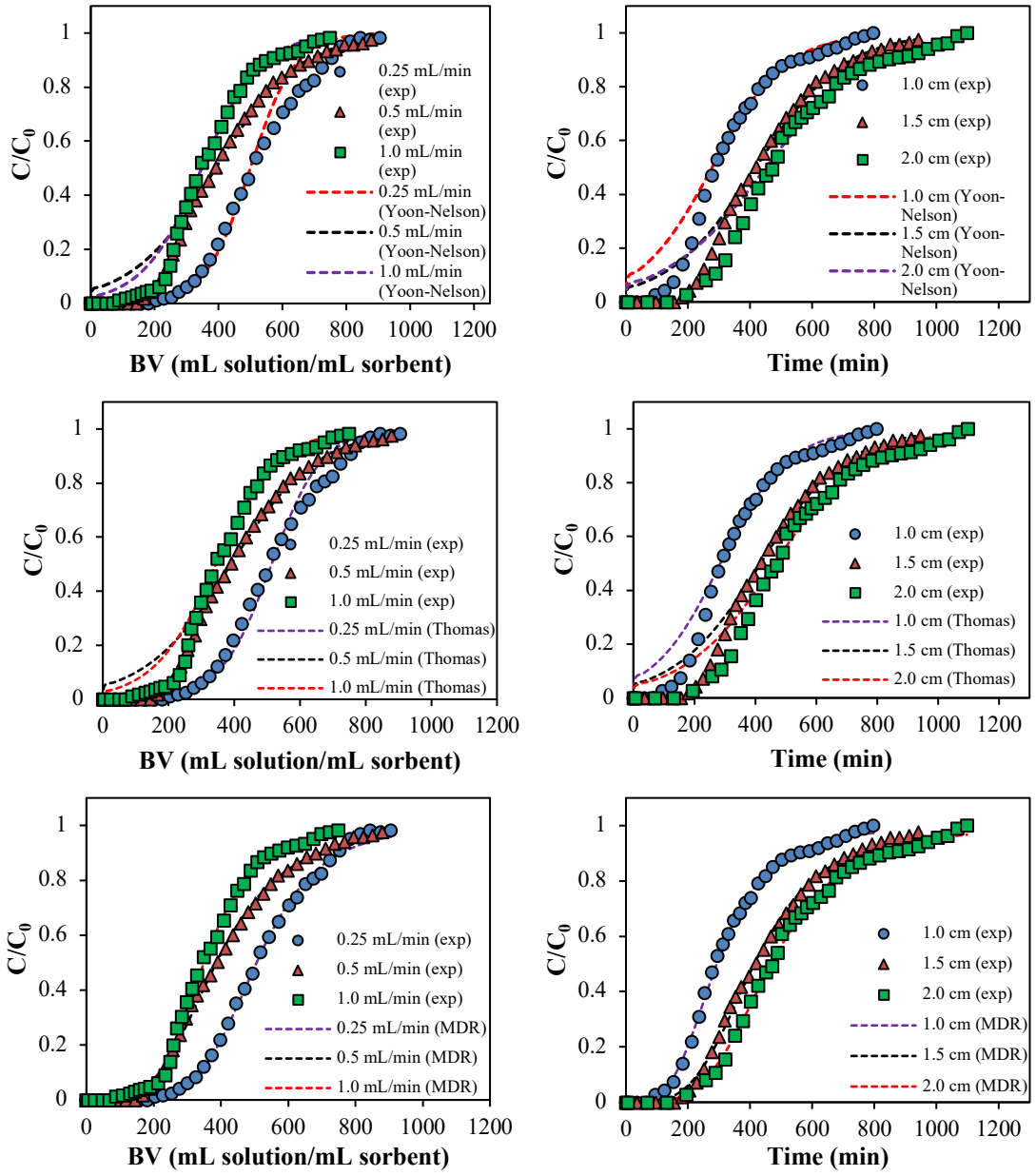

Figure 5.4. Model fittings of experimental data obtained from column study under various operating conditions.

Table 5.3. Model parameters of the breakthrough curves of Li sorption on phosphorylated functional hazelnut shell waste

Parameters			Model							
Exp. No.	Flow rate (mL min^{-1})	Bed height (cm)	Thomas		Yoon–Nelson			MDR		
			K_T	q_0	K_{YN}	τ	q_0	a	b	q_0
1	0.25	1.5	0.687	21.29	0.0072	993.10	20.69	5.423	0.294	20.96
2	0.5	1.5	0.739	16.15	0.0071	417.87	16.16	3.767	0.224	16.00
3	1.0	1.5	1.739	16.73	0.0171	218.02	16.85	4.626	0.238	16.97
4	0.5	1.0	0.866	18.43	0.0085	277.34	17.92	3.589	0.158	18.88
5	0.5	2.0	0.637	14.79	0.0061	450.87	14.38	3.969	0.253	18.50

Table 5.4. Correlation coefficients and SSE values of the models of the breakthrough curves of phosphorylated functional hazelnut shell waste

Parameters			Thomas		Yoon-Nelson		MDR	
Exp. No.	**Flow rate (mL min^{-1})**	**Bed height (cm)**	**R^2**	**SSE**	**R^2**	**SSE**	**R^2**	**SSE**
1	0.25	1.5	0.983	0.0015	0.991	0.0028	0.998	0.0003
2	0.5	1.5	0.996	0.0037	0.997	0.0036	0.998	0.0003
3	1.0	1.5	0.990	0.0043	0.992	0.0029	0.998	0.0004
4	0.5	1.0	0.993	0.0043	0.991	0.0061	0.999	0.0002
5	0.5	2.0	0.983	0.0027	0.983	0.0043	0.998	0.0002

5.4.3. Comparison of Column Performances of Functional Cellulose and Hazelnut Shell Waste

To compare the column performances of cross-linked phosphorylated functional cellulose and phosphorylated hazelnut shell waste under different conditions, the breakthrough curves were presented in Figure 5(a) and Figure 5(b) with a flow rate of 1.0 mL min^{-1} and a bed height of 1.0 cm and a flow rate of 0.25 mL min^{-1} and a bed height of 1.5 cm, respectively. Comparing the breakthrough curves in both cases showed a similar column performance profile, and according to the findings in Table 5.5, breakthrough and total capacities were comparable for phosphorylated functional cellulose and hazelnut shell waste. For example, the breakthrough capacity of phosphorylated functional cellulose with a flow rate of 1.0 mL min^{-1} and a bed height of 1.0 cm was 3.43 mg Li/mL sorbent, while it was 3.15 mg Li/mL sorbent for phosphorylated functional hazelnut shell waste. Their total capacity was 4.13 and 3.91 mg Li/mL sorbent, respectively. Meanwhile, the reason for the different capacities per g of the same volume of sorbents is due to the different densities of the materials. The density of cross-linked phosphorylated functional cellulose was 0.187 g mL^{-1}, while the density of phosphorylated functional hazelnut shell was 0.232 g mL^{-1}. Although phosphorylated functional cellulose at a higher flow rate (1.0 mL/min) and lower bed height (1.0 cm) performs relatively better with bed volumes of 411 and 918 both at the breakthrough point and at total capacity, respectively, these values for functional hazelnut shell were found to be 338 and 805, respectively. The degree of column utilization of both materials under the selected operating conditions was calculated as approximately 80%, which indicates that the utilization of the materials in the column is quite suitable. When the flow rate is 0.25 mL min^{-1} and the bed height is

1.5 cm, i.e., at a lower flow rate and higher bed height, the breakthrough curves of both materials almost overlap, and the column study findings showed similar performance in the column.

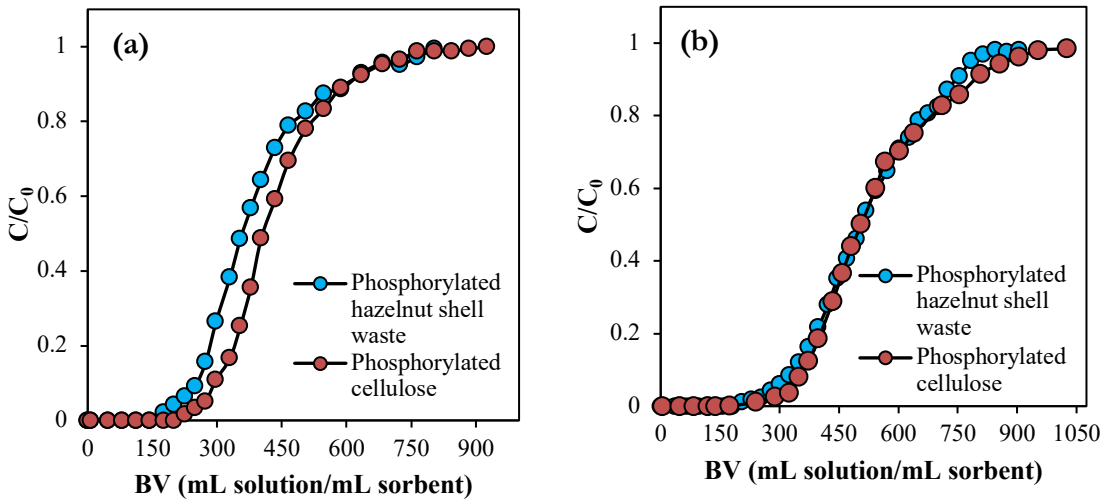

Figure 5.5.Comparison of the breakthrough curves of phosphorylated functional cellulose and hazelnut shell wastes under different conditions **(a)** C_0=10 mg L^{-1}, T=25°C, ϑ=1.0 mL min^{-1}, bed height=1.0 cm, **(b)** C_0=10 mg L^{-1}, T=25°C, ϑ=0.25 mL min^{-1}, bed height=1.5 cm

Table 5.5. Comparison of column performances of phosphorylated functional cellulose and hazelnut shell waste under different conditions.

	ϑ=1.0 mL min^{-1}, bed height=1.0 cm		**ϑ=0.25 mL min^{-1}, bed height=1.5 cm**	
Sorbent	Functional cellulose	Functional hazelnut shell waste	Functional cellulose	Functional hazelnut shell waste
Breakthrough capacity, mg Li/mL sorbent	3.43	3.15	4.83	4.20
Breakthrough capacity, mg Li/g-sorbent	18.33	13.56	25.82	18.10
BV at breakthrough point, mL solution/mL sorbent	411	338	477	477
Total capacity, mg Li/mL sorbent	4.13	3.91	6.28	5.17
Total capacity, mg Li/g-sorbent	22.08	16.84	33.56	22.29
BV at saturation point, mL solution/mL sorbent	918	805	1050	941
Degree of column utilization, %	83.02	80.52	76.92	81.20

5.4.4. Cyclic Sorption of Lithium by Functional Cellulose and Hazelnut Shell Waste

Contrary to batch regeneration of cycle studies, it is more suitable for continuous column studies to prevent material losses in repeated use. The breakthrough curves of the cycle studies of cross-linked phosphorylated functional cellulose and phosphorylated functional hazelnut shell waste are given in Figure 5.6(a) and Figure 5.6(b), respectively. As can be seen in the breakthrough curves, the profiles of the other cycles were obtained almost overlapped, except for the first cycle. This proves the reusability of the material, however, the shift in the breakthrough curve after the first cycle and the decrease in the capacity of the material is due to acid regeneration. There are similar findings in the literature, which are explained by the effect of the regenerant type used on the sorption capacity. Çiçek et al. (2018) carried out sorption/regeneration studies for Li^+ recovery from water with lithium selective commercial Lewatit TP 260 ion exchange resin with 4 cycles. The sorption capacity of the resin did not change when NaCl was used for regeneration, while the sorption capacity decreased from 99% to 53% when HCl was used. Because after regeneration with HCl, the resin was converted to H-form and used in the next sorption cycle. In the second sorption process, Li^+ exchanges with H^+, so the H^+ concentration in the solution increases, and the pH of the solution decreases. As explained in the effect of the solution pH section, the sorption capacity of the resin dec-

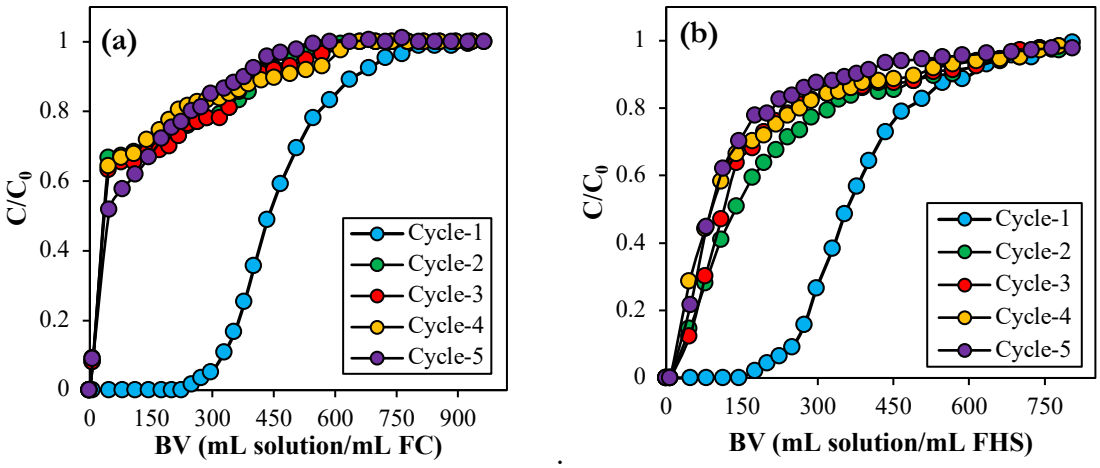

Figure 5.6. Cyclic lithium sorption-desorption breakthrough curves of **(a)** cross-linked phosphorylated functional cellulose, **(b)** phosphorylated functional hazelnut shell waste (Sorption conditions: C_0=10 mg L^{-1}, T=25°C, ϑ=1.0 mL min^{-1}, bed height=1.0 cm; desorption conditions: 5% H_2SO_4 (0.51 M), ϑ=0.12 mL/min)

reased as the pH of the solution decreased (Çiçek et al., 2018). Hence, although the capacity of the materials decreases after the first cycle depending on the type of regenerant used, the similar and approximate performance in the other four cycles showed that the materials can be used repeatedly.

5.5. Conclusions

The batch mode operation is crucial for determining the efficiency of the metal-adsorbent system. However, data obtained under batch conditions are often unsuitable for using this approach on a wide scale in most treatment procedures, particularly in a continuous-flow mode. As a result, this research is interested in developing a continuous-flow packed-bed column loaded with phosphorylated hazelnut shell waste to investigate the adsorptive behavior of lithium ions. To apply to the practical production process of lithium recovery, the breakthrough time was defined as the lithium recovery rate dropping down to 0.6. The effects of feed flow rate and bed height on the breakthrough performances were investigated. It was found that breakthrough time, exhaustion time and uptake capacity of the column bed increased with increasing column bed height, whereas decreased with increasing influent flow rate. Bed volumes at the breakthrough point were found to be 477, 369 and 347 at flow rates of 0.25, 0.5 and 1.0 mL/min, respectively. Moreover, the bed volumes required for total saturation were 941, 911 and 829, respectively, while the total capacity was calculated as 22.29, 20.07 and 17.69 mg Li/g sorbent. On the other hand, the breakthrough times were 282, 366, and 433 minutes, respectively, while the times required for saturation were 781, 897, and 1033 minutes in the 1.0, 1.5, and 2.0 cm height columns filled with phosphorylated hazelnut shell waste. In studies examining the effect of bed height, the capacity of the material was found to be 20 mg Li/g sorbent on average. The column experimental data fitted well with nonlinear Thomas and Yoon-Nelson models, confirming that both models can predict appropriately the whole breakthrough curves, and are useful for application in the large-scale field. However, the MDR model had the least relative fit error and the highest correlation coefficients and was more accurate than the conventional models. The similar and approximate performance in the other four cycles showed that the materials can be used repeatedly.

CHAPTER 6

PRELIMINARY STUDIES FOR LITHIUM RECOVERY FROM GEOTHERMAL WATER BY PHOSPHORYLATED CELLULOSE AND HAZELNUT SHELL WASTE

6.1. Introduction

Li is found in several environments on Earth such as in igneous, volcanic, and sedimentary rocks (20 to 70 ppm), the seas (0.18 ppm), brines, salt marshes (sabkhas) (1000 ppm), and thermal fluids (15 to 350 ppm) (Feininger, 2013; Kamienski et al., 2000; Swain, 2016). High volatile content in the late crystalizing magmatic fluids and slow cooling of the magma facilitates more considerable growth like pegmatites which host rich in Li, like phlogopite, tourmaline, and spodumene ($LiAlSi_2O_6$), zinwaldite (Li-bearing mica found in some granites, $K(Li,Al,Fe)_3(Al,Si)_4O_{10}(OH,F)_2$) (Garrett, 2004). It is anticipated that 31.1 Mt of Li is accessible globally in the natural sources. Brines have the highest Li concentration (21.6 Mt), followed by pegmatites (3.9 Mt), 3.4 Mt in deposits like hectorite and jadarite (3.4 Mt), and 2 Mt in geothermal fluids (Gruber et al., 2011; Kesler et al., 2012). Although Li in geothermal waters is not as high as that found in brines, they are a significant source of Li. The concentration differs widely from region to region such as the Li content in thermal waters varies from 6-33 ppm (Asal, Djibouti) (Daoud et al., 2020), 1-38 ppm (Türkiye), 10 ppm (Japan) (Yanagase et al., 1983), 239 ppm (China) (Wang et al., 2021), to 480 ppm (Mofete, Italy). In various geothermal areas of Türkiye, sediments linked with thermal springs have also a high Li concentration (Gündoğan, 2000; Helvaci et al., 2004; Ortı et al., 2002). The Li content in thermal waters from a wide geographical region is listed in Table 6.1. When the economic relevance of Li is considered, the recovery of some precious metals from geothermal fluids becomes an enormously essential process from both an environmental and an economic point of views. The increasing growth of electric cars increases Li demand dramatically. Nearly 8 kg of Li is needed in the construction of a 60 kWh Li-ion battery, and Li consumption is predicted to rise to 1.2-1.6 Mt by 2030, up from 280 kton in 2018 (Roskill, 2019).

Table 6.1. Li (ppm) content in thermal waters from a wide geographical region of the world*

Country	Geothermal site/region	Li^+ (ppm)	Reference
Argentina	Regional geothermal springs/Antuco	147.4	(Godfrey et al., 2013)
	Regional geothermal springs/Diablo	33.3	
	Regional geothermal springs/Arizaro	95.3–99.8	
	Regional geothermal springs/Aguas Calientes	7.0	
	Regional geothermal springs/Luracatao	27.7	
	Regional geothermal springs/El Tatio	14.8–47.5	
	Hot spring/ Puna plateau, Jujuy Province	29	(Arnold et al., 2017)
China	Wellbore in Tibet	25.78	(Sun et al., 2020)
	Kawu geothermal field/Tibet	23.3	(Tan et al., 2018)
	Yangbajing geothermal field/Tibet	25	
France	Vendenheim geothermal wells/Alsace	72–162	(Sanjuan et al., 2020)
	Geothermal area/Cronembourg, Buntsandstein level in North Alsace	220	(Fouillac, 1990)
	Geothermal site/Soultz Dogger	2.7–153	(Négrel et al., 2007)
Germany	Geothermal site/Groß Schönebeck	198 – 237	(Regenspurg et al., 2015)
Greece	Hot springs/Chios Island, Aghiasmata	4.55–5.5	(Dotsika et al., 2006)
	Samothraki Island geothermal area/Therma	3.7–11.4	(Dotsika, 2012)
	Vounalia Area, Milos Island	14–33	(Fytikas et al., 2005)
Iceland	Reykjanes	4.18	(Ruttinger et al., 2019)
Indonesia	Dieng geothermal power plant	40 – 60	(Pambudi et al., 2015)
	Salak geothermal site	17	(Gallup, 1998)
	Geothermal fluid/Lumpur Sidoarjo	5.81	(Noerochim et al., 2015)
Italy	Geothermal area/Cesano, near Rome	350	(Fouillac, 1990)
	Mote Amiata	21.9	(Lo et al., 2014)
	Geothermal reservoirs/Mofete	480 (deep) 28–56 (shallow)	(Dini et al., 2021)
	Geothermal fluids/Latera (Latium)	13.5	
Japan	Yamaga hot spring/Oita	41.30	(Hano et al., 1992)
	Hazama hot spring/Oita	1.54	
	Hatchobaru, Kyushu	10.80	(Park et al., 2012)
Mexico	Cerro Prieto/Baja California Peninsula	27	(Bloomquist, 2006)
	Los Azufres	0.1–65	(González-Partida et al., 2005)

(cont. on next page)

Table 6.1. (cont.)

Country	Geothermal site/region	Li^+ (ppm)	Reference
New Zealand	Wairakei Geothermal Fluid/Huka Prawn Park	11	(Mroczek et al., 2015)
	Taupo volcanic zone/Ohaaki geothermal site	6.77–12.74	(Millot et al., 2012)
	Taupo volcanic zone/Wairakei geothermal site	9.03–13.28	
	Taupo volcanic zone/Mokai geothermal site	16.88–19.94	
	Taupo volcanic zone/Kawerau geothermal site	4.46–4.97	
	Taupo volcanic zone/Rotokawa geothermal site	5.18–5.67	
Poland	Carpathian region	15.7	(Siekierka et al., 2018)
	Rabka Zdroj (southern part of Poland)	10 – 16	(Wiśniewska et al., 2018)
Russia	Pauzhetskaya geothermal station/Kamchatka	3.10	(Belova et al., 2019)
	Thermal brine/Russkiy Khutor, The Republic of Dagestan	44.9–37.5	(Alkhasov et al., 2020)
	Thermal brine/Tarumovka, The Republic of Dagestan	210	
	Thermal brine/Achikulak, Stavropol Krai	26.3	
	Thermal brine/ Datykhskiy, Chechen Republic	160	
Türkiye	Balçova geothermal field/İzmir	1.19	(Helvaci et al., 2004; Y.K. Recepoğlu et al., 2017b)
	Kızıldere geothermal power plant/Denizli	3.78	(Kabay et al., 2004)
	Alaşehir geothermal field/Manisa	5.97 – 6.29	(Rabet et al., 2017)
	Hot springs/Çan Karaılıca	1.123	(Cetiner et al., 2015)
	Hot springs/Ezine Kestanbol	12.47	
	Hot springs/Ayvacık Tuzla	34.13–38	
	Tuzla geothermal field/Çanakkale	18-24	(Baba et al., 2015; Çelik et al., 2018; Demir et al., 2014)
	Kuzuluk geothermal well/Sakarya	36	(MTA, 2005)
	Sorgun YS-1 geothermal well//Yozgat	11	
	Banza- Kızılcaören geothermal spring/Uşak	82	
Turkmenistan	Cheleken Peninsula	215	(Lo et al., 2014)
USA	Salton Sea/California	194–230	(Ruttinger et al., 2019)
	Fenton Hill/New Mexico	6–250	
	Coso hot springs/California	45	

*Table 6.1 was adapted from "D. Chandrasekharam, M. F. Şener, Y. K. Recepoğlu, T. Isık, M. M. Demir, A. Baba, Lithium: An energy transition element, its role in the future energy demand and carbon emissions mitigation strategy, Geothermics, (2022), under review."

Li extraction from brines is one of the most economical methods, and it is a well-known production strategy from ancient times (Daoud et. al, 2020; Yoshizuka et al., 2021). Precipitation, chromatography, ion exchange, liquid-liquid extraction, ionic liquids, or membrane technologies can all be used to recover Li from aqueous sources (Swain, 2017). Several authors have reported on the precipitation of Li as lithium-aluminate in the literature, with the highest yield recorded at room temperature (Pelly, 1978). Abe and Chitrakar used a titanium antimonate cation exchanger to achieve a 20-fold enrichment in recovered Li contents by chromatography (Abe and Chitrakar, 1987). Moreover, H_2TiO_3 ion exchangers have been used to extract Li as LiCl from brines by 98% elution efficiency (Hui, 2000). Traditional liquid-liquid extraction techniques have been employed to recover Li^+ ions, and Bladwin et al. patented beta-diketone/trioctylphosphine oxide in the benzene extraction method (Baldwin and Seeley, 1974). Ionic liquids have also been employed as both solvents and co-extraction agents in liquid-liquid extractions in recent years (Gao et al., 2018, 2015; Shi et al., 2016). On the other hand, the membrane method is a cutting-edge technology for Li recovery. Electro-electrodialysis with bipolar membranes has been used to recover LiOH from water (Bunani et al., 2017; Jiang et al., 2014), and Liu et al. reported a remarkable Li exchange capacity of 38.9 mg/g by membrane electrolysis (Liu et al., 2015). Membranes containing (2-ethylhexyl)-diphenyl phosphate are selective to Li^+ ions over Mg^{2+} and Ca^{2+}, and the Li^+ separation was achieved by a combination of ion exchange and membrane processes (Jagur-Grodzinski and Schori, 1985). Reverse osmosis and nanofiltration processes have also been used for pre-concentration of Li from brine NF90 membranes, exhibited 100% rejection of Mg^{2+} ions from dilute brine samples, and the final separation yield was calculated as 85% for Mg to Li (Sun et al., 2015). Beyond all, adsorption offers great promise as an effective method for the extraction of Li from aqueous sources, including brine, geothermal water, and seawater. Moreover, it exhibits environmental friendliness by being less detrimental to climate change, while also offering rapid recovery rates despite the need for large volumes of eluent and freshwater (Yoshizuka et al., 2021).

In this chapter, the focus is on exploring the potential of phosphorylated functional cellulose (FC) and hazelnut shell waste (FHS) as sustainable and efficient materials for recovering Li from geothermal water. The aim is to present the results of preliminary studies to determine the sorption capacity and selectivity of these materials towards Li^+ ions, as well as their performance in real geothermal water samples.

6.2. Materials and Methods

6.2.1. Characterization of Geothermal Water Samples

Three different geothermal water samples collected from the İzmir, Aydın, and Çanakkale provinces of Türkiye (all located in western Anatolia) as real lithium sources were used for the preliminary tests in the recovery of lithium. First, a geothermal water sample taken from a well located in İzmir province, Seferihisar district whose physicochemical properties were given in Table 3.6 was used. Then, it was continued the following studies with geothermal water having much higher lithium content obtained from the geothermal energy company (Tuzla Geothermal Energy Inc.) in the Tuzla region of Çanakkale province. Detailed physicochemical analysis of the water sample is given in Table 6.2. In addition, a milder geothermal water sample compared to Tuzla's geothermal water obtained from Germencik geothermal power plant (M11C well), whose physicochemical properties are presented in Table 6.3, was also tested.

Table 6.2. Physicochemical properties of the geothermal water sample taken from Tuzla Geothermal Energy Company, (Çanakkale).

Cation species	Concentration (mg/L)	Anion species	Concentration (mg/L)
[a]Li^+	**23.98**	[b]HCO_3^-	132.19
[a]Na^+	16602.50	[a]Cl^-	35170
[a]K^+	1608.4	[a]F^-	4.05
[a]Ca^{2+}	2768.59	[a]NO_3^-	4.64
[a]Mg^{2+}	114.96	[a]SO_4^{2-}	205.43
[a]NH_4^+	105.19	[a]PO_4^{3-}	*N.D.
[c]pH		6.71	
[d]EC (mS/cm)		83.4	
[d]Salinity (ppt)		58.6	
[e]TDS (mg/L)		62000	
[b]Total alkalinity (mg/L as $CaCO_3$)		108.36	
[f]B (mg/L)		24.56	
[f]As (µg/L)		37.11	
[g]SiO_2 (mg/L)		230	

[a]Ion Chromatography (Thermo Scientific Dionex ICS-5000), [b]Titrimetric method, [c]pH meter (Thermo, Orion Star A111), [d]Multimeter (YSI Model 30M), [e]TDS meter (TDSTestr11 Dual Range), [f]ICP-OES (Agilent Technologies, 5110), [g]Spectrophotometer (Hach-DR5000), *not determined.

Table 6.3. Physicochemical properties of the geothermal water sample taken from Germencik power plant, (Aydın).

Cation species	Concentration (mg/L)	Anion species	Concentration (mg/L)
[a]Li^+	**6.20**	[b]HCO_3^-	1264.10
[a]Na^+	980.26	[a]Cl^-	1254.99
[a]K^+	67.63	[a]F^-	9.37
[a]Ca^{2+}	20.34	[a]NO_3^-	*N.D.
[a]Mg^{2+}	2.70	[a]SO_4^{2-}	36.43
[a]NH_4^+	*N.D.	[a]PO_4^{3-}	*N.D.
[c]pH		8.94	
[d]EC (mS/cm)		2.79	
[d]Salinity (ppt)		1.5	
[b]Total alkalinity (mg/L as $CaCO_3$)		1036.15	
[e]B (mg/L)		39.48	
[e]As (µg/L)		110	
[f]SiO_2 (mg/L)		152	

[a]Ion Chromatography (Thermo Scientific Dionex ICS-5000), [b]Titrimetric method, [c]pH meter (Thermo, Orion Star A111), [d]Multimeter (YSI Model 30M), [e]ICP-OES (Agilent Technologies, 5110), [f]Spectrophotometer (Hach-DR5000), *not determined.

6.2.2. Sorbents and Chemicals

The phosphorylated functional cellulose and hazelnut shell waste were the same products previously synthesized. On the other hand, a commercially available ion exchange resin, Lewatit® TP 260 tested and compared with the phosphorylated functional cellulose and hazelnut shell waste was a gift from LANXESS–Lewatit® Ion Exchange Resins company. The chemicals used in this study such as EDTA, sodium hydroxide (NaOH), sodium carbonate (Na_2CO_3), ammonia (NH_3), were all purchased from Merck and were in analytical grade. A cation exchange resin, Purolite® C100MBH, was also used in the pretreatment of Tuzla geothermal water before lithium recovery. The properties of resins are listed in Table 6.4.

Table 6.4. The properties of commercial ion exchange resins

	Lewatit® TP 260	Purolite® C100MBH
Matrix	Cross-linked polystyrene	Cross-linked polystyrene
Functional group	Aminomethylphosphonic acid	Sulfonic acid
Ionic form	Na^+	H^+
Total capacity	2.3 eq/L (H^+-form)	2.0 eq/L (Na^+-form)
Water retention	59 – 61%	51 – 55%

6.2.3. Lithium Sorption Studies by Geothermal Water

6.2.3.1. Lithium Sorption from Seferihisar Geothermal Water

Various amounts (0.1-0.5 g) of phosphorylated functional cellulose (FC) and/or hazelnut shell waste (FHS) were placed in plastic bottles containing 25 mL of Seferihisar geothermal water at different mass/volume ratios. The suspensions were then shaken at 180 rpm at 25°C for 24 h in a water bath. Moreover, FC (12 g/L) and FHS (14 g/L) were also compared with commercially available ion exchange resin Lewatit® TP 260 (12 g/L) at optimum doses at 25°C in terms of Li separation along with major cations. Due to the limited volume of geothermal water samples, no more studies could be conducted.

6.2.3.2. Lithium Sorption from Tuzla Geothermal Water

A series of experiments were conducted with the geothermal water sample taken from Tuzla since it is a hypersaline water that led to some challenges during lithium recovery. First, proportional optimum amounts determined from previous studies for phosphorylated functional cellulose (0.6 g) and hazelnut shell waste (0.7 g) were contacted with the geothermal water sample (25 mL) for 24 h at room temperature (25°C) without pretreatment. Then, some pretreatment processes were applied to remove competitive ions such as Ca^{2+}, Mg^{2+} and Na^{+} from geothermal water before lithium sorption studies. The methods for pretreatment and lithium sorption are described as follows:

Softening of Tuzla geothermal water by EDTA

250 mL geothermal water + 7 g EDTA pH=10 (pH adjusted with NaOH.)

- 250 mL of geothermal water was filtered to remove suspended solids before use.
- Then 7 g of EDTA was added and mixed for a while.
- The pH of the geothermal water was adjusted to 10 with NaOH.
- Afterwards, the solution was left for a while to form a complex with Ca^{2+}, Mg^{2+}.
- The solution was filtered through filter paper. Li sorption experiments (25°C, 0.6/0.7 g FC/FHS, 25 mL solution, 24 h shaking) were performed using geothermal water free of Ca and Mg.

Softening of Tuzla geothermal water by Na_2CO_3

250 mL geothermal water + 5 g Na_2CO_3 pH=11 (pH adjusted with NH_3)

- 250 mL of geothermal water was filtered to remove suspended solids before use.
- Then, 5 g of Na_2CO_3 was added and mixed for a while.
- The pH of the geothermal water was adjusted to 11 with NH_3 and the formation of white precipitate was observed.
- Then the solution was allowed to form totally the white precipitate containing $CaCO_3$ and $MgCO_3$ (See Figure 6.1.)
- The solution was filtered through filter paper. Li sorption experiments (25ºC, 0.6 g FC, 25 mL solution, 24 h shaking) were performed using geothermal water free from Ca and Mg.

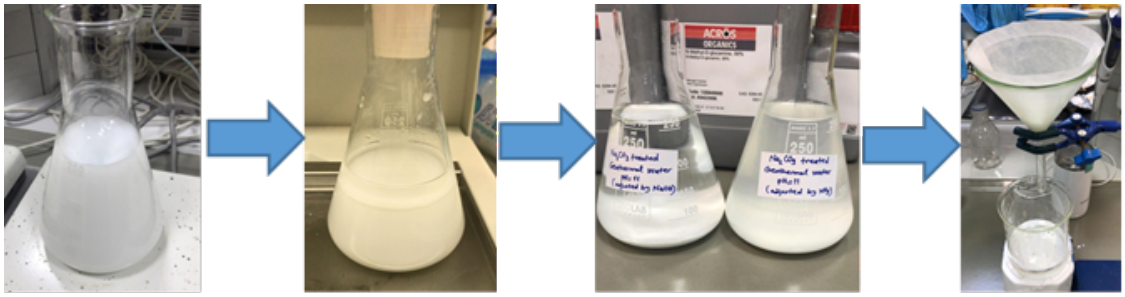

Figure 6.1. Experimental stages for pretreatment of Tuzla geothermal water by Na_2CO_3 to remove Ca and Mg.

Pretreatment of Tuzla geothermal water by gradual deionization process

Ca and Mg precipitated geothermal water (~250 mL) obtained by Na_2CO_3 softening was first applied batch adsorption for Na^+ removal using Purolite® C100MBH cation exchange resin (90 mL). Then, Li sorption experiments (25ºC, 0.6 g FC, 25 mL solution, 24 h shaking) were performed using de-ionized geothermal water.

Pretreatment of Tuzla geothermal water by gradual precipitation and evaporation method

- 250 mL of geothermal water was filtered to remove suspended solids before use.
- The pH was adjusted to=12.4 with NaOH.
- Geothermal water with a pH of 12.4 was heated to 90ºC and mixed at 90ºC for 20 min

to precipitate $MgCO_3$, $CaCO_3$, $Mg(OH)_2$, $Ca(OH)_2$ and so on.

- The sediment was allowed to settle, filtered and the filtrate analyzed (Phase-1).
- The pH of the Ca and Mg precipitated filtrate was adjusted to 12 with NaOH.
- Na_2CO_3 was added at the concentration of 1 g Na_2CO_3/1 L solution according to the remaining filtrate volume.
- The solution was heated to 100ºC and evaporated and concentrated until 50 mL of solution remained at this temperature.
- After evaporation, it was left to cool and Li_2CO_3 and other impurities were expected to precipitate.
- The solution was filtered, and the filtrate analyzed. (Phase-2)
- The solid that is expected to contain mostly Li_2CO_3 remaining from the filtered solution was washed with plenty of water on filter paper and then left to dry.
- The solid (Li_2CO_3 and other impurities) obtained in the 2nd phase and dried was transferred to a beaker with 100 mL of water, and concentrated acid was added dropwise and completely dissolved.
- Li_2CO_3 solid dissolved solution was analyzed. (Phase-3) (See Figure 6.2)

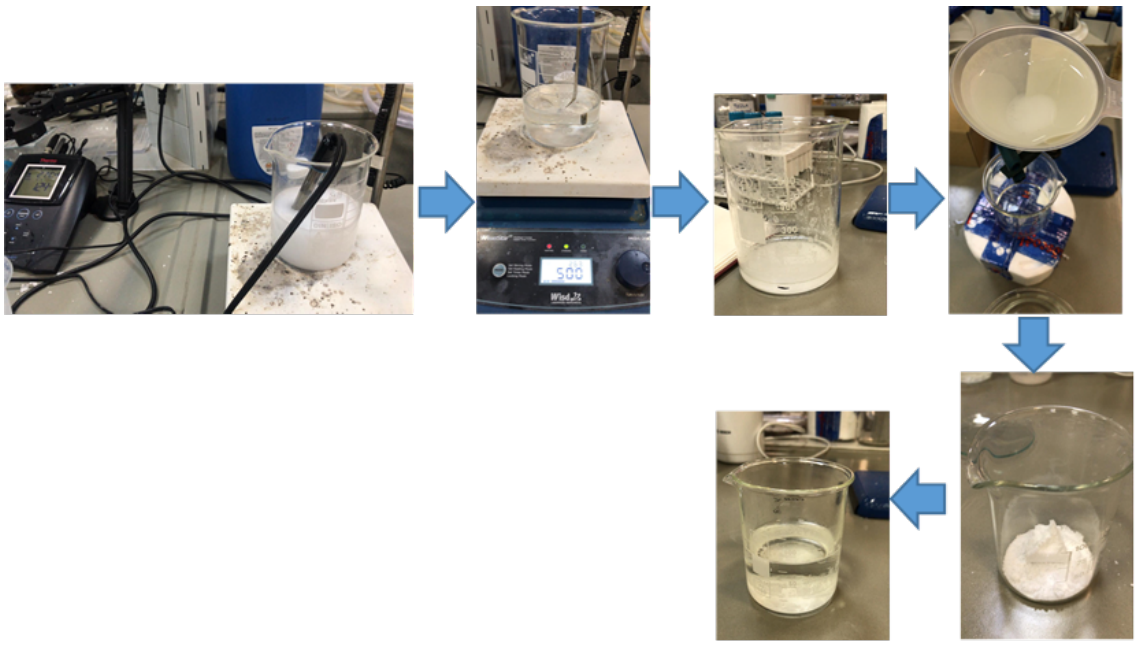

Figure 6.2. Experimental stages for pretreatment of Tuzla geothermal water by stagewise precipitation and evaporation method.

6.2.3.3. Lithium Sorption from Germencik Geothermal Water

The effect of sorbent dose was investigated with various amounts of phosphorylated functional cellulose and hazelnut shell waste ranging from 0.1 g to 0.5 g in 25 mL geothermal water at 25°C via shaking at 180 rpm for 24 h and compared with commercially available ion exchange resin, Lewatit® TP 260.

Some kinetic experiments were also run at three different temperatures (30°C, 40°C, and 50°C) using Lewatit® TP 260 and Germencik geothermal water at a 20 g/L of sorbent dose. The sampling was done periodically for 120 min.

The concentration of Li and the other cations was determined using ICP-OES (Agilent Technologies, 5110) equipment in all experiments carried out with any geothermal water.

6.3. Results and Discussion

6.3.1. Effect of Sorbent Dose on Lithium Separation from Seferihisar Geothermal Water

The lithium separation efficiency of phosphorylated functional cellulose (FC) and hazelnut shell waste (FHS) at different biosorbent doses in both LiCl solution and Seferihisar geothermal water is given in Figure 6.3 by comparison. The lithium removal effectiveness increases as the biosorbent quantity increases up to a certain dose. Quite a similar tendency was observed for both materials and in both solutions. Increased biosorbent dose increased the number of active sites available for sorption, aiding Li removal and explaining the rise in elimination percentage. While FC showed a lithium sorption efficiency of ca. 93% in solution containing only 10 mg/L Li at optimum sorbent dose (12 g/L), lithium separation efficiency was found to be ca. 50% when used in geothermal water. Under the same conditions, the Li sorption efficiency of FHS was calculated as 90% in the solution containing only Li, while it was approximately 48% in geothermal water. However, such performance comparison does not give a definitive idea because the sorption efficiency is highly dependent on the initial Li concentration along with other competitive ions. The lithium concentration of the Seferihisar geothermal

water is 7.13 mg/L and contains other ions in relatively high concentrations, but the model LiCl solution contains only 10 mg/L Li. Despite this, the phosphorylated materials demonstrated the ability to sequester lithium in actual brine, as evidenced by the materials' relatively modest yet exceptional lithium sorption efficiency.

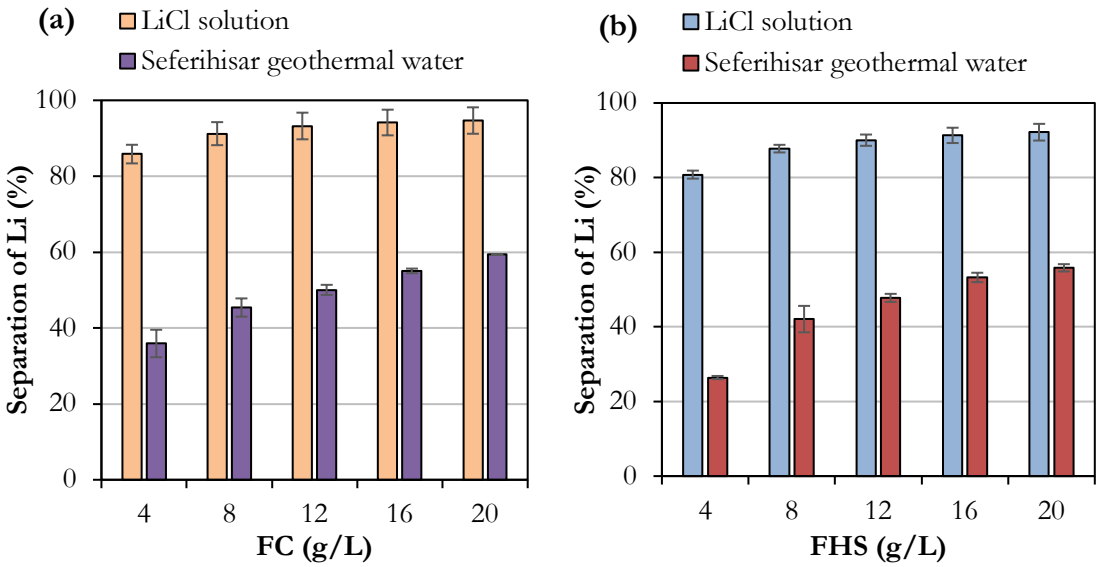

Figure 6.3. Comparison of lithium separation efficiency of phosphorylated functional **(a)** cellulose (FC), and **(b)** hazelnut shell waste (FHS) at different biosorbent doses in both LiCl solution and Seferihisar geothermal water.

On the other hand, Figure 6.4 illustrates Li^+ separation efficiencies of both FC and FHS over other major cations such as Na^+, K^+, Ca^{2+}, and Mg^{2+} by comparing with commercially available ion exchange resin, Lewatit® TP 260. From the % separation of metal ions, it was observed that FC and FHS were comparable with the commercial resin since the resin was not also separated Li alone but also other ions. FC and FHS had similar trends with the commercially available ion exchange resin in separating ions from geothermal water although they were previously shown to be extremely favorable to Li ions in model solution. Still, commercial resin and synthesized biosorbents exhibited the highest separation efficiency performance for Li so that Lewatit® TP 260 could achieve 88.3% Li separation, whereas it was 50% for FC and 50.5% for FHS. However, Ca was the dominant cation that competes with Li with 71%, 47.6%, and 43% separation for Lewatit® TP 260, FHS, and FC, respectively. As the data indicates, depending on the level of concentrations, other competing ions reduced Li separation efficiency, but Li was

concentrated almost two times higher than in the initial geothermal water. Moreover, a selective and high-affinity sorbent working with other ions would be highly desirable.

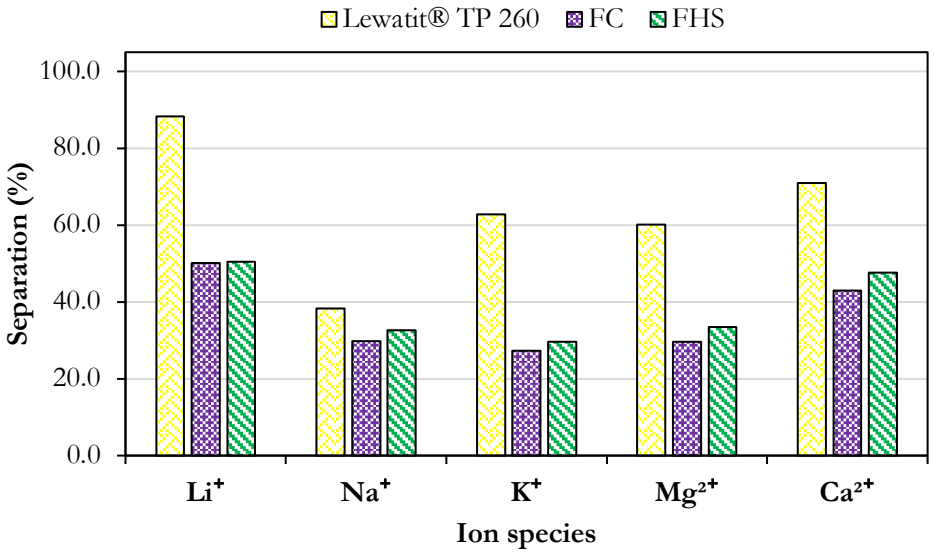

Figure 6.4. Comparison of phosphorylated functional cellulose (FC) and hazelnut shell waste (FHS) with Lewatit® TP 260 for separation of Li and other major cations from Seferihisar geothermal water.

To sum up, results from the first trials by geothermal water showed that the lithium sorption efficiencies of these biosorbents are comparable with commercially available ion exchange resin. However, the efficiency and selectivity need to be improved by pretreatment of geothermal water, such as softening with Na_2CO_3 to eliminate competitive cations (Kalmykov et al., 2021). Nonetheless, because the volume of geothermal water sample supplied from the Seferihisar district of Izmir is restricted, some pretreatment methods and additional lithium sorption investigations by FC and/or FHS could not be performed with this water sample. Therefore, some alternative geothermal water samples were provided from somewhere else such as Tuzla and Germencik.

6.3.2. Lithium Separation from Tuzla Geothermal Water

The main findings acquired under specified optimum conditions such as 0.6 g of FC and/or 0.7 g of FHS in 25 mL geothermal water sample taken from Tuzla with higher

Li and other ions concentrations and without any pretreatment are given in Table 6.5. Apparently, the presence of Ca^{2+}, Mg^{2+}, Na^{+} and K^{+} ions, which are quite high compared to lithium, adversely affected the lithium separation efficiency of the materials. Separation efficiencies of the ions were 46.3%, 30.2%, 18.7%, 16.8% and 1.4%, respectively for FC whereas they were 52.3%, 37.2%, 16.7%, 14.3% and 3.11% for FHS. It was seen that phosphorylated materials sorbed preferentially more Ca^{2+} and Mg^{2+} compared to Li^{+} ions. Moreover, relatively higher Na^{+} and K^{+} content also inhibited Li^{+} separation performance of the materials. Therefore, to increase the lithium recovery efficiency of phosphorylated functional cellulose and hazelnut shell waste, it was deemed necessary to purify the geothermal water from its main competitive ions such as Ca^{2+}, Mg^{2+}, Na^{+}, and K^{+}, and a series of pretreatment applications were applied to the geothermal water and lithium sorption experiments were carried out followingly.

Table 6.5. Ion separation efficiencies of FC and FHS with Tuzla geothermal water.

	Separation efficiency (%)				
	Li^{+}	**K^{+}**	**Na^{+}**	**Ca^{2+}**	**Mg^{2+}**
***FC**	1.36	16.84	18.74	46.32	30.21
****FHS**	3.11	14.31	16.71	52.27	37.23

*Phosphorylated functional cellulose
**Phosphorylated functional hazelnut shell waste

6.3.2.1. Effect of Pretreatment by EDTA on Lithium Separation Efficiency

After pretreatment with EDTA, Li^{+}, K^{+}, Na^{+}, Ca^{2+} and Mg^{2+} concentrations were measured as 26.25, 1974.41, 17017.50, 2216.37 and 108.36 mg/L, respectively. Approximately a 20% reduction in Ca concentration and a 6% reduction in Mg concentration were achieved in Tuzla geothermal water by using EDTA. Conversely, a slight increase was observed in Na concentration due to the addition of EDTA. Table 6.6 lists the removal percentages of lithium and other cations by FC and/or FHS from geothermal water. When compared with the conditions without any pretreatment, the lithium separation efficiency of FC in Tuzla geothermal water increased from 1.36% to 7.89%, and the separation efficiency of FHS increased from 3.11% to 10.10%. In addition, 0.02% (FC) and 0.67% (FHS) separation efficiencies for Ca proved that Ca

concentration was successfully lowered to a level that cannot compete with Li^+. However, other ions such as Na^+, Mg^{2+} and K^+ still compete with Li^+. These results showed that EDTA treatment with the specified conditions was insufficient to separate lithium selectively at a considerable level from Tuzla geothermal water by FC and/or FHS but the biosorbents proved to have a potential to recover lithium from geothermal water.

Table 6.6. Ion separation efficiencies of FC and FHS with Tuzla geothermal water pretreated with EDTA.

	Separation efficiency (%)				
	Li^+	**K^+**	**Na^+**	**Ca^{2+}**	**Mg^{2+}**
***FC**	7.89	22.57	6.25	0.02	29.12
****FHS**	10.10	29.55	7.93	0.67	31.32

*Phosphorylated functional cellulose
**Phosphorylated functional hazelnut shell waste

6.3.2.2. Effect of Pretreatment by Na_2CO_3 on Lithium Separation Efficiency

Table 6.7 gives the concentrations of Ca^{2+}, Mg^{2+}, K^+, Na^+ and Li^+ ions obtained after pretreatment of Tuzla geothermal water with Na_2CO_3 and sorption with phosphorylated functional cellulose (FC). As a result of the applied pretreatment, the initial concentrations of Ca (2768.59 mg/L) and Mg (114.96 mg/L) in geothermal water were successfully reduced to 13.01 mg/L and 7.92 mg/L, respectively. Furthermore, precipitation efficiency for Ca was 99.5% and it was 93.1% for Mg. However, Na concentration increased to 19443.17 mg/L due to the addition of Na_2CO_3 to the medium as expected. Sorption results by FC results revealed that only 2.26% of Li could be separated from the geothermal water. Still, a considerable amount of Na and K were removed at the same time, that probably inhibited effective Li sorption from geothermal water. On the other hand, 78.3% of Ca removal and 86.5% of Mg removal were also observed despite their low concentrations in geothermal water compared to Li. Meanwhile, to prevent material consumption, sorption tests by phosphorylated hazelnut shell waste were not conducted. In the next step, Ca and Mg were gradually precipitated with Na_2CO_3, then commercial cation exchange resin (Purolite® C100MBH) was used to reduce the high Na concentration, and lithium sorption study was carried out using FC.

Table 6.7. Ion concentrations in Tuzla geothermal water after pretreatment with Na_2CO_3 and sorption with phosphorylated functional cellulose

Geothermal water sample	Ca (mg/L)	K (mg/L)	Li (mg/L)	Mg (mg/L)	Na (mg/L)
After Na_2CO_3 treatment	13.01	2211.17	23.83	7.92	19443.17
After sorption by FC*	2.82	1585.55	23.29	1.07	15465.28

*Phosphorylated functional cellulose

6.3.2.3. Effect of Gradual Deionization on Lithium Separation Efficiency

Table 6.8 shows the major ion concentrations in Tuzla geothermal water by gradual ion removal studies. As a result of treatment with commercially available resin Purolite® C100MBH, the Na concentration in previously Ca and Mg precipitated Tuzla geothermal water by Na_2CO_3 decreased significantly from 19433.17 mg/L to 9102.85 mg/L. However, since the resin is a strong cation exchanger, it also captured some lithium. Despite this, the remaining 16.14 mg/L Li in the medium is still at a remarkable level to recover it. However, even though 11.65% lithium removal was achieved when phosphorylated functional cellulose was contacted with the filtrate obtained after treatment with commercial resin, lithium recovery at the desired purity and level could not be achieved in the presence of other ions. Meanwhile, to prevent sorbent consumption, sorption tests by phosphorylated hazelnut shell waste were not conducted here as well. As a result, a new strategy was used in the following pretreatment step, with the goal of gradually increasing the Li concentration to a level where it could compete with other ions through precipitation and evaporation.

Table 6.8. The major ion concentrations in Tuzla geothermal water after gradual deionization process.

Geothermal water sample	Ca (mg/L)	K (mg/L)	Li (mg/L)	Mg (mg/L)	Na (mg/L)
After Na_2CO_3 treatment	13.01	2211.17	23.83	7.92	19443.17
After Na removal by Purolite® C100MBH	78.76	1278.58	16.14	12.17	9102.85
After sorption by FC*	51.40	658.74	14.26	2.52	8446.35

*Phosphorylated functional cellulose

6.3.2.4. Effect of Gradual Precipitation and Evaporation on Major Ion Concentrations

The application of gradual precipitation and evaporation method was based on the study published by (Um and Hirato, 2013) on lithium recovery from seawater for lithium separation from hydrochloric acid solutions containing $CaCl_2$, $MgCl_2$, $MnCl_2$, NaCl, KCl and LiCl. A two-stage precipitation method was used in this procedure, with NaOH used to remove Ca, Mg, and Mn and Na_2CO_3 used to separate Li. As a result, Ca, Mg and Mn were mostly removed from the target solutions by precipitation as $Ca(OH)_2$, $Mg(OH)_2$ and $Mn(OH)_2$ in the pH range of 11.5 to 12.5. The residual Li precipitated as Li_2CO_3 by Na_2CO_3 in the second step was concentrated by evaporation at 100^oC to provide high lithium recovery. In the study, the solvent that may dissolve the salts of other ions but is not selective to Li_2CO_3 was not specified. In Table 6.9, the major ion concentrations in Tuzla geothermal water applied after the gradual precipitation and evaporation method are presented. As expected, an increase in the concentration of all ions was observed because of concentrating by evaporation and precipitation. So much so that the Li concentration increased up to 141.6 mg/L. However, when the solid precipitate obtained after evaporation was washed with water, lithium along with other ions passed into the washing water so that only 0.2 mg/L Li remained in the solution obtained by dissolving the solid of the concentrated filtrate. At this stage, washing not with water that can dissolve all ions, but with a suitable solvent that does not dissolve lithium but dissolves other ions will ensure that the desired goal is achieved. In this context, solvents such as ethanol and acetone were used, but the desired result could not also be obtained. In addition, precipitation of lithium in the form of LiF in the presence of NH_4F, not in carbonate form, was also tested, and washing was carried out with 1.5 M NH_4F solution. Although the desired target is achieved in terms of not losing Li, the Na concentration as high as 17504.9 mg/L might still be a problem for phosphorylated functional cellulose and/or hazelnut shell waste based on the previous trials. Thus, Li sorption studies were not undertaken to avoid redundant sorbent use.

Table 6.9. Ion concentrations in Tuzla geothermal water using gradual precipitation and evaporation method.

Sample	Ca (mg/L)	K (mg/L)	Li (mg/L)	Mg (mg/L)	Na (mg/L)
Ca and Mg precipitated filtrate at 90°C (Phase-1)	3936.3	2203.8	38.7	4.8	43003.8
The filtrate evaporated at 100°C (Phase-2)	8647.4	7780.3	141.6	4.0	88724.9
The solution obtained by dissolving the solid of the concentrated filtrate	1670.3	235.1	0.2	6.5	22197.3

Overall, while phosphorylated functional cellulose and hazelnut shell waste did not achieve the desired goal of high purity lithium recovery from hypersaline geothermal water like the one obtained from Tuzla, the biosorbents demonstrated the ability to concentrate lithium in geothermal water.

6.3.3. Lithium Separation from Germencik Geothermal Water

6.3.3.1. Effect of Sorbent Dose on Lithium Separation from Germencik Geothermal Water

The dependence of Li separation from Germencik geothermal water on phosphorylated functional cellulose (FC) and hazelnut shell waste (FHS) on sorbent dose was determined by varying the amounts of sorbents from 4 to 20 g/L while keeping other parameters constant. They also compared with the commercially available ion exchange resin, Lewatit® TP 260. Figure 6.5 shows the separation efficiency of FC, FHS and Lewatit® TP 260 for Li for the different doses used in Germencik geothermal water. It can be observed that, sorption efficiency of any sorbent rose with dose in general. The percentage separation of Li increased from 24% at sorbent dose of 4 g/L to around 45% at sorbent dose of 16 g/L and tended to remain constant until 20 g/L sorbent dose for FHS. On the other hand, separation efficiency of Li varied from 25% to 50% for FC with increasing sorbent dose. Furthermore, a similar effect was observed for Lewatit® TP 260 so that Li separation efficiencies of it were recorded ranging from 29% to 71.5% at doses of 4g/L and 20 g/L, respectively. The enhanced sorption pattern of Li^+ ions might be attributable to an increase in the number of accessible sorption sites with increasing dose.

This agrees well with the many observations in the literature for the recovery of lithium from brine by various adsorbents (Bao et al., 2023; Kamran and Park, 2020; Lin et al., 2019; Nampeera et al., 2022; Xie et al., 2022; Zhang et al., 2023; Zhao et al., 2022).

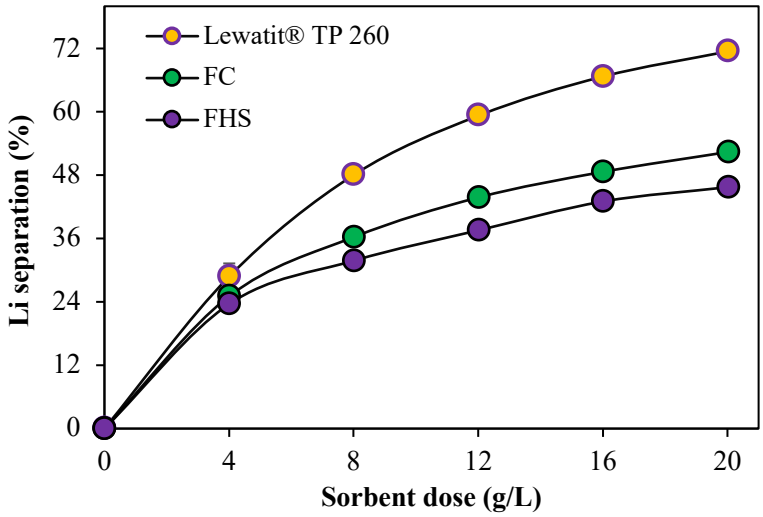

Figure 6.5. Effect of sorbent dose on Li separation from Germencik geothermal water using FC, FHS and Lewatit® TP 260.

6.3.3.2. Kinetic Studies on Lithium Separation from Germencik Geothermal Water by Lewatit® TP 260

Figure 6.6 demonstrates the effect of contact time on Li sorption capacity of commercially available ion exchange resin, Lewatit® TP 260 at different temperatures using Germencik geothermal water. At all temperatures, the quantity of Li uptake (qe) increased with increasing contact time. Furthermore, when the temperature increased from 30 to 50°C, the amount of Li separated increased somewhat. The Li sorption was rapid for the first 10 min, then it slowed and ultimately reached saturation after 20 min. These observations revealed that temperature has no influence on the time necessary for equilibrium. As a result, the initial fast stage was shown to account for up to 90% of overall Li sorption. The higher sorption rate at the initial stage might be attributed to an increase in the number of unoccupied sites accessible at the beginning, which is caused by an increase in the concentration gradients between Li^+ ions in the geothermal water and on the resin surface. As time passes, Li concentration decreases due to the

accumulation of Li^+ ions at vacant sites and competition from other ions, resulting in a decrease in sorption rate at later stages. The resulting separation curves were single, smooth, and continuous, showing monolayer coverage of Li on the surface of the resin.

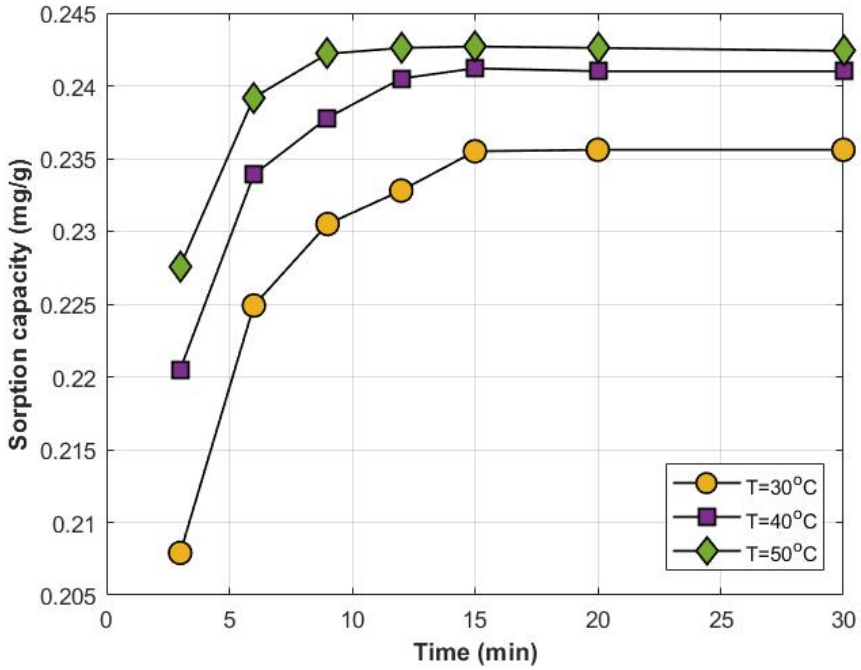

Figure 6.6. Effect of contact time on Li sorption capacity of Lewatit® TP 260 at different temperatures using Germencik geothermal water.

Moreover, kinetic models stated as a sum of first- and second-order systems were used to determine the sorption rate constants. The kinetic models are expressed as pseudo-first order (PFO) and pseudo-second order (PSO) equations in terms of $(q_e - q)$, where q_e is the sorption capacity at equilibrium (mg g^{-1}) and q is the sorption capacity (mg g^{-1}) at any time, t (min) (Islam et al., 2021; Revellame et al., 2020). The PFO equation (Lagergren, 1898) is derived as follows:

$$\frac{dq}{dt} = k_1(q_e - q) \tag{6.1}$$

where k_1 (min^{-1}) is the apparent sorption rate constant for the PFO sorption process. Integrating Eq. (6.1) for $t = 0$, $q = 0$, it gives:

$$-\ln\left(1 - \frac{q}{q_e}\right) = k_1 t \tag{6.2}$$

The PSO sorption kinetics (Ho and McKay, 1999) is derived as follows:

$$\frac{dq}{dt} = k_2(q_e - q)^2 \tag{6.3}$$

where k_2 (g mg^{-1} min^{-1}) is the apparent sorption rate constant for the PFO sorption process. Integrating Eq. (6.3) for $t = 0$, $q = 0$, and rearranging, it gives:

$$\frac{t}{q} = \frac{1}{k_2 q_e^2} + \frac{1}{q_e} t \tag{6.4}$$

The values of k_1 and k_2 can be determined by either a linear or nonlinear regression. In linear regression, if a $-\ln(1 - q/q_e)$ vs t plot gives a straight line, the value of k_1 is determined from the slope. On the other hand, if a t/q vs t plot gives a straight line, the value of k_2 is determined from the intercept of the plot. However, nonlinear regression was applied by MATLAB® to determine the values of rate constants which minimize the error caused by linearization. Thus, the nonlinear forms of PFO and PSO equations are given in Eq. (6.5) and Eq. (6.6), respectively, as follows, in which the sorption capacity (q) is defined as a function of time (t):

$$q(t) = q_e(1 - e^{-k_1 t}) \tag{6.5}$$

$$q(t) = \frac{q_e^2 k_2 t}{1 + q_e k_2 t} \tag{6.6}$$

The equation fittings and parameters of the PFO and PSO kinetic models obtained by nonlinear regression for the sorption of lithium from Germencik geothermal water onto Lewatit® TP 260 at different temperatures are provided in Table 6.10. The correlation coefficient (R^2) of the PSO equation is approximate to one in comparison with the PFO. In addition, the root mean square error (RMSE) of PSO is lower by ten than that of PFO. Therefore, the PSO model presented better fit for Lewatit® TP 260. In this model, the sorption site occupancy rate is assumed to be proportional to the square of the number of empty sites showing that the polymers have energetically non-equivalent binding sites (Tarley et al., 2015). As the temperature increased from 30 to 50^{o}C, the sorption rate constant drastically risen from 8.148 to 14.329 g mg^{-1} min^{-1}. At the point where temperature increases, the limit of the equilibrium sorption also increases from 0.234 to

0.249 mg g^{-1}. The equilibrium sorption capacity experimentally varied from 0.235 to 0.243 mg g^{-1}, also indicating that the PSO model agreed well with the experimental data. This suggests a chemisorption mechanism, in which the control step is a physical-chemical sorption or adsorption process involving valence force via electron sharing or exchange between the sorbent and sorbate (Chen et al., 2019).

Table 6.10. Equation fittings and parameters of the PFO and PSO kinetic models for the sorption of lithium from Germencik geothermal water onto Lewatit® TP 260 at different temperatures.

		Temperature		
Equations	**Parameters**	30°C	40°C	50°C
Pseudo-first order	k_1 (min^{-1})	0.765	0.862	0.943
	q_e (mg g^{-1})	0.230	0.238	0.242
	RMSE	0.00287	0.00265	0.00140
	R^2	0.957	0.941	0.974
	Adjusted R^2	0.935	0.911	0.961
	p-value	8.19E-05	6.45E-05	1.72E-05
Pseudo-second order	k_2 (g mg^{-1} min^{-1})	8.148	10.855	14.329
	q_e (mg g^{-1})	0.234	0.248	0.249
	RMSE	0.000627	0.000377	0.00100
	R^2	0.998	0.999	0.984
	Adjusted R^2	0.997	0.998	0.976
	p-value	3.92E-06	1.31E-06	1.07E-05

The kinetic data were further analysed by utilizing diffusional and reaction models as given in Table 6.11. One approach employs the infinite solution volume (ISV) model, which is based on Vermeulen's diffusion model. The alternative way, on the other hand, employs the unreacted core model (UCM) to characterize the rate-determining steps in the ion exchange process (Recepoğlu et al., 2017b). Because resistance in the bulk solution is readily regulated and low, the overall rate of the ion-exchange process is normally determined by three resistances: film diffusion, particle diffusion, and chemical reaction (Ipek et al., 2017). The plots for the fittings of experimental data with diffusional and reaction models are given in the supplementary information for Chapter 6 in Appendix E. According to Table 6.12, in which the correlation coefficient (R^2) values for lithium sorption by Lewatit® TP 260 after evaluation by ISV and UCM models are

presented, in terms of the diffusional and reaction models, the rate is controlled by particle diffusion at 30ºC, but as temperature increases, the rate is controlled by film diffusion. When evaluated kinetic data using UCM model equations, it was observed that chemical reaction was apparently rate controlling step at all temperatures.

Table 6.11. Diffusional and reaction models (Recepoğlu et al., 2017a)

Model	Equation	Rate-determining step
ISV	$-\ln(1-X) = kt \; where \; k = D_r\pi^2/r_0^2$	Film diffusion
	$-\ln(1-X^2) = K_{1i}t \; where \; K_{1i}t = 3DC/r_0\delta C_r$	Particle diffusion
UCM	$X = (3C_{A0}K_{mA}/a_{r0}C_{s0})t$	Liquid film
	$3-3(1-X)^{2/3}-2X = (6D_{eR}C_{A0}/a_{r0}2C_{s0})t$	Reacted layer
	$1-(1-X)^{1/3} = (k_sC_{A0}/a_{r0}C_{s0})t$	Chemical reaction

a: stoichiometric coefficient, C: total concentration of both exchanging species (M), C_{A0}: concentration of species A in bulk solution (M), D: diffusion coefficient in solution phase (m^2/s), D_{eR}: effective diffusion coefficient in solid phase (m^2/s), D_r: diffusion coefficient in solid phase (m^2/s), K_{1i}: rate constant for film diffusion (ISV condition, L/s), K_{mA}: mass transfer coefficient of species A through the liquid film (m/s), k: rate constant (L/s), k_s: reaction constant based on surface (m/s), r_0: average particle radius (mm), t: time (s), X: fractional attainment of equilibrium or extent of resin conversion ($X = q_e/q$), δ:film thickness (mm)

Table 6.12. Evaluation of kinetic data for Li sorption from Germencik geothermal water by Lewatit® TP 260 according to diffusional and reaction models.

Temperature (ºC)	ISV		UCM		
	Film diffusion	Particle diffusion	Liquid film	Reacted layer	Chemical reaction
30	0.9906	0.9920	0.8488	0.9345	0.9567
40	0.9786	0.9774	0.8629	0.9621	0.9863
50	0.9938	0.9933	0.7781	0.9009	0.9697

6.4. Conclusion

Preliminary studies for lithium extraction from various geothermal water sources available in Türkiye by using phosphorylated functional cellulose (FC) and/or hazelnut shell waste (FHS) were performed. The utilization of these abundant and renewable biomass-based materials not only provides an eco-friendly approach for lithium recovery but also addresses the environmental concerns associated with lithium mining and extraction from aqueous sources. Three different geothermal water samples obtained from

Türkiye's İzmir (Seferihisar), Çanakkale (Tuzla), and Aydın (Germencik) provinces (all situated in western Anatolia) as real lithium sources were utilized in this context.

FC demonstrated a lithium sorption efficiency of 50% at the optimal sorbent dosage (12 g/L) in Seferihisar geothermal water, and it was roughly 48% for FHS. Biosorbents (FC and FHS) had similar trends with the commercially available ion exchange resin, Lewatit ® TP 260, in separating ions from Seferihisar geothermal water although they were previously shown to be extremely favorable to Li ions in model solutions. Moreover, it was observed that the resin could achieve 88.3% Li separation from Seferihisar geothermal water, whereas it was 50% for FC and 50.5% for FHS.

Tuzla geothermal water required pretreatment to eliminate its main competitive ions prior to Li^+ separation with higher efficiency since it is a hypersaline water. Apparently, the presence of Ca^{2+}, Mg^{2+}, Na^+ and K^+ ions, which are quite high compared to lithium, adversely affected the lithium separation efficiency of the materials. Separation efficiencies of the ions were 46.3%, 30.2%, 18.7%, 16.8% and 1.4%, respectively for FC whereas they were 52.3%, 37.2%, 16.7%, 14.3% and 3.11% for FHS. Although the biosorbents shown a potential to recover lithium from geothermal water, EDTA treatment was inadequate to selectively extract lithium at a significant level from Tuzla geothermal water by FC and/or FHS. As a result of the Na_2CO_3 pretreatment, the initial concentrations of Ca (2768.59 mg/L) and Mg (114.96 mg/L) in geothermal water were successfully reduced to 13.01 mg/L and 7.92 mg/L, respectively. Sorption results by FC results revealed that only 2.26% of Li could be separated from the geothermal water. The effects of gradual deionization by commercial cation exchanger and gradual precipitation and evaporation were investigated to improve lithium recovery efficiency and the product purity.

The dependence of Li separation from Germencik geothermal water on FC and FHS on sorbent dose was determined by varying the amounts of sorbents and compared with the commercially available ion exchange resin, Lewatit® TP 260. The percentage separation of Li increased from 24% at sorbent dose of 4 g/L to around 45% at sorbent dose of 16 g/L and tended to remain constant until 20 g/L sorbent dose for FHS. On the other hand, separation efficiency of Li varied from 25% to 50% for FC with increasing sorbent dose. Furthermore, a similar effect was observed for Lewatit® TP 260 so that Li separation efficiencies of it were recorded ranging from 29% to 71.5% at doses of 4g/L and 20 g/L, respectively. The effect of contact time on Li sorption capacity of Lewatit® TP 260 at different temperatures were studied. The Li sorption was rapid for the first 10

min, then it slowed and ultimately reached saturation after 20 min at all temperatures. The kinetics of the sorption process was found the follow the pseudo-second-order kinetic model for all temperatures suggesting that the sorption process was controlled by chemisorption.

Overall, while FC and FHS did not achieve the desired goal of high purity lithium recovery from hypersaline geothermal water like the one obtained from Tuzla, the biosorbents demonstrated the ability to concentrate lithium in geothermal water. However, it is noteworthy to acknowledge that these studies are in their preliminary stages, and there are several challenges and variables to address before the process can be scaled up for industrial applications. Factors such as the scalability of the process, long-term stability of the sorbents, and the potential for regenerating the adsorbent for multiple cycles need to be thoroughly investigated.

CHAPTER 7

CONCLUSION

This thesis study aims to transform cellulose-based materials including pristine cellulose and lignocellulosic wastes (hazelnut shell waste) into valuable products, such as biosorbents, as part of an effort to promote circular economy practices and sustainability. Additionally, it seeks to extract lithium from water sources to address the growing need for raw materials, driven by advances in electric transportation and energy storage technologies, as well as the diminishing supply of solid mineral resources. The approaches performed in the enhancement of thesis and their benefits are summarized by chapters as follows:

Chapter 2 highlights the utilization of phosphorylated functional cellulose (FC) as a sorbent for the sorption of lithium from water, which shows a significant promise as cost-effective material. The optimal amount of FC from a 10 mg/L solution was found to be 12.0 g per liter of solution, resulting in a removal rate of ca. 94%. pH changes had minimal impact within the tested range. While the presence of other positively charged ions like Na^+ and K^+ slightly reduced efficiency, the FC exhibited a stronger affinity for lithium. Sorption of lithium was more efficient with higher initial concentrations, but less so with higher temperatures due to the exothermic nature of the process. Different models were used for analysis, with Langmuir and Freundlich models providing the best fit. At 25°C, the highest lithium uptake capacity was determined to be 9.60 mg/g. Thermodynamic analysis revealed that the process was spontaneous, exothermic, and tended towards reduced disorder. The separation of lithium was rapid, reaching equilibrium in just three minutes. Additionally, the loaded material could be easily regenerated using a 0.5 M H_2SO_4 solution, and the spent solution could be further processed to recover lithium. The study suggests the potential for synthesizing cost-effective adsorbents from various lignocellulosic waste materials, rich in cellulose, for lithium recovery from sources such as geothermal water, seawater, and brines.

In Chapter 3, hazelnut shell waste as a real cellulose resource was converted into a novel biosorbent with grafting phosphorous groups, so-called phosphorylated functional

hazelnut shell waste (FHS), aiding in lithium recovery. The optimal sorbent dose was 14.0 g/L. Thermodynamic analysis showed spontaneous, exothermic sorption, favoring metal recovery. Higher temperatures decreased lithium sorption, benefiting the exothermic nature of bisorbent. While increase in initial concentration enhanced lithium sorption, except for pH 2 there was no considerable effect of pH on lithium sorption efficiency. The sorption of lithium using FHS followed Freundlich isotherm, with maximum lithium sorption capacity at 7.71 mg/g at 25^{o}C estimated by Langmuir model. The sorption rate was rapid in a way that equilibrium achieved in three minutes. Presence of other cations slightly reduced Li sorption efficiency, but the biosorbent still performed well. Regeneration with 1.0 M HCl or H_2SO_4 was as efficient as >98%. This makes FHA a promising, cost-effective sorbent for sustainable lithium recovery from sources like geothermal water, aligning with goals of waste valorization and renewable energy promotion with supplying lithium for the recent future energy developments.

In Chapter 4, cross-linked phosphorylated functional cellulose polymers were synthesized with varying epichlorohydrin ratios. This yielded more stable and thermally robust cellulose to employ in column operations. In a packed bed column, lower feed flowrates were preferred for better Li adsorption and column utilization. With an increase in flow rate from 0.25 to 1.0 mL min^{-1}, the required bed volume (BV) for breakthrough decreased from 477 mL solution/mL sorbent to 386 mL solution/mL sorbent due to a reduced mass transfer rate, allowing lithium to move through the column more swiftly. Bed height changes didn't significantly affect sorption capacity, enabling widespread use in dynamic columns. Even though the breakthrough times varied at the three bed heights (1.0, 1.5, and 2.0 cm), being 362, 491, and 710 minutes respectively, the total capacities remained consistent at 30.85, 30.15, and 31.68 mg g^{-1}. The Thomas, Yoon–Nelson, and MDR models were used to analyze breakthrough curves. Thomas and Yoon–Nelson models were useful for forecasting lithium recovery, while MDR model excelled better in tracking effluent concentration changes over time. This cellulose-based material with phosphorous groups showed promise for lithium recovery from water due to its adaptability in continuous systems.

Chapter 5 centers on a continuous-flow column packed with phosphorylated functional hazelnut shell waste for lithium absorption. Given that batch data may not translate effectively to larger-scale applications, it's imperative to delve into continuous-flow research to assess its practical adaptability. Breakthrough time was set when lithium recovery drops to 0.6 for the practical lithium production. Higher column height increases

breakthrough time, exhaustion time, and uptake capacity but higher flow rates decrease these parameters. At different flow rates, bed volumes at breakthrough and total saturation points varied. Moreover, breakthrough times and saturation times changed with column height, but capacity was the same. Average biosorbent capacity was enhanced in column operation and was found to be 20 mg Li/g sorbent. Thomas and Yoon–Nelson models fitted experimental data, useful on a large scale to estimate breakthrough curve behavior but MDR model outperformed, being more accurate for predictions. Beyond all, the FC and FHS showed repeatable performance over multiple cycles.

In Chapter 6, preliminary research explored using phosphorylated functional cellulose (FC) and hazelnut shell waste (FHS) for lithium extraction from geothermal water in Türkiye. These eco-friendly, renewable materials aimed to address environmental concerns linked to lithium mining. In Seferihisar geothermal water, FC achieved 50% lithium sorption at 12 g/L dosage, while FHS reached about 48%. However, they performed similarly to commercially available Lewatit® TP 260 resin, achieving 50-52.3% lithium separation in Seferihisar's water. On the other hand, Tuzla's hypersaline geothermal water required pretreatment to remove competitive ions, affecting lithium separation. FC and FHS recovered only 2.26% and 3.11% lithium respectively, after Na_2CO_3 pretreatment. Increasing sorbent dosage improved lithium separation in Germencik water, with FC and FHS reaching 25-50% separation at higher doses, like Lewatit® TP 260. Overall, while FC and FHS concentrated lithium, high-purity recovery from hypersaline water like Tuzla proved challenging in preliminary studies. Scalability, sorbent stability, and regeneration for industrial use remain to be addressed.

This thesis set out to investigate the valorization of cellulose-based materials such as pristine cellulose and hazelnut shell waste for potential application in sustainable lithium recovery from water to promote circular economy. Characterization studies were elucidated in detail to verify the functionality of the newly developed biosorbents. Batch and column sorption studies with the most important operating parameters were performed comprehensively. This thesis was implemented thanks to the financial support of TUBITAK 1001 (Project no. 219M219). Moreover, the outputs of this Ph.D. thesis were widely disseminated through 5 scientific papers and 3 international conference proceedings along with 1 PhD research award. The limitations of the thesis were also presented. The most important challenge was to utilize these biosorbents in real geothermal water so that the modification of the biosorbents should be considered to increase the lithium separation efficiency in real water resources.

REFERENCES

Abe, M., Chitrakar, R., 1987. Synthetic inorganic ion-exchange materials. XLV. Recovery of lithium from seawater and hydrothermal water by titanium (IV) antimonate cation exchanger. Hydrometallurgy 19, 117–128. https://doi.org/10.1016/0304-386X(87)90045-4

Akinhanmi, T.F., Ofudje, E.A., Adeogun, A.I., Aina, P., Joseph, I.M., 2020. Orange peel as low-cost adsorbent in the elimination of Cd(II) ion: kinetics, isotherm, thermodynamic and optimization evaluations. Bioresour Bioprocess 7, 34. https://doi.org/10.1186/s40643-020-00320-y

Al-Ajji, M.A., Al-Ghouti, M.A., 2021. Novel insights into the nanoadsorption mechanisms of crystal violet using nano-hazelnut shell from aqueous solution. J Water Process Eng 44, 102354. https://doi.org/10.1016/j.jwpe.2021.102354

Alasalvar, C., Amaral, J.S., Satır, G., Shahidi, F., 2009. Lipid characteristics and essential minerals of native Turkish hazelnut varieties (Corylus avellana L.). Food Chem 113, 919–925. https://doi.org/10.1016/j.foodchem.2008.08.019

Aljarrah, S., Alsabbagh, A., Almahasneh, M., 2023. Selective recovery of lithium from Dead Sea end brines using UBK10 ion exchange resin. Can J Chem Eng 101, 1185–1194. DOI:10.1002/cjce.24559

Alkaya, E., Erguder, T.H., Demirer, G.N., 2010. Effect of operational parameters on anaerobic co-digestion of dairy cattle manure and agricultural residues: A case study for the Kahramanmaraş region in Turkey. Eng Life Sci 10, 552–559. https://doi.org/10.1002/elsc.201000037

Alkhasov, A.B., Alkhasova, D.A., Ramazanov, A.S., 2020. Technologies of geothermal resources development in South of Russia. Geomech Geophys Geo 6, 1–17. DOI: 10.1007/s40948-019-00129-w

Altun, T., Ecevit, H., Çiftçi, B., 2021. Production of chitosan coated, citric acid modified almond, and hazelnut shell adsorbents for Cr (VI) removal and investigation of equilibrium, kinetics, and thermodynamics of adsorption. Arab J Geosci 14, 439. https://doi.org/10.1007/s12517-021-06631-4

Aoki, D., Nishio, Y., 2010. Phosphorylated cellulose propionate derivatives as thermoplastic flame resistant/retardant materials: Influence of regioselective phosphorylation on their thermal degradation behaviour. Cellulose 17, 963–976. https://doi.org/10.1007/s10570-010-9440-8

Arar, Ö., 2019. Preparation of Anion-Exchange Cellulose for The Removal of Chromate. J Chil Chem Soc 64, 4471–4474. http://dx.doi.org/10.4067/S0717-97072019000204471

Arnold, Y.P., Cabassi, J., Tassi, F., Caffe, P.J., Vaselli, O., 2017. Fluid geochemistry of

a deep-seated geothermal resource in the Puna plateau (Jujuy Province, Argentina). J Volcanol Geotherm Res 338, 121–134. https://doi.org/10.1016/j.jvolgeores.2017.03.030

Arroyo, F., Morillo, J., Usero, J., Rosado, D., El Bakouri, H., 2019. Lithium recovery from desalination brines using specific ion-exchange resins. Desalination 468, 114073. https://doi.org/10.1016/j.desal.2019.114073

Attia, L.A., Sami, N.M., Hassan, H.S., Metwally, S.S., 2022. Performance evaluation of zirconium silicate composite for removal of cadmium and zinc ions. Chem Ecol 1–19. https://doi.org/10.1080/02757540.2022.2078315

Awual, M.R., Yaita, T., Shiwaku, H., 2013. Design a novel optical adsorbent for simultaneous ultra-trace cerium (III) detection, sorption and recovery. Chem Eng J 228, 327–335. https://doi.org/10.1016/j.cej.2013.05.010

Awual, M.R., Yaita, T., Suzuki, S., Shiwaku, H., 2015. Ultimate selenium (IV) monitoring and removal from water using a new class of organic ligand based composite adsorbent. J Hazard Mater 291, 111–119. https://doi.org/10.1016/j.jhazmat.2015.02.066

Awual, M.R., 2015. A novel facial composite adsorbent for enhanced copper (II) detection and removal from wastewater. Chem Eng J 266, 368–375. https://doi.org/10.1016/j.cej.2014.12.094

Awual, M.R., 2016a. Solid phase sensitive palladium (II) ions detection and recovery using ligand based efficient conjugate nanomaterials. Chem Eng J 300, 264–272. https://doi.org/10.1016/j.cej.2016.04.071

Awual, M.R., 2016b. Assessing of lead (III) capturing from contaminated wastewater using ligand doped conjugate adsorbent. Chem Eng J 289, 65–73. https://doi.org/10.1016/j.cej.2015.12.078

Awual, M.R., 2016c. Ring size dependent crown ether based mesoporous adsorbent for high cesium adsorption from wastewater. Chem Eng J 303, 539–546. https://doi.org/10.1016/j.cej.2016.06.040

Awual, M.R., 2019. A facile composite material for enhanced cadmium (II) ion capturing from wastewater. J Environ Chem Eng 7, 103378. https://doi.org/10.1016/j.jece.2019.103378

Awual, M.R., Hasan, M.M., Iqbal, J., Islam, M.A., Islam, A., Khandaker, S., Asiri, A.M., Rahman, M.M., 2020a. Ligand based sustainable composite material for sensitive nickel (II) capturing in aqueous media. J Environ Chem Eng 8, 103591. https://doi.org/10.1016/j.jece.2019.103591

Awual, M.R., Yaita, T., Kobayashi, T., Shiwaku, H., Suzuki, S., 2020b. Improving cesium removal to clean-up the contaminated water using modified conjugate material. J Environ Chem Eng 8, 103684. https://doi.org/10.1016/j.jece.2020.103684

Ayawei, N., Ebelegi, A.N., Wankasi, D., 2017. Modelling and Interpretation of Adsorption Isotherms. J Chem 2017, Article ID 3039817, 11 pages. https://doi.org/10.1155/2017/3039817

Baba, A., Demir, M.M., Koç, G.A., Tuğcu, C., 2015. Hydrogeological properties of hyper-saline geothermal brine and application of inhibiting siliceous scale via pH modification. Geothermics 53, 406–412. https://doi.org/10.1016/j.geothermics.2014.08.007

Baba, A., Şaroğlu, F., Akkuş, I., Özel, N., Yeşilnacar, M.İ., Nalbantçılar, M.T., Demir, M.M., Gökçen, G., Arslan, Ş., Dursun, N., 2019. Geological and hydrogeochemical properties of geothermal systems in the southeastern region of Turkey. Geothermics 78, 255–271. https://doi.org/10.1016/j.geothermics.2018.12.010

Bai, S., Li, J., Ding, W., Chen, S., Ya, R., 2022. Removal of boron by a modified resin in fixed bed column: Breakthrough curve analysis using dynamic adsorption models and artificial neural network model. Chemosphere 296, 134021. https://doi.org/10.1016/j.chemosphere.2022.134021

Baldwin, W., Seeley, F., 1974. Extraction of Lithium from Neutral Brines Using a Beta Diketone and Trioctylphosphine Oxide. Atomic Energy Commission. Patent No: US3793433A.

Bao, L.-R., Zhang, J.-Z., Tang, W.-P., Sun, S.-Y., 2023. Synthesis and adsorption properties of metal oxide-coated lithium ion-sieve from salt lake brine. Desalination 546, 116196. https://doi.org/10.1016/j.desal.2022.116196

Battaglia, G., Berkemeyer, L., Cipollina, A., Cortina, J.L., Fernandez de Labastida, M., Lopez Rodriguez, J., Winter, D., 2022. Recovery of lithium carbonate from dilute Li-rich brine via homogenous and heterogeneous precipitation. Ind Eng Chem Res 61, 13589–13602. https://doi.org/10.1021/acs.iecr.2c01397

Belhalfaoui, B., Aziz, A., Elandaloussi, E.H., Ouali, M.S., De Ménorval, L.C., 2009. Succinate-bonded cellulose: A regenerable and powerful sorbent for cadmium-removal from spiked high-hardness groundwater. J Hazard Mater 169, 831–837. https://doi.org/10.1016/j.jhazmat.2009.04.021

Belosinschi, D., Chabot, B., Brouillette, F., 2012. Release paper: Can phosphate esters be an alternative to silicone? Bioresources 7, 902–912. https://api.semanticscholar.org/CorpusID:35706866

Belova, T.P., Ratchina, T.I., Ershova, L.S., 2019. Lithium recovery from separate of Pauzhetskaya geothermal station by sorbents on the basis of modified silicates and aluminosilicates of the deposits of Kamchatka krai, in: IOP Conference Series: Earth and Environmental Science. IOP Publishing, p. 12032. DOI 10.1088/1755-1315/249/1/012032

Berhe, S., Ayele, D., Tadesse, A., Mulu, A., 2015. Adsorption Efficiency of Coffee Husk for Removal of Lead (II) from Industrial Effluents: Equilibrium and kinetic study. Int J Sci Res Publ 5, 1–8. https://api.semanticscholar.org/CorpusID:53140636

Bloomquist, R.G., 2006. Economic benefits of mineral extraction from geothermal brines., in: Sohn International Symposium; Advanced Processing of Metals and Materials Volume 6: New, Improved and Existing Technologies: Aqueous and Electrochemical Processing. pp. 553–558.

Bulgariu, L., Bulgariu, D., 2018. Functionalized soy waste biomass-A novel environmental-friendly biosorbent for the removal of heavy metals from aqueous solution. J Clean Prod 197, 875–885. https://doi.org/10.1016/j.jclepro.2018.06.261

Bunani, S., Arda, M., Kabay, N., Yoshizuka, K., Nishihama, S., 2017. Effect of process conditions on recovery of lithium and boron from water using bipolar membrane electrodialysis (BMED). Desalination 416, 10–15. https://doi.org/10.1016/j.desal.2017.04.017

Cagnon, B., Py, X., Guillot, A., Stoeckli, F., Chambat, G., 2009. Contributions of hemicellulose, cellulose and lignin to the mass and the porous properties of chars and steam activated carbons from various lignocellulosic precursors. Bioresour Technol 100, 292–298. https://doi.org/10.1016/j.biortech.2008.06.009

Can, M.F., Başaran, C., Yildiz, A., Demirkapi, M., 2021. Lithium extraction from geothermal waters; a case study of Ömer-Gecek (Afyonkarahisar) geothermal area. Turk J Earth Sci 30, 1208–1220. DOI:10.3906/yer-2105-29

Çelik, A., Topçu, G., Isik, T., Baba, A., Horzum, N., Demir, M.M., 2018. Investigation of lithium sorption efficiency using SWCNT functionalized electrospun fiber mats from the hypersaline geothermal brine, in: Materials Science Forum. Trans Tech Publ, pp. 121–126. https://doi.org/10.4028/www.scientific.net/MSF.915.121

Cetiner, Z.S., Doğan, Ö., Özdilek, G., Erdoğan, P.Ö., 2015. Toward utilising geothermal waters for cleaner and sustainable production: potential of Li recovery from geothermal brines in Turkey. Int J Glob Warm 7, 439–453. DOI: 10.1504/IJGW.2015.070045

Chan, W., 1993. Removal and recovery of gallium ion from solution by insoluble amphoteric starches. J Appl Polym Sci 50, 1733–1738. https://doi.org/10.1002/app.1993.070501008

Charola, S., Yadav, R., Das, P., Maiti, S., 2018. Fixed-bed adsorption of Reactive Orange 84 dye onto activated carbon prepared from empty cotton flower agro-waste. Sustain Environ Res 28, 298–308. https://doi.org/10.1016/j.serj.2018.09.003

Cha-umpong, W., Li, Q., Razmjou, A., Chen, V., 2021. Concentrating brine for lithium recovery using GO composite pervaporation membranes. Desalination 500, 114894. https://doi.org/10.1016/j.desal.2020.114894

Chen, I., Xu, C., Peng, J., Han, D., Liu, S., Zhai, M., 2019. Novel Functionalized Cellulose Microspheres for Efficient Separation of Lithium Ion and Its Isotopes: Synthesis and Adsorption Performance. Molecules 24, 2762. https://doi.org/10.3390/molecules24152762

Chen, X., Zhang, R., Zhao, B., Fan, G., Li, H., Xu, X., Zhang, M., 2020. Preparation of porous biochars by the co-pyrolysis of municipal sewage sludge and hazelnut shells and the mechanism of the nano-zinc oxide composite and Cu (II) adsorption kinetics. Sustainability 12, 8668. https://doi.org/10.3390/su12208668

Chen, Z., Zhang, J., Huang, L., Yuan, Z., Li, Z., Liu, M., 2019. Removal of Cd and Pb with biochar made from dairy manure at low temperature. J Integr Agric 18, 201–210. https://doi.org/10.1016/S2095-3119(18)61987-2

Cheruiyot, G.K., Wanyonyi, W.C., Kiplimo, J.J., Maina, E.N., 2019. Adsorption of toxic crystal violet dye using coffee husks: Equilibrium, kinetics and thermodynamics study. Scientific African 5, 1–11. https://doi.org/10.1016/j.sciaf.2019.e00116

Chitrakar, R., Kanoh, H., Miyai, Y., Ooi, K., 2001. Recovery of lithium from seawater using manganese oxide adsorbent (H1.6Mn1.6O4) derived from Li1.6Mn1.6O4. Ind Eng Chem Res 40, 2054–2058. https://doi.org/10.1021/ie000911h

Chitrakar, R., Kanoh, H., Miyai, Y., Ooi, K., 2002a. Synthesis of o-LiMnO2 by microwave irradiation and study its heat treatment and lithium exchange. J Solid State Chem 163, 1–4. doi:10.1006/jssc.2001.9403

Chitrakar, R., Kasaishi, S., Umeno, A., Sakane, K., Takagi, N., Kim, Y.S., Ooi, K., 2002b. Synthesis and characterization of lithium nickel manganese oxides and their delithiated phases. J Solid State Chem 169, 35–43. https://doi.org/10.1016/S0022-4596(02)00014-2

Chuah, T.G., Jumasiah, A., Azni, I., Katayon, S., Choong, S.Y.T., 2005. Rice husk as a potentially low-cost biosorbent for heavy metal and dye removal: an overview. Desalination 175, 305–316. https://doi.org/10.1016/j.desal.2004.10.014

Çiçek, A., Yilmaz, O., Arar, Ö., 2018. Removal of lithium from water by aminomethylphosphonic acid-containing resin. J Serb Chem Soc 83, 1059–1069. https://doi.org/10.2298/JSC170930020C

Çöpür, Y., Güler, C., Taşçıoğlu, C., Tozluoğlu, A., 2008. Incorporation of hazelnut shell and husk in MDF production. Bioresour Technol 99, 7402–7406. https://doi.org/10.1016/j.biortech.2008.01.021

Costes, L., Laoutid, F., Khelifa, F., Rose, G., Brohez, S., Delvosalle, C., Dubois, P., 2016. Cellulose/phosphorus combinations for sustainable fire retarded polylactide. European Polymer Journal 74, 218–228. https://doi.org/10.1016/j.eurpolymj.2015.11.030

Dang, V.D., Steinberg, M., 1978. Preliminary design and analysis of recovery of lithium from brine with the use of a selective extractant. Energy 3, 325–336. https://doi.org/10.1016/0360-5442(78)90029-4

Daoud A, Yokoyama, Yoshizuka, K., 2020. A Study on Recovery of Lithium from Geothermal Water and Study of Assal geothermal field, in: 8th African Geothermal Conference. Nairobi.

Das, K., Ray, D., Bandyopadhyay, N.R., Sengupta, S., 2010. Study of the properties of microcrystalline cellulose particles from different renewable resources by XRD, FTIR, nanoindentation, TGA and SEM. J Polym Environ 18, 355–363. https://doi.org/10.1007/s10924-010-0167-2

Dawood, S., Sen, T.K., Phan, C., 2018. Performance and dynamic modelling of biochar and kaolin packed bed adsorption column for aqueous phase methylene blue (MB) dye removal. Environ Technol 40, 28, 3762–3772. https://doi.org/10.1080/09593330.2018.1491065

Demir, M.M., Baba, A., Atilla, V., Inanlı, M., 2014. Types of the scaling in hyper saline geothermal system in northwest Turkey. Geothermics 50, 1–9. https://doi.org/10.1016/j.geothermics.2013.08.003

Dini, A., Lattanzi, P., Ruggieri, G., Trumpy, E., 2021. "Geothermal lithium": a new resource for Italy. Academia Letters 2.

Dotsika, E., 2012. Isotope and hydrochemical assessment of the Samothraki Island geothermal area, Greece. Journal Volcanol Geotherm Res 233, 18–26. doi:10.1016/j.jvolgeores.2012.04.017

Dotsika, E., Leontiadis, I., Poutoukis, D., Cioni, R., Raco, B., 2006. Fluid geochemistry of the Chios geothermal area, Chios Island, Greece. Journal Volcanol Geotherm Res 154, 237–250. https://doi.org/10.1016/j.jvolgeores.2006.02.013

Epstein, J.A., Feist, E.M., Zmora, J., Marcus, Y., 1981. Extraction of lithium from the dead sea. Hydrometallurgy 6, 269–275. https://doi.org/10.1016/0304-386X(81)90044-X

Feininger, T., 2013. An introduction to the rock-forming minerals. Can Mineral 51, 4, 663–664. https://doi.org/10.1180/DHZ

Flexer, V., Baspineiro, C.F., Galli, C.I., 2018. Lithium recovery from brines: A vital raw material for green energies with a potential environmental impact in its mining and processing. Sci Total Environ 639, 1188–1204. https://doi.org/10.1016/j.scitotenv.2018.05.223

Fomina, M., Gadd, G.M., 2014. Biosorption: current perspectives on concept, definition and application. Bioresour Technol 160, 3–14. https://doi.org/10.1016/j.biortech.2013.12.102

Fouillac, H.P.B.C., 1990. Lithium recovery from geothermal waters of Cesano (Italy) and Cronembourg (Alsace, France), in: Proceedings of the... New Zealand Geothermal Workshop. University of Aukland, Geothermal Institute, p. 117.

French, A.D., 2020. Increment in evolution of cellulose crystallinity analysis. Cellulose 27, 5445–5448. https://doi.org/10.1007/s10570-020-03172-z

French, A.D., 2014. Idealized powder diffraction patterns for cellulose polymorphs. Cellulose 21, 885–896. https://doi.org/10.1007/s10570-013-0030-4

French, A.D., Santiago Cintrón, M., 2013. Cellulose polymorphy, crystallite size, and the Segal Crystallinity Index. Cellulose 20, 583–588. https://doi.org/10.1007/s10570-012-9833-y

Freundlich, H., 1907. Über die adsorption in lösungen. Zeitschrift für physikalische Chemie 57, 385–470.

Fytikas, M., Radoglou, G., Karytsas, C., Mendrinos, D., Vasalakis, A., Andritsos, N., 2005. Geothermal Research in Vounalia Area, Milos Island (Greece), for Seawater Desalination and Power Production, in: Proceedings World Geothermal Congress, Antalya, Turkey.

Gallup, D.L., 1998. Geochemistry of geothermal fluids and well scales, and potential for mineral recovery. Ore Geol Rev 12, 225–236. https://doi.org/10.1016/S0169-1368(98)00004-3

Gao, D., Guo, Y., Yu, X., Wang, S., Deng, T., 2016. Extracting lithium from the high concentration ratio of magnesium and lithium brine using imidazolium-based ionic liquids with varying alkyl chain lengths. J Chem Eng Jpn 49, 104–110. https://doi.org/10.1252/jcej.15we046

Gao, D., Yu, X., Guo, Y., Wang, S., Liu, M., Deng, T., Chen, Y., Belzile, N., 2015. Extraction of lithium from salt lake brine with triisobutyl phosphate in ionic liquid and kerosene. Chem Res Chin Univer 31, 621–626. https://doi.org/10.1007/s40242-015-4376-z

Gao, J., Du, Z., Zhao, Q., Guo, Y., Cheng, F., 2021. Enhanced Li+ adsorption by magnetically recyclable iron-doped lithium manganese oxide ion-sieve: Synthesis, characterization, adsorption kinetics and isotherm. J Mater Res Technol 13, 228–240. https://doi.org/10.1016/j.jmrt.2021.04.073

Garrett, D.E., 2004. Handbook of lithium and natural calcium chloride. Elsevier.

Ghanadpour, M., Carosio, F., Larsson, P.T., Wågberg, L., 2015. Phosphorylated cellulose nanofibrils: a renewable nanomaterial for the preparation of intrinsically flame-retardant materials. Biomacromolecules 16, 3399–3410. https://doi.org/10.1021/acs.biomac.5b01117

Ghogomu, J., 2013. Removal of Pb(II) Ions from Aqueous Solutions by Kaolinite and Metakaolinite Materials. Braz J App Sci Technol 3, 942–961. DOI: 10.9734/BJAST/2013/4384

Godfrey, L. V, Chan, L.-H., Alonso, R.N., Lowenstein, T.K., McDonough, W.F., Houston, J., Li, J., Bobst, A., Jordan, T.E., 2013. The role of climate in the accumulation of lithium-rich brine in the Central Andes. Appl Geochem 38, 92–102. https://doi.org/10.1016/j.apgeochem.2013.09.002

González-Partida, E., Carrillo-Chávez, A., Levresse, G., Tello-Hinojosa, E., Venegas-Salgado, S., Ramirez-Silva, G., Pal-Verma, M., Tritlla, J., Camprubi, A., 2005. Hydro-geochemical and isotopic fluid evolution of the Los Azufres geothermal field,

Central Mexico. Appl Geochem 20, 23–39. https://doi.org/10.1016/j.apgeochem.2004.07.006

Goshadrou, A., Moheb, A., 2011. Continuous fixed bed adsorption of CI Acid Blue 92 by exfoliated graphite: An experimental and modeling study. Desalination 269, 170–176. https://doi.org/10.1016/j.desal.2010.10.058

Gozaydin, G., Yuksel, A., 2017. Valorization of hazelnut shell waste in hot compressed water. Fuel Process Technol 166, 96–106. https://doi.org/10.1016/j.fuproc.2017.05.034

Grosjean, C., Miranda, P.H., Perrin, M., Poggi, P., 2012. Assessment of world lithium resources and consequences of their geographic distribution on the expected development of the electric vehicle industry. Renew Sust Energ Rev 16, 1735–1744. https://doi.org/10.1016/j.rser.2011.11.023

Gruber, P.W., Medina, P.A., Keoleian, G.A., Kesler, S.E., Everson, M.P., Wallington, T.J., 2011. Global lithium availability: A constraint for electric vehicles? J Ind Ecol 15, 760–775. https://doi.org/10.1111/j.1530-9290.2011.00359.x

Guler, U.A., Solmaz, B., 2022. Biosorption of tetracycline and cephalexin onto surfactant-modified waste biomass using response surface methodology and ecotoxicological assessment: phytotoxicity and biotoxicity studies. Water Air Soil Pollut 233, 117. https://doi.org/10.1007/s11270-022-05590-0

Günan Yücel, H., Aksu, Z., Usta, T., Ertuğrul Karatay, S., Dönmez, G., 2021. Novel application of isolated Micrococcus luteus and Bacillus pumilus for Li+ ion biosorption: a comparative study. Prep Biochem Biotechnol 51(9), 892–900. https://doi.org/10.1080/10826068.2021.1872029

Gündoğan, İ., 2000. Geology, Mineralogy-Petrography, and Economic Potential of the Upper Miocene Evaporates in the Beypazari and Çankiri-Çorum basins, PhD Thesis. Dokuz Eylül University, İzmir, Türkiye.

Guney, M.S., 2013. Utilization of hazelnut husk as biomass. Sustain Energy Technol and Assess 4, 72–77. https://doi.org/10.1016/j.seta.2013.09.004

Guo, F., Guo, S., Niu, Y., Qiu, G., Guo, Y., Li, Y., Chen, L., Zhang, Y., Wu, J., 2023. Efficient Removal of Methylene Blue via Two-step Modification Hazelnut Shell Biochar: Process Intensification, Kinetics and Thermodynamics. J Ind Eng Chem 125, 105–116. https://doi.org/10.1016/j.jiec.2023.05.017

Gurgel, L.V.A., Gil, L.F., 2009. Adsorption of Cu(II), Cd(II), and Pb(II) from aqueous single metal solutions by succinylated mercerized cellulose modified with triethylenetetramine. Carbohydr Polym 77, 142–149. https://doi.org/10.1016/j.carbpol.2008.12.014

Gurgel, L.V.A., Júnior, O.K., Gil, R.P. de F., Gil, L.F., 2008. Adsorption of Cu(II), Cd(II), and Pb(II) from aqueous single metal solutions by cellulose and mercerized cellulose chemically modified with succinic anhydride. Bioresour Technol 99, 3077–3083.

https://doi.org/10.1016/j.biortech.2007.05.072

Gurgel, L.V.A., Perin de Melo, J.C., de Lena, J.C., Gil, L.F., 2009. Adsorption of chromium (VI) ion from aqueous solution by succinylated mercerized cellulose functionalized with quaternary ammonium groups. Bioresour Technol 100, 3214–3220. https://doi.org/10.1016/j.biortech.2009.01.068

Halsey, G., 1948. Physical adsorption on non-uniform surfaces. J Chem Phys 16, 931–937.

Hamdaoui, O., Naffrechoux, E., 2007. Modeling of adsorption isotherms of phenol and chlorophenols onto granular activated carbon. Part I. Two-parameter models and equations allowing determination of thermodynamic parameters. J Hazard Mater 147, 381–394. https://doi.org/10.1016/j.jhazmat.2007.01.021

Hameed, B.H., Tan, I.A.W., Ahmad, A.L., 2008. Adsorption isotherm, kinetic modeling and mechanism of 2,4,6-trichlorophenol on coconut husk-based activated carbon. Chem Eng J 144, 235–244. https://doi.org/10.1016/j.cej.2008.01.028

Hano, T., Matsumoto, M., Ohtake, T., Egashir, N., Hori, F., 1992. Recovery of lithium from geothermal water by solvent extraction technique. Solvent Extr Ion Exch 10, 195–206. https://doi.org/10.1080/07366299208918100

Harper, G., Sommerville, R., Kendrick, E., Driscoll, L., Slater, P., Stolkin, R., Walton, A., Christensen, P., Heidrich, O., Lambert, S., 2019. Recycling lithium-ion batteries from electric vehicles. Nature 575, 75–86. https://doi.org/10.1038/s41586-019-1682-5

Hasan, M.M., Shenashen, M.A., Hasan, M.N., Znad, H., Salman, M.S., Awual, M.R., 2021. Natural biodegradable polymeric bioadsorbents for efficient cationic dye encapsulation from wastewater. J Mol Liq 323, 114587. https://doi.org/10.1016/j.molliq.2020.114587

Heidari, N., Momeni, P., 2017. Selective adsorption of lithium ions from Urmia Lake onto aluminum hydroxide. Environ Earth Sci 76, 1–8. https://doi.org/10.1007/s12665-017-6885-1

Helfferich, F.G., 1962. Ion Exchange. McGraw-Hill, New York.

Helvaci, C., Mordogan, H., Çolak, M., Gündogan, I., 2004. Presence and distribution of lithium in borate deposits and some recent lake waters of west-central Turkey. Int Geol Rev 46, 177–190. https://doi.org/10.2747/0020-6814.46.2.177

Ho, Y.-S., McKay, G., 1999. Pseudo-second order model for sorption processes. Process Biochem 34, 451–465. https://doi.org/10.1016/S0032-9592(98)00112-5

Hokkanen, S., Repo, E., Sillanpää, M., 2013. Removal of heavy metals from aqueous solutions by succinic anhydride modified mercerized nanocellulose. Chem Eng J 223, 40–47. https://doi.org/10.1016/j.cej.2013.02.054

Hoşgün, E.Z., Bozan, B., 2020. Effect of Different Types of Thermochemical Pretreatment on the Enzymatic Hydrolysis and the Composition of Hazelnut Shells. Waste Biomass Valori 11, 3739–3748. https://doi.org/10.1007/s12649-019-00711-z

Hui, Z., 2000. Property of H2TiO3 type ion-exchangers and extraction of lithium from brine of natural gas wells. Chin J Appl Chem 17, 307–309. https://api.semanticscholar.org/CorpusID:99242664

Hussein, F.B., Mayer, B.K., 2022. Fixed-bed column study of phosphate adsorption using immobilized phosphate-binding protein. Chemosphere 295, 133908. https://doi.org/10.1016/j.chemosphere.2022.133908

I.E.A., 2021. The role of critical minerals in clean energy transitions. world energy outlook special report.

Iizuka, A., Yamashita, Y., Nagasawa, H., Yamasaki, A., Yanagisawa, Y., 2013. Separation of lithium and cobalt from waste lithium-ion batteries via bipolar membrane electrodialysis coupled with chelation. Sep Purif Technol 113, 33–41. https://doi.org/10.1016/j.seppur.2013.04.014

Illy, N., Fache, M., Ménard, R., Negrell, C., Caillol, S., David, G., 2015. Phosphorylation of bio-based compounds: The state of the art. Polym Chem 6, 6257–6291. https://doi.org/10.1039/C5PY00812C

Inagaki, N., Nakamura, S., Asai, H., Katsuura, K., 1976. Phosphorylation of cellulose with phosphorous acid and thermal degradation of the product. J Appl Polym Sci 20, 2829–2836. https://doi.org/10.1002/app.1976.070201017

Ipek, I., Kabay, N., Yüksel, M., 2017. Separation of bisphenol A and phenol from water by polymer adsorbents: Equilibrium and kinetics studies. J Water Process Eng 16, 206–211. https://doi.org/10.1016/j.jwpe.2017.01.006

İpek, İ.Y., Kabay, N., Yüksel, M., 2013. Modeling of fixed bed column studies for removal of boron from geothermal water by selective chelating ion exchange resins. Desalination 310, 151–157. https://doi.org/10.1016/j.desal.2012.10.009

Islam, M.A., Chowdhury, M.A., Mozumder, M.S.I., Uddin, M.T., 2021. Langmuir adsorption kinetics in liquid media: Interface reaction model. ACS Omega 6, 14481–14492. https://doi.org/10.1021/acsomega.1c01449

Ismail, B., Hussain, S.T., Akram, S., 2013. Adsorption of methylene blue onto spinel magnesium aluminate nanoparticles: Adsorption isotherms, kinetic and thermodynamic studies. Chem Eng J 219, 395–402. https://doi.org/10.1016/j.cej.2013.01.034

Jagur-Grodzinski, J., Schori, E., 1985. Solvent-Polymeric Membranes for Separation of Li+ From Other Alkali Metal and Alkaline Earth Ions. Isr J Chem 26, 65–70. https://doi.org/10.1002/ijch.198500070

Jamil, T.S., Gad-Allah, T.A., Ibrahim, H.S., Saleh, T.S., 2011. Adsorption and isothermal

models of atrazine by zeolite prepared from Egyptian kaolin. Solid State Sci 13, 198–203. https://doi.org/10.1016/j.solidstatesciences.2010.11.014

Jiang, C., Wang, Y., Wang, Q., Feng, H., Xu, T., 2014. Production of lithium hydroxide from lake brines through electro–electrodialysis with bipolar membranes (EEDBM). Ind Eng Chem Res 53, 6103–6112. https://doi.org/10.1021/ie404334s

Jiang, H., Yang, Y., Sun, S., Yu, J., 2020a. Adsorption of lithium ions on lithium-aluminum hydroxides: Equilibrium and kinetics. Can J Chem Eng 98, 544–555. https://doi.org/10.1002/cjce.23640

Jiang, H., Yang, Y., Yu, J., 2020b. Application of concentration dependent HSDM to the lithium adsorption from brine in fixed bed columns. Sep Purif Technol 241, 116682. https://doi.org/10.1016/j.seppur.2020.116682

Johar, N., Ahmad, I., Dufresne, A., 2012. Extraction, preparation and characterization of cellulose fibres and nanocrystals from rice husk. Ind Crops Prod 37, 93–99. https://doi.org/10.1016/j.indcrop.2011.12.016

Kabay, N., Yilmaz, I., Yamac, S., Yuksel, M., Yuksel, U., Yildirim, N., Aydogdu, O., Iwanaga, T., Hirowatari, K., 2004. Removal and recovery of boron from geothermal wastewater by selective ion-exchange resins—II. Field tests. Desalination 167, 427–438. https://doi.org/10.1016/j.desal.2004.06.158

Kalmykov, D., Makaev, S., Golubev, G., Eremeev, I., Vasilevsky, V., Song, J., He, T., Volkov, A., 2021. Operation of Three-Stage Process of Lithium Recovery from Geothermal Brine: Simulation. Membranes (Basel) 11(3), 175. https://doi.org/10.3390/membranes11030175

Kamienski, C.W., McDonald, D.P., Stark, M.W., Papcun, J.R., 2000. Lithium and lithium compounds. Kirk-Othmer Encyclopedia of Chemical Technology.

Kamran, U., Heo, Y.-J., Lee, J.W., Park, S.-J., 2019. Chemically modified activated carbon decorated with MnO2 nanocomposites for improving lithium adsorption and recovery from aqueous media. J Alloys Compd 794, 425–434. https://doi.org/10.1016/j.jallcom.2019.04.211

Kamran, U., Park, S.-J., 2020. MnO2-decorated biochar composites of coconut shell and rice husk: An efficient lithium ions adsorption-desorption performance in aqueous media. Chemosphere 260, 127500. https://doi.org/10.1016/j.chemosphere.2020.127500

Kardam, A., Raj, K.R., Srivastava, S., Srivastava, M.M., 2014. Nanocellulose fibers for biosorption of cadmium, nickel, and lead ions from aqueous solution. Clean Technol Environ Policy 16, 385–393. https://doi.org/10.1007/s10098-013-0634-2

Kaya, N., Yıldız, Z., Ceylan, S., 2018. Preparation and characterisation of biochar from hazelnut shell and its adsorption properties for methylene blue dye. Politeknik dergisi 21, 765–776.

Kesler, S.E., Gruber, P.W., Medina, P.A., Keoleian, G.A., Everson, M.P., Wallington, T.J., 2012. Global lithium resources: Relative importance of pegmatite, brine and other deposits. Ore Geol Rev 48, 55–69. https://doi.org/10.1016/j.oregeorev.2012.05.006

Khalfa, L., Sdiri, A., Bagane, M., Cervera, M.L., 2021. A calcined clay fixed bed adsorption studies for the removal of heavy metals from aqueous solutions. J Clean Prod 278, 123935. https://doi.org/10.1016/j.jclepro.2020.123935

Khambhaty, Y., Mody, K., Basha, S., Jha, B., 2009. Kinetics, equilibrium and thermodynamic studies on biosorption of hexavalent chromium by dead fungal biomass of marine Aspergillus niger. Chem Eng J 145, 489–495. https://doi.org/10.1016/j.cej.2008.05.002

Kim, Y.S., No, K.S., Chung, K.S., Lee, J.C., Ooi, K., 2003. Li+ extraction reactions with spinel-type LiM 0.5Mn1.5O4 (M=Ti, Fe) and their electronic structures. Mater Lett 57, 4140–4146. http://hdl.handle.net/10203/7899

Kim, J.S., Lee, Y.Y., Kim, T.H., 2016. A review on alkaline pretreatment technology for bioconversion of lignocellulosic biomass. Bioresour Technol 199, 42–48. https://doi.org/10.1016/j.biortech.2015.08.085

Kim, S., Joo, H., Moon, T., Kim, S.-H., Yoon, J., 2019. Rapid and selective lithium recovery from desalination brine using an electrochemical system. Environ Sci Process Impacts 21, 667–676. https://doi.org/10.1039/C8EM00498F

Kitajou, A., Suzuki, T., Nishihama, S., Yoshizuka, K., 2003. Selective recovery of lithium from seawater using a novel MnO2 type adsorbent. II–Enhancement of lithium-ion selectivity of the adsorbent. Ars Separatoria Acta 97–106. https://api.semanticscholar.org/CorpusID:91174528

Kitajou, A., Holba, M., Suzuki, T., Nishihama, S., Yoshizuka, K., 2005. Selective recovery system of lithium from seawater using a novel granulated λ-MnO2 adsorbent. Journal of Ion Exchange 16, 49–54.

Kitajou, A., Suzuka, Y., Nishihama, S., Suzuki, T., Yoshizuka, K., 2006. Development of λ-MnO2 adsorbent toward the practical recovery of lithium from seawater. J Ion Exch 17, 7–13.

Kitamura, T., Wada, H., 1978. Properties of adsorbents composed of hydrous aluminum oxide, and its selective adsorption of lithium from sea water. Nippon Kaisui Gakkai-Shi 32, 78–81.

Kofa, G.P., NdiKoungou, S., Kayem, G.J., Kamga, R., 2015. Adsorption of arsenic by natural pozzolan in a fixed bed: determination of operating conditions and modeling. J Water Process Eng 6, 166–173. https://doi.org/10.1016/j.jwpe.2015.04.006

Kokol, V., Božič, M., Vogrinčič, R., Mathew, A.P., 2015. Characterisation and properties of homo-and heterogenously phosphorylated nanocellulose. Carbohydr Polym 125, 301–313. https://doi.org/10.1016/j.carbpol.2015.02.056

Lagergren, S., 1898. Zur theorie der sogenannten adsorption geloster stoffe. Kungliga svenska vetenskapsakademiens. Handlingar 24, 1–39.

Langmuir, I., 1916. The constitution and fundamental properties of solids and liquids. Part I. Solids. J Am Chem Soc 38, 2221–2295.

Lawagon, C.P., Nisola, G.M., Mun, J., Tron, A., Torrejos, R.E.C., Seo, J.G., Kim, H., Chung, W.J., 2016. Adsorptive Li+ mining from liquid resources by H2TiO3: Equilibrium, kinetics, thermodynamics, and mechanisms. J In Eng Chem 35, 347–356. https://doi.org/10.1016/j.jiec.2016.01.015

Lee, Y., Cha, J., Jung, D., 2021. Selective Lithium Adsorption of Silicon Oxide Coated Lithium Aluminum Layered Double Hydroxide Nanocrystals and Their Regeneration. Chem Asian J 16, 974–980. DOI:10.1002/asia.202100126

Li, L., Qu, W., Liu, F., Zhao, T., Zhang, X., Chen, R., Wu, F., 2014. Surface modification of spinel λ-MnO2 and its lithium adsorption properties from spent lithium-ion batteries. Appl Surf Sci 315, 59–65. https://doi.org/10.1016/j.apsusc.2014.07.090

Li, M., Lu, J., Chen, Z., Amine, K., 2018. 30 years of lithium-ion batteries. J Adv Mater 30, 1800561. https://doi.org/10.1002/adma.201800561

Li, Y., Li, L., Cao, L., Yang, C., 2016. Promoting dynamic adsorption of Pb2+ in a single pass flow using fibrous nano-TiO2/cellulose membranes. Chem Eng J 283, 1145–1153. https://doi.org/10.1016/j.cej.2015.08.068

Lima, E.C., Hosseini-Bandegharaei, A., Moreno-Piraján, J.C., Anastopoulos, I., 2019. A critical review of the estimation of the thermodynamic parameters on adsorption equilibria. Wrong use of equilibrium constant in the Van't Hoof equation for calculation of thermodynamic parameters of adsorption. J Mol Liq 273, 425–434. https://doi.org/10.1016/j.molliq.2018.10.048

Lin, H., Han, S., Dong, Y., He, Y., 2017. The surface characteristics of hyperbranched polyamide modified corncob and its adsorption property for Cr(VI). Appl Surf Sci 412, 152–159. https://doi.org/10.1016/j.apsusc.2017.03.061

Lin, H., Yu, X., Li, M., Duo, J., Guo, Y., Deng, T., 2019. Synthesis of polyporous ion-sieve and its application for selective recovery of lithium from geothermal water. ACS Appl Mater Interfaces 11, 26364–26372. https://doi.org/10.1021/acsami.9b07401

Liu, D., Zhu, H., Wu, K., Wang, F., Zhao, X., Liao, Q., 2020. Understanding the effect of particle size of waste concrete powder on phosphorus removal efficiency. Constr Build Mater 236, 117526. https://doi.org/10.1016/j.conbuildmat.2019.117526

Liu, F., Sai, K.C.K.V., Zhang, W., 2021. Conversion of Spiky Sweetgum tree (Liquidambar styraciflua) Seeds as into Bio-adsorbent: Static and Dynamic Adsorption Assessment. J Hazard Mater Adv 1, 100001. https://doi.org/10.1016/j.hazadv.2021.100001

Liu, J., Zhang, Y., Miao, Y., Yang, Y., Li, P., 2021. Alkaline Resins Enhancing Li+/H+ Ion Exchange for Lithium Recovery from Brines Using Granular Titanium-Type Lithium Ion-Sieves. Ind Eng Chem Res 60, 45, 16457–16468. https://doi.org/10.1021/acs.iecr.1c02361

Liu, X., Chen, X., He, L., Zhao, Z., 2015. Study on extraction of lithium from salt lake brine by membrane electrolysis. Desalination 376, 35–40. https://doi.org/10.1016/j.desal.2015.08.013

Lo, Y.-C., Cheng, C.-L., Han, Y.-L., Chen, B.-Y., Chang, J.-S., 2014. Recovery of high-value metals from geothermal sites by biosorption and bioaccumulation. Bioresour Technol 160, 182–190. https://doi.org/10.1016/j.biortech.2014.02.008

Low, K.S., Lee, C.K., Mak, S.M., 2004. Sorption of copper and lead by citric acid modified wood. Wood Sci Technol 38, 629–640. https://doi.org/10.1007/s00226-003-0201-9

Lu, T., Zhu, Y., Qi, Y., Kang, Y., Wang, A., 2019. Tunable superporous magnetic adsorbent prepared via eco-friendly Pickering MIPEs for high-efficiency adsorption of Rb+ and Sr2+. Chem Eng J 368, 988–998. https://doi.org/10.1016/j.cej.2019.03.040

Luneva, N.K., Ezovitova, T.I., 2014. Cellulose phosphorylation with a mixture of orthophosphoric acid and ammonium polyphosphate in urea medium. Russ J Appl Chem 87, 1558–1565. https://doi.org/10.1134/S1070427214100243

Luo, X., Guo, B., Luo, J., Deng, F., Zhang, S., Luo, S., Crittenden, J., 2015. Recovery of lithium from wastewater using development of Li ion-imprinted polymers. ACS Sustain Chem Eng 3, 460–467. https://doi.org/10.1021/sc500659h

Malkoc, E., Nuhoglu, Y., Abali, Y., 2006. Cr (VI) adsorption by waste acorn of Quercus ithaburensis in fixed beds: Prediction of breakthrough curves. Chem Eng J 119, 61–68. https://doi.org/10.1016/j.cej.2006.01.019

Mao, L., Zhang, P., Ju, H., Zhou, X., Xue, Z., Wang, C., Sun, J., Jia, Y., Shao, F., Zou, X., 2022. Solvent extraction for lithium isotope separation by 4-NO2-B15C5/[BMIm][NTf2] system. J Mol Liq 367, 120357. https://doi.org/10.1016/j.molliq.2022.120357

Marthi, R., Smith, Y.R., 2019. Selective recovery of lithium from the Great Salt Lake using lithium manganese oxide-diatomaceous earth composite. Hydrometallurgy 186, 115–125. https://doi.org/10.1016/j.hydromet.2019.03.011

Marthi, R., Asgar, H., Gadikota, G., Smith, Y.R., 2021. On the Structure and Lithium Adsorption Mechanism of Layered H2TiO3. ACS Appl Mater Interfaces 13, 8361–8369. https://doi.org/10.1021/acsami.0c20691

Masmoudi, A., Zante, G., Trébouet, D., Barillon, R., Boltoeva, M., 2021. Solvent extraction of lithium ions using benzoyltrifluoroacetone in new solvents. Sep Purif Technol 255, 117653. https://doi.org/10.1016/j.seppur.2020.117653

Melo, J.C.P., Silva Filho, E.C., Santana, S.A.A., Airoldi, C., 2011. Synthesized cellulose/succinic anhydride as an ion exchanger. Calorimetry of divalent cations in aqueous suspension. Thermochim Acta 524, 29–34. https://doi.org/10.1016/j.tca.2011.06.007

Meng, F., McNeice, J., Zadeh, S.S., Ghahreman, A., 2021. Review of lithium production and recovery from minerals, brines, and lithium-ion batteries. Miner Process Extr Metall Rev 42, 123–141. https://doi.org/10.1080/08827508.2019.1668387.

Metwally, S.S., Rizk, H.E., Gasser, M.S., 2017. Biosorption of strontium ions from aqueous solution using modified eggshell materials. Radiochim Acta 105, 1021–1031.

Metwally, S.S., El-Sherief, E.A., Mekhamer, H.S., 2020. Fixed-bed column for the removal of cesium, strontium, and lead ions from aqueous solutions using brick kiln waste. Sep Sci Technol 55, 635–647. https://doi.org/10.1080/01496395.2019.1572189

Millot, R., Hegan, A., Négrel, P., 2012. Geothermal waters from the Taupo Volcanic Zone, New Zealand: Li, B and Sr isotopes characterization. J Appl Geochem 27, 677–688. https://doi.org/10.1016/j.apgeochem.2011.12.015

Miyai, Y., Ooi, K., Katoh, S., 1988. Recovery of Lithium from Seawater Using a New Type of Ion-Sieve Adsorbent Based on MgMn2O4. Sep Sci Technol 23, 179–191. https://doi.org/10.1080/01496398808057641

Mohamed, M.H., Wilson, L.D., Headley, J. V, 2015. Tuning the physicochemical properties of β-cyclodextrin based polyurethanes via cross-linking conditions. Microporous Mesoporous Mater 214, 23–31. https://doi.org/10.1016/j.micromeso.2015.04.029

Moubarik, A., Grimi, N., 2015. Valorization of olive stone and sugar cane bagasse by-products as biosorbents for the removal of cadmium from aqueous solution. Food Res Int 73, 169–175. https://doi.org/10.1016/j.foodres.2014.07.050

Mroczek, E., Dedual, G., Graham, D., Bacon, L., 2015. Lithium extraction from Wairakei geothermal fluid using electrodialysis, in: Proceedings World Geothermal Congress. Citeseer, p. 2015.

Munjur, H.M., Hasan, M.N., Awual, M.R., Islam, M.M., Shenashen, M.A., Iqbal, J., 2020. Biodegradable natural carbohydrate polymeric sustainable adsorbents for efficient toxic dye removal from wastewater. J Mol Liq 319, 114356. https://doi.org/10.1016/j.molliq.2020.114356

Nampeera, J., Recepoğlu, Y.K., Yuksel, A., 2022. Valorization of olive tree pruning waste for potential utilization in lithium recovery from aqueous solutions. Biomass Convers Biorefin 1–13. https://doi.org/10.1007/s13399-022-02647-2

Négrel, P., Guerrot, C., Millot, R., 2007. Chemical and strontium isotope characterization of rainwater in France: influence of sources and hydrogeochemical implications.

Isotopes Environ Health Stud 43, 179–196. https://doi.org/10.1080/10256010701550773

Ngo, H.H., Guo, W., Zhang, J., Liang, S., Ton-That, C., Zhang, X., 2015. Typical low cost biosorbents for adsorptive removal of specific organic pollutants from water. Bioresour Technol 182, 353–363. https://doi.org/10.1016/j.biortech.2015.02.003

Nishihama, S., Onishi, K., Yoshizuka, K., 2011. Selective recovery process of lithium from seawater using integrated ion exchange methods. Solvent Extr Ion Exch 29, 421–431. https://doi.org/10.1080/07366299.2011.573435

Noerochim, L., Satriawangsa, G.A., Susanti, D., Widodo, A., 2015. Synthesis and Characterization of Lithium Manganese Oxide with Different Ratio of Mole on Lithium Recovery Process from Ge-othermal Fluid of Lumpur Sidoarjo. J Mater Sci Chem Eng 3, 56. http://dx.doi.org/10.4236/msce.2015.311007

Nouri, L., Ghodbane, I., Hamdaoui, O., Chiha, M., 2007. Batch sorption dynamics and equilibrium for the removal of cadmium ions from aqueous phase using wheat bran. J Hazard Mater 149, 115–125. https://doi.org/10.1016/j.jhazmat.2007.03.055

Ohashi, F., Tai, Y., 2019. Lithium adsorption from natural brine using surface-modified manganese oxide adsorbents. Mater Lett 251, 214–217. https://doi.org/10.1016/j.matlet.2019.05.064

Oloo, C.M., Onyari, J.M., Wanyonyi, W.C., Wabomba, J.N., Muinde, V.M., 2020. Adsorptive removal of hazardous crystal violet dye form aqueous solution using Rhizophora mucronata stembarks: Equilibrium and kinetics studies. J Environ Chem Ecotoxicol 2, 64–72. https://doi.org/10.1016/j.enceco.2020.05.001

Ortı, F., Gündogan, I., Helvaci, C., 2002. Sodium sulphate deposits of Neogene age: the Kirmir formation, Beypazari basin, Turkey. Sediment Geol 146, 305–333. https://doi.org/10.1016/S0037-0738(01)00140-3

Oshima, T., Kondo, K., Ohto, K., Inoue, K., Baba, Y., 2008. Preparation of phosphorylated bacterial cellulose as an adsorbent for metal ions. React Funct Polym 68, 376–383. https://doi.org/10.1016/j.reactfunctpolym.2007.07.046

Özlem, T., 2019. Potential Use of Hazelnut Processing Plant Wastes as a Sorbent for the Simultaneous Removal of Multi-Elements from Water. Mühendislik Bilimleri ve Tasarım Dergisi 7, 301–312. DOI: 10.21923/jesd.486065

Pambudi, N.A., Itoi, R., Yamashiro, R., Alam, B.Y.C.S.S.S., Tusara, L., Jalilinasrabady, S., Khasani, J., 2015. The behavior of silica in geothermal brine from Dieng geothermal power plant, Indonesia. Geothermics 54, 109–114. https://doi.org/10.1016/j.geothermics.2014.12.003

Panda, L., Das, B., Rao, D.S., Mishra, B.K., 2011. Application of dolochar in the removal of cadmium and hexavalent chromium ions from aqueous solutions. J Hazard Mater 192, 822–831. https://doi.org/10.1016/j.jhazmat.2011.05.098

Pangeni, B., Paudyal, H., Inoue, K., Kawakita, H., Ohto, K., Alam, S., 2012. Selective recovery of gold(III) using cotton cellulose treated with concentrated sulfuric acid. Cellulose 19, 381–391. https://doi.org/10.1007/s10570-011-9628-6

Park, J., Sato, H., Nishihama, S., Yoshizuka, K., 2012. Lithium Recovery from Geothermal Water by Combined Adsorption Methods. Solvent Extr Ion Exch 30, 398–404. https://doi.org/10.1080/07366299.2012.687165

Park, H., Singhal, N., Jho, E.H., 2015. Lithium sorption properties of HMnO in seawater and wastewater. Water Res 87, 320–327. https://doi.org/10.1016/j.watres.2015.09.032

Patel, H., 2019. Fixed-bed column adsorption study: a comprehensive review. Appl Water Sci 9, 45. https://doi.org/10.1007/s13201-019-0927-7

Pelly, I., 1978. Recovery of lithium from Dead Sea brines. J Appl Chem Biotechnol 28, 469–474.

Peng, H., Zhao, Q., 2021. A Nano-Heterogeneous Membrane for Efficient Separation of Lithium from High Magnesium/Lithium Ratio Brine. Adv Funct Mater 31, 2009430. https://doi.org/10.1002/adfm.202009430

Poletto, M., Zattera, A.J., Forte, M.M.C., Santana, R.M.C., 2012. Thermal decomposition of wood: Influence of wood components and cellulose crystallite size. Bioresour Technol 109, 148–153. https://doi.org/10.1016/j.biortech.2011.11.122

Puliga, F., Leonardi, P., Minutella, F., Zambonelli, A., Francioso, O., 2022. Valorization of hazelnut shells as growing substrate for edible and medicinal mushrooms. Horticulturae 8, 214. https://doi.org/10.3390/horticulturae8030214

Qian, F., Zhao, B., Guo, M., Wu, Z., Zhou, W., Liu, Z., 2021. Surface trace doping of Na enhancing structure stability and adsorption properties of Li1.6Mn1.6O4 for Li+ recovery. Sep Purif Technol 256, 117583. https://doi.org/10.1016/j.seppur.2020.117583

Rabet, R.S., Simsek, C., Baba, A., Murathan, A., 2017. Blowout mechanism of Alasehir (Turkey) geothermal field and its effects on groundwater chemistry. Environ Earth Sci 76, 49. https://doi.org/10.1007/s12665-016-6334-6

Recepoğlu, Y.K., Kabay, N., Yılmaz-Ipek, İ., Arda, M., Yoshizuka, K., Nishihama, S., Yüksel, M., 2017a. Equilibrium and Kinetic Studies on Lithium Adsorption from Geothermal Water by λ-MnO2. Solvent Extr Ion Exch 35, 221–231. https://doi.org/10.1080/07366299.2017.1319235

Recepoğlu, Y.K., Kabay, N., Yılmaz-İpek, İ., Arda, M., Yüksel, M., Yoshizuka, K., Nishihama, S., 2017b. Deboronation of geothermal water using N-methyl-D-glucamine based chelating resins and a novel fiber adsorbent: batch and column studies. J Chem Technol Biotechnol 92, 7, 1540–1547. https://doi.org/10.1002/jctb.5234

Recepoğlu, Y.K., Kabay, N., Yoshizuka, K., Nishihama, S., Yılmaz-Ipek, İ., Arda, M., Yüksel, M., 2018a. Effect of Operational Conditions on Separation of Lithium from Geothermal Water by λ-MnO2 Using Ion Exchange–Membrane Filtration Hybrid Process. Solvent Extr Ion Exch 36, 499–512. https://doi.org/10.1080/07366299.2018.1529232

Recepoğlu, Y.K., Kabay, N., Ipek, I.Y., Arda, M., Yüksel, M., Yoshizuka, K., Nishihama, S., 2018b. Packed bed column dynamic study for boron removal from geothermal brine by a chelating fiber and breakthrough curve analysis by using mathematical models. Desalination 437, 1–6. https://doi.org/10.1016/j.desal.2018.02.022

Recepoğlu, Y.K., Yüksel, A., 2021a. Synthesis, Characterization and Adsorption Studies of Phosphorylated Cellulose for the Recovery of Lithium from Aqueous Solutions. Cellul Chem Technol 55, 385–401. https://doi.org/10.35812/CelluloseChemTechnol.2021.55.37

Recepoğlu, Y.K., Yüksel, A., 2021b. Phosphorylated hazelnut shell waste for sustainable lithium recovery application as biosorbent. Cellulose 28, 9837–9855. https://doi.org/10.1007/s10570-021-04148-3

Redlich, O., Peterson, D.L., 1959. A useful adsorption isotherm. J Phys Chem 63, 1024.

Regenspurg, S., Feldbusch, E., Byrne, J., Deon, F., Driba, D.L., Henninges, J., Kappler, A., Naumann, R., Reinsch, T., Schubert, C., 2015. Mineral precipitation during production of geothermal fluid from a Permian Rotliegend reservoir. Geothermics 54, 122–135. https://doi.org/10.1016/j.geothermics.2015.01.003

Reichel, S., Aubel, T., Patzig, A., Janneck, E., Martin, M., 2017. Lithium recovery from lithium-containing micas using sulfur oxidizing microorganisms. Miner Eng 106, 18–21. https://doi.org/10.1016/j.mineng.2017.02.012

Revellame, E.D., Fortela, D.L., Sharp, W., Hernandez, R., Zappi, M.E., 2020. Adsorption kinetic modeling using pseudo-first order and pseudo-second order rate laws: A review. Clean Eng Technol 1, 100032. https://doi.org/10.1016/j.clet.2020.100032

Rol, F., Belgacem, N., Meyer, V., Petit-Conil, M., Bras, J., 2019. Production of fire-retardant phosphorylated cellulose fibrils by twin-screw extrusion with low energy consumption. Cellulose 26, 5635–5651. https://doi.org/10.1007/s10570-019-02447-4

Romero-Cano, L.A., Gonzalez-Gutierrez, L. V, Baldenegro-Perez, L.A., 2016. Biosorbents prepared from orange peels using Instant Controlled Pressure Drop for Cu (II) and phenol removal. Ind Crops Prod 84, 344–349. https://doi.org/10.1016/j.indcrop.2016.02.027

Roskill, 2019. Lithium: Outlook to 2028. Retrieved from Roskill Information Services Ltd.

Ruthven, D.M., 1984. Principles of adsorption and adsorption processes. John Wiley & Sons.

Ruttinger, A.W., Pálsdóttir, A., Tester, J.W., Clancy, P., 2019. A quantitative metric for the design of selective supercritical CO2 extraction of lithium from geothermal brine. ChemSusChem 12, 3532–3540. https://doi.org/10.1002/cssc.201901200

Sagara, F., Ning, W.B., Yoshida, I., Ueno, K., 1989. Preparation and adsorption properties of λ-MnO2-cellulose hybrid-type lon-exchanger for lithium ion. Application to the enrichment of lithium ion from seawater. Sep Sci Technol 24, 1227–1243. https://doi.org/10.1080/01496398908049899

Sakaguchi, T., Horikoshi, T., Nakajima, A., 1981. Adsorption of Uranium by Chitin Phosphate and Chitosan Phosphate. Agric Biol Chem 45, 2191–2195. https://doi.org/10.1080/00021369.1981.10864862

Salehi, E., Madaeni, S.S., Vatanpour, V., 2012. Thermodynamic investigation and mathematical modeling of ion-imprinted membrane adsorption. J Membr Sci 389, 334–342. https://doi.org/10.1016/j.memsci.2011.10.045

Sanjuan, B., Negrel, G., Le Lous, M., Poulmarch, E., Gal, F., Damy, P.-C., 2020. Main geochemical characteristics of the deep geothermal brine at Vendenheim (Alsace, France) with constraints on temperature and fluid circulation, in: World Geothermal Congress 2020.

Sarker, T.C., Azam, S.M.G.G., El-Gawad, A.M.A., Gaglione, S.A., Bonanomi, G., 2017. Sugarcane bagasse: a potential low-cost biosorbent for the removal of hazardous materials. Clean Technol Environ Policy 19, 2343–2362. https://doi.org/10.1007/s10098-017-1429-7

Segal, L., Creely, J.J., Martin Jr, A.E., Conrad, C.M., 1959. An empirical method for estimating the degree of crystallinity of native cellulose using the X-ray diffractometer. Text Res J 29, 786–794. https://doi.org/10.1177/004051755902901003

Segovia-Sandoval, S.J., Ocampo-Pérez, R., Berber-Mendoza, M.S., Leyva-Ramos, R., Jacobo-Azuara, A., Medellín-Castillo, N.A., 2018. Walnut shell treated with citric acid and its application as biosorbent in the removal of Zn (II). J Water Process Eng 25, 45–53. https://doi.org/10.1016/j.jwpe.2018.06.007

Sengupta, D., Pike, R.W., 2012. Chemicals from biomass: Integrating bioprocesses into chemical production complexes for sustainable development. CRC Press.

Şenol, H., 2019. Biogas potential of hazelnut shells and hazelnut wastes in Giresun City. Biotechnol Rep 24, e00361. https://doi.org/10.1016/j.btre.2019.e00361

Shi, C., Jing, Y., Jia, Y., 2016. Solvent extraction of lithium ions by tri-n-butyl phosphate using a room temperature ionic liquid. J Mol Liq 215, 640–646. https://doi.org/10.1016/j.molliq.2016.01.025

Shi, C., Jing, Y., Xiao, J., Wang, X., Yao, Y., Jia, Y., 2017. Solvent extraction of lithium from aqueous solution using non-fluorinated functionalized ionic liquids as extraction agents. Sep Purif Technol 172, 473–479.

https://doi.org/10.1016/j.seppur.2016.08.034

Shi, Y., Belosinschi, D., Brouillette, F., Belfkira, A., Chabot, B., 2014. Phosphorylation of Kraft fibers with phosphate esters. Carbohydr Polym 106, 121–127. https://doi.org/10.1016/j.carbpol.2014.01.070

Shin, J., Jeong, J.-M., Lee, J.B., Cho, H.-J., Kim, Y.H., Ryu, T., 2022. Preparation of lithium carbonate from waste lithium solution through precipitation and wet conversion methods. Hydrometallurgy 210, 105863. https://doi.org/10.1016/j.hydromet.2022.105863

Siekierka, A., Tomaszewska, B., Bryjak, M., 2018. Lithium capturing from geothermal water by hybrid capacitive deionization. Desalination 436, 8–14. https://doi.org/10.1016/j.desal.2018.02.003

Singh, M., Kaiser, J., Hahn, H., 2016. A systematic study of thick electrodes for high energy lithium-ion batteries. J Electroanal Chem 782, 245–249. https://doi.org/10.1016/j.jelechem.2016.10.040

Socrates, G., 2004. Infrared and Raman characteristic group frequencies: tables and charts. John Wiley & Sons.

Somrani, A., Hamzaoui, A.H., Pontie, M., 2013. Study on lithium separation from salt lake brines by nanofiltration (NF) and low pressure reverse osmosis (LPRO). Desalination 317, 184–192. https://doi.org/10.1016/j.desal.2013.03.009

Srivastava, V.C., Prasad, B., Mishra, I.M., Mall, I.D., Swamy, M.M., 2008. Prediction of breakthrough curves for sorptive removal of phenol by bagasse fly ash packed bed. Ind Eng Chem Res 47, 1603–1613. https://doi.org/10.1021/ie0708475

Stjepanović, M., Velić, N., Habuda-Stanić, M., 2022. Modified hazelnut shells as a novel adsorbent for the removal of nitrate from wastewater. Water (Basel) 14, 816. https://doi.org/10.3390/w14050816

Stringfellow, W.T., Dobson, P.F., 2021. Technology for the Recovery of Lithium from Geothermal Brines. Energies (Basel) 14, 6805. https://doi.org/10.3390/en14206805

Suflet, D.M., Chitanu, G.C., Popa, V.I., 2006. Phosphorylation of polysaccharides: New results on synthesis and characterisation of phosphorylated cellulose. React Funct Polym 66, 1240–1249. https://doi.org/10.1016/j.reactfunctpolym.2006.03.006

Sun, N., Dou, P., Zhai, W., He, H., Nghiem, L.D., Vatanpour, V., Zhang, Y., Liu, C., He, T., 2022. Polyethylene separator supported thin film composite forward osmosis membranes for concentrating lithium enriched brine. Water Res 216, 118297. https://doi.org/10.1016/j.watres.2022.118297

Sun, Q., Chen, H., Yu, J., 2022. Investigation on the lithium extraction process with the TBP–FeCl3 solvent system using experimental and DFT methods. Ind Eng Chem Res 61, 4672–4682. https://doi.org/10.1021/acs.iecr.1c05072

Sun, S., Yu, X., Li, M., Duo, J., Guo, Y., Deng, T., 2020. Green recovery of lithium from geothermal water based on a novel lithium iron phosphate electrochemical technique. J Clean Prod 247, 119178. https://doi.org/10.1016/j.jclepro.2019.119178

Sun, S.-Y., Cai, L.-J., Nie, X.-Y., Song, X., Yu, J.-G., 2015. Separation of magnesium and lithium from brine using a Desal nanofiltration membrane. J Water Process Eng 7, 210–217. https://doi.org/10.1016/j.jwpe.2015.06.012

Swain, B., 2016. Separation and purification of lithium by solvent extraction and supported liquid membrane, analysis of their mechanism: a review. J Chem Technol Biotechnol 91, 2549–2562. https://doi.org/10.1002/jctb.4976

Swain, B., 2017. Recovery and recycling of lithium: A review. Sep Purif Technol 172, 388–403. https://doi.org/10.1016/j.seppur.2016.08.031

Tan, H., Su, J., Xu, P., Dong, T., Elenga, H.I., 2018. Enrichment mechanism of Li, B and K in the geothermal water and associated deposits from the Kawu area of the Tibetan Plateau: Constraints from geochemical experimental data. Appl Geochem 93, 60–68. https://doi.org/10.1016/j.apgeochem.2018.04.001

Tang, L., Huang, S., Wang, Yan, Liang, D., Li, Y., Li, J., Wang, Yonggui, Xie, Y., Wang, W., 2020. Highly Efficient, Stable, and Recyclable Hydrogen Manganese Oxide/Cellulose Film for the Extraction of Lithium from Seawater. ACS Appl Mater Interfaces 12, 9775–9781. https://doi.org/10.1021/acsami.9b21612

Tarley, C.R.T., Corazza, M.Z., Somera, B.F., Segatelli, M.G., 2015. Preparation of new ion-selective cross-linked poly (vinylimidazole-co-ethylene glycol dimethacrylate) using a double-imprinting process for the preconcentration of Pb2+ ions. J Colloid Interface Sci 450, 254–263. https://doi.org/10.1016/j.jcis.2015.02.074

Tempkin, M.I., Pyzhev, V., 1940. Kinetics of ammonia synthesis on promoted iron catalyst. Acta Phys. Chim. USSR 12, 327.

Thomas, H.C., 1948. Chromatography: a problem in kinetics. Ann N Y Acad Sci 49, 161–182. https://doi.org/10.1111/j.1749-6632.1948.tb35248.x

Ting, T.M., Nasef, M.M., Aravindan, D., Rosslan, I.F.N., Ruslan, N., 2021. Selective removal of boron from industrial wastewater containing high concentration of ammonia by radiation grafted fibrous adsorbent in fixed bed column. J Environ Chem Eng 9, 104993. https://doi.org/10.1016/j.jece.2020.104993

Tomul, F., Arslan, Y., Başoğlu, F.T., Babuçcuoğlu, Y., Tran, H.N., 2019. Efficient removal of anti-inflammatory from solution by Fe-containing activated carbon: Adsorption kinetics, isotherms, and thermodynamics. J Environ Manage 238, 296–306. https://doi.org/10.1016/j.jenvman.2019.02.088

Torres Castillo, N.E., Ochoa Sierra, J.S., Oyervides-Muñoz, M.A., Sosa-Hernández, J.E., Iqbal, H.M.N., Parra-Saldívar, R., Melchor-Martínez, E.M., 2021. Exploring the potential of coffee husk as caffeine bio-adsorbent – A mini-review. Case Stud Chem Environ Eng 3, 100070. https://doi.org/10.1016/j.cscee.2020.100070

Tran, H.N., You, S.-J., Chao, H.-P., 2016. Thermodynamic parameters of cadmium adsorption onto orange peel calculated from various methods: a comparison study. J Environ Chem Eng 4, 2671–2682. https://doi.org/10.1016/j.jece.2016.05.009

Tran, H.N., You, S.-J., Nguyen, T.V., Chao, H.-P., 2017. Insight into the adsorption mechanism of cationic dye onto biosorbents derived from agricultural wastes. Chem Eng Commun 204, 1020–1036. https://doi.org/10.1080/00986445.2017.1336090

Turan, A.Z., Turan, M., 2022. Removal of Heavy Metals and Dyes from Wastewaters by Raw and Activated Carbon Hazelnut Shells, in: Progress in Nanoscale and Low-Dimensional Materials and Devices: Properties, Synthesis, Characterization, Modelling and Applications. Springer, pp. 907–933.

Udoetok, I.A., Dimmick, R.M., Wilson, L.D., Headley, J. V, 2016. Adsorption properties of cross-linked cellulose-epichlorohydrin polymers in aqueous solution. Carbohydr Polym 136, 329–340. https://doi.org/10.1016/j.carbpol.2015.09.032

Ulatowska, J., Polowczyk, I., Bastrzyk, A., Koźlecki, T., Sawiński, W., 2019. Fly ash as a sorbent for boron removal from aqueous solutions: Equilibrium and thermodynamic studies. Sep Sci Technol 55(12), 2149–2157. https://doi.org/10.1080/01496395.2019.1612434

Um, N., Hirato, T., 2013. A Study on Lithium Recovery from Seawater: Separation of Lithium from Hydrochloric Acid Solutions Containing CaCl2, MgCl2, MnCl2, NaCl, KCl, and LiCl, in: Zero-Carbon Energy Kyoto 2012. Springer, pp. 149–154.

Velazquez-Jimenez, L.H., Pavlick, A., Rangel-Mendez, J.R., 2013. Chemical characterization of raw and treated agave bagasse and its potential as adsorbent of metal cations from water. Ind Crops Prod 43, 200–206. https://doi.org/10.1016/j.indcrop.2012.06.049

Wang, C., Zheng, M., Zhang, X., Wu, Q., Liu, X., Ren, J., Chen, S., 2021. Geothermal-type Lithium Resources in Southern Xizang, China. Acta Geologica Sinica-English Edition.

Wang, L., Rehman, D., Sun, P.-F., Deshmukh, A., Zhang, L., Han, Q., Yang, Z., Wang, Z., Park, H.-D., Lienhard, J.H., 2021. Novel Positively Charged Metal-Coordinated Nanofiltration Membrane for Lithium Recovery. ACS Appl Mater Interfaces 13, 16906–16915. https://doi.org/10.1021/acsami.1c02252

Wang, S., Chen, X., Zhang, Ying, Zhang, Yang, Zheng, S., 2018. Lithium adsorption from brine by iron-doped titanium lithium-ion sieves. Particuology 41, 40–47. https://doi.org/10.1016/j.partic.2018.02.001

Wang, S., Li, P., Zhang, X., Zheng, S., Zhang, Y., 2017. Selective adsorption of lithium from high Mg-containing brines using HxTiO3 ion sieve. Hydrometallurgy 174, 21–28. https://doi.org/10.1016/j.hydromet.2017.09.009

Wang, X., Li, Y., Li, H., Yang, C., 2016. Chitosan membrane adsorber for low concentration copper ion removal. Carbohydr Polym 146, 274–281.

https://doi.org/10.1016/j.carbpol.2016.03.055

Weber, W.J., Morris, J.C., 1963. Kinetics of adsorption on carbon from solution. J Sanit Eng Div 89, 31–60. https://doi.org/10.1061/JSEDAI.0000430

Wekoye, J.N., Wanyonyi, W.C., Wangila, P.T., Tonui, M.K., 2020. Kinetic and equilibrium studies of Congo red dye adsorption on cabbage waste powder. J Environ Chem Ecotoxicol 2, 24–31. https://doi.org/10.1016/j.enceco.2020.01.004

Wesselborg, T., Virolainen, S., Sainio, T., 2021. Recovery of lithium from leach solutions of battery waste using direct solvent extraction with TBP and FeCl3. Hydrometallurgy 202, 105593. https://doi.org/10.1016/j.hydromet.2021.105593

Winarti, C., Kurniati, M., Arif, A.B., Sasmitaloka, K.S., 2018. Cellulose-based nanohydrogel from corncob with chemical crosslinking methods, in: IOP Conference Series: Earth and Environmental Science. IOP Publishing, p. 12043.

Wiśniewska, M., Fijałkowska, G., Ostolska, I., Franus, W., Nosal-Wiercińska, A., Tomaszewska, B., Goscianska, J., Wójcik, G., 2018. Investigations of the possibility of lithium acquisition from geothermal water using natural and synthetic zeolites applying poly (acrylic acid). J Clean Prod 195, 821–830. https://doi.org/10.1016/j.jclepro.2018.05.287

Witek-Krowiak, A., Szafran, R.G., Modelski, S., 2011. Biosorption of heavy metals from aqueous solutions onto peanut shell as a low-cost biosorbent. Desalination 265, 126–134. https://doi.org/10.1016/j.desal.2010.07.042

Wu, F.C., Liu, B.L., Wu, K.T., Tseng, R.L., 2010. A new linear form analysis of Redlich-Peterson isotherm equation for the adsorptions of dyes. Chem Eng J 162, 21–27. https://doi.org/10.1016/j.cej.2010.03.006

Xiao, H., Chai, M., Abdollahzadeh, M., Ahmadi, H., Chen, V., Gore, D.B., Asadnia, M., Razmjou, A., 2022. A lithium ion selective membrane synthesized from a double layered Zrbased metalorganic framework (MOF-on-MOF) thin film. Desalination 532, 115733. https://doi.org/10.1016/j.desal.2022.115733

Xie, Y., Zhang, Y., Qin, J., Samadiy, M., Deng, T., 2022. Synthesis of Spherical Composite CMC-LTO-EGDE-ME for Lithium Recovery from Geothermal Water. J Chem. 6884947. https://doi.org/10.1155/2022/6884947

Xu, C., Yu, T., Peng, J., Zhao, L., Li, J., Zhai, M., 2020. Efficient Adsorption Performance of Lithium Ion onto Cellulose Microspheres with Sulfonic Acid Groups. Quantum Beam Sci 4, 6. https://doi.org/10.3390/qubs4010006

Xu, N., Li, S., Guo, M., Qian, Z., Li, W., Liu, Z., 2019. Synthesis of H4Mn5O12 Nanotubes Lithium-Ion Sieve and Its Adsorption Properties for Li+ from Aqueous Solution. ChemistrySelect 4, 9562–9569. https://doi.org/10.1002/slct.201901764

Xu, R., Kang, Y., Zhang, W., Zhang, X., Pan, B., 2022. Oriented UiO-67 metal–organic framework membrane with fast and selective lithium-ion transport. Angewandte

Chemie International Edition 61, e202115443. https://doi.org/10.1002/anie.202115443

Xu, X., Chen, Y., Wan, P., Gasem, K., Wang, K., He, T., Adidharma, H., Fan, M., 2016. Extraction of lithium with functionalized lithium ion-sieves. Prog Mater Sci 84, 276–313. https://doi.org/10.1016/j.pmatsci.2016.09.004

Xu, X., Gao, Y., Gao, B., Tan, X., Zhao, Y.-Q., Yue, Q., Wang, Y., 2011. Characteristics of diethylenetriamine-crosslinked cotton stalk/wheat stalk and their biosorption capacities for phosphate. J Hazard Mater 192, 1690–1696. https://doi.org/10.1016/j.jhazmat.2011.07.009

Yabusaki, K., 2010. Cellulose II phosphate ester and metal-adsorbing material using the same. Google Patents September 28, 2010, Patent No: US 7,803,937 B2.

Yagub, M.T., Sen, T.K., Afroze, S., Ang, H.M., 2015. Fixed-bed dynamic column adsorption study of methylene blue (MB) onto pinecone. Desalination Water Treat 55, 1026–1039. https://doi.org/10.1080/19443994.2014.924034

Yanagase, K., Yoshinaga, T., Kawano, K., Matsuoka, T., 1983. Recovery of Lithium from Geothermal Water in the Hatchobaru Area of Kyushu, Japan. Bull Chem Soc Jpn. 56, 8, 2490–2498. https://doi.org/10.1246/bcsj.56.2490

Yang, S., Liu, G., Wang, J., Cui, L., Chen, Y., 2019. Recovery of lithium from alkaline brine by solvent extraction with functionalized ionic liquid. Fluid Phase Equilib 493, 129–136. https://doi.org/10.1016/j.fluid.2019.04.015

Yelatontsev, D., 2023. Production of versatile biosorbent via eco-friendly utilization of non-wood biomass. Chem Eng J 451, 138811. https://doi.org/10.1016/j.cej.2022.138811

Yetgin, A.G., Dündar, O.A., Çakmakçı, E., Arar, Ö., 2022. Removal of boron from aqueous solution by modified cellulose. Biomass Convers Biorefin 1–10. https://doi.org/10.1007/s13399-021-02133-1

Yilmaz Ipek, I., 2014. Application of Kinetic, Isotherm, and Thermodynamic Models for Atrazine Adsorption on Nanoporous Polymeric Adsorbents. Sep Sci Technol (Philadelphia) 49, 2358–2365. https://doi.org/10.1080/01496395.2014.915415

Yoon, Y.H., Nelson, J.H., 1984. Application of gas adsorption kinetics I. A theoretical model for respirator cartridge service life. Am Ind Hyg Assoc J 45, 509–516. https://doi.org/10.1080/15298668491400197

Yoshizuka, K., Fukui, K., Inoue, K., 2002. Selective recovery of lithium from seawater using a novel MnO2 type adsorbent. Ars Separatoria Acta 79–86.

Yoshizuka, K., Nishihama, S., Takano, M., Asano, S., 2021. Lithium Recovery from Brines with Novel λ-MnO2 Adsorbent Synthesized by Hydrometallurgical Method. Solvent Extr Ion Exch 39(5-6), 604–621. https://doi.org/10.1080/07366299.2021.1876443

Yousef, R., Qiblawey, H., El-Naas, M.H., 2020. Adsorption as a Process for Produced Water Treatment: A Review. Processes 8, 12, 1657. https://doi.org/10.3390/pr8121657

Yu, J., Wu, Q., Bu, L., Nie, Z., Wang, Y., Zhang, J., Zhang, K., Renchen, N., He, T., He, Z., 2022. Experimental study on improving lithium extraction efficiency of salinity-gradient solar pond through sodium carbonate addition and agitation. Solar Energy 242, 364–377. https://doi.org/10.1016/j.solener.2022.07.027

Yu, Q., Sasaki, K., Hirajima, T., 2013. Bio-templated synthesis of lithium manganese oxide microtubes and their application in Li+ recovery. J Hazard Mater 262, 38–47. https://doi.org/10.1016/j.jhazmat.2013.08.027

Yu, X., Tong, S., Ge, M., Wu, L., Zuo, J., Cao, C., Song, W., 2013. Adsorption of heavy metal ions from aqueous solution by carboxylated cellulose nanocrystals. J Environ Sci (China) 25, 933–943. https://doi.org/10.1016/S1001-0742(12)60145-4

Yue, X., Huang, J., Jiang, F., Lin, H., Chen, Y., 2019. Synthesis and characterization of cellulose-based adsorbent for removal of anionic and cationic dyes. J Eng Fiber Fabr 14. https://doi.org/10.1177/1558925019828194

Zandvakili, S., Ranjbar, M., 2018. Preparation and characterisation of lithium-ion exchange composite for the recovery of lithium from brine. Mineral Processing and Extractive Metallurgy 127, 176–181. https://doi.org/10.1080/03719553.2017.1334983

Zhang, C., Yao, J., Zhai, W., Chen, H., He, H., Zhang, Y.-B., He, T., 2023. Lithium extraction from geothermal brine by granulated HTO titanium-based adsorbent with block-co-polymer poly (ethylene-co-vinyl alcohol)(EVAL) as binder. Chem Eng J 467, 143526. https://doi.org/10.1016/j.cej.2023.143526

Zhang, L., Li, L., Shi, D., Peng, X., Song, F., Nie, F., Han, W., 2018. Recovery of lithium from alkaline brine by solvent extraction with β-diketone. Hydrometallurgy 175, 35–42. https://doi.org/10.1016/j.hydromet.2017.10.029

Zhang, M., Yin, Q., Ji, X., Wang, F., Gao, X., Zhao, M., 2020. High and fast adsorption of cd (ii) and pb (ii) ions from aqueous solutions by a waste biomass-based hydrogel. Sci Rep 10, 1–13. https://doi.org/10.1038/s41598-020-60160-w

Zhang, S., Shi, Q., Christodoulatos, C., Korfiatis, G., Meng, X., 2019. Adsorptive filtration of lead by electrospun PVA/PAA nanofiber membranes in a fixed-bed column. Chem Eng J 370, 1262–1273. https://doi.org/10.1016/j.cej.2019.03.294

Zhang, Y., Liu, J., Yang, Y., Lin, S., Li, P., 2021. Preparation of granular titanium-type lithium-ion sieves and recyclability assessment for lithium recovery from brines with different pH value. Sep Purif Technol 267, 118613. https://doi.org/10.1016/j.seppur.2021.118613

Zhao, B., Qian, Z., Guo, M., Wu, Z., Liu, Z., 2021. The performance and mechanism of recovering lithium on H4Ti5O12 adsorbents influenced by (1 1 0) and (1 1 1) facets

exposed. Chem Eng J 414, 128729. https://doi.org/10.1016/j.cej.2021.128729

Zhao, K., Tong, B., Yu, X., Guo, Y., Xie, Y., Deng, T., 2022. Synthesis of porous fiber-supported lithium ion-sieve adsorbent for lithium recovery from geothermal water. Chem Eng J430, 131423. https://doi.org/10.1016/j.cej.2021.131423

Zhou, C.H., Zhang, D., Tong, D.S., Wu, L.M., Yu, W.H., Ismadji, S., 2012. Paper-like composites of cellulose acetate-organo-montmorillonite for removal of hazardous anionic dye in water. Chem Eng J 209, 223–234. https://doi.org/10.1016/j.cej.2012.07.107

Zhou, Y., Jin, Q., Hu, X., Zhang, Q., Ma, T., 2012. Heavy metal ions and organic dyes removal from water by cellulose modified with maleic anhydride. J Mater Sci 47, 5019–5029. https://doi.org/10.1007/s10853-012-6378-2

Zhou, Y., Zhang, M., Wang, X., Huang, Q., Min, Y., Ma, T., Niu, J., 2014. Removal of crystal violet by a novel cellulose-based adsorbent: Comparison with native cellulose. Ind Eng Chem Res 53, 5498–5506. https://doi.org/10.1021/ie404135y

Zinicovscaia, I., Yushin, N., Pantelica, A., Demčák, Š., Mitu, A., Apostol, A.I., 2020. Lithium biosorption by Arthrospira (Spirulina) platensis biomass. Ecol Chem Eng S 27, 271–280. DOI: 10.2478/eces-2020-0017

APPENDIX A

PERMISSIONS TO REPRODUCE FIGURES AND TEXTS

The necessary authorizations have been obtained to replicate the entire content featured in Chapters 2, 3, and 4 via the Copyright Clearance Center. The documentation confirming these approvals can be found on the subsequent pages.

Chapter 2

COPYRIGHT PERMISSION REQUEST FORM

FROM: Name: Yaşar Kemal Recepoğlu

Address: Izmir Institute of Technology

Faculty of Engineering, Department of Chemical Engineering

35430, Gulbahce, Urla, Izmir/Turkey

Dear Editors:

I am requesting permission to reprint [a portion of] the following work:

[Y.K. Recepoğlu, A. Yüksel, Synthesis, Characterization and Adsorption Studies of Phosphorylated Cellulose for the Recovery of Lithium from Aqueous Solutions, Cellulose Chemistry and Technology 55(3-4) (2021) 385-401.]

This request is for permission to include the above content as part of the following project that I am preparing:

[In a Thesis Submitted to the Graduate School of İzmir Institute of Technology in Partial Fulfillment of the Requirements for the Degree of DOCTOR OF PHILOSOPHY in Chemical Engineering, titled: VALORIZATION OF LIGNOCELLULOSIC WASTES ABUNDANT IN TURKEY FOR POTENTIAL APPLICATION IN SUSTAINABLE LITHIUM RECOVERY, by Yaşar Kemal Recepoğlu, November 2023]

Your permission confirms that you hold the right to grant this permission.

This request is for a non-exclusive, irrevocable, and royalty-free permission, and it is not intended to interfere with other uses of the same work by you. I would be pleased to include a full citation to your work and acknowledgement as follows:

"Reproduced by permission of Romanian Academy Publishing House, the owner of the publishing rights"

Sincerely,

Yaşar Kemal Recepoğlu

Permission is hereby granted:

Iuliana Spiridon, PhD

Associate Editor *Cellulose Chemistry and Technology*

September 13, 2023

Chapter 3

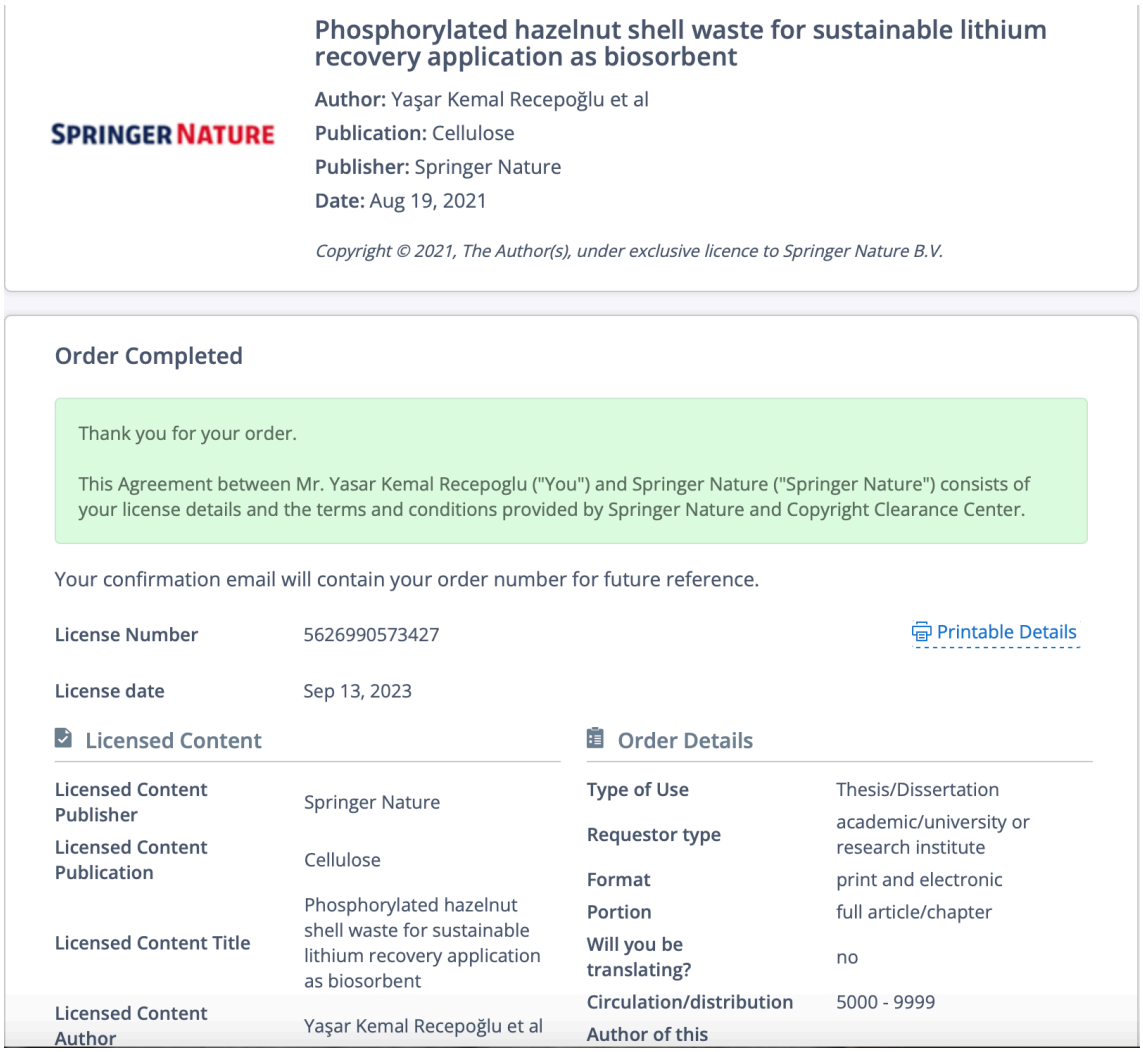

SPRINGER NATURE

Phosphorylated hazelnut shell waste for sustainable lithium recovery application as biosorbent

Author: Yaşar Kemal Recepoğlu et al
Publication: Cellulose
Publisher: Springer Nature
Date: Aug 19, 2021

Order Completed

Thank you for your order.

This Agreement between Mr. Yasar Kemal Recepoglu ("You") and Springer Nature ("Springer Nature") consists of your license details and the terms and conditions provided by Springer Nature and Copyright Clearance Center.

Your confirmation email will contain your order number for future reference.

License Number	5626990573427
License date	Sep 13, 2023

Printable Details

Licensed Content

Licensed Content Publisher	Springer Nature
Licensed Content Publication	Cellulose
Licensed Content Title	Phosphorylated hazelnut shell waste for sustainable lithium recovery application as biosorbent
Licensed Content Author	Yaşar Kemal Recepoğlu et al

Order Details

Type of Use	Thesis/Dissertation
Requestor type	academic/university or research institute
Format	print and electronic
Portion	full article/chapter
Will you be translating?	no
Circulation/distribution	5000 - 9999
Author of this	

Chapter 4

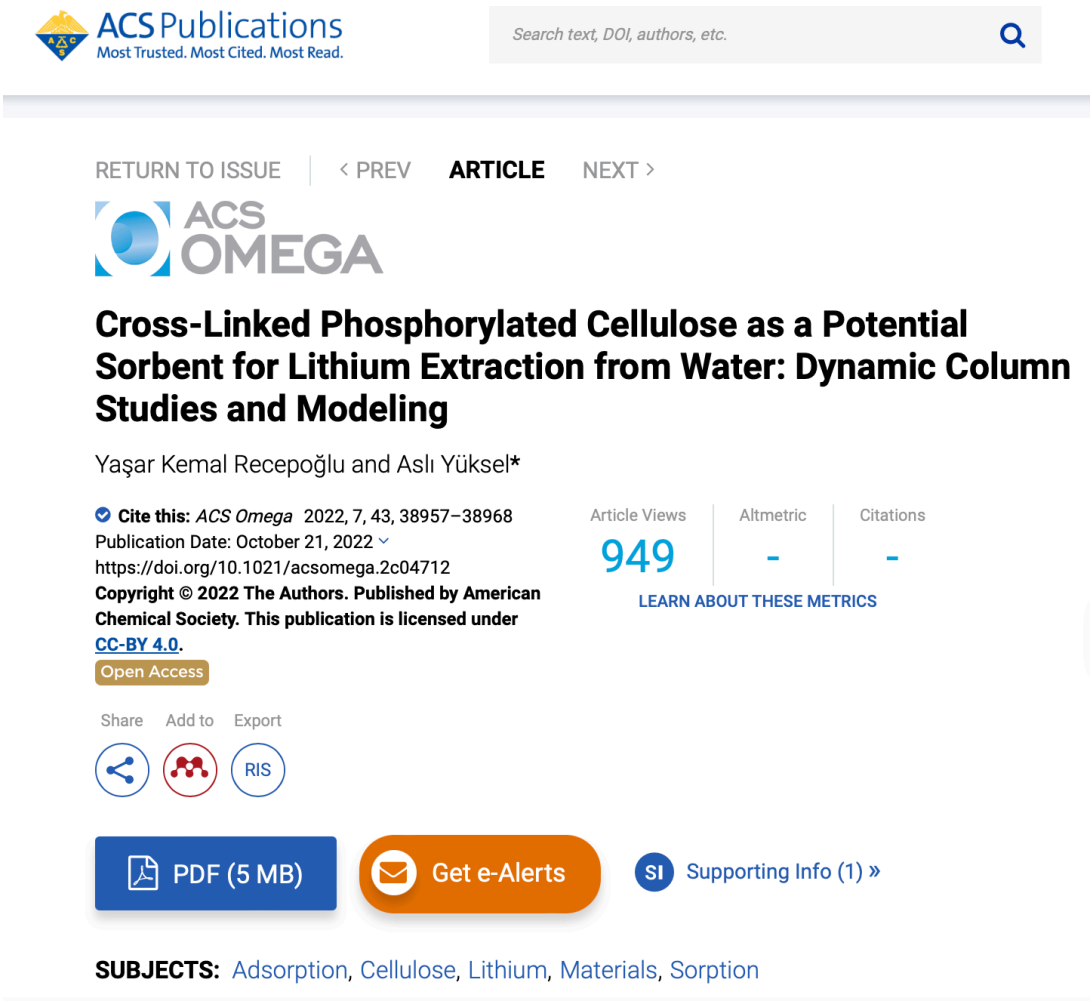

Chapter 5

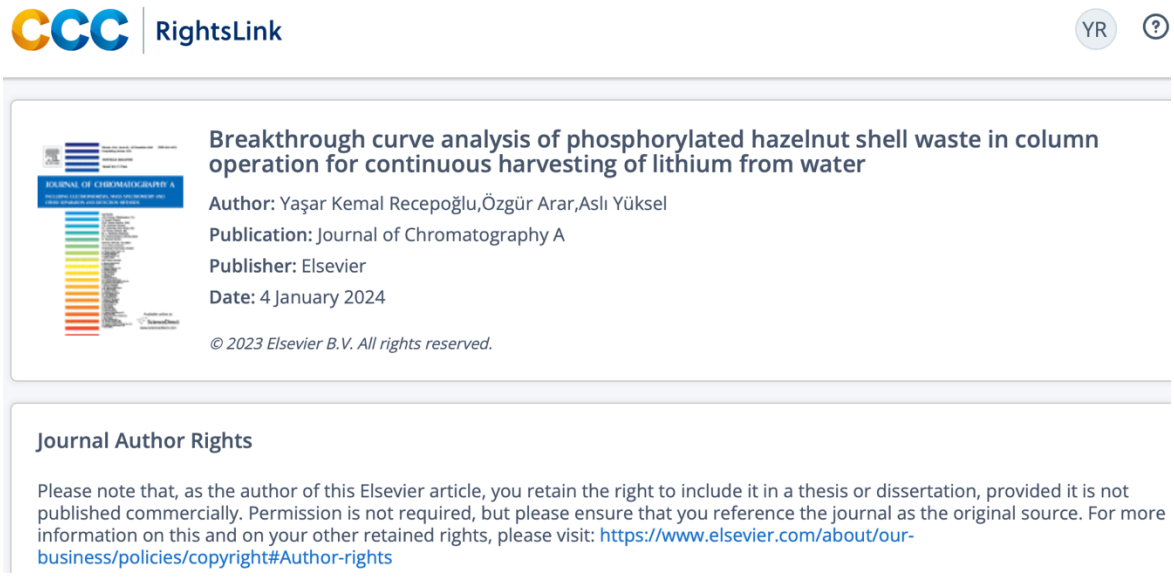

APPENDIX B

SUPPLEMENTARY INFORMATION FOR CHAPTER 2

Table B.1. XPS information of pristine cellulose, phosphorylated functional cellulose, and lithium loaded phosphorylated functional cellulose.

	Pristine cellulose		Phosphorylated functional cellulose		Li-loaded phosphorylated functional cellulose	
Atom	**Binding energy (eV)**	**Peak area**	**Binding energy (eV)**	**Peak area**	**Binding energy (eV)**	**Peak area**
C1s Scan A	286.99	3053.47	286.71	2407.01	286.70	2183.01
C1s Scan B	286.61	3174.93	287.12	4178.64	287.05	5357.69
C1s Scan C	286.33	4201.86	285.44	1319.11	286.36	2794.94
C1s Scan D	287.43	2622.41	287.78	2551.17	285.20	1148.31
C1s Scan E	288.47	408.81	286.32	2898.67	288.09	1226.51
C1s Scan F	286.48	1337.15	284.82	703.35	284.73	1137.89
C1s Scan G	285.17	3589.25	284.96	2126.28	286.37	2916.17
C1s Scan H	288.01	805.67	288.62	426.03	286.96	800.48
C1s Scan I	288.30	3991.57	288.22	3908.73	284.28	438.03
C1s Scan J	-	-	-	-	286.68	8051.17
C1s Scan K	-	-	-	-	287.28	5871.12
O1s Scan A	533.22	2736.41	532.96	7825.05	533.05	4743.4
O1s Scan B	533.45	5978.64	533.49	10984.45	532.64	12580.24
O1s Scan C	533.73	1729.53	532.54	6078.99	532.12	7222.23
O1s Scan D	533.92	6945.39	533.96	3373.3	531.60	1892.65
O1s Scan E	533.03	6081.8	531.86	508.36	531.29	5563.34
O1s Scan F	532.71	6454.17	531.42	4485.64	530.84	2924.76
O1s Scan G	534.08	415.56	532.09	4678.07	531.87	15413.28
O1s Scan H	532.35	4978.31	534.42	1431.55	533.01	6385.36
O1s Scan I	532.19	3008.95	533.25	11643.37	533.39	10900.16
O1s Scan J	534.08	5109.97	-	-	533.71	6393.96
O1s Scan K	-	-	-	-	534.09	3596.87
O1s Scan L	-	-	-	-	534.45	1558.56
O1s Scan M	-	-	-	-	534.95	704.97
O1s Scan N	-	-	-	-	535.50	477.42
O1s Scan O	-	-	-	-	536.35	565.54
P2p Scan A	-	-	134.21	2603.76	133.70	4114.23
Li1s Scan A	-	-	-	-	55.43	297.31

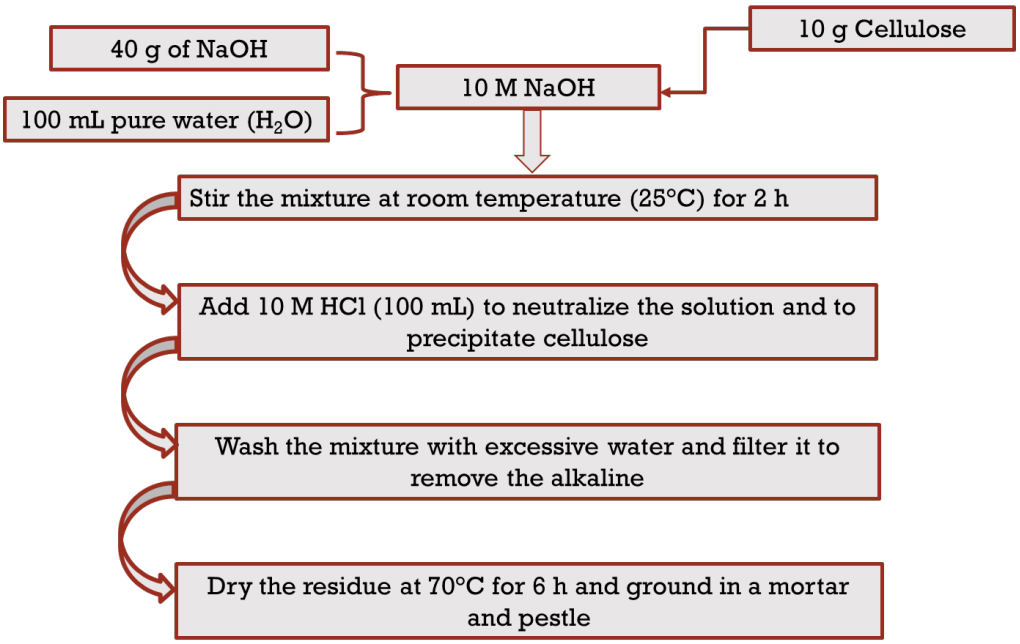

Figure B.1. Alkali treatment procedure for the activation of cellulose prior to phosphorylation.

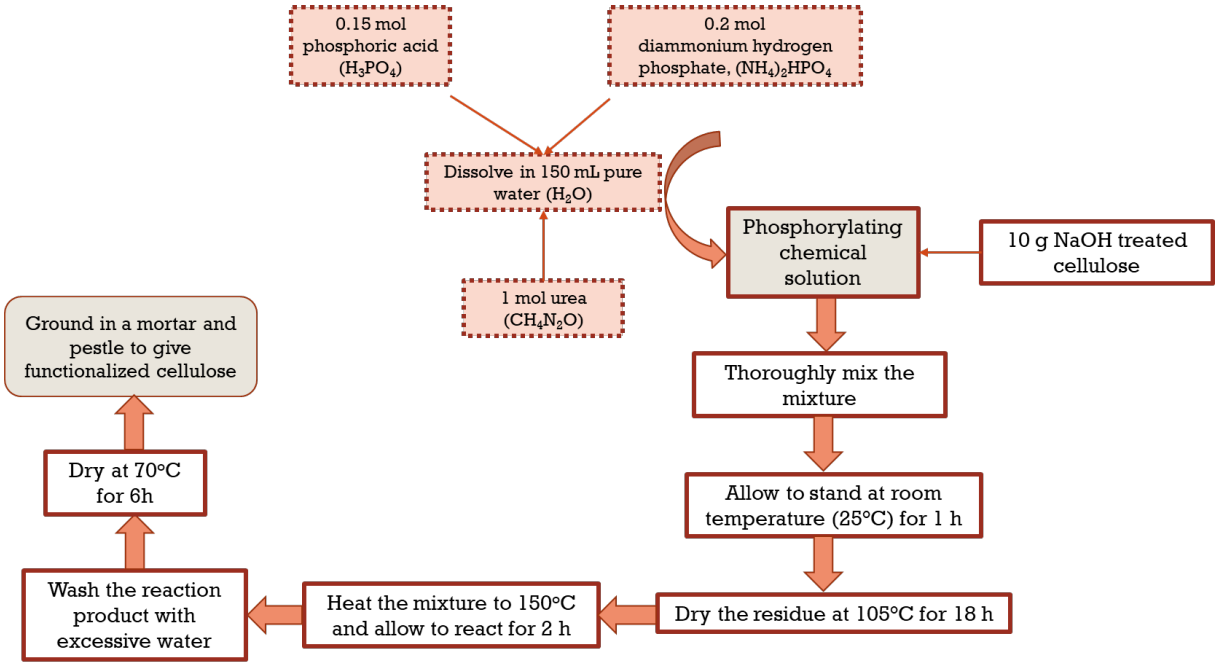

Figure B.2. The synthesis route for cellulose phosphorylation.

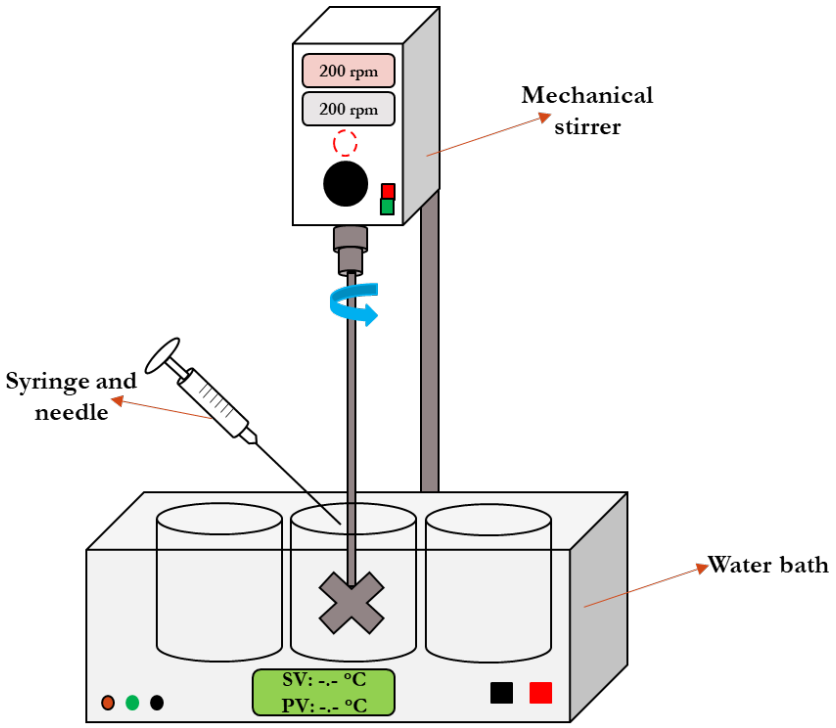

Figure B.3. Schematic representation for the general procedure of kinetic study.

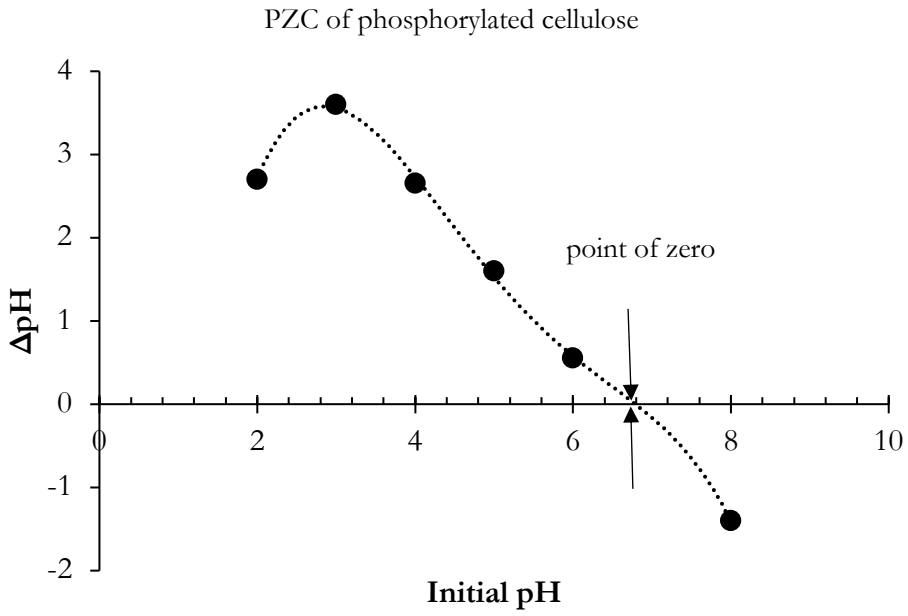

Figure B.4. Determination of zero-point charge for phosphorylated cellulose ($C_0 = 10\ mgL^{-1}$, $T = 25$°C *and Adsorbent dosage* $= 12.0\ g/L$)

APPENDIX C

SUPPLEMENTARY INFORMATION FOR CHAPTER 3

Table C.1. The characteristics of hazelnut shell waste as proximate, structural, and ultimate analysis (Gozaydin and Yuksel, 2017).

Proximate analysis (wt%)		Structural analysis (wt%)		Ultimate analysis (wt%)	
Moisture	8.93	Lignin	40.14	C	50.44
Protein	3.11	Cellulose	36.02	O	41.92
Ash	1.48	Hemicellulose	12.66	H	6.76
		Extractives	7.86	N	0.76
				S	0.11

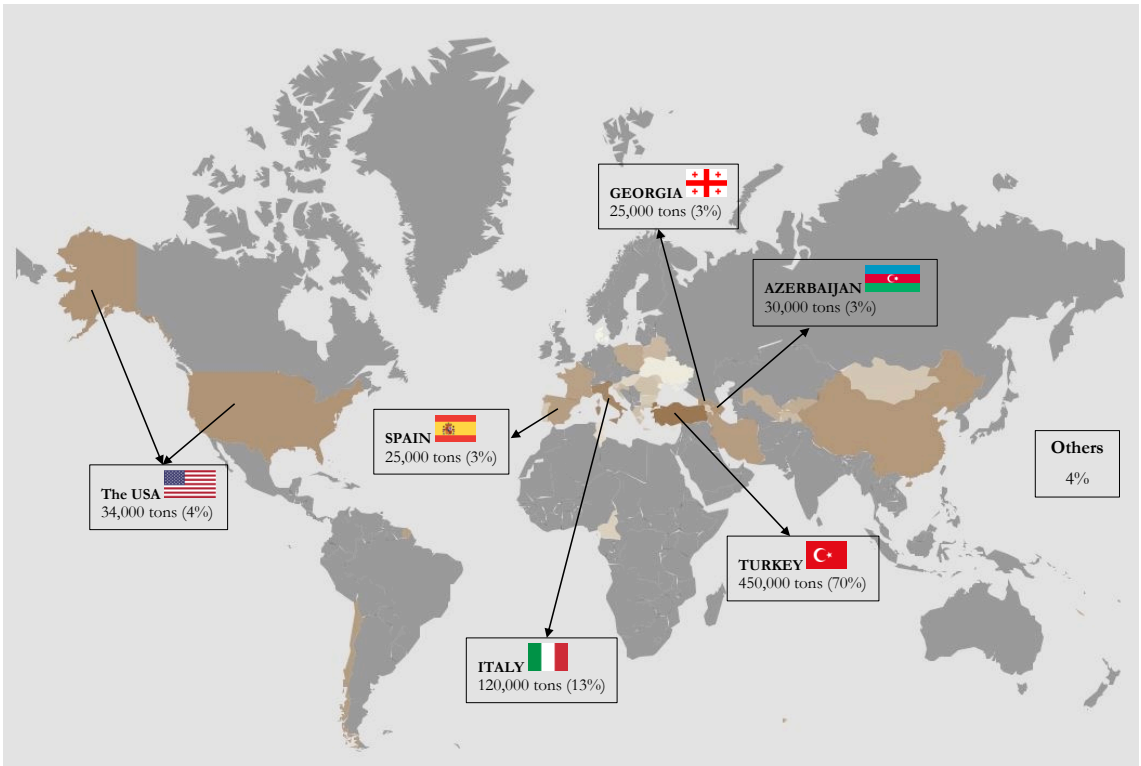

Figure C.1. Main hazelnut producing countries at worldwide market level (in shell) in 2017.

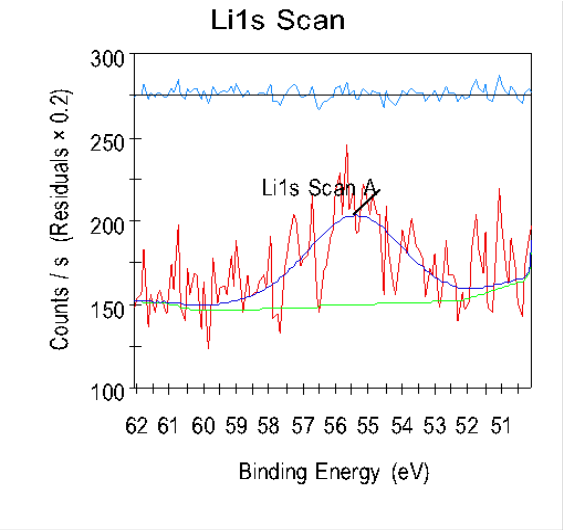

Figure C.2. High-resolution XPS spectra acquired at room temperature for a lithium-loaded phosphorylated hazelnut shell with binding energy (BE, eV) that correspond to Li 1s electron

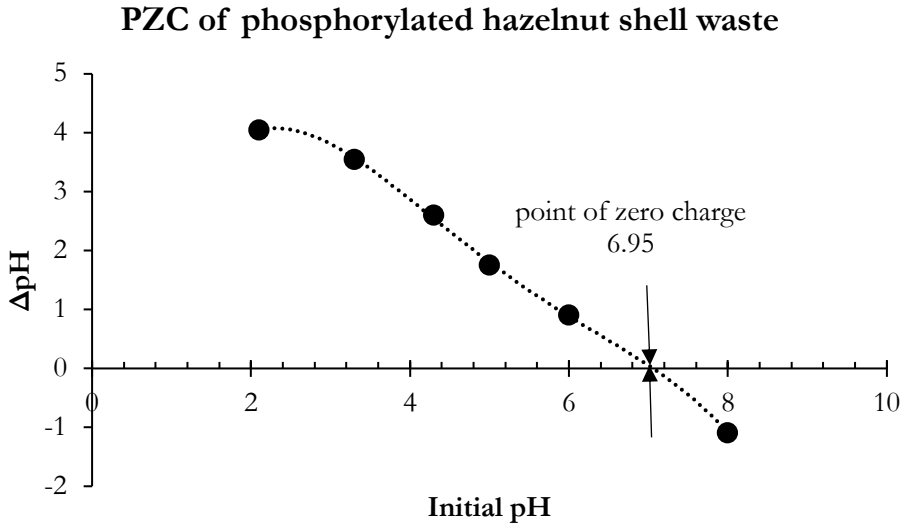

Figure C.3. Determination of zero-point charge for phosphorylated hazelnut shell waste ($C_0 = 10\ mgL^{-1}$, $T = 25℃\ and\ Adsorbent\ dosage = 14.0\ g/L$)

APPENDIX D

SUPPLEMENTARY INFORMATION FOR CHAPTER 4

Table D.1. Amount of phosphorylated functional cellulose and epichlorohydrin in the synthesis of cross-linked materials.

Reaction inputs	2-ECH*	4-ECH**	8-ECH***
Amount of functional material, g	10	10	10
Epichlorohydrin (ECH), mL	0.2	0.4	0.8

*0.02 mL ECH/g functional material; **0.04 mL ECH/g functional material; ***0.08 mL ECH/g functional material

Table D.2. Equilibrium swelling data of phosphorylated functional cellulose and its cross-linked forms in water at 25°C.

Material	W_s (g)	W_d (g)	Swelling ratio (%)
FC	0.42	0.0506	727.1
2-ECH	0.37	0.0508	626.2
4-ECH	0.30	0.0506	498.2
8-ECH	0.27	0.0508	438.4

Table D.3. Equilibrium swelling data of phosphorylated functional cellulose and its cross-linked forms in water at 25°C.

	Parameters		Thomas		Yoon-Nelson		MDR	
Exp. No.	Flow rate (mL/min)	Bed height (cm)	R^2	SSE	R^2	SSE	R^2	SSE
1	0.25	1.5	0.96	0.0033	0.98	0.0034	0.99	0.0003
2	0.5	1.5	0.99	0.0013	0.99	0.0009	0.99	0.0002
3	1.0	1.5	0.98	0.0094	0.99	0.0053	0.99	0.0007
4	0.5	1.0	0.99	0.0015	0.99	0.0012	0.99	0.0005
5	0.5	2.0	0.98	0.0004	0.99	0.0004	0.99	0.0002

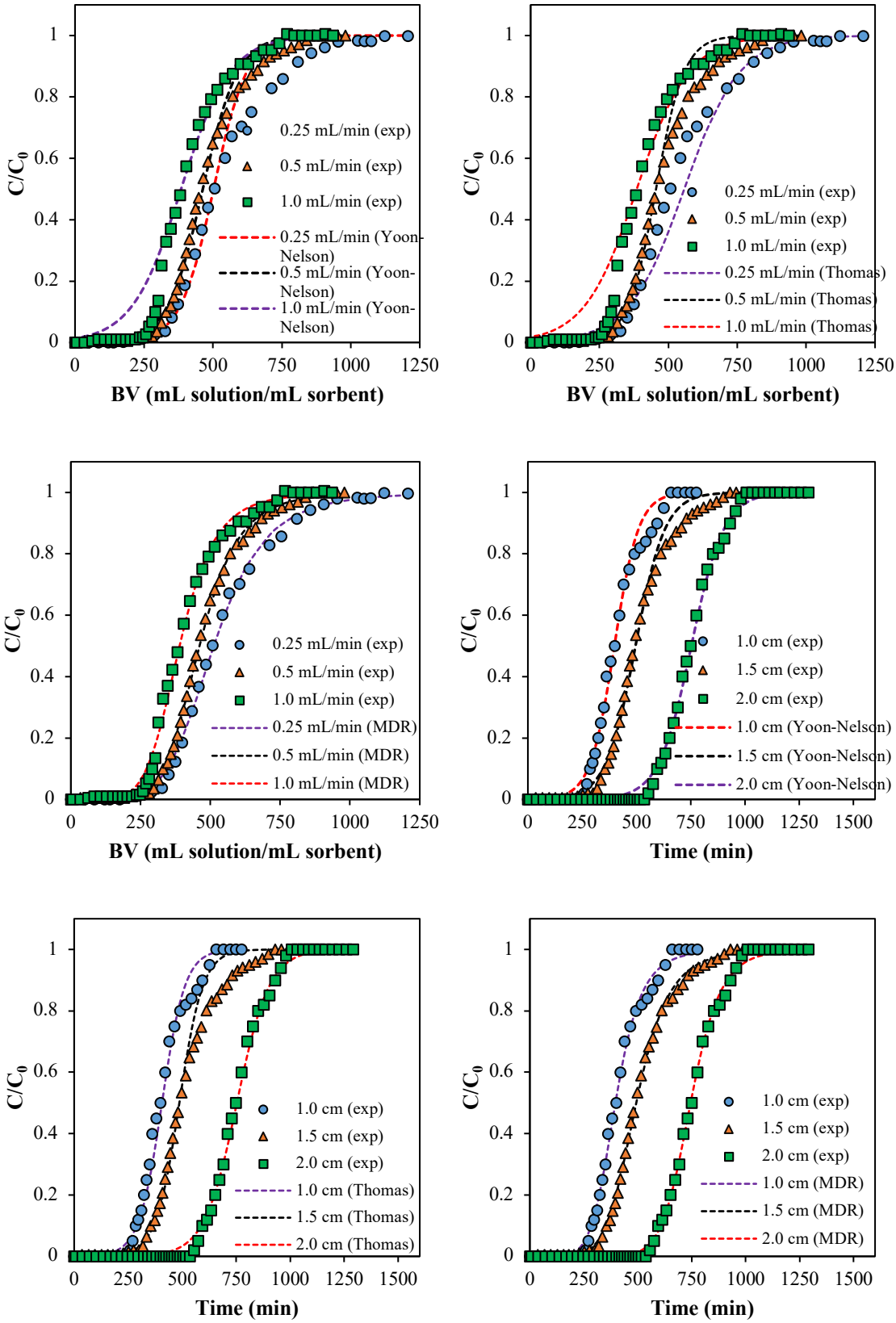

Figure D.1. Model fittings of experimental data obtained from column study under various operating conditions.

APPENDIX E

SUPPLEMENTARY INFORMATION FOR CHAPTER 6

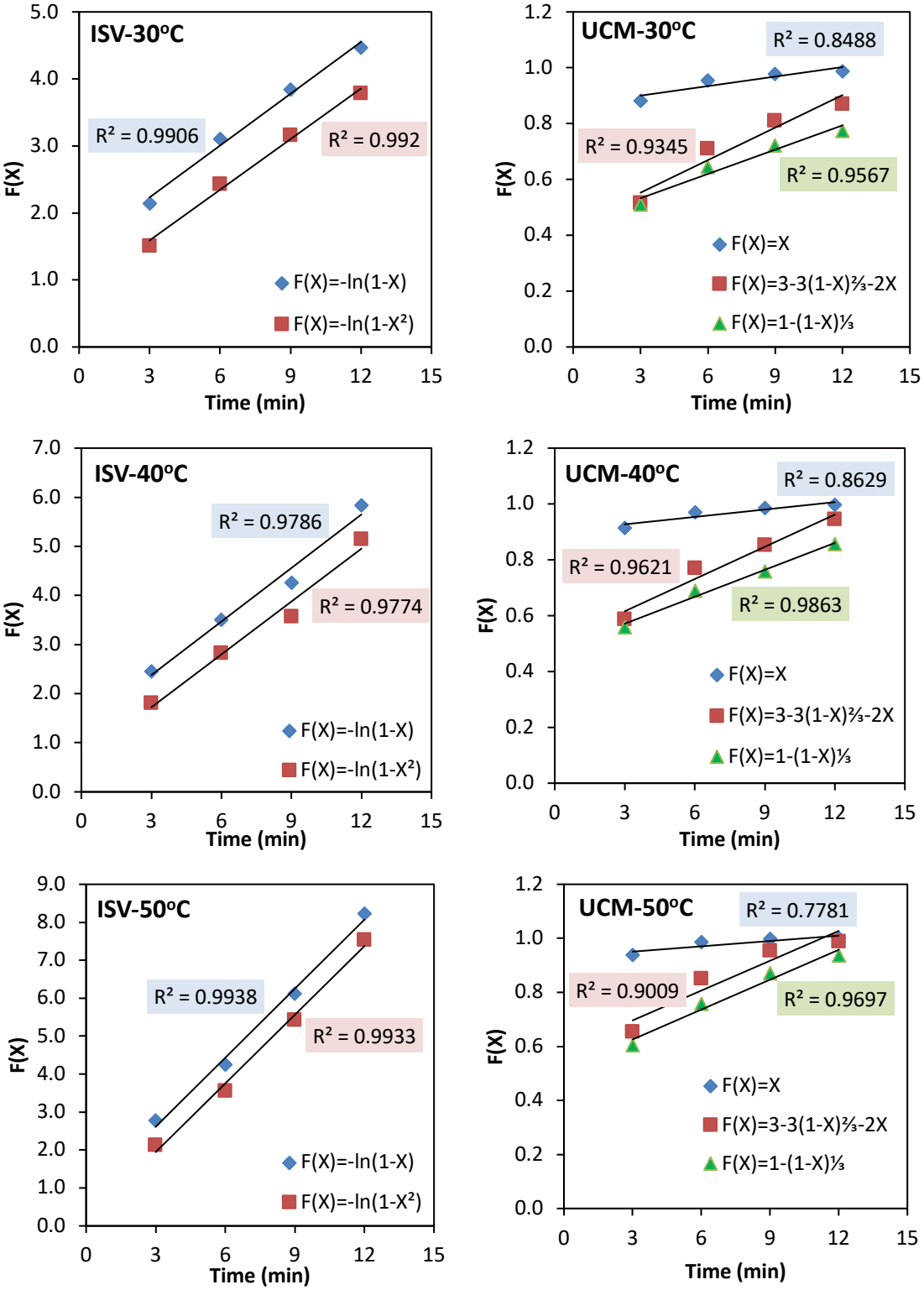

Figure E.1. ISV and UCM model fittings of kinetic data obtained by Lewatit® TP 260 for Li sorption from geothermal water.

VITA

Education

PhD:

2017 – 2023	Izmir Institute of Technology The Graduate School Department of Chemical Engineering (English) Urla/İzmir, TÜRKİYE

MSc:

2015 – 2017	Ege University Graduate School of Applied and Natural Sciences Department of Chemical Engineering (English) Bornova/İzmir, TÜRKİYE

BSc:

2010 – 2015	Ege University Faculty of Engineering Department of Chemical Engineering (English) Bornova/İzmir, TÜRKİYE Graduation Degree: 3.91/4.00 (1st Rank)

Work Experience

Feb 2017 – ...	Research and Teaching Assistant İzmir Institute of Technology Department of Chemical Engineering Gülbahçe, Urla/İzmir, TÜRKİYE
June 2023 – Aug 2023	PhD Student Internship Institut Mines-Télécom (IMT Mines-Alès) Polymer Composites and Hybrids Research Center Alès, FRANCE
Sept 2016 – Nov 2016	MSc Student Internship The University of Kitakyushu Faculty of Environmental Engineering Department of Chemical Engineering Hibikino, Kitakyushu, JAPAN
Aug 2014 – Sept 2014	Internship Student The University of Twente Faculty of Science and Technology (MST Group) Enschede, THE NETHERLANDS

Awards & Honors

- PhD Research Fellowship 2023 from the French Embassy in Türkiye for 2 months mobility at Institut Mines-Telecom, Ales, France (June – August 2023).
- PhD research award from Activity B of the 2nd edition of the Mediterranean PhD School, European Green Deal. The Contribution from Civil, Architectural and Environmental Engineering, The University of Naples Federico II (11 - 16 October 2021).
- The Best Poster Award (1st Place) at 1st International Black Sea Congress on Environmental Sciences (IBCESS), August 31–September 03, 2016, Giresun, TÜRKİYE

Projects Involved

- Project Title: **Separation and Recovery of Lithium from Geothermal Water with New Type Chitosan-Lithium Manganese Oxide Composite Material.** Project No: 2022IYTE-2-0009 AÜDP (Research Universities Support Program by Higher Education Council of Türkiye) (2022 – …)

- Project Title: **Phosphoryl-functional Cellulose-Based Adsorbents for Lithium Recovery from Water Sources: Synthesis, Adsorption, and Kinetic Studies.** Project No: 219M219 TÜBİTAK 1001 (The Scientific and Technological Research Council of Türkiye) (2020 – 2022)

- Project Title: **Synthesis of Cellulose-Based Lithium Selective Adsorbents and Their Application in Batch Adsorption Studies.** Project No: 2019IYTE0178 (Scientific Research Projects of Izmir Institute of Technology) (2019 – 2020)

- Project Title: **Recovery of Lithium and Boron from Geothermal Waters by Adsorption-Electrodialysis Hybrid Process.** Project No: 214M360 TÜBİTAK-JSPS (The Scientific and Technological Research Council of Türkiye – Japan Society for the Promotion of Science) (2015 – 2017)

Academic

Publications in Indexed Journals and Books

- **Y. K. Recepoğlu,** Ö. Arar, A. Yüksel, Breakthrough curve analysis of phosphorylated hazelnut shell waste in column operation for continuous harvesting of lithium from water, *Journal of Chromatography A*, (2024), 1713: 464510.

- **Y. K. Recepoğlu,** A. Y. Gören, Y. Orooji, V. Vatanpour, N. Kudaibergenov, Polyoxometalate-Based Hybrid Composites in Multi-Functional Wastewater Treatment Applications, *Journal of Water Process Engineering*, (2023), 53: 103863.

- A. Y. Gören, **Y. K. Recepoğlu**, Y. Yoon, A. Khataee, Insights into Sustainability of Engineered Carbonaceous Material-Based Technologies for Advanced Cyanide Removal from Wastewater, *Alexandria Engineering Journal*, (2023), 73: 169–88.

- A. Y. Gören, **Y. K. Recepoğlu**, V. Vatanpour, Y. Yoon, A. Khataee, Insights into Engineered Graphitic Carbon Nitride Quantum Dots for Hazardous Contaminants Degradation in Wastewater, *Environmental Research*, (2023), 223: 115408.

- **Y.K. Recepoğlu**, G. Gümüşbulut, A. Yüksel, A Comparative Assessment for Efficient Oleuropein Extraction from Olive Leaf (Olea Europaea L. Folium), *Turkish Journal of Engineering*, (2023), 7(2): 116-124.

- A. Y. Gören, **Y. K. Recepoğlu**, Ö. Edebali, Ç. Şahin, M. Genişoğlu, H. E. Ökten, Electrochemical Degradation of Methylene Blue by Flexible Graphite Electrode: Techno-Economic Evaluation, *ACS Omega*, (2022), 7(36): 32640–32652.

- A. Mott, A. Baba, M. Hadi Mosleh, H. E. Ökten, M. Babaei, A. Y. Gören, C. Feng, **Y. K. Recepoğlu**, T. Uzelli, H. Uytun, D. Morata, A. Yüksel, M. Sedighi, Boron in Geothermal Energy: Sources, Environmental Impacts, and Management in Geothermal Fluid, *Renewable and Sustainable Energy Reviews*, (2022), 167: 112825.

- J. Nampeera, **Y. K. Recepoğlu**, A. Yüksel, Valorization of Olive Tree Pruning Waste for Potential Utilization in Lithium Recovery from Aqueous Solutions, *Biomass Conversion and Biorefinery*, (2022), 1-13.

- **Y. K. Recepoğlu**, A. Y. Gören, V. Vatanpour, Y. Yoon, A. Khataee, Boron Carbon Nitride Nanosheets in Water and Wastewater Treatment: A Critical Review, *Desalination*, (2022) 533: 115782.

- A. Y. Gören, **Y. K. Recepoğlu**, A. Khataee, Chapter 4: Language of Response Surface Methodology as An Experimental Strategy for Electrochemical Wastewater Treatment Process Optimization. In: Asadnia M., Razmjou A., Beheshti A. (eds) *Artificial Intelligence and Data Science in Environmental Sensing*. Academic Press, Elsevier (2022), 57–92.

- A. Y. Gören, **Y. K. Recepoğlu**, A. Karagündüz, A. Khataee, Y. Yoon, A Review of Boron Removal from Aqueous Solution Using Carbon-Based Materials: An Assessment of Health Risks, *Chemosphere*, (2022), 293: 133587.

- **Y. K. Recepoğlu**, A. Y. Gören, Y. Orooji, A. Khataee, Carbonaceous Materials for Removal and Recovery of Phosphate Species: Limitations, Successes and Future Improvement, *Chemosphere*, (2022), 287: 132177.

- **Y. K. Recepoğlu**, A. Yüksel, Cross-Linked Phosphorylated Cellulose as A Potential Sorbent for Lithium Extraction from Water: Dynamic Column Studies and Modeling, *ACS Omega*, (2022), 7(43): 38957–38968.

- **Y. K. Recepoğlu**, A. Yüksel, Phosphorylated Hazelnut Shell Waste for Sustainable Lithium Recovery Application as Biosorbent, *Cellulose*, (2021), 28: 9837-9855.

- A. Baba, **Y. K. Recepoğlu**, H. Yazdani, Chapter 18: Naturally Occurring Arsenic and Boron in Geothermal Systems and Their Health Effects: A Case Study from Turkey. In: Siegel M., Selinus O., Finkelman R. (eds) *Practical Applications of Medical Geology*. Springer, Cham. (2021), 615–635.

- **Y. K. Recepoğlu**, A. Yüksel, Synthesis, Characterization and Adsorption Studies of Phosphorylated Cellulose for the Recovery of Lithium from Aqueous Solutions, *Cellulose Chemistry and Technology*, (2021), 55 (3-4): 385–401.

- M. Genişoğlu, A.Y. Gören, E. Balcı, **Y. K. Recepoğlu**, H. E. Ökten, Methylene Blue Removal of Fixed-Bed Column Reactor with Pumice and nZVI-Pumice: Experimental and Modeling

Study, *Süleyman Demirel University Journal of Natural and Applied Sciences*, (2019), 23(2): 298–305.

- **Y. K. Recepoğlu,** N. Kabay, K. Yoshizuka, S. Nishihama, İ. Yılmaz-İpek, M. Arda, M. Yüksel, Effect of Operational Conditions on Separation of Lithium from Geothermal Water by λ-MnO_2 Using Ion Exchange–Membrane Filtration Hybrid Process, *Solvent Extraction and Ion Exchange,* (2018), 36(5): 499–512.

- **Y. K. Recepoğlu,** N. Kabay, İ. Yılmaz-İpek, M. Arda, M. Yüksel, K. Yoshizuka, S. Nishihama, Packed Bed Column Dynamic Study for Boron Removal from Geothermal Brine by A Chelating Fiber and Breakthrough Curve Analysis by Using Mathematical Models, *Desalination*, (2018), 437: 1–6.

- **Y. K. Recepoğlu,** N. Kabay, İ. Yılmaz-İpek, M. Arda, M. Yüksel, K. Yoshizuka, S. Nishihama, Elimination of Boron and Lithium Coexisting in Geothermal Water by Adsorption-Membrane Filtration Hybrid Process, *Separation Science and Technology*, (2018), 53(6): 856–862.

- **Y. K. Recepoğlu,** N. Kabay, İ. Yılmaz-İpek, M. Arda, K. Yoshizuka, S. Nishihama, M. Yüksel, Equilibrium and Kinetic Studies on Lithium Adsorption from Geothermal Water by λ-MnO_2, *Solvent Extraction and Ion Exchange*, (2017), 35(3): 221–231.

- **Y. K. Recepoğlu,** N. Kabay, İ. Yılmaz-İpek, M. Arda, M. Yüksel, K. Yoshizuka, S. Nishihama, Deboronation of Geothermal Water Using N-Methyl-D-Glucamine Based Chelating Resins and A Novel Fiber Adsorbent: Batch and Column Studies, *Journal of Chemical Technology and Biotechnology*, (2017), 92: 1540–1547.

Oral Presentations at International Symposiums, Congresses, and Conferences

- **Y. K. Recepoğlu**, A. Yüksel, Utilization of Phosphorylated Hazelnut Shell Waste in a Column for Continuous Lithium Recovery from Water, 5th International Environmental Chemistry Congress (EnviroChem), October 30 – November 2, 2023, Antalya, TÜRKİYE

- **Y. K. Recepoğlu**, A. Yüksel, Synthesis and Application of Cellulose-Based Functionalized Adsorbent for The Recovery of Lithium from Aqueous Solutions, IEX 2022: Ion Exchange – a continuing success story, September 07–09, 2022, UK (virtual)

- **Y. K. Recepoğlu**, A. Yüksel, Development of sustainable and cost effective biosorbent from hazelnut shell waste for lithium extraction from water, the 7th International Conference Ecological and Environmental Chemistry, March 3–4, 2022, Chisinau, Republic of Moldova (virtual)

- A. Y. Gören, **Y. K. Recepoğlu**, Ö. Edebali, Ç. Şahin, M. Genişoğlu, H. E. Ökten, Techno-Economic Assessment of Electrochemical Process for Sustainable Removal of Methylene Blue, the 7th International Conference Ecological and Environmental Chemistry, March 3–4, 2022, Chisinau, Republic of Moldova (virtual)

- **Y. K. Recepoğlu,** N. Kabay, İ. Yılmaz-İpek, M. Arda, M. Yüksel, K. Yoshizuka, S. Nishihama, A Comparative Study for Removal of Arsenic from Water by a Cellulose Based Functional Fiber, Ion Exchange Resins and Inorganic Adsorbents, Uluslararası Su ve Çevre Kongresi (SUCEV 2018), March 22–24, 2018, Bursa, TÜRKİYE

- **Y. K. Recepoğlu,** N. Kabay, İ. Yılmaz-İpek, M. Arda, M. Yüksel, K. Yoshizuka, S. Nishihama, Simultaneous Separation of Boron and Lithium from Geothermal Water by Adsorption-Membrane Filtration Hybrid Process, 2nd IWA Regional International Symposium on Water, Wastewater and Environment (IWA-PPFW2017), March 22–24, 2017, Çeşme, İzmir, TÜRKİYE

- **Y. K. Recepoğlu,** N. Kabay, İ. Yılmaz-İpek, M. Arda, M. Yüksel, K. Yoshizuka, S. Nishihama, Chromatographic Separation of Boron from Geothermal Water using a Boron Selective Chelating Fiber Adsorbent, III. International Porous Powder Materials Symposium & Exhibition (PPM 2017), September 12–15, 2017, Kuşadası, Aydın, TÜRKİYE

- **Y. K. Recepoğlu,** N. Kabay, İ. Yılmaz-İpek, M. Arda, M. Yüksel, K. Yoshizuka, S. Nishihama, A Comparative Study for Selective Separation of Boron from Geothermal Water by A Novel Chelating Fiber Adsorbent and Boron Selective Ion Exchange Resins, IEX 2016: Ion Exchange – a continuing success story, July 06–08, 2016, Robinson College, Cambridge, UK

Poster Presentations at International Symposiums, Congresses, Conferences

- **Y. K. Recepoğlu,** N. Kabay, İ. Yılmaz-İpek, M. Arda, M. Yüksel, K. Yoshizuka, S. Nishihama, Comparison of Adsorption and Desorption Performances of Boron Selective Chelating Resins and Fibers for Separation of Boron from Geothermal Water, 9th Eastern Mediterranean Chemical Engineering Conference (EMCC 9), August 31–September 02, 2018, Ankara, TÜRKİYE

- **Y. K. Recepoğlu,** N. Kabay, İ. Yılmaz-İpek, M. Arda, M. Yüksel, K. Yoshizuka, S. Nishihama, Removal of Boron from Geothermal Water by a Novel Chelating Fiber, 1st International Black Sea Congress on Environmental Sciences (IBCESS), August 31–September 03, 2016, Giresun, TÜRKİYE *(The Best Poster Award – 1st Place)*

- E. Altıok, **Y. K. Recepoğlu,** N. Kabay, M. Arda, İ. İpek, M. Yüksel, S. Nishihama, K. Yoshizuka, Preparation of Solvent Impregnated Composite Fibre Adsorbents for Cr(VI) Removal from Aqueous Solution, IEX 2016: Ion Exchange – a continuing success story, July 06–08, 2016, Robinson College, Cambridge, UK

Poster Presentations at National Symposiums, Congresses, Conferences

- E. Altıok, **Y. K. Recepoğlu**, B. Çokçalışır, N. Kabay, İ. İpek, M. Yüksel, S. Nishihama, K. Yoshizuka, Removal of Cr(VI) from Aqueous Solution by Functional Composite Fiber, Activated Carbon and Polymer Adsorbent, III. Ege Composite Materials Symposium by International Participation, November 05–07, 2015, Kuşadası, Aydın, TÜRKİYE